PNNL-11595
UC-2030

Pacific Northwest
National Laboratory

Operated by Battelle for the
U.S. Department of Energy

Developing a Model for Moisture in Saltcake Waste Tanks: Progress Report

C. S. Simmons
N. Aimo
M. J. Fayer
M. D. White

July 1997

Prepared for the U.S. Department of Energy
under Contract DE-AC06-76RLO 1830

PNNL-11595

PACIFIC NORTHWEST NATIONAL LABORATORY
operated by
BATTELLE
for the
UNITED STATES DEPARTMENT OF ENERGY
under Contract DE-AC06-76RLO 1830

Printed in the United States of America

Available to DOE and DOE contractors from the Office of Scientific and Technical Information, P.O. Box 62, Oak Ridge, TN 37831; prices available from (615) 576-8401.

Available to the public from the National Technical Information Service, U.S. Department of Commerce, 5285 Port Royal Rd., Springfield, VA 22161


This document was printed on recycled paper.

PNNL-11595
UC-2030

Developing a Model for Moisture in Saltcake Waste Tanks: Progress Report

C. S. Simmons
N. Aimo
M. J. Fayer
M. D. White

July 1997

Prepared for
the U.S. Department of Energy
under Contract DE-AC06-76RLO 1830

Pacific Northwest National Laboratory
Richland, Washington 99352

Summary

This report describes a modeling effort to provide a computer simulation capability for estimating the distribution and movement of moisture in the saltcake-type waste contained in Hanford's single-shell radioactive waste storage tanks. This moisture model goes beyond an earlier version because it describes water vapor movement as well as the interstitial liquid held in a saltcake waste. The work was performed by Pacific Northwest National Laboratory to assist Duke Engineering and Services Hanford with the Organic Tank Safety Program.

The Organic Tank Safety Program is concerned whether saltcake waste, when stabilized by jet pumping, will retain sufficient moisture near the surface to preclude any possibility of an accidental ignition and propagation of burning. The nitrate/nitrite saltcake, which might also potentially include combustible organic chemicals might not always retain enough moisture near the surface to preclude any such accident. Draining liquid from a tank by pumping, coupled with moisture evaporating into a tank's head space, may cause a dry waste surface that is not inherently safe. The moisture model was devised to help examine this safety question.

The model accounts for water being continually cycled by evaporation into the head space and returned to the waste by condensation or partly lost through venting to the external atmosphere. Water evaporation occurs even in a closed tank, because it is driven by the transfer to the outside of the heat load generated by radioactivity within the waste. How dry a waste may become over time depends on the particular hydraulic properties of a saltcake, and the model uses those properties to describe the capillary flow of interstitial liquid as well as the water vapor flow caused by thermal differences within the porous waste.

The possible directions of migration and the precipitation of dissolved organic chemicals at the waste surface are other physical aspects that can be quantified by using this new moisture model, but this subject of salt transport is a future application of the model.

The computer code STOMP (Subsurface Transport Over Multiple Phases) is used as the computational foundation for this moisture model. This code solves the relevant conservation equations for the flow of both liquid and gas (air with water vapor) phases in a porous matrix confined in a cylindrical shape. It can also calculate the associated flow of heat when the system is treated as nonisothermal (depending on temperature). By itself, the code does not constitute the moisture model; it also requires measurements of relevant physical parameters that describe the waste. The code helps to clarify the importance of measuring the hydraulic properties of waste to make predictions about moisture retention.

The following four development activities were completed to prepare the moisture model for application to saltcake-type waste contained in a tank:

- The STOMP code was modified to include the influence of dissolved salt concentration on the water vapor partial pressure within the porous waste matrix.

- The moisture model was applied to test cases involving both interstitial liquid and water vapor flow for nonisothermal conditions

- Supporting simulations were run to test the influence of surface evaporation on the waste moisture distribution by using the UNSAT-H code, a simulator for water flow in an unsaturated porous medium.

- A simplified model was developed for steady-state evaporation into a tank's head space to define the waste surface boundary condition.

The relevance of these four model development activities is described further below. In addition to obtain better estimates of hydraulic properties of saltcake waste that is now actually held in Hanford's stabilized tanks, the drainable porosity of the waste was evaluated; and the results are provided in Appendix E.

Model Development. The STOMP code as used for the moisture model was modified to include the influence of dissolved salt concentration on the water vapor pressure, and the mathematical revision is discussed in Appendix A. A further test case also described in Appendix A shows that the code can model the counter balanced flow of water vapor and a salty liquid compelled by a thermal gradient acting in an unsaturated porous medium held in a closed container. The test cases showed that moisture accumulates at the cool end of a porous medium while being reduced in amount at the warmer end. Furthermore, dissolved salt concentration increases at the warmer end, when compared with the cooler end. It demonstrated that, under final steady-state conditions, liquid flow driven by capillary forces acting from the cooler to the warmer end is balanced by an equal flow of water vapor in the opposite direction. This simulated behavior confirmed the STOMP code's capability for describing the coupled flow of salty liquid, water vapor and heat in an unsaturated porous medium, such as a saltcake above the interstitial liquid level.

Test Cases for Vapor Flow. A group of test cases were run using the STOMP code to demonstrate the code's capability for describing the circulation of moisture in a tank's waste profile. The test cases demonstrated the importance of the waste surface boundary condition for the head space. Because the exact evaporation rate at the waste surface of a particular tank is not certain, various extreme situations were simulated to test the consequences. It was assumed in the test cases that evaporated moisture returns to the waste edge by condensation near the tank side. These cases used a four-layer saltcake presumed to imitate the waste profile of Tank BY-104. The extreme hypothetical situations of having either no evaporation with only radiant heat loss at the waste surface or having entirely evaporative heat transfer to the dome were simulated. These extremes were intended to bound the conditions in a waste tank.

The outcome was that the liquid distribution in the waste was not changed by a detectable amount from the initial static condition produced by stabilization and determined by liquid capillarity acting against gravity. This result was a consequence of the particular high hydraulic conductivity presumed appropriate for a saltcake and the constraint that moisture did not leave

the tank over the model's 10-year simulation period. Thus, cycling of moisture in saltcake via the flow of water vapor did not dry out the waste surface, and liquid is continually replenished to keep the surface moisture content the same.

Surface Evaporation Conditions. The UNSAT-H code for simulating one-dimensional, unsaturated vertical moisture flow for nonisothermal conditions was used independently of the STOMP code to examine the influence of the waste surface boundary condition. The impact of the surface evaporation rate on the waste moisture distribution was thereby examined. The modeling results and implications are discussed in Appendix B. This study was done as a confirmation of the STOMP code's prediction capability. Related to the possibility of a waste surface drying out, the code showed that the relative value of the emissivity for head space air and the waste surface is critical for determining the proportion of heat transferred by evaporation, compared with the heat load transferred by convection and radiation into the head space. It was found that the radiant emissivity for head space air must be much less than that for the waste surface for heat to mainly be transferred by convection and radiation. Moreover, the air flow speed across the waste surface has an important influence on evaporation rate into the head space. These findings were incorporated into a simplified steady-state evaporation model for the waste surface and head space of a tank.

Head Space Evaporation Model. A revised model was developed to calculate the rate of moisture evaporation into the head space of a tank, based on how the heat load transfer is partitioned between the convection, thermal radiation, and latent heat modes. The model is intended to describe the waste surface boundary condition for input to the STOMP code, which only describes the subsurface system. The model makes use of the relative humidity in the head space air and within the porous matrix along with a tank's known heat load to estimate the evaporation rate. The revised version accounts for water vapor diffusion toward the surface from within the waste matrix and the moisture loss by breathing of a tank. This revised model is described in Appendix C.

Using this model to simulate a waste tank like BY-104 showed that the evaporative part of the heat transfer is about 9% of the total transferred through the waste surface. That evaporation results in about 2000 kg/yr of moisture cycled within a tank's head space, while only about 20 kg/yr of water is lost by passive breathing of 2000 cubic meters/year of air. As demonstrated by the test cases using the STOMP code, this evaporation rate would not alter the moisture distribution, which is mainly set by the capillary equilibrium distribution, because the permeability was great enough to continually allow the resupply of evaporated moisture.

Testing the moisture model for hypothetical cases showed the importance of having exact data for the physical parameters in order to predict the ultimate dryness of waste in a tank. To predict the moisture distribution in a waste tank requires specific data for the saltcake: porosity; permeability; pore-size index for the capillary liquid retention; depth to the interstitial liquid level determined by stabilization; existing waste temperatures for the particular heat load; and properties of any dense crust, which might be covering the surface and limiting evaporation.

A final question relevant to the Organic Tank Safety Program is whether remediation steps can be taken effectively to re-wet a dry saltcake surface and return it to a safe condition. The model also examined this possibility. It was found that moisture applied to the surface of a highly permeable saltcake would not remain long at the surface but would rapidly drain downward, making it difficult to maintain moisture at the waste surface without continually applying water. This conclusion, however, does not account for the continual dissolution of the saltcake that might occur at the surface.

Contents

Figures

Tables

1.0 Introduction

A computer simulation model has been developed to describe the distribution and movement of moisture in stabilized saltcake waste stored in single-shell tanks at Hanford. Stabilizing the saltcake waste usually involves jet-pumping out the excess liquid that could possibly leak from a tank. Stabilized saltcake waste is different from the same material saturated with interstitial liquid because it constitutes an unsaturated porous material when drained. In this unsaturated material above the interstitial liquid level of the saturated region, moisture moves by capillary conduction as liquid and as vapor, driven by thermal gradients. The study discussed in this report was conducted by Pacific Northwest National Laboratory (PNNL)[a] under the Organic Tank Safety Program to determine whether sufficient water would be retained at the surface of a stabilized saltcake to prevent accidental ignition and combustion of organic-nitrate waste mixtures. The moisture model developed for this project can also help quantify the stabilization process itself and estimate the resulting dryness of drained saltcake waste.

The moisture model discussed here is an extension of an earlier version (Simmons 1995), which was limited to describing only vertical, steady upward flow of liquid in a drained saltcake. The earlier version did not account for the role of water vapor movement in the waste, which is usually being heated by radioactive decay. The advanced version can estimate the movement of water as both interstitial liquid (salty water) and vapor. It also incorporates the cylindrical shape of the waste tank and describes the pattern of moisture movement in such a container.

The moisture model is based on an advanced simulator called the STOMP (Subsurface Transport Over Multiple Phases) code, which calculates the flow of both liquid and gas phases in an unsaturated porous medium through which heat is also passing (White and Oostrum 1996). The earlier model (Simmons 1995) used a simplified analytical solution for one-dimensional, vertical unsaturated flow in a system with constant temperature, whereas the STOMP code is a much more general numerical solution of all the governing equations that describe the multiphase flow processes acting under nonisothermal conditions. (Nonisothermal means that thermal conditions are spatially variable, and temperature is not the same everywhere. Liquid and vapor flows are dependent on the temperature gradient.)

Modeling is an indispensable approach for gaining a better understanding of moisture behavior in drained saltcake. An overview of how the model is designed and applied to describe basic flow processes in saltcake is provided in this section. Section 2 discusses the physical processes that influence the moisture distribution and movement in porous material. Section 2 is a conceptual synopsis of the processes simulated by the STOMP code. More technical explanations about the simulated processes are found in White and Oostrum (1996).

Section 3 describes boundary conditions necessary to simulate moisture migration behavior in waste tanks. Boundary conditions acting at the waste surface determine the potential

---

(a) Pacific Northwest National Laboratory is operated by Battelle for the U.S. Department of Energy under Contract DE-AC06-76RLO 1830.

pattern of moisture movement in a drained saltcake. Section 4 examines how moisture might migrate inside a stabilized saltcake profile for conditions that do not involve the influence of water vapor movement or heat transfer, and discusses the test cases run to show the STOMP code's capability. Section 5 addresses the movement of moisture under nonisothermal conditions (depending on thermal differences) applicable to a waste tank with a heat load. Section 5 also presents some nonisothermal test cases for water vapor movement. Conclusions from this study and model development are given in Section 6. Cited references can be found in Section 7.

Appendixes to this report include information on the technical aspects of various modifications to the STOMP code needed to account for the influence of salt concentration on water vapor movement and a simulation example addressing the potential drying out of a waste profile. A model for evaporation occurring within the head space of a tank is also given, as well as a revised estimation of capillary parameters for actual stabilized Hanford waste tanks.

1.1 Reasons for Moisture Modeling

Saltcake waste undergoes considerable change in density and porosity as a result of stabilization. Modeling the moisture in tank waste is a way to determine the dryness condition following stabilization that cannot be estimated by measuring the waste characteristics before drainage has occurred.

Because radioactive tank systems cannot be easily entered safely, obtaining direct measurements of moisture at the surface of a stabilized waste is a very difficult technical problem. Moreover, core samples obtained by drilling and used for analyzing the chemical constituents of waste do not always accurately reflect the moisture content under actual in-tank conditions. Core samples are usually taken before the tank is stabilized and do not reflect the drained moisture condition. Drilling and core extraction change the moisture condition of the waste because most of the moisture is held physically as interstitial liquid rather than chemically bound to the solids. Extracting a core sample disturbs the true physical association of the interstitial liquid with the solid saltcake matrix as held by the tank. For instance, the interstitial liquid and salt solids often separate in a drilled core, and the matrix structure collapses from its original in-situ bulk density to some other density value. Furthermore, instrumentation methods for measuring in-situ moisture content cannot predict the future state of a waste surface following stabilization. Thus the future state must be forecast through modeling.

The moisture model can be used for forecasting in the following ways:

- to determine the potential dryness of the waste surface after stabilization
- to understand the moisture cycle dynamics in saltcake waste held by a tank
- to examine transport of dissolved organic chemicals by leaching or evaporation.

Another reason for developing the more advanced model is to determine how adequate the simplifying assumptions were as used in the earlier model (Simmons 1995). If the simplified model is an adequate description, then the hydraulic properties of the waste (liquid retention relationship and conductivity) were sufficient information to model the moisture distribution,

without accounting for the more complex influences of water vapor flow or heat transfer. It is useful to know when the influence of water vapor flow and heat transfer can be neglected for using a more simplified analysis of the waste moisture distribution. Then, also, less information about the waste may be adequate to predict its future safety.

1.2 Overview of Moisture Model

Water moves in saltcake as part of the interstitial liquid and as vapor passing through drained interstices of air-filled pores. In a nonisothermal system like tank waste, water vapor flows as a result of the vapor pressure gradient acting in the air or gas phase. Mostly, spatial changes in temperature cause the vapor pressure to vary in a drained waste. Also, liquid flows as a result of capillary forces whenever the liquid content anywhere is changed by evaporation or condensation of water vapor.

The processes that move water can be described using the STOMP code, which solves the relevant conservation equations for the coupled flow of interstitial liquid, water vapor, and heat in an unsaturated porous waste. The STOMP code solves the mathematical equations that describe the appropriate physical mechanisms governing moisture transport via both liquid and vapor phases. Under long-term, steady-state conditions following stabilization, the moisture distribution in waste may not appear to change with time. However, in a nonisothermal system such as radioactively heated tank waste, the moisture will be in continual flux as a result of a balanced evaporation and condensation cycle occurring within the waste profile. (Of course, in a highly ventilated tank, which has a substantial moisture loss by breathing, the cycle is not in balance.)

Also, a waste profile, when being pumped for stabilization, exhibits a dynamic change in the interstitial liquid distribution as the interstitial liquid level (ILL) is drawn down. Because the STOMP code gives a general solution for moisture flow in an unsaturated porous medium, it can model all of these circumstances involving stabilization and moisture evaporating from the waste surface. (STOMP was applied already to evaluate the diffusive movement of released entrapped gas in stabilized waste [Peurrung et al. 1996]. Entrapped gas can alter the hydraulic properties of waste and influence liquid flow behavior, but this influence was not examined here.)

In general, the STOMP code can be used to determine the outcome of a final steady-state condition by simulating when it is reached as the limit of dynamic processes that eventually approach the final state. In other words, the STOMP code does not simulate a final hypothetical steady-state situation directly but obtains it as the limit of changing conditions. For instance, pumping a tank is a dynamic process that finally achieves a static distribution of liquid in a saltcake profile when no more liquid can be removed because it is retained by capillarity.

Thus, the STOMP code implements the mathematical theory and performs calculations of water and thermal energy transport. The flow of water mass and thermal energy quantities is described by conservation equations (Section 3 of White and Oostrom 1996) that give the time rate of change of these quantities in control volumes as a result of the fluxes of each crossing the control volume surfaces. Control volumes are defined for a problem by the discretization of the

system domain into subunit cells. Primary physical variables such as pressures, mole fractions, and temperatures are treated as constant (uniform) within a subunit cell but vary spatially over the cells. The state of the system at each time is described in terms of the primary physical variables by solving the governing conservation equations. White and Oostrom (1996) give detailed mathematical procedures for how these calculations are accomplished.

1.2.1 Model Limitations

Certain assumptions about the characteristics of saltcake are necessary. The exact nature of waste material has not been completely quantified nor have the hydraulic properties been directly measured on core samples. First, it is assumed that a saltcake crystal matrix is a rigid porous medium with liquid retention behavior due to capillarity, which is described by the traditional Brooks-Corey equation (Simmons 1995). The prior modeling was predicated on this equation, which is a common relationship used in soil physics for granular subsurface media. Based on the Brooks-Corey equation, which is also incorporated in the STOMP code, the holdup height of capillary rise, the porosity, and a pore-size index are sufficient parameters to represent capillary retention. This is a key assumption that requires further confirmation for actual saltcake.

Additionally, with information about the intrinsic permeability and liquid viscosity, the hydraulic conductivity, as it depends on the volumetric liquid content, can also be described mathematically by using the Brooks-Corey model. Then, assuming Darcy's law of liquid flow, the flow velocity or flux is equal to the product of the hydraulic conductivity with the pressure gradient in the liquid acting in union with the added gravitational gradient.

The Brooks-Corey equation gives the capillary pressure as a function of the volumetric liquid content at each location. From the capillary pressure, which is the difference in the air phase and liquid phase pressures, the required pressure in the liquid phase is found. This pressure, which is actually a tension within the liquid phase, is negative under unsaturated conditions because the adhesion to the drained saltcake draws the liquid into the porous matrix. The pulling of liquid into a drained saltcake matrix is called capillarity. In contrast, the liquid pressure below the ILL in the saturated zone is a positive hydrostatic head, except within the depth of the holdup height just below the ILL, where capillarity still draws liquid up.

The Brooks-Corey model is known to apply to granular subsurface media such as sand and soils. Thus it is presumed that a solid saltcake is a pack of crystal grains. If, instead, saltcake is a fractured solid with mainly fissures as the interstitial space, this model may not apply. Also, it is known that the Brooks-Corey model for liquid retention applies to liquids other than pure water, such as oil or brines. Thus, a reasonable assumption is that it also applies to sodium nitrate/nitrite brine in solubility equilibrium with the saltcake. That is, the model likely applies for a fixed pore-index and porosity as long as the matrix is not undergoing change by dissolution.

Presently, the code does not account for the salt crystal matrix dissolving and changing over time. The hydraulic properties and parameters of the matrix, therefore, are assumed to be constant over time. In reality, this assumption is probably not correct.

It is also assumed that the pore-size index could be estimated by considering the volume of liquid that could be pumped from a stabilized saltcake profile that becomes partially drained. The calculation of pore-size index was explained in the earlier report (Simmons 1995). Interstitial liquid is only partly water; it is also saturated with soluble salts that constitute a brine with density greater than that of water. That is, only a certain percentage (usually, 40 to 60 wt%) of brine is water. The holdup height is given in terms of the brine density, so that liquid pressure can be expressed in terms of the equivalent liquid column height for the brine.

Another important limitation of the present conceptualization of saltcake is that water combined or associated chemically (e.g., water of hydration) with the salt crystal matrix is not considered. The model discussed here is concerned with only the water included in the interstitial liquid, which is free enough to conduct through the interstices under a mechanical pressure gradient. If it is known how much water by weight percent is bound to the saltcake matrix by mechanisms other than capillarity, then given the volumetric liquid content of the interstitial liquid and its weight percent water, a straightforward calculation of the total weight percent water is easily done, provided the porosity, crystal density, and liquid density are known. However, this bound percentage of water is not yet known for typical saltcake in waste tanks. Future measurements of tank waste need to evaluate the amount of bound or immobile water.

1.2.2 Unsaturated Flow Processes

Drainage, evaporation, and leaching are three important unsaturated flow processes relevant to stabilized saltcake. When excess liquid is pumped from a tank to stabilize the waste, the porous matrix drains until the amount of liquid held up by capillary force against gravity cannot be removed further by pumping from a salt well. This report demonstrates (Section 4.1) that draining a saltcake by pumping from a salt well can be simulated for a tank's cylindrical shape. The drained or stabilized state represents a starting point or initial condition for which evaporation at the surface becomes important in determining the long-term moisture content of the waste.

In a nonisothermal, drained waste profile having a heat load, water vapor is continually evolving and diffusing upward, where it condenses and returns as liquid flowing back down into the unsaturated matrix. This process is only important in a stabilized profile that has drained interstices containing interconnected passageways that allow air movement. The upward and outward movement of water vapor is one important mode by which the tank's heat load is transferred to the outside. At the same time, heat is conducted through the solid and liquid masses to the outside. Such heat conduction must be calculated simultaneously with the mass transport of water to accurately explain the moisture condition of saltcake held in a closed tank.

Surface drying may occur, depending on the amount of evaporation that potentially transfers water to the tank dome and sides, which are cooler than the waste core. This evaporation may be continually reabsorbed in the cooler waste along the tank sides, provided that vapor is not being removed by ventilation of the tank's head space from between the dome and

waste surface. The degree of potential evaporation depends on the distribution and transfer of heat within a particular tank. The STOMP code must be used to examine the complicated coupling of all mass and heat transfer mechanisms acting within a tank that influence internal evaporation.

If a waste surface contains an unsafe concentration of organic chemicals along with nitrate/nitrate salts, and it becomes too dry to naturally suppress any possible accidental ignition event, then it might be necessary to apply water to the waste surface. Because the drained saltcake waste is porous and dry, infiltrated water would seep down from the surface and begin refilling the tank with liquid that could potentially leak. Therefore, it is important to design an effective method of adding moisture that keeps the moisture near the surface long enough before redistribution occurs. Moreover, infiltration of water might accomplish leaching of unwanted soluble organic species on the surface. Leached organics could be transported deeper into the waste this way. When transported by leaching down to the ILL, soluble organics could be removed from the vulnerable surface region. The STOMP code can be applied to examine this subject of transport.

1.2.3 Boundary Conditions

To simulate heat transfer and moisture movement in a domain such as a cylindrical tank, various boundary conditions must be applied to specify a problem uniquely. The STOMP code incorporates many special boundary conditions to solve the governing conservation equations for a specific domain. The values of moisture flux and heat transfer rate or temperature can be set on the tank boundaries, which are the sides, bottom, and waste surface facing into the head space. The head space itself, however, is not simulated by STOMP (see Section 3).

The test cases discussed in Sections 4 and 5 presume that no liquid flows out the sides or bottom of a tank; that is, a leaking tank is not considered here. The loss of heat through the sides and bottom is specified because the appropriate temperature is unknown there. Liquid flux leaving as water vapor will be specified at the waste surface, while the evaporated water is returned as condensation along the tank side where the waste surface contacts it. Other boundary information, however, can be applied if specific measurements for those boundary values become available.

2.0 Processes of Moisture Transport

The physical processes discussed in this section act on the pore scale to determine the distribution of moisture in a porous medium like saltcake. Mathematical descriptions of these processes are included in the STOMP code's formulation (White and Oostrum 1996). The STOMP code calculates the distribution of moisture at the tank's spatial scale based on these pore-scale processes. Figure 2.1 depicts the processes involved with liquid and vapor movement at the pore scale.

In Figure 2.1, the volumetric liquid content of the saltcake matrix depends on the local capillary pressure, as described by the Brooks-Corey retention relationship (Simmons 1995). The directions of flow (indicated in parentheses) of moisture and heat may be different than indicated, depending on detailed conditions. The pressure gradients acting in the gas (air including water vapor) and liquid phases determine the flow directions, while permeability of the matrix determines the rate of fluid flow under these pressure gradients. Gauges indicate the sign of the pressure in the liquid and gas phases. Heat is transferred by conduction through both solid and the liquid phases and as latent heat of water vaporization by evaporation and condensation. Salts dissolved in the liquid phase lower the water vapor partial pressure relative to the saturated vapor condition for the prevailing temperature.

2.1 Capillary Retention of Interstitial Liquid

The interstitial liquid distribution in a drained saltcake is set primarily by the capillary retention relationship as expressed in terms of the Brooks-Corey model, which depends on the holdup height and pore-size index. The absolute porosity of the saltcake matrix also determines on a volumetric basis how much liquid can be held in the interstices. When drained, the liquid distribution with depth takes the shape of the liquid retention relationship. Capillary pressure of liquid (in units of equivalent liquid column height) in the interstices at a location is essentially the height of the location above the ILL plus the holdup height. In equilibrium under isothermal conditions, the capillary rise in the interstices and the downward gravitational force are in balance. Condensation and evaporation of water vapor under nonisothermal conditions tend to perturb the moisture distribution from its static equilibrium distribution for isothermal conditions. The moisture distribution is perturbed in a way that produces a liquid flux that balances the flow of water in the vapor phase.

The Brooks-Corey retention equation gives the volumetric liquid content divided by the porosity (actually the saturation) as an exponential function of capillary pressure (Simmons 1995). As capillary pressure becomes greater relative to a reference location the volumetric liquid content decreases, as liquid is held by smaller interstices. Liquid is held in the interstices by capillarity with a greater strength when its surface tension is greater than, say, that for pure water as the standard reference. The influence of surface tension is presumed already accounted for in the Brooks-Corey model, as found from the response to drainage during stabilization. However, by using fluid property scaling, it is possible to consider an interstitial liquid with

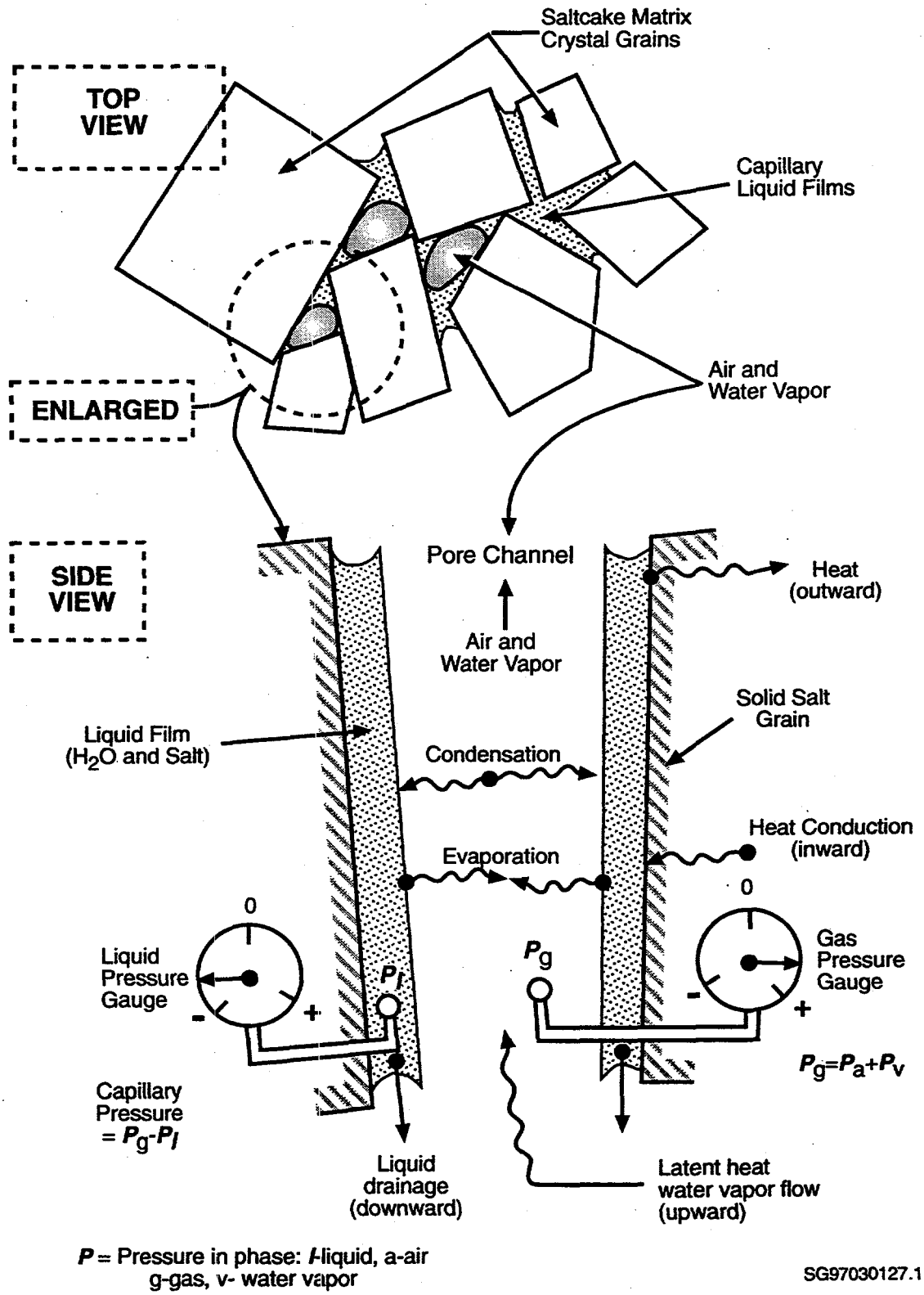

Figure 2.1. Physical Processes for Nonisothermal Moisture Transport in Saltcake

some other value of surface tension, as possibly changed by the presence of dissolved organics. Measurements of actual surface tension are needed to consider this possibility further.

2.2 Darcy Flow of Liquid

Darcy's law is assumed for the flow of liquid in interstices of saltcake. Flow is proportional to the sum of the pressure gradient in the liquid and the gravitational force. The proportionality coefficient is called the liquid conductivity, which equals the relative permeability times the intrinsic permeability of the matrix multiplied by liquid density and divided by kinetic viscosity (the common viscosity divided by g) for the liquid. Relative permeability, with its greatest value equal to one when the matrix is saturated with liquid, decreases to zero very steeply when the liquid content drops below its maximum value equal to the porosity. Thus, the Darcy flow velocity in a drained situation will be many orders of magnitude smaller than that exhibited during pumping in the saturated zone.

The relative permeability function is obtained as part of the Brooks-Corey model, as described in the first version of the moisture model (Simmons 1995). As liquid occupies smaller pores, for higher capillary pressures given by the Brooks-Corey retention curve, the relative permeability decreases exponentially for a small percentage decrease of volumetric liquid content. Thus, the relative permeability and liquid conductivity will be very small near the surface, where drainage and evaporation diminish the liquid content, compared with the saturated value below the ILL. At the surface of drained saltcake, because the conductivity becomes small there, the upward flow of liquid might not be able to replenish a substantial evaporation rate, and the surface material would then dry out. However, the condensation rate of water vapor near the surface must also be accounted for to determine if drying would actually occur. The advanced model includes vapor condensation.

2.3 Temperature Distribution

The transfer of thermal energy as a result of the radioactive decay generated heat load controls the potential surface evaporation rate. Heat that is not conducted through the solid matrix and liquid phase is transferred through the porous matrix as latent heat of evaporation and condensation. The amount of heat transferred as latent heat is key to estimating the evaporation rate, which in turn controls the dryness of the waste surface.

The STOMP code uses Fourier's law of heat conduction along with thermal conductivity for the solid and liquid fractions to determine the temperature distribution in the waste. It also calculates the flow of heat carried by water vapor transfer. Vapor pressure gradient and the resulting flow of water vapor through the drained waste is determined by the temperature distribution associated with the loss of heat from the tank into the bottom, sides, and dome top. The STOMP code takes into account the reduction of thermal conductivity as the liquid phase is reduced in any way by drainage or evaporation. However, in the current simulation tests, the precipitation of dissolved salts to become part of the solid matrix and the resulting changes of the hydraulic properties were not accounted for. At this stage, this effect is not believed to substantially alter the temperature distribution for a stabilized profile. Test cases discussed in

Section 4 indicate that the liquid distribution and its associated thermal conductivity field are not altered greatly from the pattern imposed by capillary forces acting in the matrix.

2.4 Water Vapor Flow

The STOMP code calculates the flow of the gas phase (air including water vapor), as well as the liquid phase, within the interstitial space of the porous material. Air (with vapor) fills and moves in the interstitial space that is not occupied by the liquid, which is held by capillarity in the smaller pores. Air, containing water vapor or any other gases, flows in proportion to the pressure gradient in that gas phase. The proportionality factor is the relative permeability of the pore space not occupied by the liquid. This gas-phase relative permeability and resulting conductivity for air are obtained as part of the Brooks-Corey model for multiphase flow. References for this complex theory are given in White and Oostrum (1996). This flow of air caused by the pressure differences is called advection.

Water vapor is also moved by diffusion in the air as well as by advection of the gas phase. Advection is determined by the pressure gradient in the gas phase and by the relative permeability for air flow in the drained pores. Note that the gas phase pressure is the sum of the air pressure and the partial pressure of water vapor for the particular local temperature. Differences in water vapor concentration within the gas phase determine the diffusive flux that contributes to the overall flow of gas through the drained interstices. Vapor concentration is calculated directly from the prevailing water vapor pressure by assuming the ideal gas law applies locally for the particular local temperature.

The diffusive flux conforms to Fick's law and is determined by the vapor concentration gradient multiplied by a diffusion coefficient, which is a function of the local temperature. Under certain situations, usually near the surface, the advection of water vapor and diffusive flux could be in opposite directions. (Actually, in the STOMP code's formulation, the diffusive flux of a component species in a particular phase is determined by the gradient of the mole fraction of the component, then multiplied by the phase density. Also, the effective diffusion coefficient for each component is modified by the porosity, tortuosity, phase saturation, and ratio of molecular weights, all multiplied times the binary diffusion coefficient for the species in the particular phase. This effective diffusion coefficient multiplied by phase density and the mole fraction gradient gives the diffusive flux.)

Water vapor movement transfers latent heat of vaporization as part of the heat transfer process. The temperature distribution is a consequence of both heat conduction and latent heat transfer by water vapor. (Transfer of heat by water vapor is actually thermodynamically more complicated by the transfer of enthalpy, which is the sum of internal energy and the work performed by pressure changes. The detailed equations are discussed in the STOMP code documentation.)

Local equilibrium thermodynamic conditions determine the water vapor partial pressure as a function of temperature. The water vapor partial pressure is lowered exponentially in association with the capillary pressure. An increased capillary pressure produces a decreased

water vapor pressure, but such lowering does not become an influence until the medium is very dry with capillary pressures greater than 10 million Pa (100 kPa is an atmosphere of pressure). Plots of the saturated water vapor pressure as a function of temperature and the lowering of water vapor pressure by capillarity are provided by White and Oostrom (1996) in the STOMP theory documentation. Note, however, that lowering water vapor pressure by capillarity is nearly negligible compared with the dominating influence of the dissolved salts in the interstitial liquid.

2.5 Reduction of Water Vapor Partial Pressure by Salts

The presence of ionic salts in the aqueous phase lowers the water vapor partial pressure in equilibrium with the liquid phase. Sodium chloride is treated as the model salt in the STOMP code formulation. (Specific physical and chemical properties of sodium nitrate/nitrite have not yet been included in the code. A more complex solubility model is needed in the code to accurately describe the wide range of solutes present in tank liquids, especially the influence of sodium hydroxide.) A high concentration of dissolved salts will affect the density and viscosity and hence also affect the hydraulic conductivity for the Darcy liquid flow. Moreover, the salt concentration would move in the liquid phase by advection and diffusion. Also, the thermal conductivity of salt brine depends on concentration. These effects are all accounted for by the STOMP code. For application to waste tanks, it is presumed that the behavior of sodium nitrate/ nitrite salt is similar to that of sodium chloride. However, the presence of strong concentrations of sodium hydroxide would have substantially different influence on water vapor pressures. It can lower the vapor pressure considerably more than sodium chloride or sodium nitrate salts. This solute is not yet accounted for in the STOMP code but can easily be incorporated.

Modifications were made to the STOMP code to include the capability of treating systems with high salt concentration in the aqueous phase. Prior to this moisture model, STOMP did not include the appropriate mathematical theory. Appendix A details the equations included in the code that deal with problems of liquid flow involving high salt concentration. Mainly, an equation for the lowering of water vapor partial pressure by the osmotic coefficient for sodium chloride was included, as well as an expression for the osmotic pressure in the liquid phase. The osmotic pressure represents the tendency of liquid with less salt concentration to be drawn to a region with liquid of greater concentration. This osmotic pressure results from water moving to dilute the region of greater salt concentration while salt diffused out from that region into lower concentration regions.

The code modifications are necessary to describe the phenomenon of counter liquid and water vapor flow in a unsaturated porous system, which is subjected to a thermal gradient. In an unsaturated column of porous material, which is heated at one end and cooled at the other, the vapor evaporates from the hotter end to condense on the cooler end. At the same time, liquid flows back, drawn by capillarity to the hotter end that has a reduced volumetric liquid content. Salt in solution will increase in concentration at the hotter end and decrease at the cooler end. This same process would operate in a drained saltcake, as water vapor moves toward the cooler surface and returns downward as condensed liquid. In a tank's vertical waste profile, the excess liquid produced by condensation of vapor near the cooler surface is drawn downward again by gravity.

Appendix A also describes a well-documented test case for the counter flow of moisture phenomenon: a closed horizontal column, maintained at a constant hotter and cooler temperature at opposite ends; initially, partially saturated with salty liquid. In the test case, the influence of osmotic pressure was still dominated by the capillary pressure for the particular salt concentration. In contrast, for a vertical tank profile, the gravitational force enhances the liquid's downward return flow. In a tank profile, the liquid content would still remain greater in the deeper, hotter depth, while water vapor would condense toward the drier surface. The process is the same, but the liquid content distribution would be reversed as a result of drainage by gravity in a vertical waste profile.

In a drained saltcake profile, the dissolved salt would be advected downward with a net downward transport of salt. However, in the test case described in Appendix A, the salt advection from the cooler to the hotter end is counterbalanced by an equal magnitude but opposite diffusive flux of salt from the greater salt concentration at the hotter end. Regardless of conceptual distinction with a tank waste profile, the test case represents the simultaneous flow of water vapor, liquid, and dissolved salt in a nonisothermal system under steady-state conditions of heat transfer. The case, nevertheless, demonstrates the code's intended mathematical capabilities.

3.0 Waste Surface Boundary Condition

This section discusses modeling the evaporation of moisture at the waste surface. The estimated evaporation rate is then used to define the surface boundary condition that determines the subsurface moisture distribution in the waste.

Modeling the moisture distribution below a drained waste surface requires accurately estimating the flow of liquid either upward toward or downward from the surface. This liquid flow is determined either by evaporation or condensation of water vapor at the surface, and measurements of liquid content alone cannot indicate which way the liquid is moving at the surface. Only modeling using prevailing temperature gradients and water vapor pressure gradients can predict what the magnitude and direction of the liquid flux is at the surface. Because the STOMP code simulates only the subsurface conditions within a porous saltcake, another model must be used to determine the possible liquid flux for the surface boundary condition.

Conceivably, water can either evaporate from the waste surface as part of the heat transferred out as latent heat of vaporization or condense from the vapor diffusing toward the surface through the drained zone. The earlier model (Simmons 1995) examined only the steady loss or gain of liquid at the surface and the resulting influence on the moisture profile. An additional model for the surface boundary was needed to explain what might occur over time in a nearly closed head space, which perhaps still breathes passively. (Although a tank head space is nearly a closed container, there is a relatively small vent that balances atmospheric pressure inside and outside. This causes breathing and a small volume of air carrying moisture flows in and out over time.) The objective of this boundary condition model, therefore, was to establish if there could be a substantial moisture flux out of the surface that would influence the liquid distribution held by capillarity in the waste.

As an extreme bounding situation for the maximum possible evaporation, it is instructive to determine how rapidly a waste profile could dry out if subject to continual loss of moisture, as if, hypothetically, a tank were entirely open to the atmosphere. This situation was tested by applying an unsaturated flow code, UNSAT-H (Fayer and Jones 1990). This code represents an intermediate design between the earlier model based on presumed steady-state conditions and STOMP's generality. The UNSAT-H code is nearly as mechanistically complete as the STOMP code and able to model unsteady conditions occurring in conjunction with heat transfer; but it describes only one-dimensional, vertical moisture flow. The UNSAT-H code was applied to help understand the results that would be produced by using the more complicated STOMP code.

Evaporation from an open tank is discussed in Section 3.1. Section 3.2 describes a more general model for evaporation within a nearly closed tank allowed to breathe passively.

3.1 Surface Dryout in an Open Tank

An open tank exposed to continual evaporation should exhibit a profile that dries out; that is, the moisture content in the entire profile decreases over time. This behavior is confirmed by applying the UNSAT-H code. However, the contribution of water vapor movement below the waste surface was not certain, when compared with the direct loss of moisture from only the surface, as liquid is draw up by evaporation. Previous modeling did not consider the subsurface movement of water vapor. The UNSAT-H code predicts how transient variations in surface conditions would influence the moisture profile in an unsaturated subsurface. In the code, liquid flow is described by Richard's equation for unsaturated flow; diffusive water vapor flow is described by Fick's law; and heat conduction is described by Fourier's law.

The code was also applied with a different equation for the hydraulic properties to evaluate the sensitivity of results to the particular mathematical description. The results, when applied to a tank profile similar to BY-104, are discussed in Appendix B. Since such an open-surface condition was not the main concern of this study; the details are discussed only in Appendix B. However, the main conclusion related to potential dryout of the waste surface in a closed tank is that the radiant emissivity of the surface relative to that of air is crucial. Radiant emissivity is the fraction of radiant heat energy given off by a black body at a particular temperature, as given by the Stefan-Boltzman law.

The modeling using UNSAT-H showed that the relative value of emissivity for the head space air and the waste surface is critical for determining whether substantial evaporation occurs. A key technical issue is whether heat is transferred mainly by convection or radiation or by latent heat of evaporation. It is thought that heat transfer for a drained waste occurs mainly via convection and radiation in a tank's head space (Crowe et al. 1993). But the simulations (Appendix B) showed that substantial evaporation does occur if the emissivity of head space air is greater than that for the waste surface. If the emissivity of head space air is less, most of the heat transfer at a waste surface would occur via convection and radiation. If these emissivities are nearly the same, the speed of air flowing across the waste surface determines how great moisture evaporation will be. Thus it is essential to know the emissivity of the waste relative to that of air and the speed of air circulation across the surface to determine the dominant mode of thermal energy transfer.

This finding showed that any model for heat transfer at the waste surface inside a closed tank must properly account for the radiant heat in the head space air. Based on this recognition, a model for steady heat and moisture transfer for a closed head space was formulated as a boundary condition model for the STOMP code.

3.2 Head Space Evaporation Model

A model was devised to estimate the possible water evaporation rate at the waste surface of a nearly closed tank, which may be vented either passively or actively. The model is a modification of one developed by Fauske & Associates, Inc. (1994) that was intended to estimate

evaporative losses from single-shell tanks. Recently, the FAI model was used in the preliminary safety analysis for the organic watch list tanks at Hanford (Webb et al. 1995). The original model was intended for use with waste profiles for which the liquid reaches the surface or is saturated up to the surface. The present, revised formulation, however, addresses a drained waste profile for which diffusion of water vapor through the dry surface region limits how rapidly moisture is evolved. Also, the original model was mainly intended to estimate the relative humidity or moisture density within the head space, whereas this new version also provides the rate of evaporation that cycles in the closed head space.

In this model, conceptualized in Figure 3.1, evaporation as a result of the heat load transfer through the waste surface is returning to the tank sides via condensation on the dome. However, evaporated moisture could be returning directly to the cooler waste region just adjacent to the tank side walls.

The head space evaporation model is designed to describe only the steady-state transfer of heat and the connected evaporation in only the vertical direction. This new version is implemented in a Mathcad program called EVAPLOSS and is provided in Appendix C. Mathematical details can be read directly from the program. The concepts and notations used are similar to those explained in the report by Fauske & Associates (1994). This model is a precursor to a code that would eventually be built into STOMP to define the upper surface boundary condition of the waste. However, this application has not yet been implemented. Instead, a simplified model was used in STOMP for the simulation cases (Section 5).

3.2.1. Conceptual Formulation

Heat is transferred through the waste surface by radiation, convection, and latent heat of evaporation. Figure 3.1 shows the sequence of heat and water vapor transfer in a waste tank. The heat load portion expelled through the surface to the tank dome and head space sides that does not occur by combined radiation and convection must necessarily occur via evaporation. This is the conceptual basis of the model. Heat transfer by convection and associated vapor mass transfer are described by transfer coefficients, where the rate of transfer is proportional to the differences in temperature and relative vapor density in two adjacent regions. The regions are the air at the waste surface, the middle volume of head space, and the air near the dome top. Also, a region is included below the waste surface in the drained waste above the ILL. Only heat is transferred to the outside air through the ground cover region above the dome. Thus, in the new formulation, the heat load is passed to the outside through five adjacent regions: drained subsurface, waste surface, head space, dome, and ground cover. Heat and moisture may also be lost or gained by breathing through the riser vent to the outside.

In the ground cover region, heat can only be conducted out. In the head space region, heat is transferred by thermal radiation, air convection, and condensation. In the drained subsurface, heat is conducted through the solid waste and is also transferred as evaporated moisture. Fourier's law describes the rate of heat conduction, whereas Fick's law, expressed in terms of an effective diffusion coefficient, describes the rate of vapor flow in the drained subsurface.

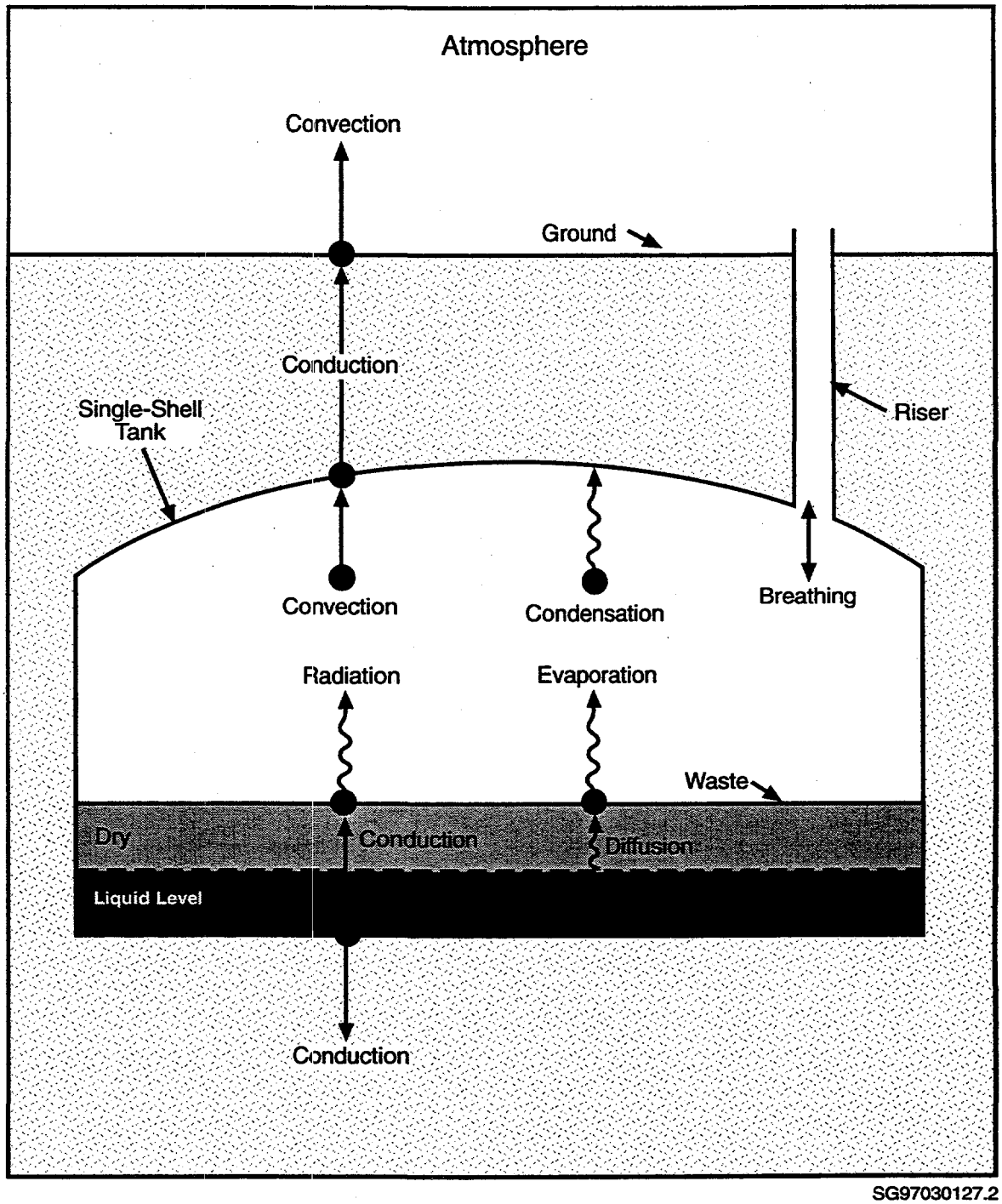

Figure 3.1. Heat and Water Vapor Transfer in the Head Space of a Single-Shell Tank

3.2.1.1 Radiant Heat Transfer

In the original formulation of the model, heat transfer by radiation was conceptualized as going from the surface to the head space gas and then onto the dome. This was a sequential transfer, which made it possible to define radiation transfer coefficients between the waste surface, head space, and dome. This radiation transfer was applied with a single emissivity coefficient, which was taken as equal for all three adjacent regions.

Subsequently, it was determined that this conceptualization of thermal radiation transfer was incorrect, because most radiant heat is believed to be transferred directly through the head space gas to the tank dome. Crowe et al. (1993) stated this viewpoint in their calculation of tank heat loads. An approach for dealing with heat transfer between surfaces with an intervening thermally absorptive gas has been known for years (e.g., Kreith 1973). A gas containing water vapor as the heat-absorbing substance is treated as a "gray" gas in an enclosure. Most radiant heat is transmitted directly between the enclosing surfaces, and a smaller fraction is absorbed by the gas and emitted back to the surfaces. The fraction of thermal energy transmitted through the gas is determined by the gas emissivity as 1 minus this emissivity. The gas emissivity determines what fraction of the black body radiation emitted from the gas is returned to the enclosure surfaces. Thus, radiant heat is transferred in parallel through and from the gas to the surfaces, and a net thermal resistance can be defined so that the difference in the Stefan-Boltzman radiation from the two surfaces is proportional to the radiant heat transmitted between them.

By the Stefan-Boltzman law, thermal radiant energy is emitted from a black body in proportion to the temperature with the fourth power exponent. The proportionality factor is the Stefan-Boltzman constant, common to all materials. The emissivity of each surface determines the fraction of black body thermal radiation that will be emitted. The theory described by Kreith (1973) in his third edition of the *Principles of Heat Transfer* is implemented in the EVAPLOSS program (Appendix C). In this heat transfer model, the shape factors or view factors, which describe the fraction of radiant energy absorbed from another radiating surface, are taken as unity to simplify the calculation of the heat transfer.

Therefore, in the model, the radiant heat transfer between the waste surface and dome depends on the temperatures and the emissivities of each surface along with the emissivity of the head space gas. Emissivity of water vapor in the head space air, given as a function of water vapor pressure, was determined in the early 1940s (Hottel and Egbert in Krieth 1973); the graphs reproduced by Kreith are found in most texts on heat transfer. These standard graphs are also found in the sixth edition of *Perry's Chemical Engineers' Handbook* (Perry et al. 1984). Specifically, the head space gas emissivity depends on the water vapor pressure multiplied by the beam length, which is the effective separation distance between the gas enclosure surfaces, the waste, and the dome. For conceptualized infinite parallel surfaces (planes), the beam length is the distance between the planes multiplied by 1.8. For separation distance of 10 to 20 ft and saturated water vapor pressures associated with typical head space temperatures (27°C for BY-104), the gas emissivity is between 0.2 and 0.3. Crowe et al. (1993) suggested a value of 0.25. Emissivities of the waste surface and dome are not known, but the values are presumed to fall between 0.7 and 0.95, typical of rusted steel and concrete.

3.2.1.2 Water Vapor Diffusion

The evaporation of water is coupled to the rate of vapor diffusion through the drained subsurface region. This rate of diffusion or vapor flux is proportional to the difference in the vapor concentrations in the interstices at some depth above the liquid level and the surface. The effective diffusion coefficient divided by that depth is the proportionality factor (a vapor mass transfer coefficient) that defines that vapor flux. This effective diffusion coefficient is the molecular diffusion coefficient for water vapor in air multiplied by an air-filled porosity and an enhancement factor. The enhancement factor accounts for the fact that apparent diffusion flux associated with a thermal gradient is augmented by a microscopic temperature gradient that is often greater than the macroscopic gradient associated with heat conduction. Apparently, in an unsaturated porous medium, the transport of moisture as vapor between microscopic droplets of liquid filling some interstitial pores is faster or enhanced (Nassar and Horton 1989). The enhancement phenomenon for vapor flow in unsaturated porous media was first explained by Philip and De Vries in 1957 (see Nassar and Horton 1989).

At the other extreme, if the waste surface has a compacted crust that impedes the escape of water vapor, the diffusion flux could be substantially reduced or limited. This concept of a diffusion-limiting crust was incorporated in the moisture loss model devised by Heard (1993) for the evaporation analysis of the actively vented Tank SX-105. In that model, it was conceptualized that a dry surface crust reduced the amount of moisture that could be lost if water evaporated directly from a liquid saturated surface. Heard suggested that the crust in SX-105 had a vapor diffusion coefficient typical of concrete and much less than the molecular diffusion coefficient for vapor in air. Heard used a value of 0.018 ft^2/hr for the diffusion coefficient in crust instead of 1.03 ft^2/hr (2.67 E^{-5} m^2/s) for water molecular diffusion in air. This corresponded to an enhancement (reduction) factor of about 0.02 by the crust. The interstitial pores in such a crust would have small air-filled porosity and would likely be plugged or not well interconnected. In this model, the enhancement factor can represent either an increase or decrease in the evaporation rate, depending on the particular physical circumstances relevant for a tank waste.

3.2.1.3 Water Vapor Concentration

The water vapor concentration in the drained region and head space is calculated from the local temperatures and is expressed by a standard formula for the saturated water vapor density for the temperature to be determined. If the activity factor for reducing vapor pressure caused by the dissolved salt concentration is known, that factor can be applied for vapor below the waste surface. Both Heard (1993) and Barney (1976) give information on how much the saturated water vapor pressure is reduced for various dissolved salt concentrations of nitrates/nitrites and sodium hydroxide. When setting the relative humidity value at a depth below the waste surface, such information should be used when the appropriate dissolved salt concentrations are known. That information, however, is not available for most tanks. Instead, the relative humidity value at depth below the surface must be chosen so that the estimated heat load transferred through the surface matches that estimated by another method (Crowe et al. 1993; Kummerer 1994).

3.2.1.4 Model Solution

A solution for steady-state transfer of heat and water vapor mass passing through the head space is obtained by equating the fluxes of each quantity through the five adjacent regions. However, water vapor does not flow through the ground cover region; it stops at the dome cover as condensation. Flow of heat and water vapor removed by venting is also included in the balance equations. The equations for the various fluxes are given in the EVAPLOSS program, and the Mathcad software is used to solve the system of coupled equations for the unknown quantities. (The program actually includes three cases that apply when certain information is assumed already known and the solution is constrained to comply.) However, because the equation system is very nonlinear in the variables of temperature and vapor concentration, starting values for the unknown quantities must be provided to begin the solving process. This is usually not a problem, because even approximate values of unknown quantities are adequate to find the solution.

To apply the program, the following quantities should be known:

- heat load fraction removed from the waste surface (W)
- breathing rate as air volume vented per unit of time (m^3/yr)
- thermal conductivity of soil cover and waste (W/m/K)
- vapor diffusion and thermal conductivity depth below the surface (surface level minus the ILL) (meters)
- measurements of temperature in the waste, at the surface, and in the head space, if known. Waste temperature is most essential to be consistent with heat load.
- emissivities for the waste and dome surfaces and the head space air with vapor
- volumetric liquid content of the drained subsurface and its porosity.

3.2.2 Application to Tank BY-104

The model was tested successfully for Tank BY-104, for which the heat load and temperatures are known. Relative humidity (RH) in the head space was also measured and estimated to be about 55% for a temperature of 26.8°C. The data on tank temperature and RH were compiled by J. Huckaby of PNNL. Similar temperature in the waste and head space is reported by Kummerer (1994). Table 3.1 contains the parameter value used to test the waste evaporation model on Tank BY-104.

The solution to the problem for Tank BY-104 is shown graphically in Figure 3.2. RH in the five regions is given for the indicated temperature profile. The solution for which the RH is held at 60% in the waste depth results in a value for the head space of nearly 55%. It should be noted that these RH values are in terms of the saturated vapor pressure for the given local temperatures.

Table 3.2 provides specifics for the possible solutions based on different values of RH at depth in the waste. The table also demonstrates the sensitivity to a 1% change above or below the 60% RH value.

Table 3.1. Physical Parameters for Tank BY-104

Parameter	Value	Units	Reference
Heat load	2550	W	Crowe et al. 1993; Kummerer 1994
Surface fraction of heat	0.66	none	Crowe et al. 1993
Ground temperature	13.5	°C	Crowe et al. 1993
Air temperature outside	12	°C	Heard 1993
Head space temperature	26.6	°C	Huckaby (PNNL)
Breathing rate, passive	2000	m^3/yr	Fauske & Assoc. 1994
Tank relative humidity	55	%	Huckaby (PNNL)
Waste temperature	52.5	°C	Huckaby (PNNL)
Soil cover conductivity	1.04	W/m/K	Kummerer 1994
Waste heat conductivity	0.25	W/m/K	Kummerer 1994
Ground cover depth	13	ft	Crowe et al. 1993
Waste level	13	ft	Hanlon 1995
Liquid level	7.44	ft	Whitney 1995

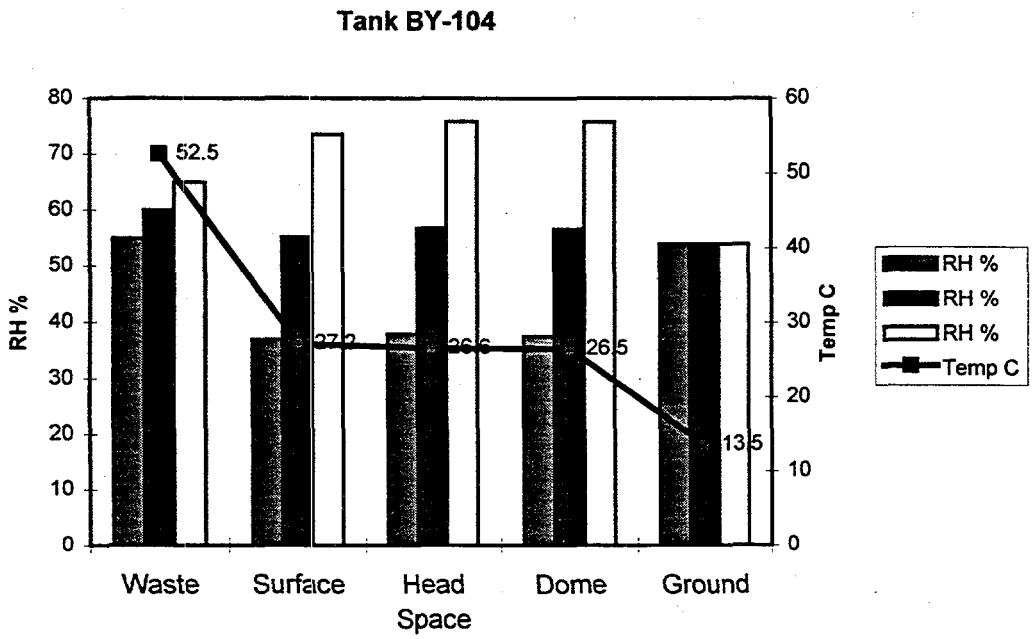

Figure 3.2. Heat Transfer Solution for Tank BY-104. Relative humidity in tank is determined by the value set at depth in the waste below the surface. Heat flux through the waste surface is 4.105 W/m^2 with 9.1% latent heat for evaporation. Radiant heat is 67.6% of the surface heat flux.

Table 3.2. Solution of Heat Transfer from Waste Surface of Tank BY-104

Surface heat flux (W/m^2)	4.105	4.105	4.105	4.105	4.105
Radiant heat %	67.6	67.6	67.6	67.6	67.6
Latent heat %	9.17	9.15	9.14	9.14	9.12
RH% at depth	55	59	60	61	65
RH% waste surface	37.02	51.62	55.27	58.92	73.53
RH% head space gas	37.96	53.08	56.86	60.64	75.78
RH% dome cover	37.63	---	56.69	60.50	75.76
Temp. waste surface (°C)	27.22	27.22	27.22	27.22	27.21
Temp. head space (°C)	26.63	26.62	26.62	26.62	26.61
Temp. at dome (°C)	26.5	---	26.49	26.49	26.48

The surface heat flux in Table 3.2 is the heat load expelled through the waste surface divided by the surface area (410 m^2) for a 75-ft-diameter tank. The fraction of heat passing out of the waste surface is calculated from the total heat load in Table 3.1 and the fraction exiting the dome cover and sides within the head space. Remaining fractions of the heat load are passed through the waste sides and bottom. The surface fraction of heat is taken from Crowe et al. (1993, Figure 6-1), which gives the relative fractions of heat passing through various surfaces for different capacity tanks. Tank BY-104 has about 406 kgal of waste in a 750 kgal capacity.

To confirm the uniqueness of the solution indicated in Figure 3.2, a number of sensitivity calculations were performed with the model to check its response to other values for the parameters. Values not listed in the various sensitivity tables given below are the same as those given in Table 3.1.

3.2.2.1 Sensitivity to Humidity

Table 3.3 shows how the heat flux changes for various values of RH at depth. After the likely value for the vapor diffusion enhancement factor of 0.834 was determined, it appeared that 60% RH gave a heat flux approximately equal to the reference target value of 4.105 W/m^2. Table 3.3 indicates that RH at depth in the waste is very sensitive to small changes in the surface heat flux. A 2.8% change in surface heat flux is associated with a 20% increase or decrease in RH.

Table 3.3. Sensitivity to Waste Relative Humidity at Depth

Surface heat flux (W/m^2)	Percent deviation from reference value [a]	Latent heat % evaporation	Relative humidity % at depth in waste
3.99	-2.8	5.35	40
4.05	-1.34	7.32	50
4.108	0.07	9.23	60
4.165	1.46	11.1	70
4.22	2.8	12.9	80
(a) Reference surface heat flux is 4.105 W/m^2, for an enhancement factor of 0.834.			

3.2.2.2 Sensitivity to Enhancement Factor

Table 3.4 shows how the heat flux and latent heat percent change with different values of enhancement factor. The enhancement factor has the strongest influence on evaporation. A crust with a factor of less than 0.05 would reduce evaporation to less than 1% of the surface heat flux, while a large enhancement factor of 3, typical of fairly moist unsaturated porous material, would increase evaporation to nearly 28%. Such a large enhancement factor is common for subsurface media (Nassar and Horton 1989) that are not air dry. Table 3.4 indicates that the enhancement factor of 0.83 is most consistent with the expected surface heat flux.

Table 3.4. Sensitivity to Water Vapor Diffusion Enhancement Factor for 60% RH at Depth

Surface heat flux (W/m^2)	Percent deviation from reference value[a]	Latent heat % evaporation	Enhancement factor
3.86	-6.0	0.6	0.05
3.88	-5.5	1.19	0.1
4.00	-2.6	5.72	0.5
4.108	0.07	9.23	0.83
4.16	1.34	10.9	1.0
4.46	8.6	19.93	2.0
4.75	15.7	27.51	3.0
(a) Reference surface heat flux is 4.105 W/m^2, for an enhancement factor of 0.834.			

3.2.2.3 Sensitivity to Temperature

Table 3.5 shows the response of the surface heat flux estimate to different values of waste and ground cover temperature. These temperatures determine the boundary conditions for the heat transfer problem in a tank when viewed as a vertical, one-dimensional system. Surface heat flux increases if the waste temperature is greater than 52.5°C and also if the ground temperature is less than 13.5°C.

Table 3.5. Sensitivity to Waste and Ground Cover Temperatures for 60% RH in Waste

Surface heat flux (W/m^2)	Percent deviation from reference value[a]	Latent heat % evaporation	Temperature °C	
			Waste	Ground top
4.27	4.0	9.62	54	13.5
4.108	0.07	9.23	52.5	13.5
3.83	-6.7	8.64	50	13.5
4.26	3.8	9.07	52.5	12
4.36	6.2	8.96	52.5	11
(a) Reference surface heat flux is 4.105 W/m^2, for an enhancement factor of 0.834.				

3.2.2.4 Sensitivity to Waste Conductivity

Table 3.6 shows that a greater thermal conductivity than 0.25 W/m/K would be associated with a greater surface heat flux. The surface heat flux increases directly with an increase in this waste conductivity, which determines how much heat would flow out for the given temperature gradient in the waste. Note that the evaporation percent would actually decrease if the thermal conductivity were greater. Also, different temperatures would prevail if the conductivity value were different from the value suggested in Table 3.1. Notice that the surface heat flux is most sensitive to deviations in the waste thermal conductivity.

Table 3.6. Sensitivity to Waste Thermal Conductivity

Surface heat flux (W/m^2)	Percent deviation from reference value[a]	Latent heat % evaporation	Waste thermal conductivity (W/m/K)	Waste surface temperature	Head space gas temperature
3.23	-21.3	12.32	0.17	24.28	23.8
3.58	-12.8	10.91	0.20	25.47	24.94
4.108	0.07	9.23	0.25	27.23	26.63
4.57	11.3	8.07	0.30	28.77	28.11
5.34	30.1	6.54	0.40	31.34	30.59
(a) Reference surface heat flux is 4.105 W/m^2 for an enhancement factor of 0.834.					

3.2.2.5 Sensitivity to Emissivity

Table 3.7 indicates how the latent heat and RH respond to the emissivity values for the internal radiating surfaces and head space vapor. The solution for the heat transfer is constrained to have the reference value of surface heat flux, 4.105 W/m^2. A change in the emissivity of the internal surfaces has greater impact on the RH than that for the head space gas. Apparently, the head space RH would be greater for a smaller vapor emissivity.

Table 3.7. Sensitivity to Radiant Emissivity for 60% RH at Waste Depth

Latent heat %	RH% waste surface	RH% head space	Emissivity of surfaces	Emissivity of head space gas
9.06	56.7	58.32	0.8	0.1
9.14	55.27	56.86	0.8	0.2
9.23	53.7	55.27	0.8	0.3
9.59	47.14	48.57	0.7	0.2
9.36	51.35	52.87	0.75	0.2
8.76	62.34	64.05	0.9	0.2
8.58	65.54	67.31	0.95	0.2

3.2.2.6 Sensitivity to Breathing Rate

The sensitivity to breathing rate through the riser vent of Tank BY-104 is important for the implications of long-term dryout of the waste. The head space RH should decrease as more dry air flows through the head space. Moreover, the moisture loss should increase if the breathing rate is increased. However, as seen in Figure 3.3, the loss of moisture from a breathing tank is perhaps more complicated if the observed temperatures remain the same while the air flow rate is increased. In Figure 3.3, there is an optimal flow rate near 20,000 m^3/yr for which the moisture loss is maximum. If the flow rate is further increased, eventually moisture is deposited in the tank instead of being removed, as indicated by the negative loss of moisture. Nevertheless, the head space RH always decreases for an increased flow rate.

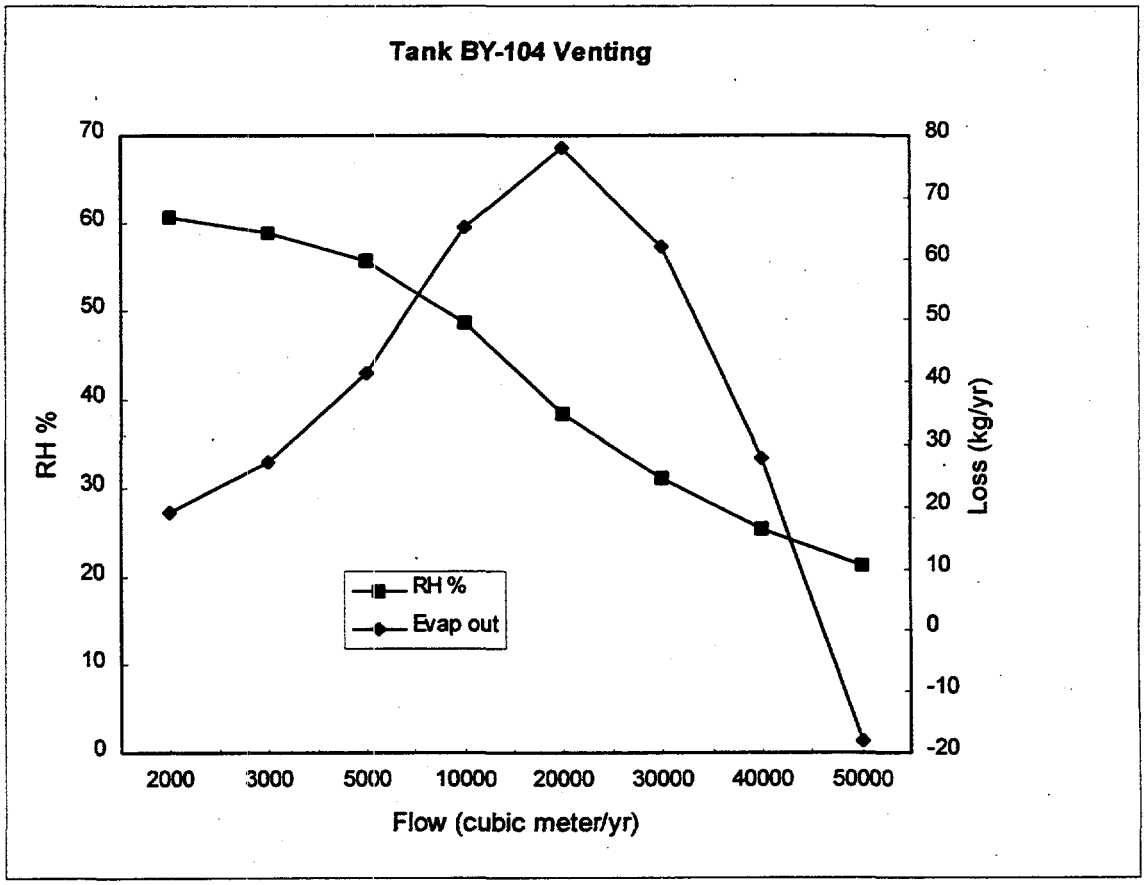

Figure 3.3. Breathing of Tank BY-104. RH in head space and evaporative loss depend on venting flow rate of the breathing. Temperature of waste and head space are fixed at 52.5 and 26.6°C, respectively, for each venting flow rate. Waste has 60% RH at depth.

In actuality, however, the boundary temperature in the waste would not remain fixed as was imposed but would decrease when the flow rate is increased in order to maintain the same given surface heat flux. Surface heat flux for the fixed temperatures of Figure 3.3 show an increase above the reference value as breathing is increased, as expected. Specifically, the surface heat flux increases by only 2.1% from 4.1 W/m^2 at 2000 m^3/yr of breathing when raised to 50,000 m^3/yr. To maintain the same surface heat flux, the waste temperature would need to be reduced in conjunction with any increased breathing. In other words, the waste surface would actually exhibit cooling if the breathing rate were increased. Simulations were not performed to demonstrate that cooling but could be done if such an analysis were required for BY-104.

Note that for an enhancement factor with values of 0.7, 0.8, 1, and 1.2, the corresponding moisture loss is 4.5, 15.8, 31.9, and 42.8 kg/yr, respectively, for the same breathing rate of 2000 m^3/yr. At the same time, there would be an internal moisture evaporation of about 2000 kg/yr cycled in the head space. So the condition of the waste surface as reflected by the enhancement factor would have a strong effect on the actual moisture loss due to breathing.

3.2.2.7 Water Vapor Pressure

To calculate the flow of water vapor, the model uses the concentration of water vapor in the air present in each tank region: waste depth, surface, head space, and dome. This vapor concentration is the saturated water vapor density multiplied by the prevailing relative humidity for the particular temperature. This required relative humidity was found for each region by solving the heat and water vapor transfer equations. By using the ideal gas law, the water vapor pressure at each location can be estimated as well. In particular, for the heat transfer solution having 60% RH in the waste depth, the vapor pressures are about 63, 15, and 14.9 torr (mm Hg) for the waste, surface, and head space air, respectively. The waste surface has only slightly higher vapor pressure than the head space, but the vapor pressure is substantially greater at depth as a consequence of greater temperature there and, possibly, because of higher moisture content.

The measurements obtained by Scheele et al. (1996) that relate moisture content as a weight fraction or percent to the equilibrium water vapor pressure (called water partial pressure) could be used to assess the dryness of waste at depth below the surface. For example, in their report, a graph is provided of the weight fraction of water depending on the water partial pressure for 65°C. By adjusting the equilibrium partial pressure to correspond to the actual tank waste temperature of 52.5°C, it could be possible to estimate the moisture content of the surrogate wastes that were studied by Scheele et al. (1996) as if within Tank BY-104. Thus this evaporation model provides a means to connect the vapor pressure observed originally in the head space—55% RH for BY-104—with the moisture content at depth in drained saltcake waste. The waste must be drained or unsaturated, because the vapor pressure gradient is being determined by the diffusion of water vapor through it under steady-state thermodynamic conditions. Furthermore, the effective diffusion coefficient that determines the water vapor flux is dependent on the volumetric liquid content by being proportional to the air-filled porosity, which equals the total porosity less the volumetric liquid content. However, in this test example, the appropriate volumetric liquid content is actually unknown; and instead, the influence of the air-filled porosity

on diffusion was accounted for by the enhancement factor. Regardless, the model could be modified to make the volumetric liquid content and the associated weight percent water consistent with the heat and moisture transfer balance equations. This modification would actually be accomplished by using the more detailed solution provided by the STOMP code, which describes the detailed moisture conditions below the waste surface.

For this example calculation, it was assumed that the waste was totally drained by having a volumetric liquid content of 0.05 for a total porosity of 0.5. Such an assumption was not necessary. If the volumetric liquid content were taken as 0.2, instead, then an enhancement factor of 1.25, rather than 0.834, would produce the same heat transfer solution. Such an enhancement factor value would still be consistent with a typical observation of vapor flux in moist soils. This theoretical role of the vapor diffusion enhancement factor has been discussed in detail for soil materials (Cass et al. 1984; Campbell 1985). But the factor's relationship to salt-cake waste is not yet known, and its value must be selected to be consistent with expected results. The relationship of sensitivity and enhancement factor was calculated to achieve the needed match of the solution to this example.

Another theoretical difficulty with connecting the water partial pressure in the waste with the weight fraction of water is that the vapor pressure may only reflect equilibrium with respect to the weight fraction of water in the liquid phase instead of representing the total mass included in the waste matrix. This technical question must be resolved before making a direct association between the water vapor partial pressure and the total liquid content contained in the waste matrix.

4.0 Modeling Test Cases for Moisture in Tank Waste

This section discusses test case simulations performed to confirm the STOMP code's capabilities for describing the distribution and movement of moisture in saltcake tank waste. The test cases described here were intended to demonstrate how various unsaturated flow processes, including drainage and evaporation, would determine the moisture distribution in a tank. These test cases, however, do not describe the true moisture distribution in a specific tank because the exact physical properties of saltcake and its spatial variability, as well as the precise boundary conditions that control behavior, are not known adequately. Pumping to stabilize an initially liquid-saturated saltcake waste profile is also demonstrated using the STOMP code. In all cases, the code was used to simulate the approach of tank conditions to a steady state, which would describe the ultimate long-term moisture distribution in a stabilized tank.

The purpose of these test cases is to examine the STOMP code's simulation capability in a step-wise manner, by first disregarding nonisothermal effects on the potential for drying out a waste surface in a closed tank. It is also useful to know whether a simple one-dimensional model for the moisture distribution is adequate to explain the conditions seen in stabilized saltcake tanks. A simple model in which nonisothermal aspects could be neglected would make the evaluation of tank safety easier, requiring less information about each saltcake tank.

A hypothetical saltcake profile that represents Tank BY-104 was used based on previous one-dimensional simulations (Simmons 1995), where it was determined that four layers with slightly different capillary retention parameters composed the saltcake profile on top of a sludge layer. This four-layer system was used for all test cases. Figure 4.1 shows the assumed stratigraphy for the saltcake profile and the parameter values used in all test cases. These are the parameters defined in the Brooks-Corey model to describe capillary retention of interstitial liquid. The pore-size index, "b," capillary holdup height, Ho, and saturated and residual liquid contents were estimated by matching the modeled moisture profile to a neutron probe scan taken within Tank BY-104. But direct characterization by core samples has not confirmed whether this tank actually includes four such distinct layers.

The parameter values in Figure 4.1 were obtained by fitting the model's description to available moisture information based on neutron scans and the quantity of liquid pumped during stabilization (Simmons 1995). For instance, the drainage response to pumping was used to estimate the pore-size index. Also, the saturated permeability, which is not indicated in Figure 4.1, is generally taken as 22.2 darcy but is varied in some test cases. This permeability value was obtained from laboratory measurements on simulated saltcake and has a value near that reported by Metz (1976), based on a pumping response analysis of a tank. Presently, physical measurements (e.g., density and crystal grain size) on cores cannot be converted theoretically into estimates of the hydraulic properties or the parameter values needed for modeling saltcake. Therefore, hydraulic properties for tank simulations must be inferred from the response to pumping.

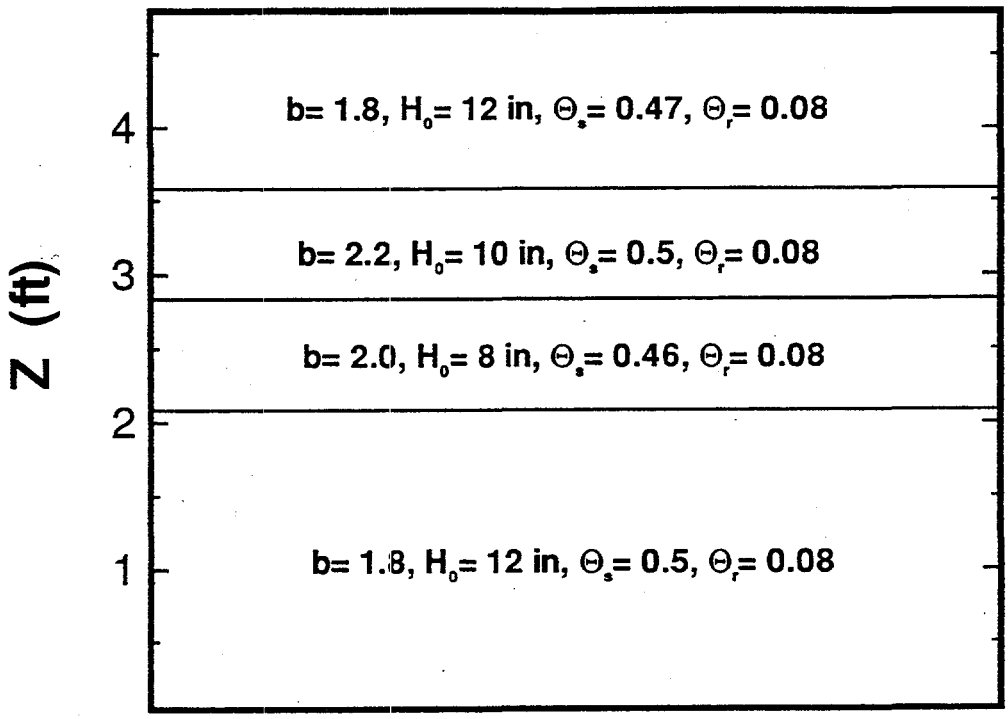

Figure 4.1. Layers and Hydraulic Parameters for a Hypothetical Saltcake Profile in Tank BY-104. B is pore-size index; Ho is capillary holdup height; theta is volumetric liquid content; subscripts "s" and "r" denote saturated and residual values, respectively; Z (ft) is height above sludge layer top.

As the tank moisture model was developed using the STOMP code, it was first tested for isothermal conditions, which disregard the influence of the heat load and the movement of water as vapor by evaporation within the drained waste. For instance, it was not expected that the conduction of heat during stabilization would have much effect on the nearly saturated flow and rapid removal of liquid from a draining profile. Moreover, during the brief pumping period, it is not likely that movement of water vapor would play a role in the overall movement of moisture. Thus pumping down a tank could be appropriately modeled as an isothermal process.

Using the two-dimensional capability of the STOMP code, it was also possible to examine whether a surface spot with an evaporation rate greater than that of the surrounding surface area could cause a localized drying out of the waste. A so-called "hot spot" associated with a higher concentration of radioactive decay might potentially cause such drying out. Section 4.2 describes a test case that examined whether the unsaturated liquid flow replenished moisture loss from the surface by evaporation so that drying would not occur. In this test case, the evaporation coupled to the heat transfer was modeled as though it took place only at the waste surface and the system treated as if still isothermal. For the test cases discussed in this

section, it is not known whether any nonisothermal flow mechanisms would override the capillary influence on the liquid distribution in saltcake. That question is addressed in Section 5.

4.1 Pumping Saltcake Waste

The STOMP code was used first to demonstrate draining a tank by pumping out interstitial liquid not held up by capillarity against gravity. The final drained conditions in the tank were used as initial conditions for all other simulations. This test case was intended to show how a pumped tank reaches its final stabilized condition, which could then be altered by other flow mechanisms such as evaporation.

Calculations on pumping liquid-saturated saltcake have been discussed previously (Metz 1976). Past analyses, however, did not account for the true tank boundary conditions or the unsaturated drainage behavior. The STOMP code made it possible to remove all such modeling limitations because the STOMP code accounts for the boundary condition of the tank sides and for the unsaturated drainage behavior above the ILL as well as the saturated flow below it.

Figure 4.2 shows the drawdown in the waste profile defined in Figure 4.1. The liquid surface is shown for 10, 90, and 200 days of pumping. The figure displays one-half of a vertical plane section with radial distance measured from the central salt well. The salt well at the left edge is the vertical axis of the cylindrical coordinate system used to perform the simulation. This perspective is repeated in all other test cases. The radial distance is compressed (37.5 ft) and the vertical axis is exaggerated (only 5 ft). Notice also that the liquid level drops to that maintained by pumping from the salt well.

Figure 4.3 shows the rate of discharge to a 10-in.-diameter salt well as the system of Figure 4.2 is pumped. The rate of pumping is constrained by how rapidly liquid flows into the well as determined by the permeability and hydraulic gradient. Rate of pumping must decrease as the liquid level declines in Figure 4.2. If the pumping rate were greater than indicated, the well would empty out, and the pump would stop operating.

The resulting saturation contours in the tank profile after 200 days are shown in Figure 4.4. Saturation, which is the ratio of the liquid content to its saturated value, is sometimes discontinuous across the layer boundary or experiences an abrupt deviation caused by the unsaturated drainage in the layers. Because the saturation is not zero above the ILL, where saturation is unity, the remaining liquid is held up by capillarity. Thus, a tank containing a porous saltcake does not empty the same way as a tank containing only a liquid phase. Moreover, the saltcake above the ILL that is detectable by neutron scanning remains partially saturated to the extent predicted by the saturation distribution.

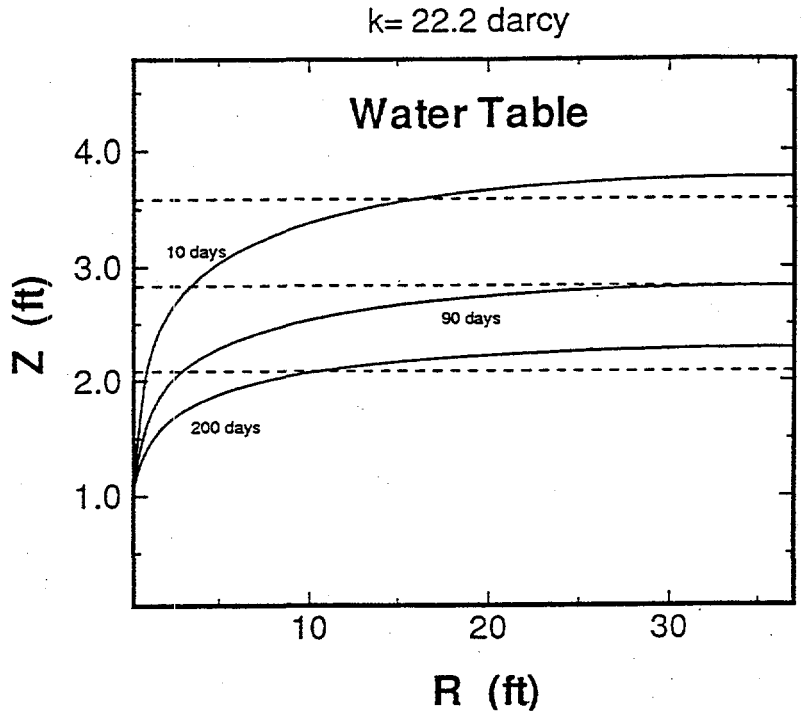

Figure 4.2. Interstitial Liquid Level (water table) in a Tank Pumped from a Central Salt Well. Four layers are separated by dashed lines with hydraulic parameters of Figure 4.1. Liquid level is 5 ft before pumping.

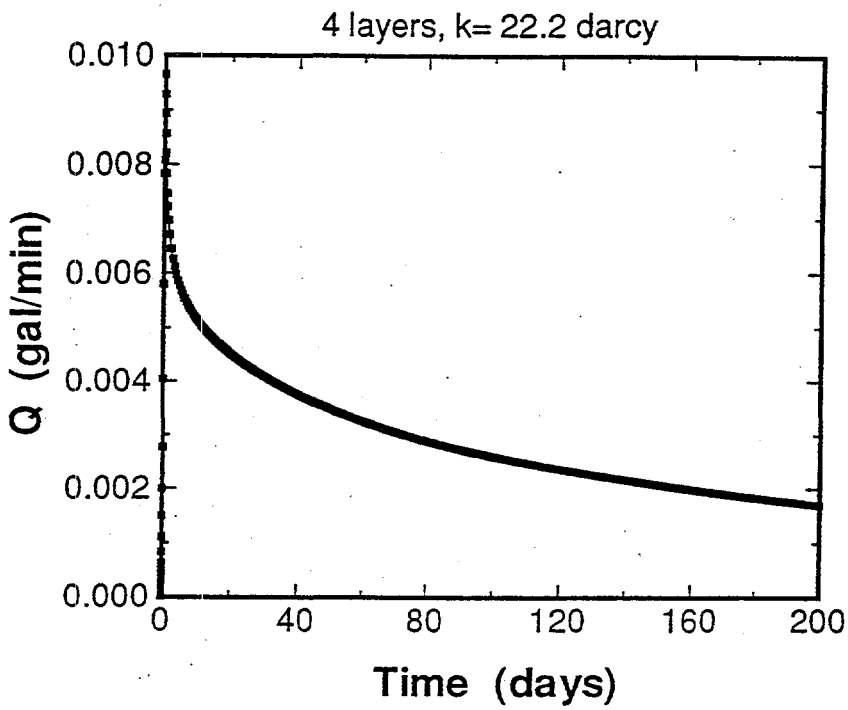

Figure 4.3. Discharge to a Salt Well with a 10-in. diameter

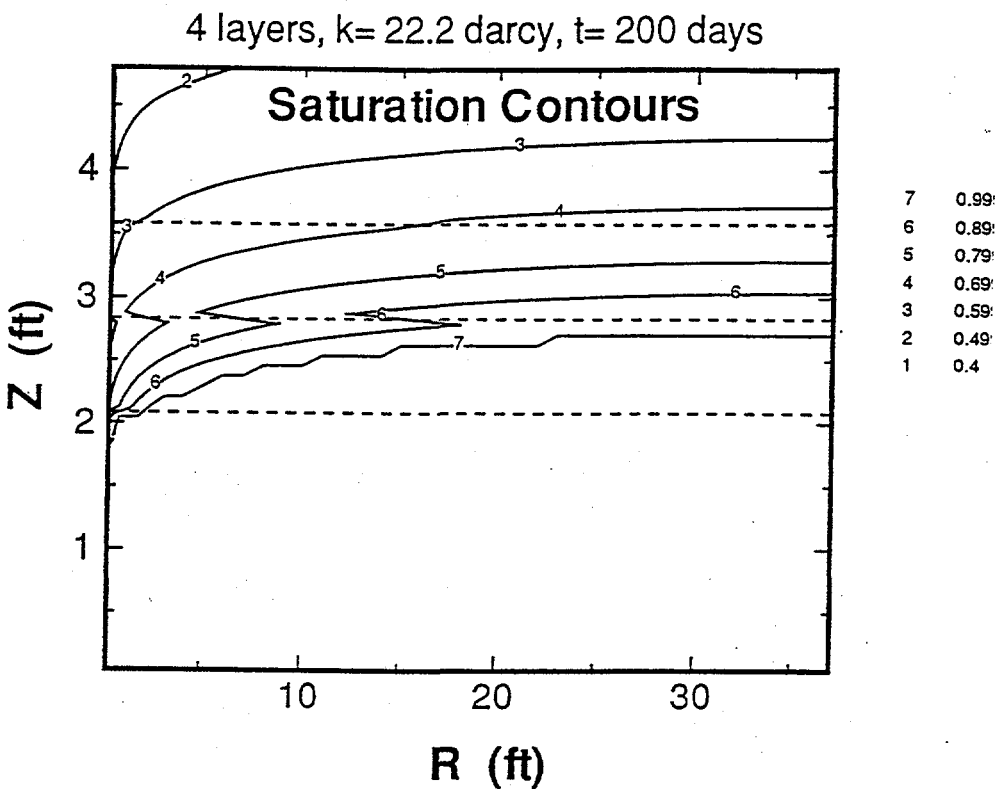

Figure 4.4. Relative Saturation after Pumping a Tank Waste Profile

After being pumped down, the liquid level in a tank would recover and become level again, not curved at the well. Figure 4.5 shows this recovery behavior. The waste profile has been made homogeneous by using the same average hydraulic parameters throughout. so the layers are removed in this simulation. The liquid level established at 200 days continues to decline away from the well but rises near the well to gradually refill the level within the well. For permeability of 22 darcy, about 100 days are needed to recover the equilibrium liquid level. For much less permeability, the recovery would take much longer. Thus, the level in a salt well does not indicate the true liquid level in the waste until a certain recovery time has passed.

4.2. Hot-Spot Dryout Case

This test case demonstrates the evaporation of liquid from a localized central spot on the waste surface after the profile has been drained and becomes unsaturated. It is supposed that the entire heat flux of 3.6 W/ m^2 associated with the transfer of the heat load at the surface is delivered entirely to evaporation over a 5.5-ft-radius disk. It is supposed also that only about 1/50th of the heat flux goes to evaporation elsewhere. The remainder of the heat transfer that is not from the disk area would occur via radiation and convection. Movement of water vapor in the porous matrix is disregarded, and no heat conduction is coupled with the liquid movement. This is intended to be a worst-possible case of isothermal evaporation at the surface.

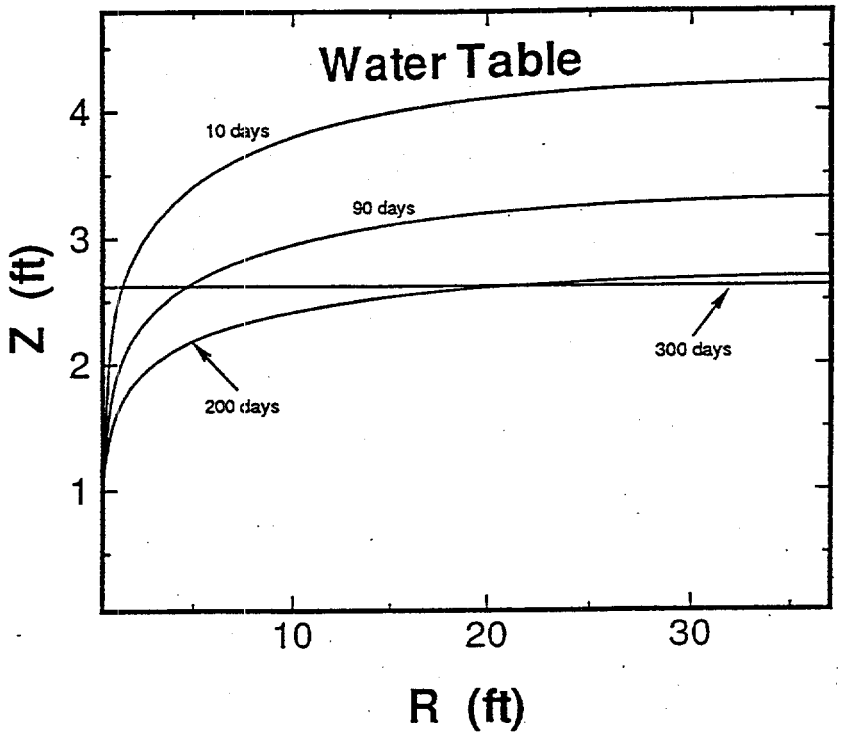

Figure 4.5. Draw-Down and Recovery of Liquid in a Homogeneous Profile (average values of hydraulic parameters define homogeneous profile without layers)

The STOMP code is used to simulate the dynamic conditions for which the evaporation begins instantly, for instance, by stopping the radiative and convective loss of heat from the spot, and then continuing until a steady state is achieved. During the evaporation inside the tank, the moisture is condensed on the tank dome and sides and returned to the profile along the side wall. The head space is closed to vapor loss.

The flow velocity field in a tank that is just beginning to evaporate from a hot spot with a radius of 5.5 ft is shown in Figure 4.6. The sizes of the vectors indicate the relative magnitude and direction of the flow velocity after being in progress for only 10 days. However, this short time is sufficient to influence the flow response at depth in the waste profile. Streamlines of liquid flow returning down the tank rim wall are also displayed. They indicate downward flow that then returns to the surface where moisture is being withdrawn by evaporation. The vertical perspective is exaggerated in the figure.

By 200 days of evaporation, the liquid flow field has attained the pattern shown in Figure 4.7. Both flow velocity vectors and streamlines are shown to display the pattern, which indicates the strong evaporation from the hot spot disk. A steady-state condition is nearly achieved by 200 days. The tendency of the flow is nearly vertical beneath the hot spot as liquid is more easily drawn up directly from the ILL than from across the waste profile.

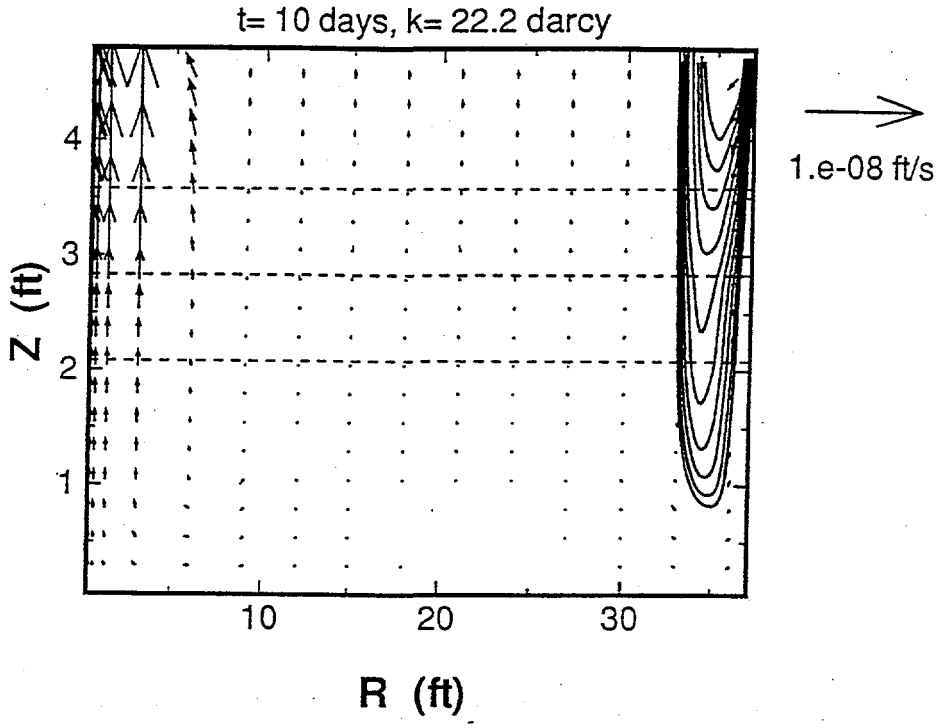

Figure 4.6. Flow Velocity in Layered Saltcake Profile Subject to Evaporation from a Hot Spot with Condensation along the Tank Rim. ILL is Z=0; evaporation is from a centered hot spot of radius 5.5 ft, shown 10 days later. Evaporation is 3.6 W/m^2 on the hot spot area and 1/50th outside.

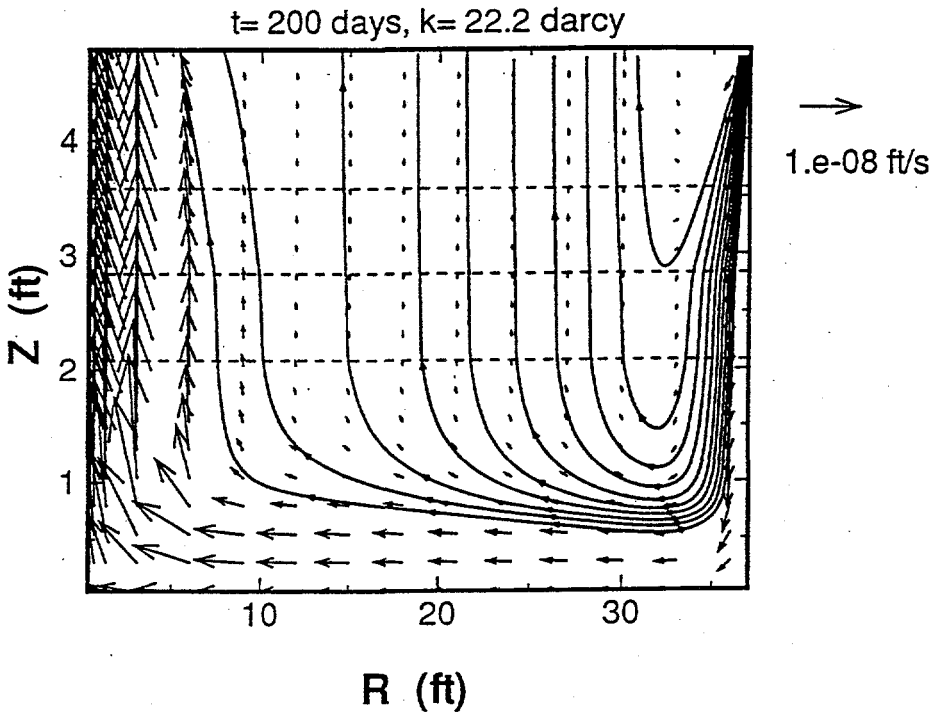

Figure 4.7. Flow Velocity in Layered Saltcake Profile after 200 Days of Evaporation from Hot Spot

Figure 4.8 demonstrates what the steady-state flow field would look like if the permeability in three layers were reduced to 10 darcy while keeping the 22.2 darcy permeability in the second layer below the surface. The reduced permeability effectively reduces the liquid flow velocity and distorts the streamline pattern. Such streamline patterns would be useful for calculating the trajectory of dissolved chemicals that would be drawn along by the flow. The magnitude of the velocity along a streamline would determine how long it would take a dissolved chemical species to traverse the profile.

Saturation contours for the layered profile subject to the hot spot of evaporation are shown in Figure 4.9. The lowest saturation contour, the 0.4 level, displays a depression below the surface area of the hot spot. This demonstrates the degree of drying out that occurs after 200 days. A slight rise in saturation is seen near the rim where condensation returns to the waste.

Figure 4.10 shows the volumetric liquid content distribution in the profile at two locations, below the hot spot and nearer to the tank rim. The liquid content distribution is only slightly changed from the initial shape. Very little decrease in the liquid content near the surface is indicated. Apparently, the surface even below the hot spot is not dried out when the permeability is 22.2 darcy.

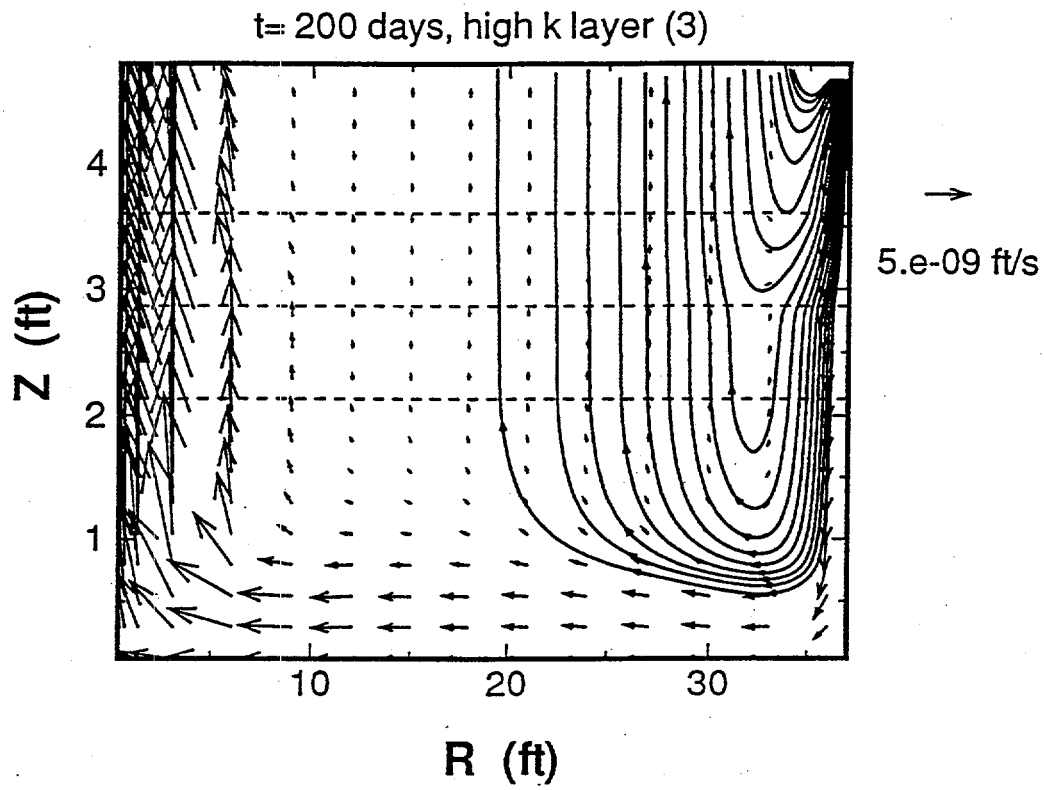

Figure 4.8. Flow Velocity in Layered Saltcake Profile after 200 Days of Evaporation from Hot Spot

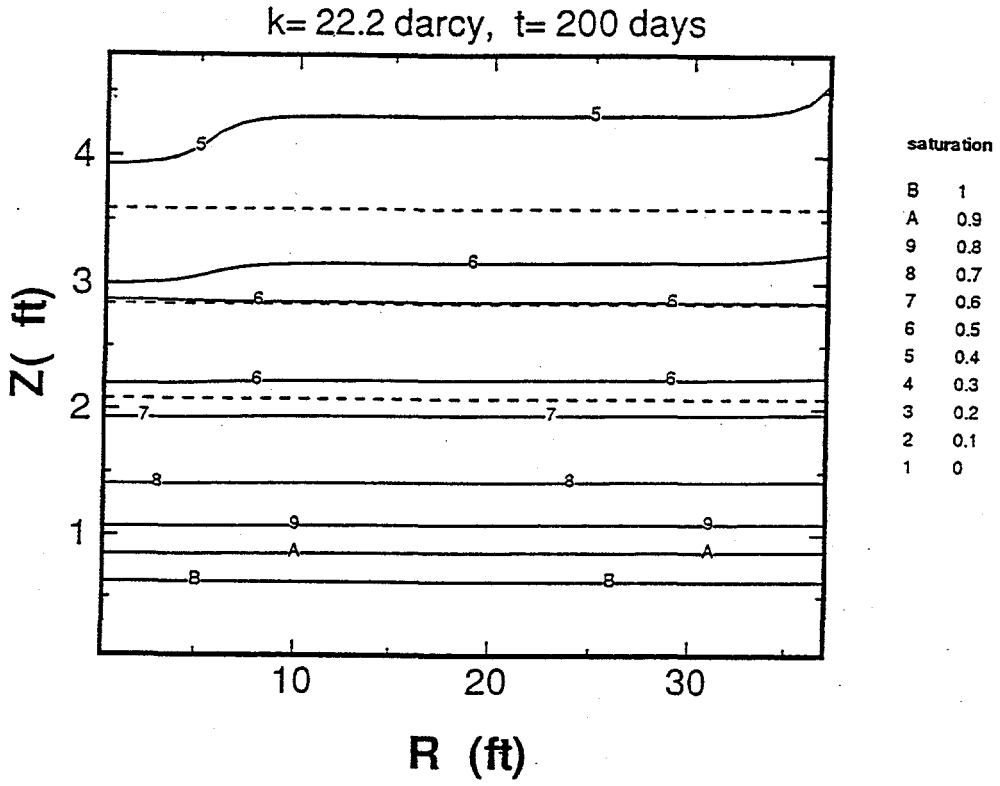

Figure 4.9. Liquid Saturation Contours in Layered Saltcake Profile after 200 Days of Evaporation from Hot Spot

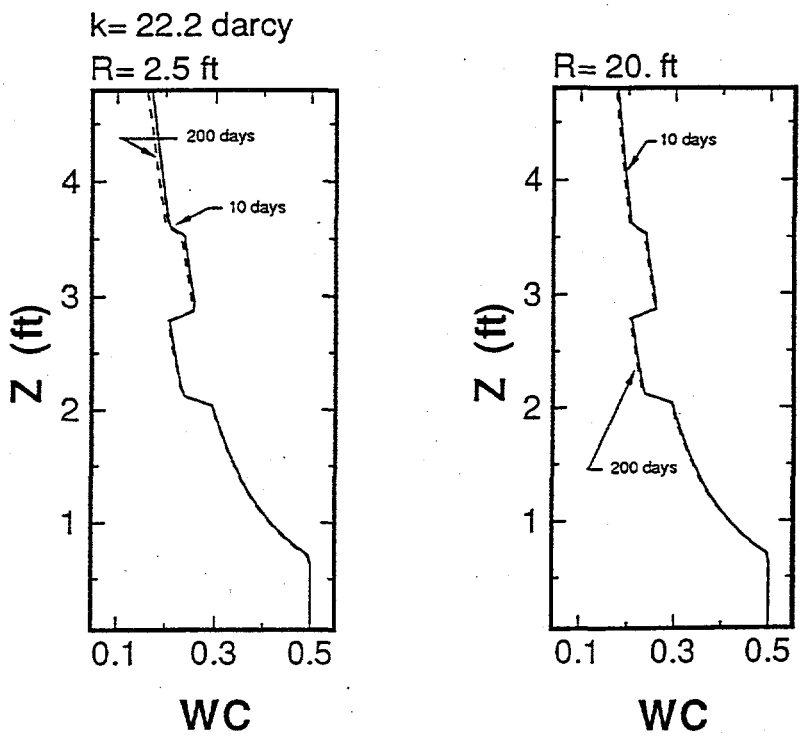

Figure 4.10. Volumetric Liquid Content (WC) in the Layered Saltcake Profile Subject to Evaporation from Hot Spot

If the permeability is reduced to 2.2 darcy in all layers, then the surface will begin to dry out beneath the hot spot as shown in Figure 4.11. Also, the drying occurs in only 90 days. However, the surface still does not dry out away from the hot spot at a radius of 20 ft, for instance. The influence of having a second layer down with higher permeability of 22.2 darcy is shown in Figure 4.12. More moisture can then be pulled toward the surface. However, the dryout is still not substantial, compared with initial moisture conditions determined by drainage.

The actual extent of drying that would occur in the three different layered saltcake profiles is shown more graphically by Figure 4.13, which gives the weight percent moisture content at the surface, depending on evaporation time. The same physical parameters applied previously (Simmons 1995) are used to convert the volumetric liquid content into wt% water. The surface begins with about 12 wt% water and dries out to 5 wt% for the lower permeability case but not for the higher permeability case. Figure 4.13 indicates that the steady-state condition is still not quite reached after 200 days of drying.

The test cases indicate that the potential for localized dryout at the surface of a saltcake profile depends on the permeability value near the surface. Therefore, it is important to know the permeability near the waste surface to evaluate the possibility of drying out there. Also, the pore-size index value would have the stronger effect of determining the initial moisture content after drainage, from which further drying would begin by evaporation.

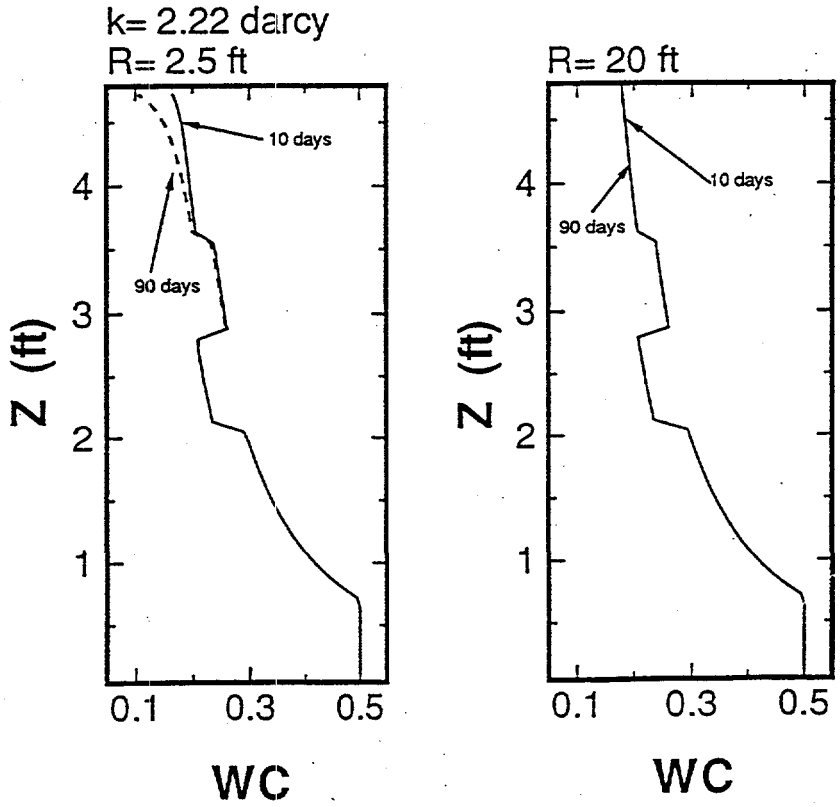

Figure 4.11. Volumetric Liquid Content (WC) in Layered Saltcake Profile Subject to Evaporation from Hot Spot (permeability in each layer reduced to 2.2 darcy)

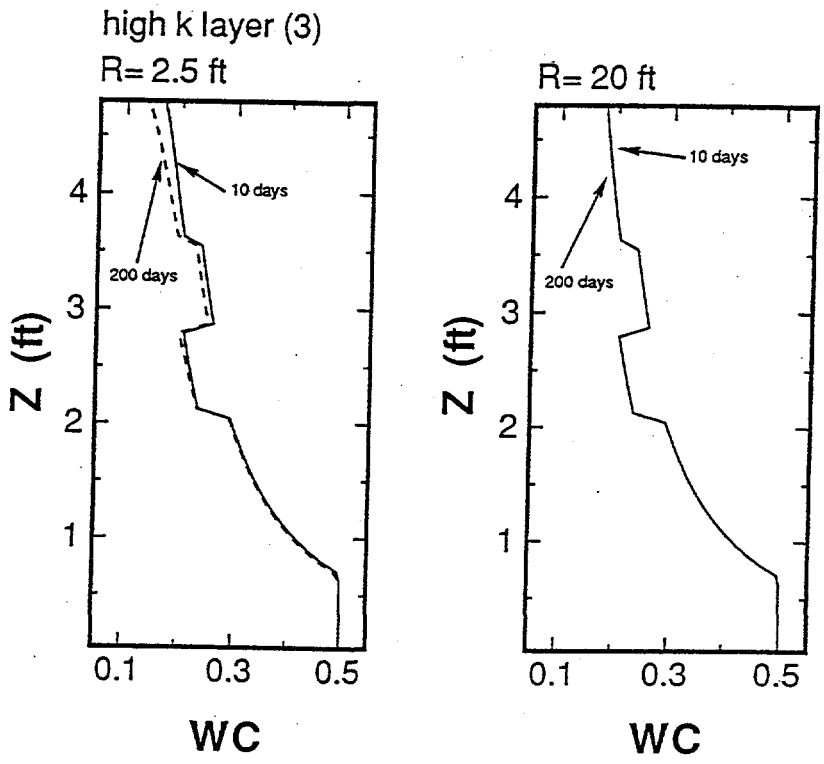

Figure 4.12. Volumetric Liquid Content (WC) in a Heterogeneous Layered Saltcake Profile Subject to Evaporation from Hot Spot (second layer down has permeability of 22.2 darcy; others have 2.2 darcy)

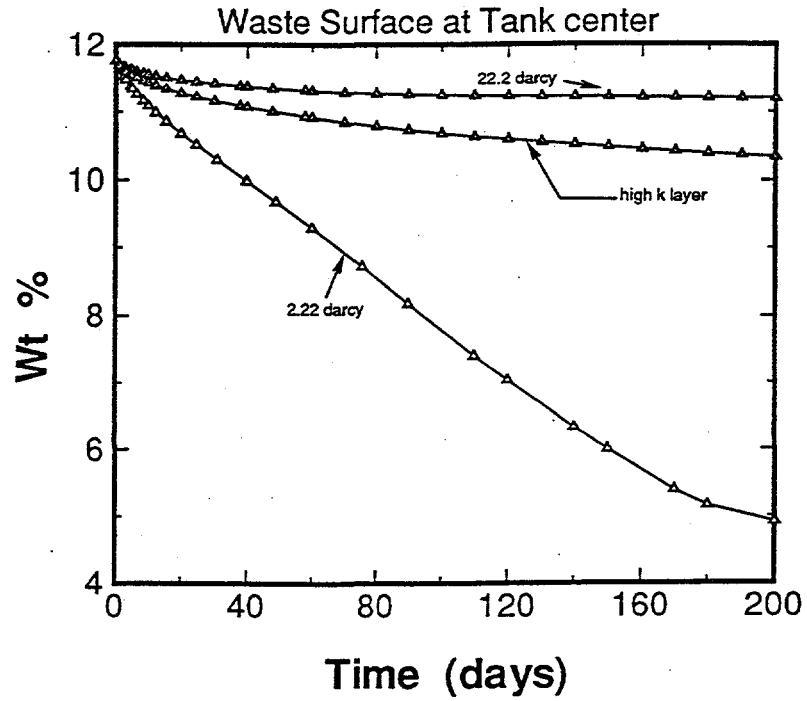

Figure 4.13. Moisture Content at Surface of Layered Saltcake Profile Subject to Hot Spot Drying (wt% water is given for center of hot spot)

4.3. Liquid Application Case

A test case was performed to demonstrate the remediation of a drained waste surface by addition of liquid (saturated salt brine) that infiltrates from the surface. The infiltration over a localized region (disk area) was simulated to show the STOMP code's capability for describing liquid application and removal by pumping. By applying the liquid over a disk region smaller than the tank surface area, the rate of horizontal liquid movement and the downward vertical flow could be examined.

The applied liquid is brine, so it is not necessary to attempt modeling the simultaneous dissolution of saltcake that would result if the liquid were pure water. Currently, there is no theory in the STOMP code to describe how the hydraulic properties change if the interstitial pore-size distribution were changed by dissolving the saltcake matrix. Also, the infiltration simulation neglects the influence of temperature differences between the matrix and applied liquid. It is assumed the liquid has the same temperature as waste.

A pulse of liquid 5 minutes in duration is applied over a disk area of 5-ft radius. In Figure 4.14, a pulse of liquid enters the surface disk area and begins moving downward. Twenty-four hours later, the pulse has vanished, as indicated by the decrease in the liquid saturation near the surface, but it has reached the ILL and increased the saturation slightly at all depths. The layers are displayed in the profile by their different degree of saturation. All layers have the same permeability of 22.2 darcy, as in the other test cases.

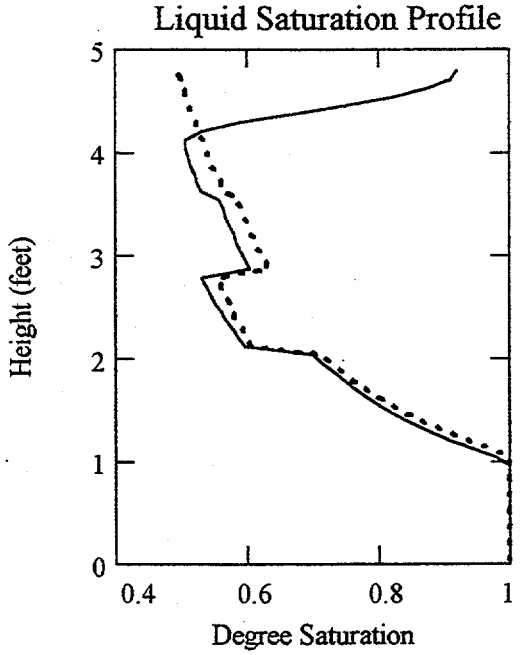

Figure 4.14. Degree of Saturation Distributions in Saltcake Profile following a 5-Minute Pulse of Brine. Dashed line is 24 hr later. Distributions shown for a radius of 3 ft within 5 ft radius of hot spot.

Figure 4.15a shows that during infiltration liquid moves outward very little at first but spreads outward more at depth (Figure 4.15b). Figures 4.15a and 4.15b confirm that applied liquid moves rapidly down and does not spread much horizontally. In Figure 4.15b, liquid spreads to about a 10 ft radius at the 1 ft depth after 24 hours. After 5 minutes, the applied liquid has not reached the 1 ft depth.

The simulation demonstrates that the applied liquid is not retained very long near the surface but rapidly redistributes downward, mainly, and outward. Thus it is not possible to maintain a safe limit (15 wt% water) of moisture near the surface without a continuous application of liquid. A continuous application of liquid to maintain the wt% water at the surface would require an inundation that would rapidly raise the ILL to the surface unless a tank waste was continually pumped down to keep the ILL static. The implication is that the surface permeability would need to be considerably reduced in order to hold the liquid up to maintain the surface liquid content. This simulation suggests that it would be necessary to add fine insoluble particles or another hygroscopic salt to the surface to retain water there. This conclusion does not depend on how the water is applied, either sprinkled liquid or condensation from circulated air with a high RH in the head space.

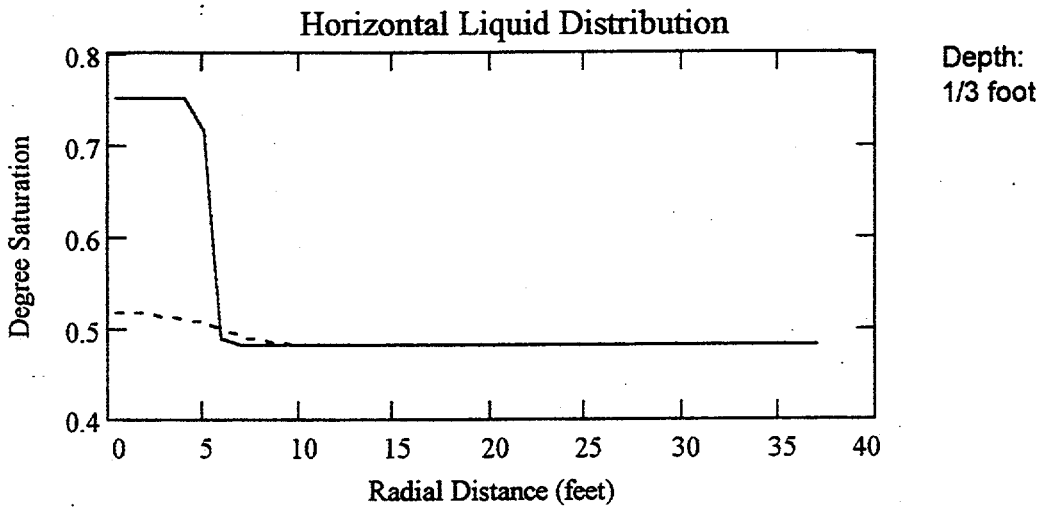

Figure 4.15a. Degree Saturation at Horizontal Distance from Tank Center (solid line is for 5 minutes of applied pulse at 1/3 foot; dashed line is for 24 hours)

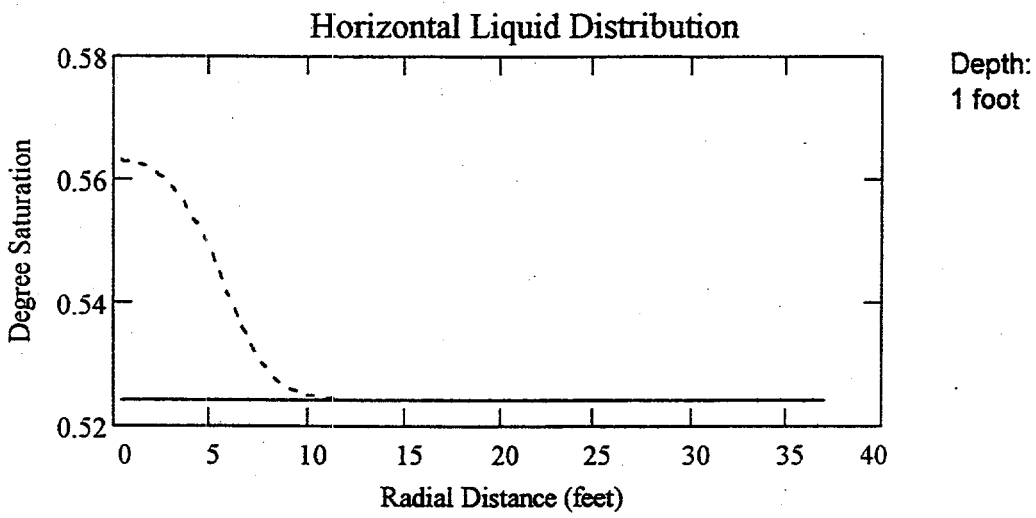

Figure 4.15b. Degree of Saturation at Horizontal Distance from Tank Center (curves are for depth of 1 ft)

5.0 Moisture Cycles Under Nonisothermal Tank Conditions

Predicting the simultaneous, coupled flow of liquid and water vapor in a drained saltcake is the most complicated application of the STOMP code to a waste tank. The flow of water vapor depends on the prevailing temperature gradient. At the same time, the transfer of heat and the resulting temperature distribution depend on the flow of water vapor and its condensation. Water vapor pressure is generally greatest at depth where temperature is highest relative to the surface, and, as a result, vapor flows toward the surface. At the surface, the vapor may escape the waste by going into the head space or may condense higher in the waste profile and drain back down as liquid. These are the possible moisture cycles that must be examined for the actual nonisothermal (temperature-dependent) conditions that exist in most tanks.

To simulate these moisture cycles, the STOMP code must calculate the simultaneous flow of liquid, water vapor, and heat in an unsaturated porous matrix. The test cases described here were run to demonstrate this required modeling capability. The moisture cycles are assumed to take place in a closed tank. Moisture produced at the waste surface is condensed and returned to the tank wall, where it again enters the waste profile. A fraction of the internal evaporation, however, can be specified as lost by breathing. So a tank may not be a completely closed system and may lose some water over time.

As the test cases demonstrate, the moisture cycle and direction of fluid flow depends on the particular surface boundary conditions established by the heat transfer and evaporation rates at the surface. In Section 3 we described a model for the surface boundary condition that depended on how heat is transferred through the head space. This head space evaporation model has not yet been implemented in the STOMP code as a final boundary condition for modeling a tank system. Instead, the test cases here suppose certain extreme situations in order to judge the maximum impact on the moisture movement below the waste surface.

The hypothesis being tested with these cases is that the surface dryness of a stabilized saltcake is not altered substantially from the moisture distribution established by capillarity at equilibrium, even when nonisothermal flow is accounted for, at least when the hydraulic conductivity is sufficient to allow rapid replacement of evaporated water. For the assumed hydraulic property values to represent a typical saltcake, this hypothesis appears true, as the test cases demonstrate. Thus the continual transfer of heat (uniformly) through the waste surface does not appear to cause dryout there.

5.1 Base-Case Simulation Test

The test case simulations of nonisothermal moisture flow were developed from a base case by changing its parameter values. These values are listed in Table 5.1. Simulations are performed using a cylindrical coordinate system and are two-dimensional, having a vertical and radial direction only. The region treated in the STOMP code solution is a 30-degree wedge of

Table 5.1. Parameters for the Base-Case Simulation Test

Parameter	Value (Units)
Permeability of saltcake	22 (darcy)
Liquid specific gravity	1.4 (density in g/cc)
Liquid viscosity	12.5 (cP)
Heat source within waste	2.66 (W/m^3)
Salt thermal conductivity	0.434 (W/m/°C)
Liquid thermal conductivity	1.75 (W/m/°C)
Saltcake heat capacity	860.3 (J/kg/°C)
Initial waste temperature	40 (°C)
Condensate returning temperature	30 (°C)
RH at surface	50 (%)
Gas pressure at waste surface	101.3 (kPa) (1 atm)
Heat flux at profile bottom	-0.871 (W/m^2)
Heat flux at waste tank wall	1.827 (W/m^2)

the cylinder; this is the discretized domain for the calculations. There is no flow of heat or mass in the angular direction through the sides of this wedge domain by rotational symmetry.

For the base case, the waste permeability and viscosity together define the liquid conductivity of 2.5E-3 cm/s. The boundary conditions include the constraint of having no flow (zero flux) of either liquid or gas at the walls or the bottom of the cylindrical profile. Simulations start from the initial conditions of being drained to equilibrium and having a uniform temperature for the profile, and run for 10 years. The boundary condition at the saltcake bottom accounts for the flow of heat from the sludge into the bottom of the saltcake profile without any exchange of liquid. This assumption is consistent with the very low permeability of sludges. Saltcakes are typically a thousand times more permeable to liquid flow.

The heat fluxes result from a heat load of 5500 Btu/hr (2550 W) with 1221 Btu/hr going out the bottom and 660 Btu/hr going out the side wall at its contact with the waste. The fraction exiting the bottom and wall was determined from the heat load fractions in Crowe et al. (1993).

The four-layer saltcake profile described in Figure 4.1 is presumed for all test cases. The liquid retention properties change over the profile, but the permeability and heat conductivity are the same (uniform) over all layers. The code does allow the values for each layer to vary if required and if known. For this study, the test cases were not intended to examine the influence of heterogeneous waste properties but to demonstrate the interaction of the physical processes.

5.2. Simulation Test Cases

The 12 test cases described were run with the STOMP code. These cases, defined as a variation on the base case, are described in Table 5.2. Each case produced graphical results that required a set of 13 plots (see Appendix D). Each plot represents a 30-degree wedge of the tank.

The first set of graphs gives the water vapor and gas flux as well as the heat flux at the waste surface. The second set gives the profiles (two radial distances) of volumetric liquid content, gas moisture content, and temperature that result after 10 years, starting with the initial conditions. The third set of graphs consists of contour plots of hydraulic head, liquid saturation, liquid content, liquid velocity vectors, gas moisture content, and temperature. Those last plots are needed to describe the complexity of the nonisothermal vapor flow behavior in a cylinder. The plots show how rapidly the final steady-state conditions of heat and vapor transfer are achieved for each case. A graph on heat flux shows how the heat transfer is partitioned over advection of the gas and diffusion of water vapor from the surface.

The test cases were devised mainly to test the simulation performance of STOMP, not to represent the waste profile of any actual tank. Unfortunately, there are no measurements of actual tanks in sufficient detail to verify these predictions. The idealized stratigraphy used in the test cases does not describe the complex variation that is typical in a heterogeneous waste profile, but the qualitative results are nonetheless informative.

A general conclusion for all test cases, except for situations in which evaporation is completely stopped, is that liquid is drawn toward the surface without changing the liquid content much from the equilibrium distribution. This is exactly what was found in the earlier simplified modeling, which conceptualized the waste as being one-dimensional in the vertical and without any radial dependence. These two-dimensional simulations, therefore, tend to support the viewpoint used in the simplified modeling.

Table 5.2. Simulation Test Case Conditions

Case Number	Description
1	Base case
2	Heat source halved to 1.33 W/m^3
3	Thermal conductivity of saltcake doubled to 1 W/m/°C
4	RH at surface set to 90%
5	Initial saltcake temperature raised to 80°C
6	Moisture loss fraction from head space at 1%
7	Temperature at waste surface held at 36°C
8	RH at surface set to 99.9% (saturated)
9	Sealed waste surface: no gas flow through surface
10	Convective heat transfer only to 30°C dome with heat transfer coefficient of 5.67 $W/m^2/°C$
11	Convective and radiative heat transfer with 30°C dome
12	Case 11 without advective gas flow from surface

Case 1. This is the base case and demonstrates the transfer of heat from the waste surface entirely by evaporation, which would lead to the greatest possible evaporation rate. The opposite situation is described in case 9. No transfer of heat by convection or radiation is allowed. It is assumed—not realistically—that the surface is insulated to thermal transfer and that only water vapor can escape the surface.

Case 2. If the heat load is reduced by half, the final temperature is reduced everywhere in the waste, and less moisture is evaporated.

Case 3. If the thermal conductivity is doubled, the profile will be cooler than in case 1. Also, the steady-state vapor flux is achieved more rapidly from the given initial temperature.

Case 4. The RH at the waste surface and the gas pressure (1 atm) there determine the rate of vapor flow out of the waste. In this case, the RH is increased to 90%. This case is intended to test sensitivity to the boundary conditions. Case 8 has even higher RH at the waste surface. If surface RH is increased, the profile becomes hotter, and the vapor content increases drastically to balance the high RH in the head space.

Case 5. A higher initial temperature of 80°C, instead of 40°C, requires the waste to cool down before reaching steady state. The vapor flux also decreases to reach the final steady state.

Case 6. A small percentage loss of moisture by breathing, 1%, does not alter the results of the base case very much. (Compare with case 1 [Appendix D]).

Case 7. In case 1, surface temperature is determined by the other boundary conditions. In case 7, a fixed surface temperature is imposed at 36°C, which is lower than that achieved in case 1. Note that the temperature profiles at different radial distances are nearly the same. This condition has a strong effect on the temperature profile and gas moisture content distribution.

Case 8. RH is raised to nearly saturated vapor conditions. This condition would exhibit a dramatic associated temperature increase in the waste profile. Also the water vapor density must increase throughout to be consistent; it is nearly 10 times greater than in case 1. Therefore, RH prevailing in the head space at the surface boundary has a dramatic effect on the profile conditions but not on the equilibrium liquid content distribution. Also, in this situation, about 2000 days were required to achieve steady state, whereas case 1 took only about 750 days.

Case 9. No heat is lost by water vapor flux escaping at the surface—no evaporation. The liquid flow is now directed downward, whereas it is always upward for the other cases. Apparently, vapor moving upward in the profile is condensing and returning downward as liquid. In Appendix D, instead of the gas moisture content contour plot, the gas velocity field is shown.

Case 10. Heat flux at the surface is now carried partly by convection instead of entirely by evaporation, as in case 1, which reduces liquid flow toward the surface and vapor flux. Notice that the influence of the boundary condition is similar to a fixed and uniform temperature at the surface, as in case 7; a common sink temperature on the dome causes the temperature at the

waste surface to be nearly the same at different radial distances—not a realistic situation. But the waste is now much cooler, because heat is being convected away rather than carried entirely by evaporation. Note that now the heat flux rate carried by vapor advection and diffusion does not add up to 90 watts because the remainder is carried by convection.

Case 11. Both convective and radiative heat transfer take place. The vapor flux is determined by the remaining heat load part that is going into evaporation.

Case 12. The advective transport of water vapor out of the surface has been turned off, while only diffusion is allowed to remove vapor. This substantially reduces the outflow of moisture and also the amount of liquid returning along the rim as condensation. As seen in the heat flux rate plot, almost the entire surface heat is now transferred by other than evaporation.

5.3. Moisture Movement in a Saltcake Tank

Although the test cases demonstrate the impact of changing various physics-controlling parameters, only three cases are actually needed to examine the implications for drying out at the surface. Apparently, no matter how the heat loss through the waste surface is partitioned among evaporation, thermal radiation, and convection, the moisture distribution as determined by capillarity cannot be perturbed much from its equilibrium with gravity. In other words, the liquid content at the surface and throughout the profile is not altered by any of the conceived evaporation scenarios. Regardless of whether all the heat load was transferred by evaporation or, in the opposite situation, if the water vapor did not leave the surface, the moisture content distribution remained nearly the same. Cases 1, 9, and 11 together indicate this conclusion.

In these three test cases the liquid flows upward or downward in a way that balances the movement of water vapor. Figures 5.1 through 5.4 reinforce the conclusion that the equilibrium moisture distribution was not disturbed whether or not evaporation occurred . Figure 5.1 describes case 1, and Figure 5.2 describes case 11, for which part of the surface heat loss is by thermal radiation and convection. As seen in Figure 5.3 for case 9, when no evaporation occurs, the liquid flow is downward, while the vapor flow is toward the surface. In case 9, apparently, condensation of water vapor occurs entirely within the waste profile, not on the head space dome. Condensation is returning down the tank rim in Figures 5.1 and 5.2 in the liquid velocity plot. In Figure 5.3, liquid is also flowing toward the tank side where condensation must be occurring within the waste matrix and not in the head space; vapor is seen moving in that direction, too.

Figure 5.4 shows that the liquid distribution is not altered, but the gas moisture content and temperature profiles are quite different for cases 1 and 11. The surface temperature in case 11 is somewhat unrealistic because the heat transfer takes place to a single dome temperature as the heat sink. In reality, the dome would be expected to be cooler toward the rim, and the waste surface temperature should follow that trend.

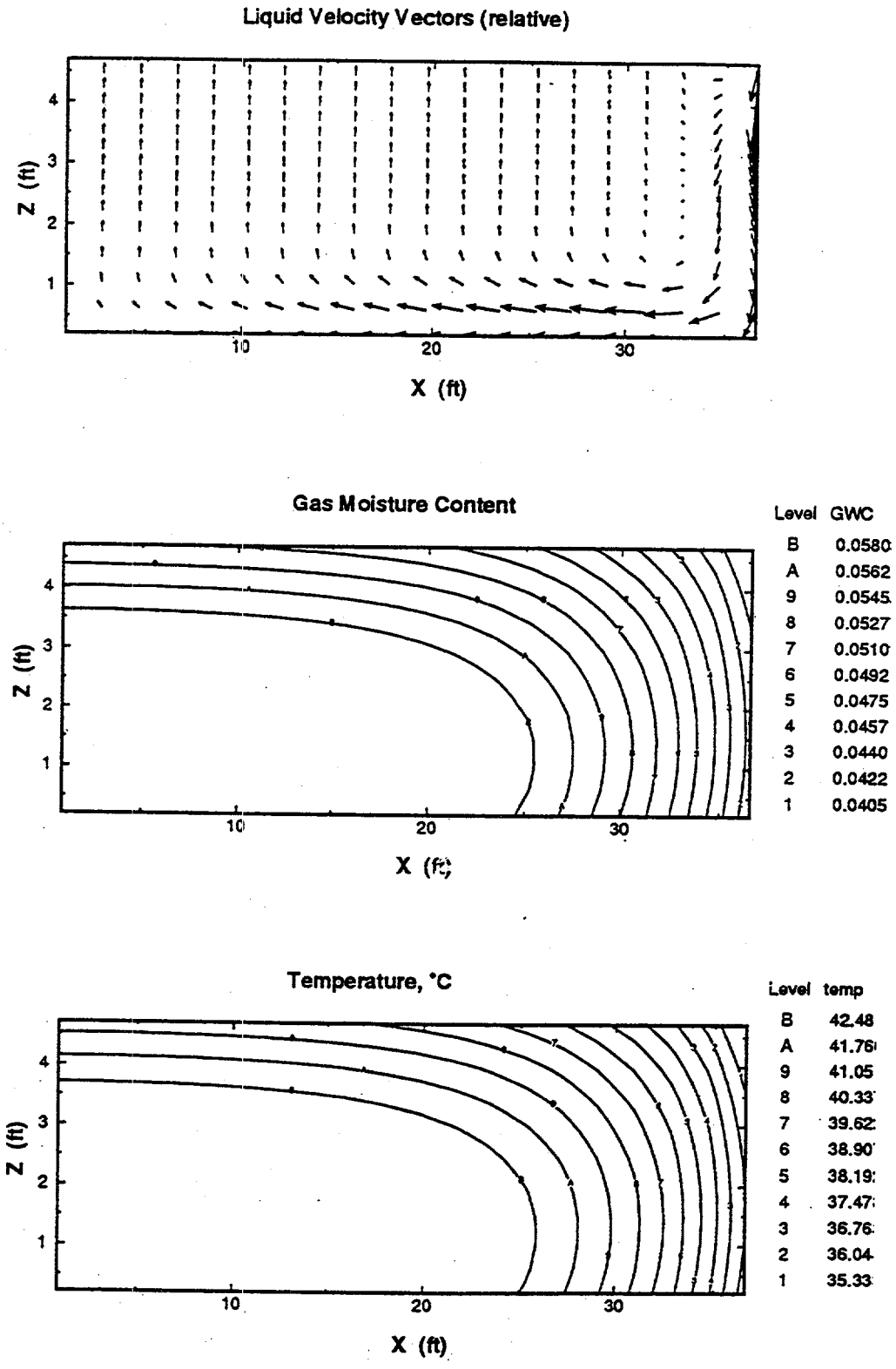

Figure 5.1. Simulation of Liquid Flow, Water Vapor Content, and Temperature Distribution in a Waste Tank, Test Case 1. All surface heat transfer (1080 W) is by evaporation. Total heat load is 1610 W (5500 Btu/hr) in the saltcake. Water vapor content (moisture content plot) of gas has units kg/m^3. Height in waste is Z, and X is radial distance from tank center.

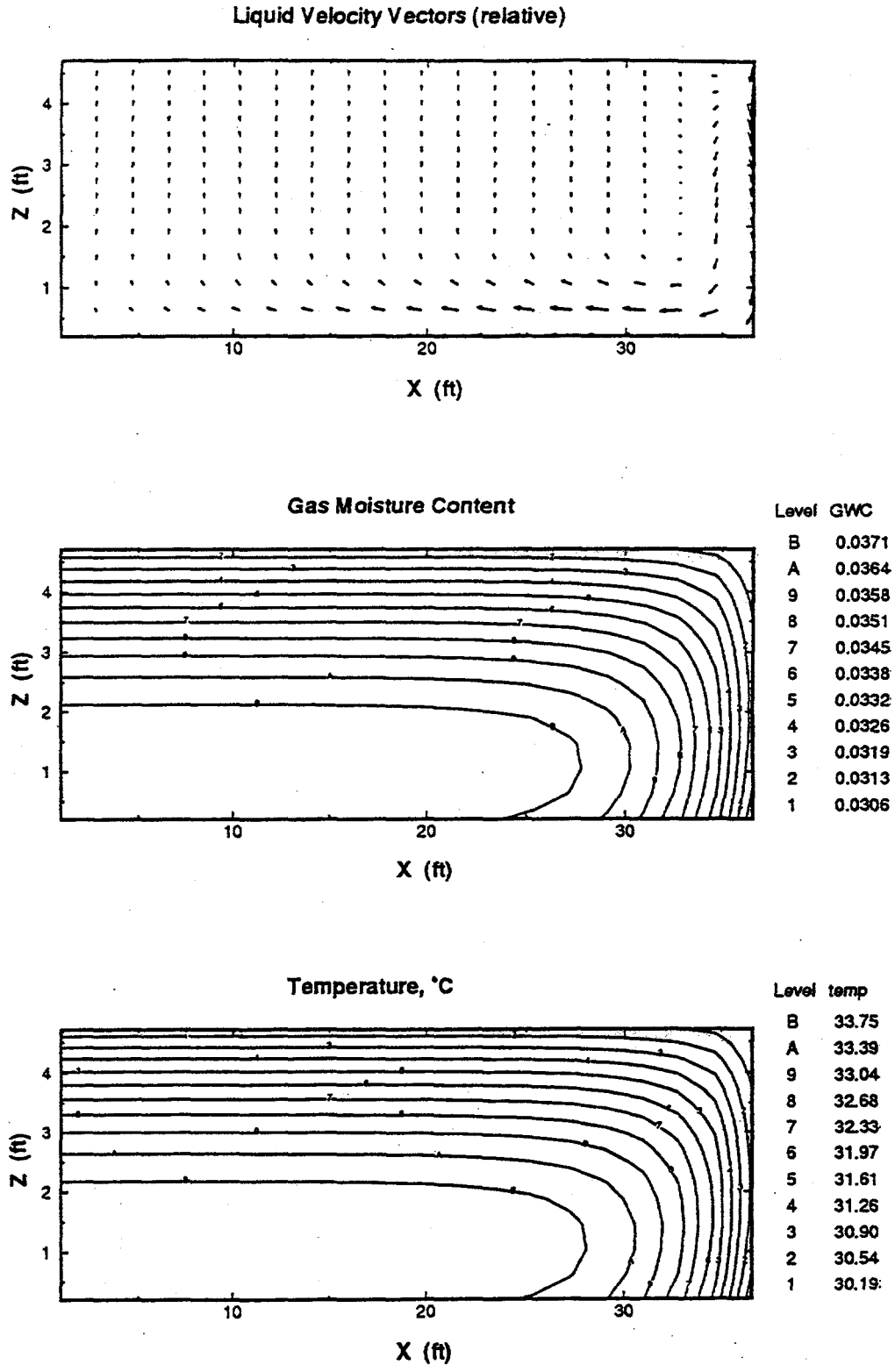

Figure 5.2. Simulation of Liquid Flow, Water Vapor Content, and Temperature in Waste Tank, Test Case 11. Surface heat transfer includes convection and radiation (430 W) with evaporation (650 W).

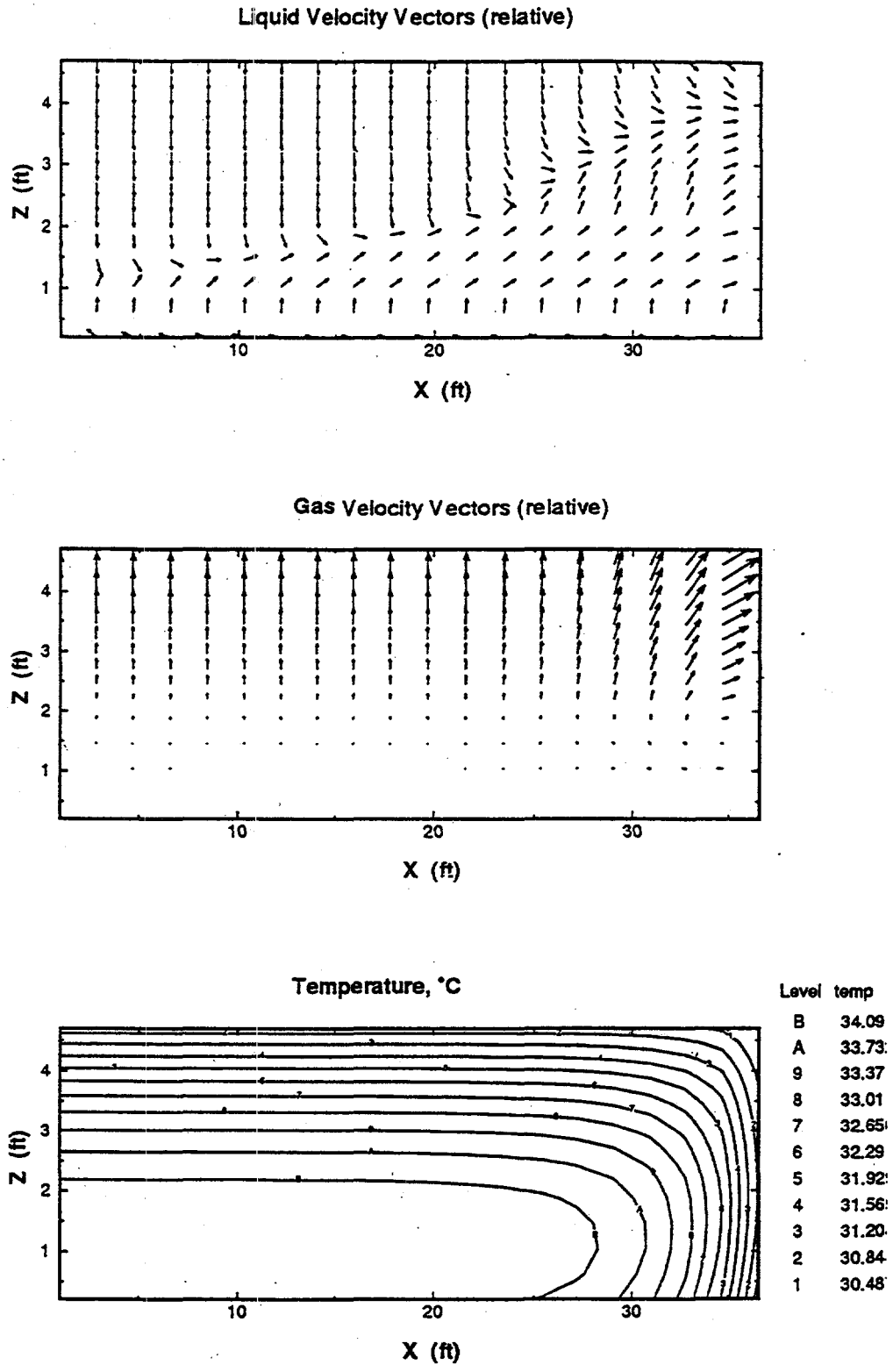

Figure 5.3. Simulation of Liquid Flow, Gas Flow, and Temperature Distribution in Waste Tank, Test Case 9. All surface heat transfer is by convection and radiation without allowing evaporation.

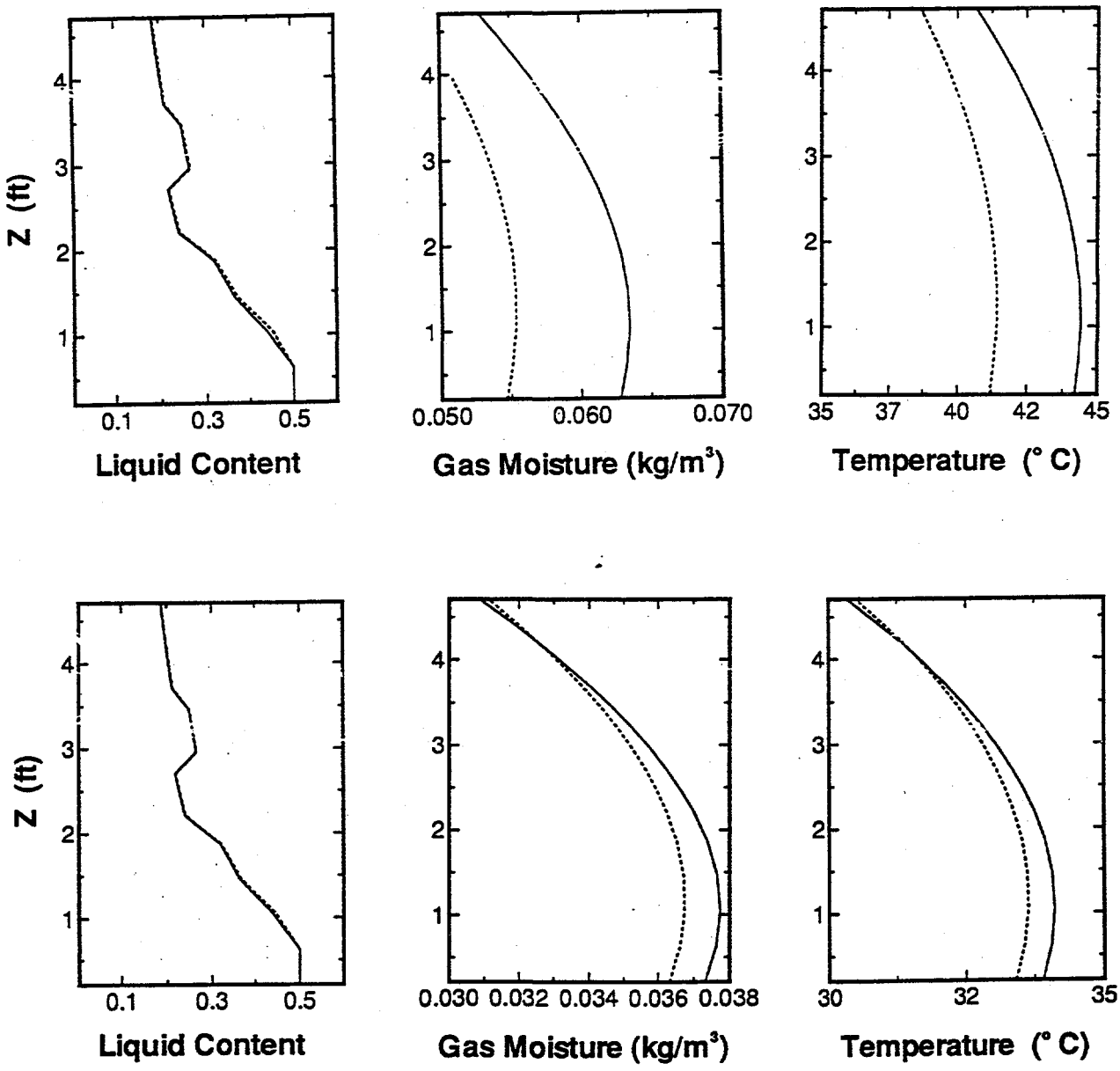

Figure 5.4. Liquid Content, Gas Moisture Content, and Temperature Profiles for Test Cases 1 and 11. First plots correspond to Figure 5.1 (surface heat loss by evaporation only) and second correspond to Figure 5.2. Solid curve is for radius 4.7 ft, and dot curve is for radius 30 ft.

6.0 Conclusions

A model for the moisture distribution and movement in a saltcake waste was developed using the STOMP code (White and Oostrum 1996) as the computational engine. STOMP can predict liquid and water vapor flow in a porous matrix under nonisothermal conditions. Moreover, the code calculates the temperature profile in the waste that results from conduction of the radioactive heat load from the waste tank into the surroundings. The code's capability was demonstrated for a variety of test cases. Because of its complicated pattern, the thermal energy transfer in the head space of a tank is not yet accurately described. Future modeling, therefore, must emphasize improvements of the head space model for waste moisture evaporation.

Despite the limitation in modeling evaporation within the head space, the modeling test cases suggested that the liquid distribution determined by capillarity would not be altered much by the moisture evaporation rate, as long as most of the moisture returns to the waste by condensation within the tank. This result depends considerably on the assumed saltcake permeability. In contrast, if evaporation occurs to the open air, the waste would instead eventually dry out. A test simulation using the UNSAT-H code (Fayer and Jones 1990) demonstrated this drying out process in a stabilized saltcake.

Several other conclusions where drawn from this study:

- A lack of data on the unsaturated hydraulic properties of saltcake in tanks is the most severe impediment to using the STOMP code to predict moisture distributions. The pore-size index and absolute porosity of saltcake layers in tanks are simply not known for wastes that have probably undergone decades of transformation from their original physical characteristics. A method to deduce the needed hydraulic properties by matching simulations with neutron scans was demonstrated in the earlier modeling effort (Simmons 1995). However, there is insufficient data on moisture content in the profiles of actual stabilized waste to verify or test the calibration approach. As a result of this lack of hydraulic data, a detailed study of the modeling sensitivity to different parameter values was not accomplished. A lack of measurements of hydraulic conductivity or permeability of saltcake presents a limitation to using the moisture model for predicting surface drying.

- To overcome the lack of hydraulic data, a reevaluation of the drainable porosity and pore-size index for existing stabilized saltcake tanks was undertaken recently. This work, provided in Appendix E, is a revision of the analysis performed by Simmons (1995). Appendix E improves the estimation of pore-size index by taking into account the collapse of the waste profile caused by pumping out the drainable porosity fraction. An average pore-size index is found for each waste profile of a stabilized saltcake tank. This index describes liquid retention in an entire tank as it is being drained, but it is not known whether the range of index values found for all stabilized tanks reflects the variability of layers that might exist in any particular tank. The relationship of the pore-size index

estimate to the actual liquid retention by capillarity in saltcake waste is still being studied. These values may be useful in a future study of the moisture model's sensitivity.

- If the waste permeability at the surface is an order of magnitude less than the presumed value of about 10 to 20 darcy, the response to internal evaporation may be different than found in the test cases. A stabilized saltcake having a crust with a much lower permeability may be subject to drying out at the surface. Unfortunately, the nature of the surface crust material relative to the bulk of a saltcake profile is unknown for tank waste. Hence, the moisture model cannot be used to predict water content accurately for a waste surface at this time.

- The most valuable contribution of the modeling is an understanding of how various physical mechanisms may affect the moisture condition in a drained saltcake profile. Although the exact value of moisture content at the waste surface cannot be predicted, the moisture modeling nonetheless contributes to understanding the possible moisture cycles inside a waste profile. Two possible moisture cycles were studied: 1) water vapor evaporating from the surface and returning near the tank rim or 2) condensing within the saltcake and draining back down as interstitial liquid while remaining confined to the porous matrix. These two cycles potentially produce either a steady upward movement of liquid—except near the tank rim—or a downward liquid flow, respectively. It is not yet known which possibility occurs in a particular stabilized saltcake tank. But the STOMP code provides a tool to further analyze these possibilities, which have important implications for transport of dissolved organics over time.

- The flow of interstitial liquid and associated evaporation cycle is key to estimating the potential for accumulation of dissolved salts or soluble organics anywhere in a waste profile, especially at the surface. A shallow profile in a tank with a high heat load may produce substantial internal evaporation with resulting advection of solutes upward to the surface. On the other hand, soluble organic-nitrates may naturally be continually leached downward, provided that the drained profile is high enough that cooling confines the condensation of water vapor in the saltcake. A future study should determine which of these transport patterns predominates under what tank conditions.

Certain technical advances to the STOMP code are needed. To model the simultaneous transfer of water vapor and liquid in saltcake waste, it was necessary to extend the code's capabilities so that the influence of dissolved salt on vapor pressure was accounted for. The modifications were discussed as a technical update of the code. However, these advances were not actually employed in the test cases discussed in this report. But the new capabilities were tested and demonstrated as explained in Appendix A. At this time, the code treats the particular salt as being sodium chloride rather than sodium nitrate or nitrite. Sodium chloride has a similar vapor-pressure lowering range as nitrate. Future revisions must take into account the properties of sodium hydroxide, which has a much stronger effect on lowering vapor pressure.

7.0 References

Barney GS. 1976. *Vapor-Liquid-Solid Phase Equilibria of Radioactive Sodium Salt Wastes at Hanford.* ARH-ST-133, Atlantic Richfield Hanford Company, Richland, Washington.

Campbell GS. 1985. *Soil Physics with BASIC Transport Models for Soil-Plant Systems.* Elsevier, New York.

Cass A, GS Campbell, and TL Jones. 1984. "Enhancement of Thermal Water Vapor Diffusion in Soil." *Soil Sci. Soc. Am. J.,* 48:25-32.

Crowe RD, M Kummerer, and AK Postma. 1993. *Estimation of Heat Load in Waste Tanks Using Average Vapor Space Temperatures.* WHC-EP-0709, Westinghouse Hanford Company, Richland, Washington.

Fauske & Associates, Inc. 1994. *Evaporative Losses from Hanford Single Shell Tanks.* FAI/94-95, Fauske & Associates, Inc., Burr Ridge, Illinois.

Fayer MJ and TL Jones. 1990. *UNSAT-H Version 2.0: Unsaturated Soil Water and Heat Flow Model.* PNL-6779, Pacific Northwest National Laboratory, Richland, Washington.

Hanlon BM. 1995. *Waste Tank Summary Report for Month Ending March 31, 1995.* WHC-EP-0182-84, Westinghouse Hanford Company, Richland, Washington.

Heard FJ. 1993. *Evaporation Analysis for Tank SX-105.* WHC-SD-WM-ER-202 Rev. 0, Westinghouse Hanford Company, Richland, Washington.

Kreith J. 1973. *Principles of Heat Transfer, Third Edition.* Intext Educational Publishers, New York.

Kummerer M. 1994. *Topical Report on Heat Removal Characteristics of Waste Storage Tanks.* WHC-SD-WM-SARR-010 Rev. 0, Westinghouse Hanford Company, Richland, Washington.

Metz WP. 1976. *A Topical Report on Interstitial Liquid Removal from Hanford Saltcakes.* ARH-CD-545, Atlantic Richfield Hanford Company, Richland, Washington.

Nassar IN and R Horton. 1989. "Water Transport in Unsaturated Nonisothermal Salty Soil: II. Theoretical Development." *Soil Sci. Soc. Am. J.,* 53:1330-1337.

Perry RH, DW Green, and JO Maloney. 1984. *Perry's Chemical Engineers' Handbook, Sixth Edition.* McGraw-Hill Book Company, New York.

Peurrung LM, SM Caley, EY Bian, and PA Gauglitz. 1996. *Gas Release During Salt-Well Pumping: Model Predictions and Comparisons to Laboratory Experiments*. PNNL-11310, Pacific Northwest National Laboratory, Richland, Washington.

Scheele RD, PR Bredt, and RL Sell. 1996. *Organic Tank Safety Project: Development of a Method to Measure the Equilibrium Water Content of Hanford Organic Tank Wastes and Demonstration of Method on Actual Waste*. PNNL-11227, Pacific Northwest National Laboratory, Richland, Washington.

Simmons CS. 1995. *A Simplified Model of Saltcake Moisture Distribution.* PNL-10803, Pacific Northwest National Laboratory, Richland, Washington.

Webb AB, JL Stewart, DA Turner, MG Plys, B Malinovic, JM Grigsby, DM Camaioni, PG Heasler, WD Samuels, and JJ Toth. 1995. *Preliminary Safety Criteria for Organic Watch List Tanks at the Hanford Site*. WHC-SD-WM-SARR-033 Rev. 0, Westinghouse Hanford Company, Richland, Washington.

White MD and M Oostrom. 1996. *STOMP Subsurface Transport Over Multiple Phases. Theory Guide*. PNNL-11217, Pacific Northwest National Laboratory, Richland, Washington.

Whitney PE. 1995. *Screening the Hanford Tanks for Trapped Gas*. PNL-10821, Pacific Northwest National Laboratory, Richland, Washington.

Appendix A

Salt Transport Modifications to the STOMP Simulator

M. D. White

Appendix A

Salt Transport Modifications to the STOMP Simulator

A.1 Background

The STOMP (Subsurface Transport Over Multiple Phases) engineering simulator was developed for the U.S. Department of Energy (DOE), Office of Environmental Restoration and Waste Management, in conjunction with the Volatile Organic Compounds in Arid Soils Integration Demonstration Program (ARID-ID). The ARID-ID program, which has been concluded, was directed toward the remediation of sites where the subsurface environment had been contaminated with volatile organic compounds and/or radioactive material. The STOMP engineering simulator provides a variety of capabilities to evaluate subsurface remediation technologies. Specifically, the engineering simulator has been designed to provide engineers and scientists with multidimensional analysis capabilities of subsurface flow and transport phenomena for multiple phase and noniso-thermal systems in saturated or partially saturated environments. The engineering simulator offers a variable source code configuration, which allows the user to optimize the source code, in terms of execution speed and memory, to the specifics of the subsurface system under consideration. Construction of the variable source code and input files can be performed through an associated interactive graphical user interface, sTeP. Documentation for the simulator is available in three guide manuals that completely describe the use, numerical theory, algorithmic structure, and application: *STOMP Theory Guide* (White and Oostrom 1996), *STOMP User's Guide*, and *STOMP Application Guide*.(a)

The engineering simulator employs an integrated-volume finite-difference approach for the physical domain and a backwards Euler approach for the time domain to discretize the governing partial differential conservation equations. Coupled solutions of component mass and energy conservation equations over four immiscible phases (aqueous, gas, ice, and nonaqueous liquid) are possible. Simulation of freezing conditions is currently limited to air-water systems. Solute transport problems with equilibrium partitioning among four phases (aqueous, gas, nonaqueous liquid, and solid) may be solved for multiple dilute solutes with radioactive decay. The solute transport equations are solved sequentially to the coupled flow and heat transport equations. Nonlinearities in the discretized coupled flow and heat transport equations are resolved with a Newton-Raphson iteration scheme. Phase appearances and transitions are handled through variable switching schemes. The saturation-relative permeability-pressure constitutive theory for describing both two-phase (water-air) and three-phase (water-oil-air) systems include fluid entrapment and hysteretic effects. The simulator allows a variety of boundary conditions, both internally and externally with respect to the computational domain. The simulator allows computation domains with both permanent and dynamically defined inactive nodes. The simulator currently provides two linear system solvers, a directed banded scheme and an iterative conjugate gradient algorithm.

Heat transfer, fluid migration, localized heat generation, and salt deposition phenomena within the waste tanks on the Hanford Site is not well understood. Remediation decisions and safety analyses would benefit from having a better understanding of the physical processes occurring within these waste tanks. Because of the porous structure of the dried waste tank

---

(a) White MD and M Oostrom. 1995. *STOMP Subsurface Transport Over Multiple Phases, User's Guide* (draft), and *STOMP Application Guide* (draft). Pacific Northwest Laboratory, Richland, Washington.

material, it has been hypothesized that these physical processes could be approximated with numerical tools for predicting flow and transport in conventional porous media. Unfortunately, few numerical tools have been written for solving the governing equations involving the simultaneous flow and transport of water, air, salt, and heat. STOMP, the numerical simulator described above, had proven capabilities for solving problems involving the simultaneous flow and transport of water, air, and heat but lacked capabilities for modeling the transport of nondilute solutes (e.g., brines). By adjusting the density, thermal capacitance, and viscosity of the aqueous solution, heat transfer and fluid migration processes could be investigated using the documented version of the STOMP simulator. To simulate the processes involving localized heat generation and salt deposition, however, the STOMP simulator would require modifications. This document briefly describes the modifications that were made to the STOMP simulator for simulating nonisothermal brines. A demonstration application of these new capabilities is included.

A.2 Theory

Numerical modeling of salt transport in variably-saturated, nonisothermal porous media requires the simultaneous solution of four nonlinear, partial differential equations for the conservation of water mass, air mass, salt, and thermal energy. Transport of these components occurs over three phases: aqueous, gas, and solid; the aqueous phase comprises liquid water, dissolved salt, and dissolved air; the gas phase comprises air and water vapor; and the solid phase represents a porous media. Modification to the STOMP simulator required the additional solution of the salt mass conservation equation simultaneously with the water, air, and thermal energy conservation equations. The salt mass conservation equation added to the STOMP simulator is shown in Equation (A.1):

$$\frac{\partial S}{\partial t} = -\nabla\left[S_\ell \mathbf{V}_\ell\right] + \nabla\left[\left(\tau_\ell s_\ell n_D D_\ell^S + s_\ell n_D \mathbf{D}_{h_\ell}\right)\nabla S_\ell\right] + \dot{m}^S \qquad \text{(A.1)}$$

where S is the salt volumetric concentration, S_ℓ is the dissolved-salt volumetric concentration, $\mathbf{V}_\ell$ is the aqueous phase Darcy velocity vector, τ_ℓ is the aqueous-phase tortuosity, s_ℓ is the aqueous-phase saturation, n_D is the diffusive porosity, D_ℓ^S is the molecular diffusion coefficient for salt in the aqueous phase, is the hydraulic dispersion coefficient tensor, and $\dot{m}^S$ is the salt mass source rate. Salt transport occurs by advection and diffusion-dispersion through the aqueous phase. Solubility of salt in the gas phase is neglected, as is a transport effect known as pressure diffusion, which accounts for dispersive salt mass flux from aqueous phase pressure gradients.

Simultaneous solution of the salt mass conservation equation with the conservation equations for the other active components is required because of the property dependencies on the salt concentration. Properties that were recognized as being dependent on the salt concentration are generally nonlinear: water-vapor partial pressure, aqueous-phase density, aqueous-phase viscosity, aqueous-phase enthalpy, and osmotic pressure. Water-vapor pressure was computed as a function of salt concentration through the brine osmotic coefficient shown in Equation (A.2):

$$P_g^{wS} = P_g^w \exp\left(-\frac{m_\ell^S M^w \phi_\ell^S}{1000}\right) \qquad \text{(A.2)}$$

where P_g^{wS} is the water vapor pressure for brine in porous media, P_g^w is the water vapor pressure for pure water in porous media, m_ℓ^S is the molarity of the dissolved salt, M^w is the molecular

weight of water, and ϕ_ℓ^S is the brine osmotic coefficient. The osmotic coefficient was computed from a fit to tabular data as shown in Equation (A.3) for sodium chloride.

$$\phi_\ell^S = 1 - m_\ell^S \left(a + bT + \frac{c}{T} \right) \tag{A.3}$$

where

$$a = -0.41103 - 1.9084 \exp\left(-0.54744 m_\ell^S\right) - 5.7481 \exp\left(-6.6873 m_\ell^S\right)$$

$$b = 6.7496 x 10^{-4} + 3.2743 x 10^{-3} \exp\left(-0.67161 m_\ell^S\right) + 1.1208 x 10^{-2} \exp\left(-7.1134 m_\ell^S\right)$$

$$c = 49.433 + 355.41 \exp\left(-0.502371 m_\ell^S\right) + 1028.0 \exp\left(-6.5851 m_\ell^S\right)$$

The aqueous-phase density and viscosity were computed as a function of salt concentration for sodium chloride, according to the expressions shown in Equations (A.4) and (A.5), respectively.

$$\rho_\ell^S = \rho_\ell^w \exp\left(0.7 \omega_\ell^S\right) \tag{A.4}$$

$$\mu_\ell^S = \mu_\ell \left(1.0 + 1.85 \omega_\ell^S + 4.1 \left(\omega_\ell^S\right)^2 + 44.5 \left(\omega_\ell^S\right)^3 \right) \tag{A.5}$$

where ρ_ℓ^S is the aqueous-phase density, ρ_ℓ^w is the density of pure water, ω_ℓ^S is the mass fraction of salt in the aqueous phase, μ_ℓ^S is the aqueous-phase viscosity, and μ_ℓ is the viscosity of pure water. The aqueous-phase enthalpy as a function of salt concentration for sodium chloride was computed according to the expression shown in Equation (A.6).

$$h_\ell^S = \frac{\chi_\ell^w M^w h_\ell^w + \chi_\ell^S \left(h_\ell^{S^o} + h_\ell^{S^{ex}} + \Delta h_\ell^{S^o} \right)}{\chi_\ell^w M^w + \chi_\ell^S M^S} \tag{A.6}$$

where h_ℓ^S is the aqueous-phase enthalpy, χ_ℓ^w is the mole fraction of water in the aqueous phase, h_ℓ^w is the enthalpy of pure liquid water, χ_ℓ^S is the mole fraction of salt in the aqueous phase, $h_\ell^{S^o}$ is the molar infinite-dilution enthalpy, $h_\ell^{S^{ex}}$ is the molar excess enthalpy for nondilute salt-water solution, $\Delta h_\ell^{S^o}$ is the molar heat of solution at the reference temperature, and M^S is the molecular weight of salt. The molar infinite-dilution enthalpy is computed as a function of temperature according to Equation (A.7).

$$h_\ell^{S^o} = 77.734 - 0.60371 T + 1.5662 x 10^{-3} T^2 - 1.3913 x 10^{-6} T^3 \tag{A.7}$$

The molar excess enthalpy for nondilute salt-water solutions is computed as a function of salt concentration and temperature according to Equation (A.8):

$$h_\ell^{S^{ex}} = a+bT+cT^2+dT^3 \tag{A.8}$$

where

$$a = -93.34+68.661\exp\left(-0.34452 m_\ell^S\right)+16.031\exp\left(-3.585 m_\ell^S\right)$$

$$b = 0.67174-0.47246\exp\left(-0.36703 m_\ell^S\right)-0.12881\exp\left(-3.5899 m_\ell^S\right)$$

$$c = -1.6263x10^{-3}+1.0999x10^{-3}\exp\left(-0.39371 m_\ell^S\right)+3.3829x10^{-4}\exp\left(-3.6424 m_\ell^S\right)$$

$$d = 1.3749x10^{-6}-9.0136x10^{-7}\exp\left(-0.41024 m_\ell^S\right)-3.0285x10^{-7}\exp\left(-3.6789 m_\ell^S\right)$$

The molar heat of solution for sodium-chloride in water at reference conditions is a constant as shown in Equation (A.9):

$$\Delta h_\ell^{S^o} = 3883 \ J/mol \tag{A.9}$$

The osmotic pressure is computed as a function of salt concentration from the osmotic coefficient according to Equation (A.10):

$$P_\ell^o = -\phi_\ell^S C_\ell^S T R \bar{\rho}_\ell \tag{A.10}$$

where P_ℓ^o is the osmotic pressure, ϕ_ℓ^S is the osmotic coefficient, C_ℓ^S is the molar aqueous-phase concentration of salt, R is the universal gas constant, and g is the acceleration of gravity. The osmotic pressure acts as an additional component in the total water potential. Considering osmotic pressure, matric pressure, and gravitational effects, Darcy's law for volumetric flux of the aqueous phase appears as shown in Equation (A.11):

$$\mathbf{V}_\ell^S = -\frac{k_{r\ell}\mathbf{k}}{\mu_\ell^S}\left[\nabla P_\ell+\sigma_\ell^S \nabla P_\ell^o+\rho_\ell^S g \mathbf{z}_g\right] \tag{A.11}$$

where $k_{r\ell}$ is the aqueous-phase relative permeability, $\mathbf{k}$ is the intrinsic permeability, P_ℓ is the aqueous-phase pressure, σ_ℓ^S is the osmotic efficiency coefficient, P_ℓ^o is osmotic pressure, ρ_ℓ^S is the aqueous phase density, and $\mathbf{z}_g$ is the gravitational vector. The osmotic efficiency coefficient expresses the degree to which dissolved salt would be effective in reducing the total pressure and is computed by assuming the water exists as a film around soil particles according to this equation:

$$\sigma_\ell^S = \frac{r^S-r^W}{b-r^W} \tag{A.12}$$

where, r^S is the hydrated radius of the salt (~2.8 A), r^W is the radius of a water molecule (1.5A), and b is one-half of the water film thickness. The one-half water film thickness is computed as a function of saturation according to Equation (A.13).

$$b = \left[\frac{3 k_{r\ell} \mathbf{k}}{\tau_\ell s_\ell n_D} \right]^{1/2} \qquad \text{(A.13)}$$

The osmotic coefficient varies from 0 to 1, increasing with decreasing film thickness (i.e., the osmotic coefficient increases with decreasing aqueous saturation). An average hydraulic effective film thickness as defined above is reportedly better than that obtained by dividing the volumetric water content with by the product of the soil specific surface and bulk density (i.e., assuming water to be distributed uniformly over the all soil particle surfaces). The latter approach ignores the fact that water preferentially flows through the larger pore spaces. An osmotic coefficient of 1 is assigned to one-half film thickness, which is computed to be less than the radius of a water molecule.

A.3 Application

These modeling capabilities were demonstrated by solving a series of nonisothermal transport problems in unsaturated soils following the work of Nassar and Horton (1989). In these experiments, heat and mass transport were investigated by imposing temperature gradients across closed cylinders filled with partially saturated salty soil. Temperature, water content, and salt concentrations were determined after steady-state conditions were reached. Four initial condition scenarios were investigated: 1) salt-free moist soil, 2) salt-free dry soil, 3) salinized moist soil, and 4) salinized dry soil. The STOMP simulator was executed on four similar scenarios with the addition of considering and excluding osmotic pressure effects on the salinized soils. All simulated scenarios involved a closed horizontal cylinder (0.14 m long and 0.04 m in diameter) that was packed with soil and had the properties shown in Table A.1. The temperature at the cold end of the cylinder was maintained at 9.19°C, whereas the temperature on the warm end was 18.96°C. The cylinder was considered sealed to mass loss, and the side walls were adiabatic.

Six simulations were executed until steady-state conditions were reached. All simulations were executed from the initial conditions having uniform distributions of temperature, aqueous saturation, and salt concentration. Initial temperatures equaled that of the warm end. The six simulations were characterized according to initial saturation, salt concentration, and osmotic pressure effects: 1) salt-free moist soil, 2) salt-free dry soil, 3) salinized moist soil-no osmotic pressure, 4) salinized dry soil-no osmotic pressure, 5) salinized moist soil with osmotic pressure, 6) salinized dry soil with osmotic pressure.

Table A.1. Soil Properties

Grain Density	2650 kg/m^3
Porosity	0.68
Tortuosity	Millington and Quirk Model, 1.0 (aqueous factor), 1.5 (gas factor)
Saturated Conductivity	2.65 x 10^{-6} m/s
Thermal Conductivity	Somerton Model, 0.582 W/m·K (unsat.), 1.13 W/m·K (sat.)
Grain Specific Heat	700 J/kg·K
Vapor Diffusion	Enhanced (0.01 clay fraction)
Saturation Function	van Genuchten Model, α = 0.7026 1/m, n = 1.464, s_m = 0.047
Relative Permeability	Mualem Model
Salt Molecular Diffusion	18.86 x 10^{-6} m^2/s

Moisture content and temperature profiles are shown in Figures A.1 and A.2 for the moist and dry initial soil water contents, respectively. The profiles display minor effects of the salt concentration and redistribution on the moisture content and temperature profiles for both the moist and dry soils. Moisture is slightly shifted toward the warmer end of the heat pipe for salty soil when compared with the salt-free soil. Osmotic pressure effects have a negligible impact on the steady-state distribution of pore water and temperature. Salt concentrations, in terms of aqueous volumetric and total volumetric, are shown in Figures A.3 and A.4 for the moist and dry soil-moisture conditions, respectively. Both aqueous concentration profiles, for the moist and dry soil-moisture conditions, show strong concentration gradients with strong moisture content gradients. For the moist soil-moisture condition the moisture content and salt concentration vary rapidly between 0.1 and 0.12 m from the cold end. Likewise, the dry soil shows strong moisture and salt concentration gradients between 0.04 and 0.06 m from the cold end. The moisture content and salt concentration profiles develop from the countercurrent flow of salt-free water-vapor in the gas phase and dissolved salt in the aqueous phase. This result was also observed in the experiments of Nassar and Horton; where in particular the steep concentration gradients in the dissolved salt occurred closer to the cold end for the dry soil compared against the moist soil. Osmotic and aqueous pressure profiles are shown for the simulations with salinized soil in Figure A.5. For both the dry and moist initial soil moisture conditions the osmotic pressure gradients which develop in response to the redistribution of salt are significantly lower than those for the aqueous pressure. This indicates that the steady-state flow field is dominated by the aqueous pressure gradients and water vapor fluxes in the gas phase. These osmotic pressure gradients are further reduced by the osmotic efficiency coefficient which is shown in Figure 6 for the simulations with salinized soil. Osmotic efficiency coefficients are generally higher for drier soil-moisture conditions because the dissolved salts are more strongly retained by the thinner pore fluid film.

A.4 Conclusions

The STOMP simulator has been modified to solve problems involving the simultaneous flow of water, air, heat, and dissolved salt through porous media. The thermophysical properties of aqueous viscosity, aqueous density, aqueous enthalpy, water vapor partial pressure, osmotic pressure, and osmotic efficiency coefficient have been defined as functions of the aqueous salt concentration. Nonideal solution thermodynamics are considered using functional fits to tabular data for osmotic coefficient, infinite dilution enthalpy, and excess enthalpy for sodium chloride-water solutions. This capabilities have been demonstrated through the application of the simulator to a series of heat pipe problems involving both salt-free and salinized soils. Numerical results generated with the STOMP simulator were compared qualitatively with the experimental results of Nassar and Horton (1989) for similar experiments.

A.5 References

Nassar IN and R Horton. 1989. "Water Transport in Unsaturated Nonisothermal Salty Soil: 1. Experimental Results." *Soil Sci. Soc. Am. J.*, 53:1323-1329.

White MD and M Oostrom. 1996. *STOMP Subsurface Transport Over Multiple Phases, Theory Guide*. PNNL-11217, Pacific Northwest National Laboratory, Richland, Washington.

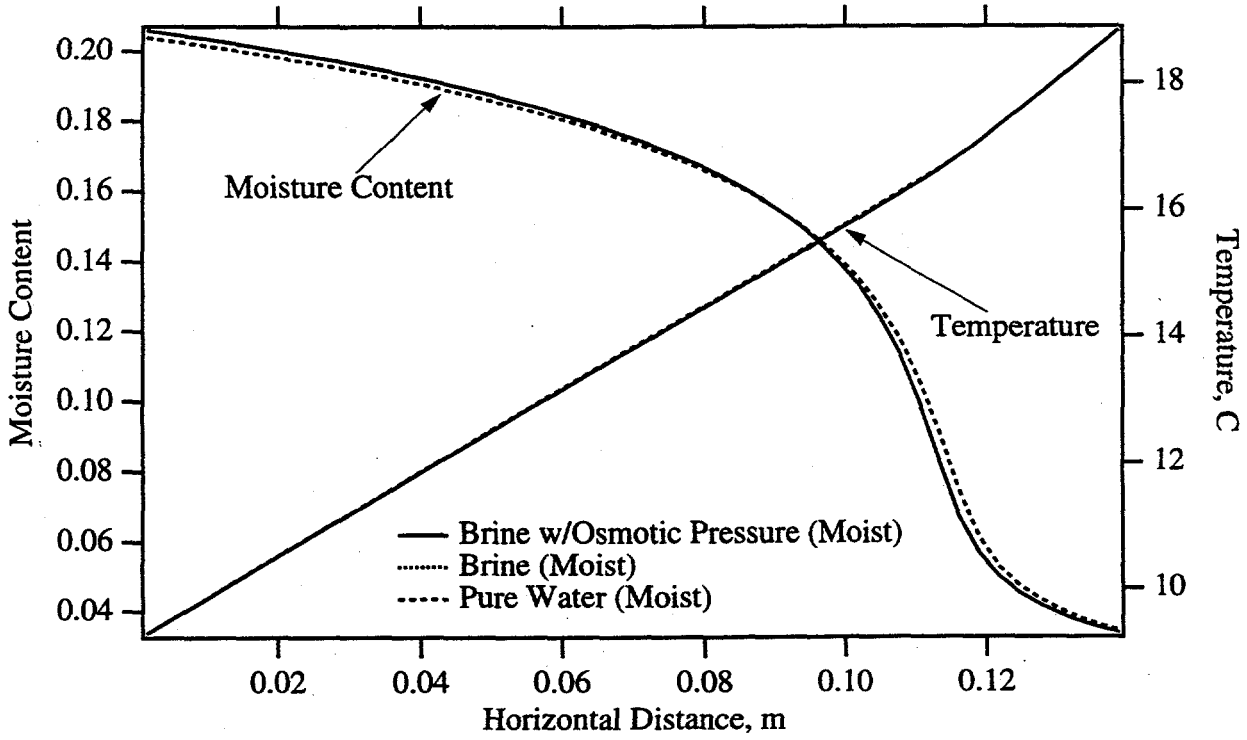

Figure A.1. Moisture Content and Temperature Profiles for Moist Soil Conditions

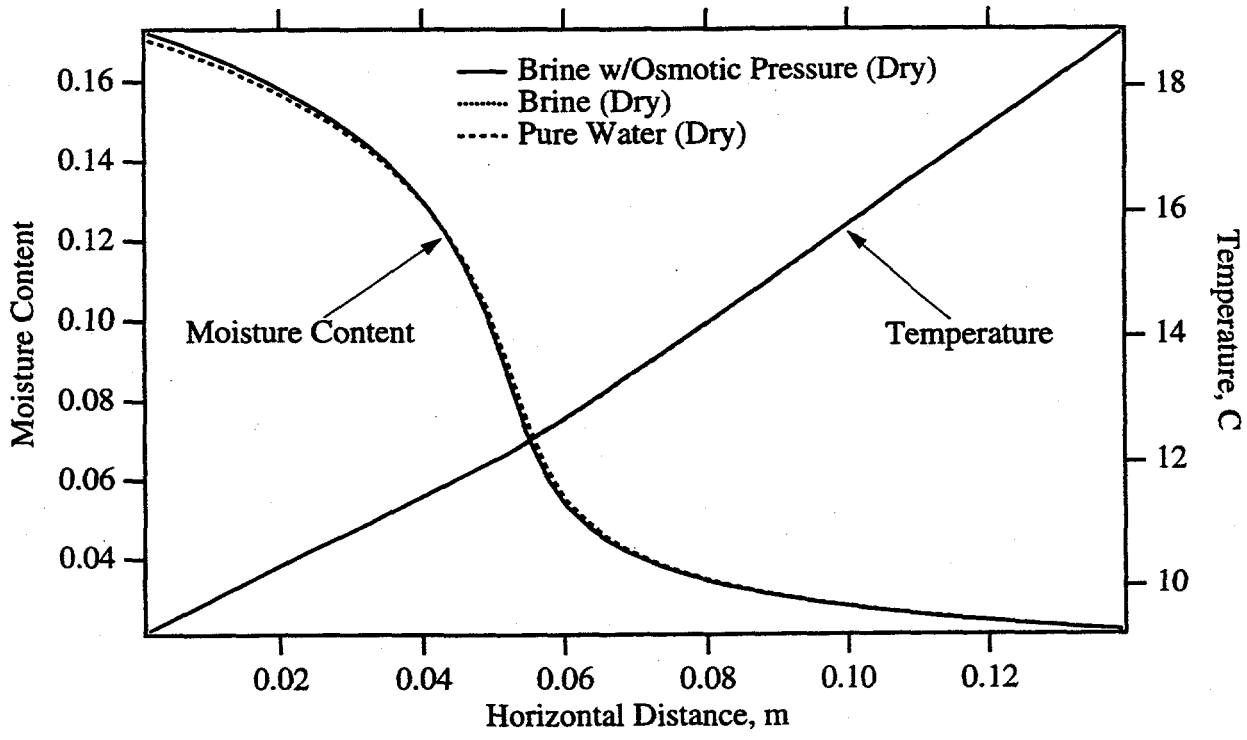

Figure A.2. Moisture Content and Temperature Profiles for Dry Soil Conditions

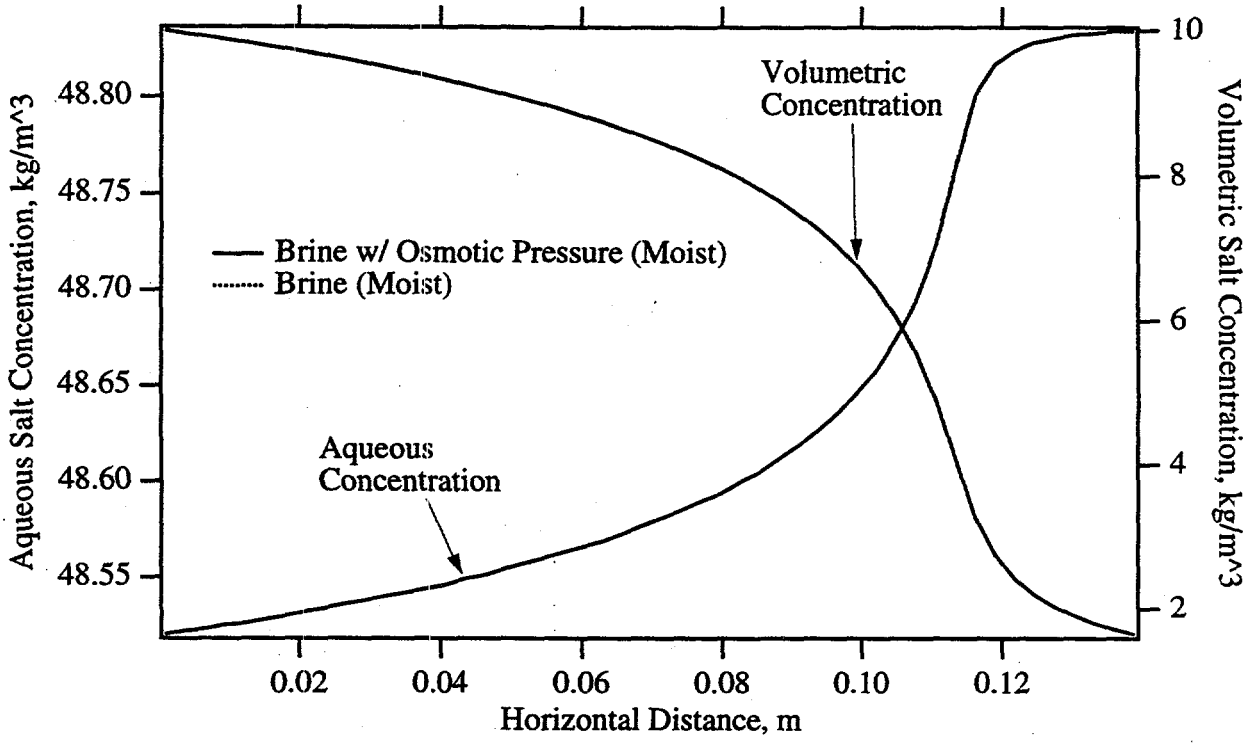

Figure A.3. Salt Concentration Profiles for Moist Soil Conditions

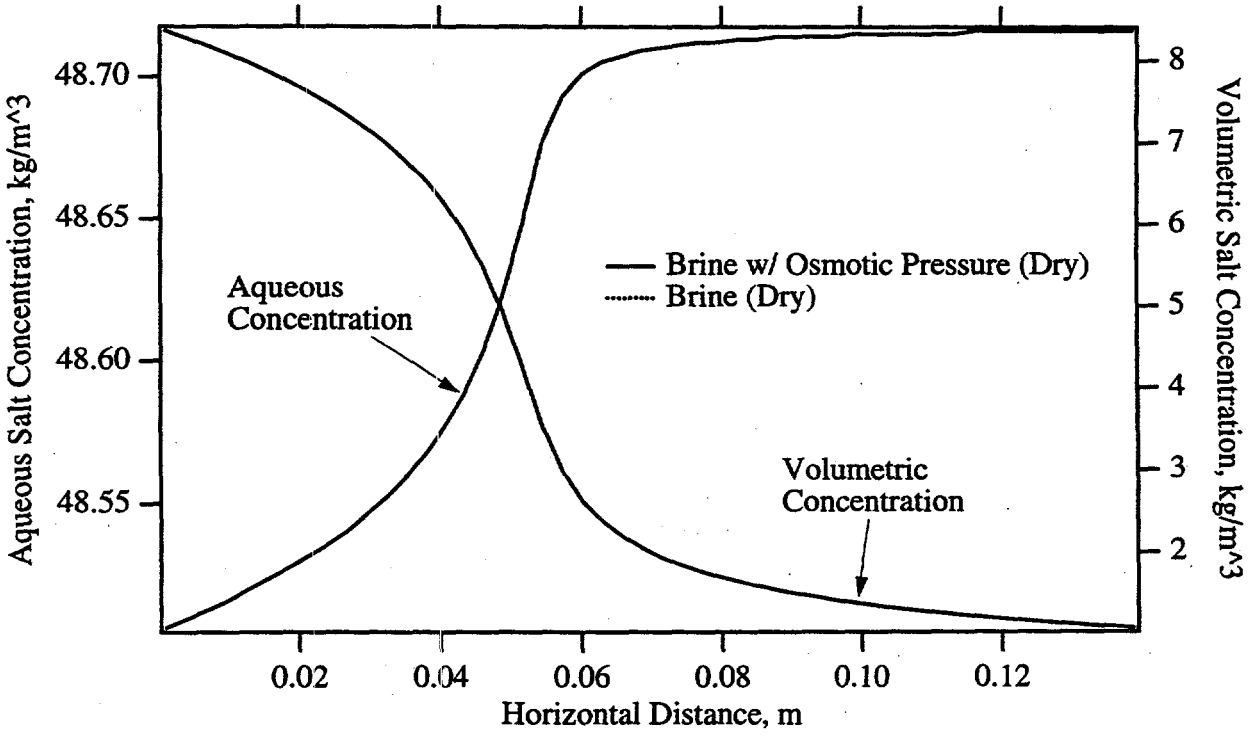

Figure A.4. Salt Concentration Profiles for Dry Soil Conditions

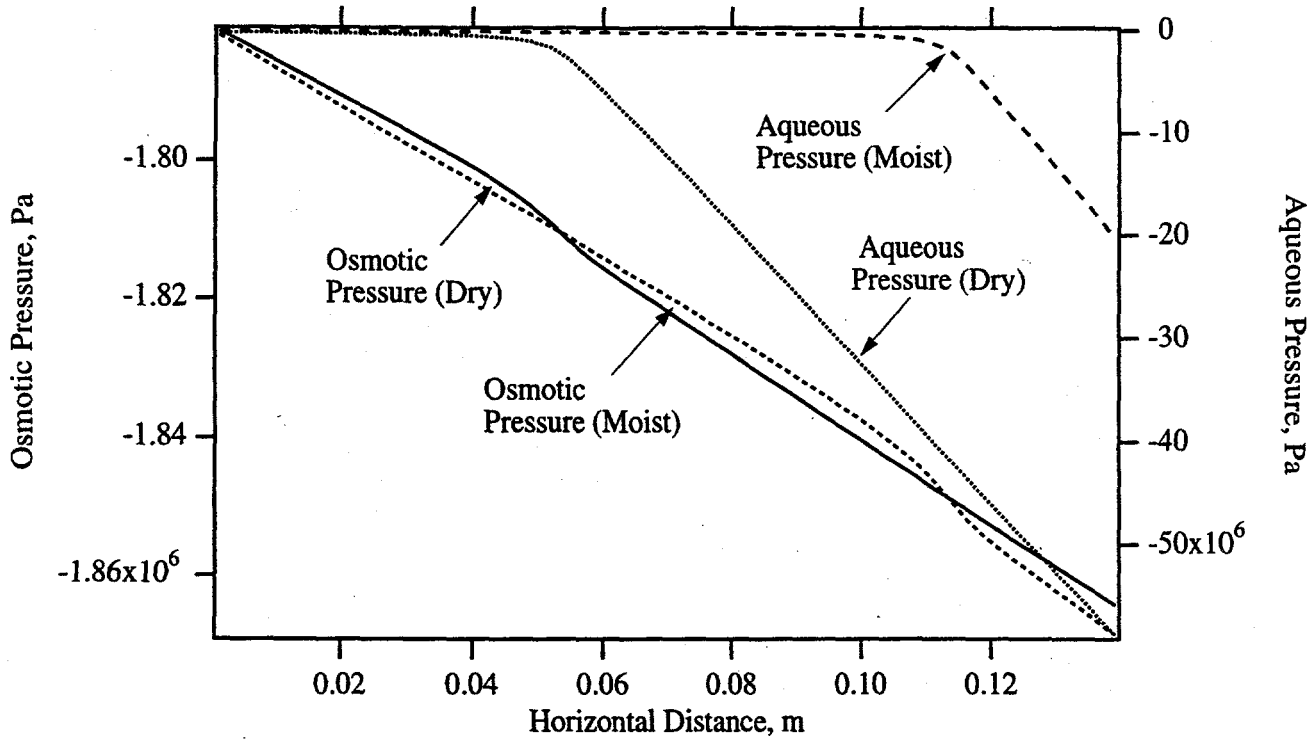

Figure A.5. Osmotic and Aqueous Pressure Profiles

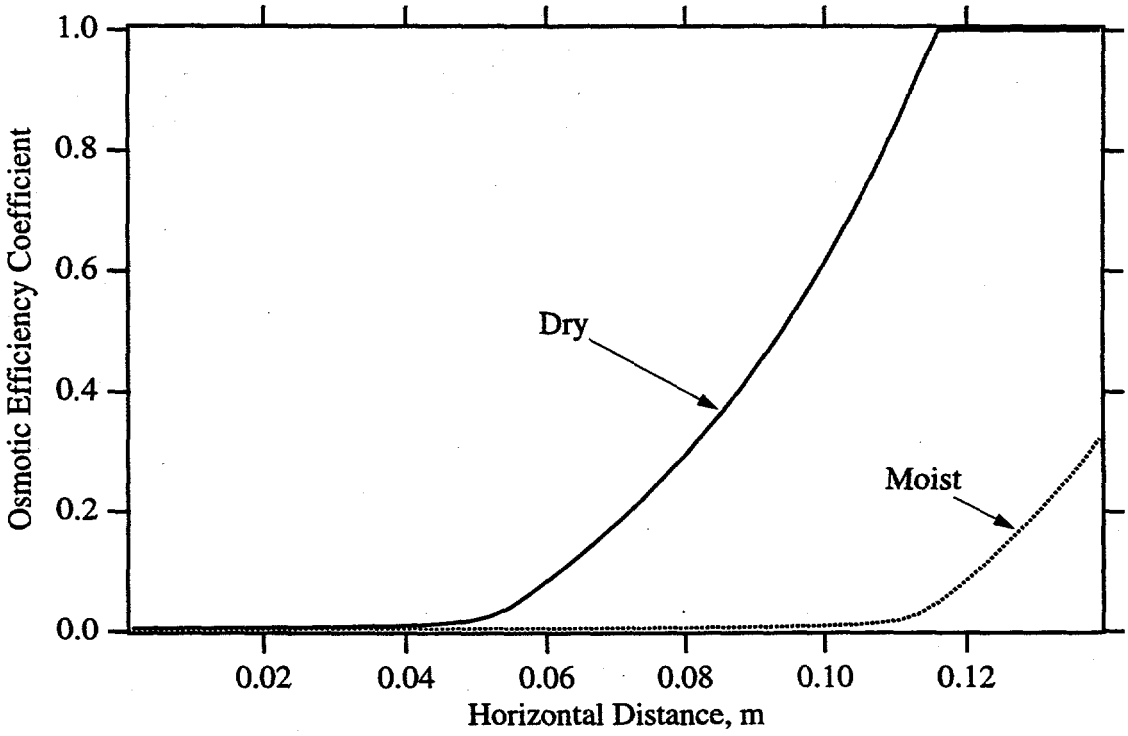

Figure A.6. Osmotic Efficiency Coefficient Profiles

Appendix B

Evaporation Modeling of Tank BY-104

M. J. Fayer

Appendix B

Evaporation Modeling of Tank BY-104

B.1 Introduction

Evaporation of water from tank wastes could lower the water content of the wastes to the point where safety is affected (Epstein et al. 1994). Therefore, estimates of evaporation rates in tanks are needed to better understand the potential for the tank constituents to dry out. The objectives of this study were to estimate evaporation rates from the surface of the waste in a tank such as BY-104 and identify some of the most significant parameters controlling the rates.

B.2 Methods

Evaporation rates were estimated using the UNSAT-H computer code and published or estimated values of the pertinent parameters. Although many of the parameters were determined for Tank BY-104, the conclusions should be applicable to all similar tanks.

The UNSAT-H computer code is a one-dimensional, finite difference computer code that was designed to estimate evaporation rates from surface soils (Fayer and Jones 1990). Liquid water flow is described using Richard's Equation, diffusive vapor flow is described using Fick's law, and conductive heat flow is described using Fourier's law. The code was parameterized by providing information on the problem dimensions, media properties, initial and boundary conditions, heat source terms, and water chemistry effects.

The computer code uses specified temperatures and humidities in the air above the waste to calculate the water and heat fluxes between the surface and air. The code assumes no direct connection between these fluxes and the air temperature and humidity. The net effect of this assumption is that any water that evaporates from the waste surface is immediately removed by some mechanism (e.g., venting), thus preventing a buildup of humidity and a concomitant decrease in the evaporation rate.

B.2.1 Dimensions

The conceptual model of the waste layers in the tank comprises five materials. The total thickness of the five waste layers was a nominal 3.0 m (according to Epstein et al. 1994, the actual waste depth in BY-104 was 3.9 m). The layering scheme and dimensions were provided by C.S. Simmons. Table B.1 shows the specific assignments for the computational nodes.

B.2.2 Media Properties

The required media properties are hydraulic and thermal. The hydraulic properties include the water retention and conductivity functions and the vapor diffusion coefficient. The thermal properties include the thermal conductivity and enhancement factor functions and heat capacity of each material. Tables B.2 to B.6 contain the function parameters.

C.S. Simmons provided the parameters for the Brooks-Corey retention function (see Table B.2). Another common retention function is the van Genuchten function. To demonstrate the degree of sensitivity to the choice of retention function, the appropriate Brooks-Corey parameters were transformed to yield the van Genuchten parameters shown in Table B.3.

Table B.1. Problem Dimensions Showing Node Numbers, Materials, Depth Below Surface, and Initial Suction Head

Node Number	Material Number	Depth Below Surface (cm)	Initial Suction Head (cm)
1	4	0.0	147.6
2	4	0.2	147.4
3	4	0.4	147.2
4	4	0.7	146.9
5	4	1.2	146.4
6	4	2.0	145.6
7	4	3.0	144.6
8	4	4.5	143.1
9	4	7.0	140.6
10	4	10.5	137.1
11	4	15.0	132.6
12	4	19.0	128.6
13	4	24.0	123.6
14	4	29.0	118.6
15	4	35.0	112.6
16	3	41.0	106.6
17	3	47.0	100.6
18	3	52.0	95.6
19	3	58.0	89.6
20	2	64.0	83.6
21	2	70.0	77.6
22	2	76.0	71.6
23	2	81.0	66.6
24	1	87.0	60.6
25	1	93.0	54.6
26	1	100.0	47.6
27	1	110.0	37.6
28	1	120.0	27.6
29	1	130.0	17.6
30	1	138.0	9.6
31	1	144.0	3.6
32	5	150.0	-2.4
33	5	156.0	-8.4
34	5	165.0	-17.4
35	5	180.0	-32.4
36	5	200.0	-52.4
37	5	230.0	-82.4
38	5	265.0	-117.4
39	5	300.0	-152.4

Table B.2. Parameters for the Brooks-Corey Retention Function

Material Number	θs	θr	he	b	Ks (cm/h)	Conductivity Model	l
1	0.50	0.08	30.5	1.8	0.9	Mualem	0.5
2	0.46	0.08	20.3	2.0	0.9	Mualem	0.5
3	0.50	0.08	25.4	2.2	0.9	Mualem	0.5
4	0.47	0.08	30.5	1.8	0.9	Mualem	0.5
5	0.50	0.08	200	1.8	0.009	Mualem	0.5

Table B.3. Parameters for the van Genuchten Retention Function

Material Number	θs	θr	α	n	Ks (cm/h)	Conductivity Model	*l*
1	0.50	0.08	0.0328	1.56	0.9	Mualem	0.5
2	0.46	0.08	0.0493	1.5	0.9	Mualem	0.5
3	0.50	0.08	0.0394	1.45	0.9	Mualem	0.5
4	0.47	0.08	0.0328	1.56	0.9	Mualem	0.5
5	0.50	0.08	0.005	1.8	0.009	Mualem	0.5

Table B.4. Parameters for the Thermal Conductivity Function (values reported for a silt loam soil by Cass et al. 1984)

Material Number	Thermal Conductivity (W/(m K) Parameters				
	A	B	C	D	E
1	0.4	0.8	4.5	0.22	6.0
2	0.4	0.8	4.5	0.22	6.0
3	0.4	0.8	4.5	0.22	6.0
4	0.4	0.8	4.5	0.22	6.0
5	0.4	0.8	4.5	0.22	6.0

Table B.5. Parameters for the Enhancement Factor Function (values reported for a silt loam soil by Cass et al. 1984)

Material Number	Enhancement Factor Parameters				
	A	B	C	D	E
1	9.5	3.0	3.5	1.0	4.0
2	9.5	3.0	3.5	1.0	4.0
3	9.5	3.0	3.5	1.0	4.0
4	9.5	3.0	3.5	1.0	4.0
5	9.5	3.0	3.5	1.0	4.0

Table B.6. Volumetric Specific Heat (bulk density was calculated from particle density and porosity [i.e., θ_s] in Table B.2)

Material Number	Particle Specific Heat J/(g K)	Particle Density Mg/m^3	Particle Volumetric Specific Heat J/(m^3 K)	Bulk Density Mg/m^3	Bulk Volumetric Specific Heat J/(m^3 K)
1	0.9	2.60	2.34	1.30	1.17
2	0.9	2.60	2.34	1.40	1.26
3	0.9	2.60	2.34	1.30	1.17
4	0.9	2.60	2.34	1.38	1.24
5	0.9	2.60	2.34	1.38	1.24

Two water vapor parameters were used: the diffusion coefficient in air and the tortuosity. The diffusion coefficient was determined for the initial waste temperature of 26.1°C, yielding a value of 0.255 cm^2/s (Campbell 1985). The tortuosity for all materials was specified as 0.66, the value determined for soil by Penman (Campbell 1985).

Thermal conductivities and enhancement factors are functions of water content. Such relationships have not been developed for the tank wastes. In lieu of actual measurements, surrogate properties were identified. Cass et al. (1984) reported measurements of thermal properties for a silt loam soil; these properties were used to represent the materials in the tank (Tables B.4 and B.5). The resulting estimate of thermal conductivity for a saturated silt loam is 1.49 W/(m·K). This value is about 50% higher than the estimate used by Epstein et al. (1994) for Tank BY-104.

The volumetric heat capacity of each waste material was represented by the mass specific heat of clay (Campbell 1985) and an assumed particle density (Table B.6). As supporting information, the bulk density and bulk volumetric specific heat were calculated using the porosity information in Tables B.2 and B.3 and the particle density information in Table B.6; the results are in Table B.6.

B.2.3 Initial Conditions

Initial conditions include both suction heads and temperatures. The suction heads were assigned by assuming that the wastes were in hydraulic equilibrium with a water table at the depth of 147.6 cm, which was 152.4 cm above the bottom of the tank. The initial temperatures were equated with the head space temperature of 26.1°C (79°F), which was roughly equal to the 78.5°F value reported by Crowe et al. (1993).

B.2.4 Boundary Conditions

Boundary conditions include both the surface and the bottom of the waste. The surface was described by imposing daily values of air temperature, dewpoint temperature, and wind speed. The air temperature was held constant at 26.1°C (79°F). The dewpoint temperature was determined relative to the osmotic potential of the waste. For those simulations in which the osmotic potential was set to zero so that there was no vapor pressure lowering, the dewpoint set to either 0 or 1°C below the air temperature (100.0 or 94.8% relative humidity (RH), respectively). For those simulations with a finite osmotic potential, the dewpoint temperature was set to 1°C below the temperature at which the saturated vapor density would be at equilibrium with the osmotic potential (75.0 or 70.8% RH, respectively). The wind speed (which entered into the calculation of aerodynamic resistance) was set to either 0 or 0.447 m/s (1 mph). The resulting resistances were roughly 10^4 or 360 s/m, respectively

Net longwave radiation at the waste surface was calculated as a function of the surface and air temperatures and their emissivities. Figure B.1 shows how atmospheric emissivity varied as a function of dewpoint temperature. Soil emissivity was allowed to vary between 0.9 and 1.0, depending on the water content. During the course of this study, we discovered that the results were sensitivity to the emissivity difference between the surface and the air (or tank ceiling). Included in Figure B.1 are emissivities of other materials to give some indication of the possible variation that might be expected in this parameter.

Sensible and latent heat fluxes were calculated as functions of the differences in the surface and air temperatures and vapor pressures, and the aerodynamic resistance. Soil heat flux was the difference between the net radiation and the sensible and latent heat fluxes. The calculations are explained more fully in Fayer and Jones (1990).

Actual measurements of the heat flux through the bottom of the tank were not available. Crowe et al. (1993) estimated that the heat loss through the bottom of BY-104 was roughly 22% of the tank heat load. Based on the work by Crowe et al. (1993), the bottom boundary was assigned a constant heat flux of 0.861 W/m^2.

B.2.5 Source Terms

A feature of the tank waste that is of interest to evaporation modeling is the in situ source of heat from the decay of radioactive elements. Two situations were investigated, no heat source and a heat source uniformly distributed throughout the waste. According to Epstein et al. (1994), estimates of the heat load in Tank BY-104 have recently ranged from 2.3 to 2.6 kW. Using a nominal value of 2.4 kW, a tank area of 406 m^2, and a waste depth of 3.9 m, a heat load of 1.5 W/m^3 was calculated and used for this study. The computer code was modified to allow the user to specify a constant heat source.

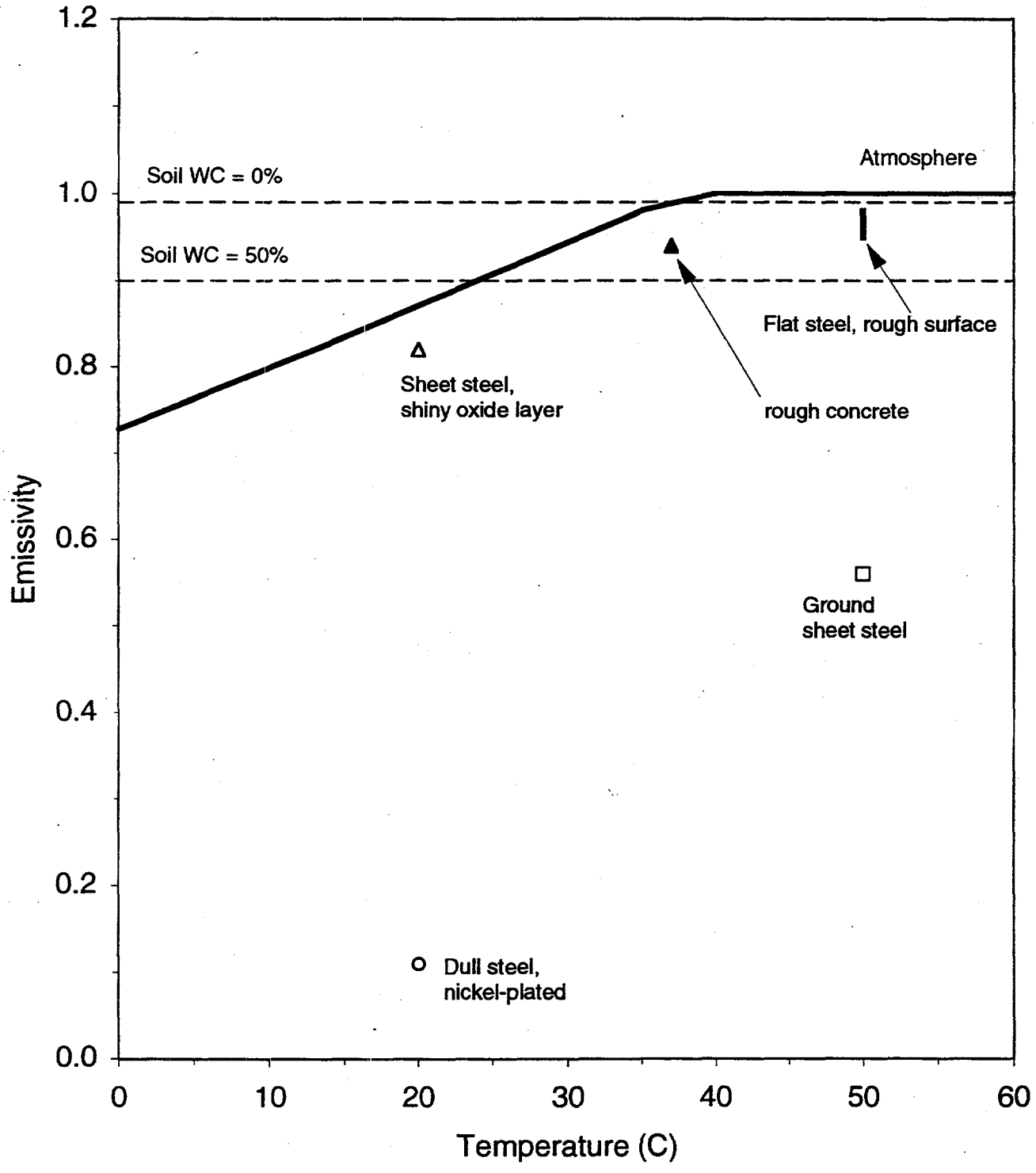

Figure B.1. Variation of Emissivity as a Function of Temperature, Material, and Water Content

B.2.6 Waste Chemistry

The concentrations of the waste constituents are high enough to affect certain properties. For this study, only the chemistry impacts on hydraulic conductivity and relative humidity were considered. Simmons (1995) used the measured permeability (2.19×10^{-7} cm^2) of a synthetic saltcake along with the liquid density of 1.43 g/cm^3 and viscosity of 0.125 g/(cm s) to calculate the hydraulic conductivity of the saltcake. That value was used in Tables B.2 and B.3.

The relative humidity in equilibrium with the water in a porous medium is a function of total water potential determined as the sum of the matric and osmotic potentials. The osmotic potential can be determined from a measurement of the relative humidity in equilibrium with the saturated porous medium (i.e., when the matric potential is zero). Although the humidities measured in the tanks are highly variable, a mean value appears to be 75%. Using this value of humidity and the initial temperature of 26.1°C, the osmotic potential is -39.7 MPa, which is roughly equivalent to a suction head of 4.05×10^5 cm. The computer code was modified to allow the user to specify a constant osmotic potential.

B.3 Results

The simulation results are grouped into four categories to highlight the influences of emissivity, osmotic potential, water retention function, and vapor flow on evaporation rates. Unless stated otherwise, the simulations were conducted with the standard formulation for calculating atmospheric emissivity (ε_a). Figure B.2 shows an example input file.

B.3.1 Emissivity

The method for calculating ε_a does not account for the limited atmospheric volume in the tank and the possible dominating influence of the tank ceiling in regulating longwave radiation exchange. Because of the uncertain nature of thermal radiation exchange within the tank, additional simulations were conducted in which the computer code was modified to set εa equal to either the waste emissivity (ε_s) or to a value that was about 3% higher than ε_s.

The results in Table B.7 show that, for all atmospheric parameters, slight changes in the atmospheric emissivity relative to the waste emissivity can dramatically increase the evaporation rate from the waste surface. When ε_a was 3% less than ε_s, the evaporation rate was effectively zero. When the emissivities were equal, evaporation rates were small but detectable when there was no air movement, and the rates were significant when the wind speed was 0.447 m/s. When ε_a was 3% greater than ε_s, the evaporation rates were 0.1 to 0.2 cm/yr when there was no air movement and more than 14 cm/yr when the wind speed was 0.447 m/s.

B.3.2 Osmotic Potential

Two sets of simulations were performed, one with no osmotic potential and the other with a potential of -4.05×10^5 cm. The results in Table B.7 show that the presence of a significant osmotic potential reduced the evaporation rate. This result was expected because a significant osmotic potential lowers the vapor pressure of the waste, thus reducing the vapor gradient that drives the evaporation process.

```
BY104-k.inp: calculation of evaporation from tank BY-104; -e; dT=1.0 C, 1 mph
    0    4    1    1    1    0    3        IPLANT,LOWER,NGRAV,ISWDIF,IHEAT,UPPER
    0  365  365    1    0    1 1.000E+00  NPRINT,DAYEND,NDAYS,NYEARS,IRAIN,ICON
    1    2    0    1    1                 NSURPE,NFHOUR,ITOPBC,ET_OPT,ICLOUD
    3    3    1    0   10    1            KOPT,KEST,IVAPOR,SH_OPT,INMAX,INHMAX
    0    0    0                           IHYS,IHYST,IRES
 0.000E+00 1.000E+07       0.0       0.0  HIRRI,HDRY,HTOP,DHMAX
 1.000E-05 1.000E+00 1.000E-08 2.400E+01  DMAXBA,DELMAX,DELMIN,STOPHR
      0.66    288.46     0.255       0.0  TORT,TSOIL,VAPDIF
-0.000E-00 2.880E+02 1.000E+01 3.1000E-1  TGRAD,TSMEAN,TSAMP,QHLEAK
       0.5       1.6 1.000E-05       0.0  WTF,RFACT,RAINIf,DHFACT
       0.0    0.0001                      SMETH,DHTOL
       0.0       0.0       0.0           AIRTOL,HYSTOL,HYSMXH
   5   39                                 MATN,NPT
   4     0.000   4     0.200   4     0.400   4     0.700   MAT,Z
   4     1.200   4     2.000   4     3.000   4     4.500   MAT,Z
   4     7.000   4    10.500   4    15.000   4    19.000   MAT,Z
   4    24.000   4    29.000   4    35.000   3    41.000   MAT,Z
   3    47.000   3    52.000   3    58.000   2    64.000   MAT,Z
   2    70.000   2    76.000   2    81.000   1    87.000   MAT,Z
   1    93.000   1   100.000   1   110.000   1   120.000   MAT,Z
   1   130.000   1   138.000   1   144.000   5   150.000   MAT,Z
   5   156.000   5   165.000   5   180.000   5   200.000   MAT,Z
   5   230.000   5   265.000   5   300.000
Mat. No. 1 Brooks-Corey retention
     0.500       0.08      30.48       1.80    0.0,0.0         THET,THTR,A,N
   Brooks-Corey K parameters and Ks(cm/hr)
         2       0.90      30.48       1.80       0.5          KMODEL,SK,A,N,EPIT
Mat. No. 2 Brooks-Corey retention
     0.460       0.08      20.32       2.00    0.0,0.0         THET,THTR,A,N
   Brooks-Corey K parameters and Ks(cm/hr)
         2       0.90      20.32       2.00       0.5          KMODEL,SK,A,N,EPIT
Mat. No. 3 Brooks-Corey retention
     0.500       0.08      25.40       2.20    0.0,0.0         THET,THTR,A,N
   Brooks-Corey K parameters and Ks(cm/hr)
         2       0.90      25.40       2.20       0.5          KMODEL,SK,A,N,EPIT
Mat. No. 4 Brooks-Corey retention
     0.470       0.08      30.48       1.80    0.0,0.0         THET,THTR,A,N
   Brooks-Corey K parameters and Ks(cm/hr)
         2       0.90      30.48       1.80       0.5          KMODEL,SK,A,N,EPIT
Mat. No. 5 Brooks-Corey retention
     0.500       0.08     200.00       1.80    0.0,0.0         THET,THTR,A,N
   Brooks-Corey K parameters and Ks(cm/hr)
         2      0.009     200.00       1.80       0.5          KMODEL,SK,A,N,EPIT
Mat. No. 1 Thermal conductivity
 0.400e+00 0.800e+00 4.500e+00 0.220e+00 6.000e+00 2.340e+00 TCON(A,B,C,D,E),CHS
Mat. No. 1 Enhancement Factor
 9.500e+00 3.000e+00 3.500e+00 1.000e+00 4.000e+00           EF(A,B,C,D,E)
Mat. No. 2 Thermal conductivity
 0.400e+00 0.800e+00 4.500e+00 0.220e+00 6.000e+00 2.340e+00 TCON(A,B,C,D,E),CHS
```

Figure B.2. Sample UNSAT-H Input File

```
Mat. No. 2 Enhancement Factor
 9.500e+00 3.000e+00 3.500e+00 1.000e+00 4.000e+00           EF(A,B,C,D,E)
Mat. No. 3 Thermal conductivity
 0.400e+00 0.800e+00 4.500e+00 0.220e+00 6.000e+00 2.340e+00 TCON(A,B,C,D,E),CHS
Mat. No. 3 Enhancement Factor
 9.500e+00 3.000e+00 3.500e+00 1.000e+00 4.000e+00           EF(A,B,C,D,E)
Mat. No. 4 Thermal conductivity
 0.400e+00 0.800e+00 4.500e+00 0.220e+00 6.000e+00 2.340e+00 TCON(A,B,C,D,E),CHS
Mat. No. 4 Enhancement Factor
 9.500e+00 3.000e+00 3.500e+00 1.000e+00 4.000e+00           EF(A,B,C,D,E)
Mat. No. 5 Thermal conductivity
 0.400e+00 0.800e+00 4.500e+00 0.220e+00 6.000e+00 2.340e+00 TCON(A,B,C,D,E),CHS
Mat. No. 4 Enhancement Factor
 9.500e+00 3.000e+00 3.500e+00 1.000e+00 4.000e+00           EF(A,B,C,D,E)
   0                                                        NDAY
        147.6         147.4         147.2         146.9    Initial heads
        146.4         145.6         144.6         143.1
        140.6         137.1         132.6         128.6
        123.6         118.6         112.6         106.6
        100.6          95.6          89.6          83.6
         77.6          71.6          66.6          60.6
         54.6          47.6          37.6          27.6
         17.6           9.6           3.6          -2.4
         -8.4         -17.4         -32.4         -52.4
        -82.4        -117.4        -152.4
       299.27        299.27        299.27        299.27    Initial temperatures
       299.27        299.27        299.27        299.27
       299.27        299.27        299.27        299.27
       299.27        299.27        299.27        299.27
       299.27        299.27        299.27        299.27
       299.27        299.27        299.27        299.27
       299.27        299.27        299.27        299.27
       299.27        299.27        299.27        299.27
       299.27        299.27        299.27
  0.00100   0.00100     2.000       2.00      0.00    46.57  ZH,ZM,ZT,ZU,D,LAT
   1   79   79 68.1   0.  1.0  0.0 0.00
   2   79   79 68.1   0.  1.0  0.0 0.00
   3   79   79 68.1   0.  1.0  0.0 0.00
...intermediate lines removed for brevity...
 363   79   79 68.1   0.  1.0  0.0 0.00
 364   79   79 68.1   0.  1.0  0.0 0.00
 365   79   79 68.1   0.  1.0  0.0 0.00
   0                NWATER
```

Figure B.2 (contd)

Table B.7. Evaporation During the First Simulation Year as a Function of Atmospheric Emissivity and Relative Humidity, Osmotic Potential, and Wind Speed

Variables			Evaporation (cm/yr)		
RH (%)	Wind (m/s)	Vapor Flow?	$\varepsilon_a < \varepsilon_s$	$\varepsilon_a = \varepsilon_s$	$\varepsilon_a > \varepsilon_s$
Osmotic Potential = -4.05 x 10^5 cm (equilibrium RH = 75.0%)					
75.0	0.0	yes	0.0	0.0178	0.129
70.8	0.0	yes	8.24×10^{-7}	0.0569	0.168
70.8	0.447	yes	1.60×10^{-5}	3.74	14.2
70.8	0.447	no	1.42×10^{-5}	3.68	14.2
Osmotic Potential = 0 cm (equilibrium RH = 100%)					
100.0	0.0	yes	0.0	ns	0.169
94.6	0.0	yes	5.9×10^{-6}	ns	0.219
94.6	0.447	yes	1.02×10^{-4}	ns	16.1
94.6	0.447	no	8.68×10^{-5}	ns	16.0

B.3.3 Hydraulic Function

Most of the simulations conducted for this study used the Brooks-Corey function. To demonstrate the impact of using a different retention function, a series of simulations was conducted with the van Genuchten function. Furthermore, the simulations were conducted for 10 years to highlight impacts as the waste dried out. For this comparison, the only emissivity case studied was $\varepsilon_a > \varepsilon_s$, because evaporation rates were highest for this case (e.g., see Table B.7), and higher rates would tend to highlight any differences between the two retention functions.

Table B.8 shows that, in the first year, the evaporation rate using the van Genuchten function was less than half of the rate estimated when using the Brooks-Corey function. Near saturation, the van Genuchten function begins to release water gradually over a range of matric potential ,whereas the Brooks-Corey function begins releasing water dramatically, precisely at the air-entry potential.

Table B.8. Evaporation as a Function of the Retention Function (the osmotic potential was -4.05 x 10^5 cm, the RH 70.8%, wind speed 0.447 m/s; vapor flow was included)

Retention Function	Simulation Year	Evaporation (cm/yr)		
		$\varepsilon_a < \varepsilon_s$	$\varepsilon_a = \varepsilon_s$	$\varepsilon_a > \varepsilon_s$
Brooks-Corey	1	ns	ns	14.2
	10	ns	ns	1.61
van Genuchten	1	ns	ns	6.53
	10	ns	ns	1.38

In the tenth year, Table B.8 shows that the gap between the predicted annual evaporation rates narrowed to 86%. The shape of the retention function is used to calculate unsaturated conductivity values. Because the two retention functions have different shapes, they have different unsaturated conductivity functions. Thus long-term evaporation rates, which are dominated by the unsaturated conductivity, will differ for these two retention functions.

B.3.4 Vapor Flow

One of the questions to be answered was whether vapor flow was a significant process in the evaporation of water from the waste. Ten-year simulations, with and without vapor flow, were conducted and compared. Table B.9 shows that, during the first year, evaporation rates were identical. This result was not surprising because the waste was very wet initially. When the porous media are wet, liquid conductivities are highest, and air space (for vapor flow) is minimal.

After 10 years, the simulations appeared to be approaching steady conditions. Evaporation rates were 90% less than they were during the first year, which indicates that surface drying has occurred. Drier sediments have lower conductivities, which limits water movement. In the tenth year, the annual evaporation rate without vapor flow was 25% less than the rate with vapor flow. As the waste dried out, the liquid conductivities dropped dramatically, and the air space increased. Vapor flow led to more water withdrawal. Figure B.3 shows the water content profiles after 10 years, during which the inclusion of vapor flow resulted in a total of 4.7 cm more water removal. Figure B.3 also shows that the extra water removal occurred at the waste surface and from the waste layer located below 1.5 m. This behavior is consistent with the hydraulic properties of the materials.

Figure B.4 shows that using vapor flow resulted in higher temperatures throughout the profile. The temperature difference was anywhere from 0K at the surface to as much as 1K below a depth of 1.5 m. As water is removed, the head capacity of the waste decreases such that the temperature rises higher for a given unit of energy input. In addition, the thermal conductivity of drier wastes is less, meaning that the waste is less able to remove the internally generated heat by conduction, although this is ameliorated by the increased heat removal by vapor flow.

Table B.9. Evaporation as a Function of Vapor Flow (osmotic potential was -4.05 x 10^5 cm, RH was 70.8%, and wind speed was 0.447 m/s)

Vapor Flow	Simulation Year	Evaporation (cm/yr)		
		$\varepsilon_a < \varepsilon_s$	$\varepsilon_a = \varepsilon_s$	$\varepsilon_a > \varepsilon_s$
Yes	1	ns	ns	14.2
	10	ns	ns	1.61
No	1	ns	ns	14.2
	10	ns	ns	1.17

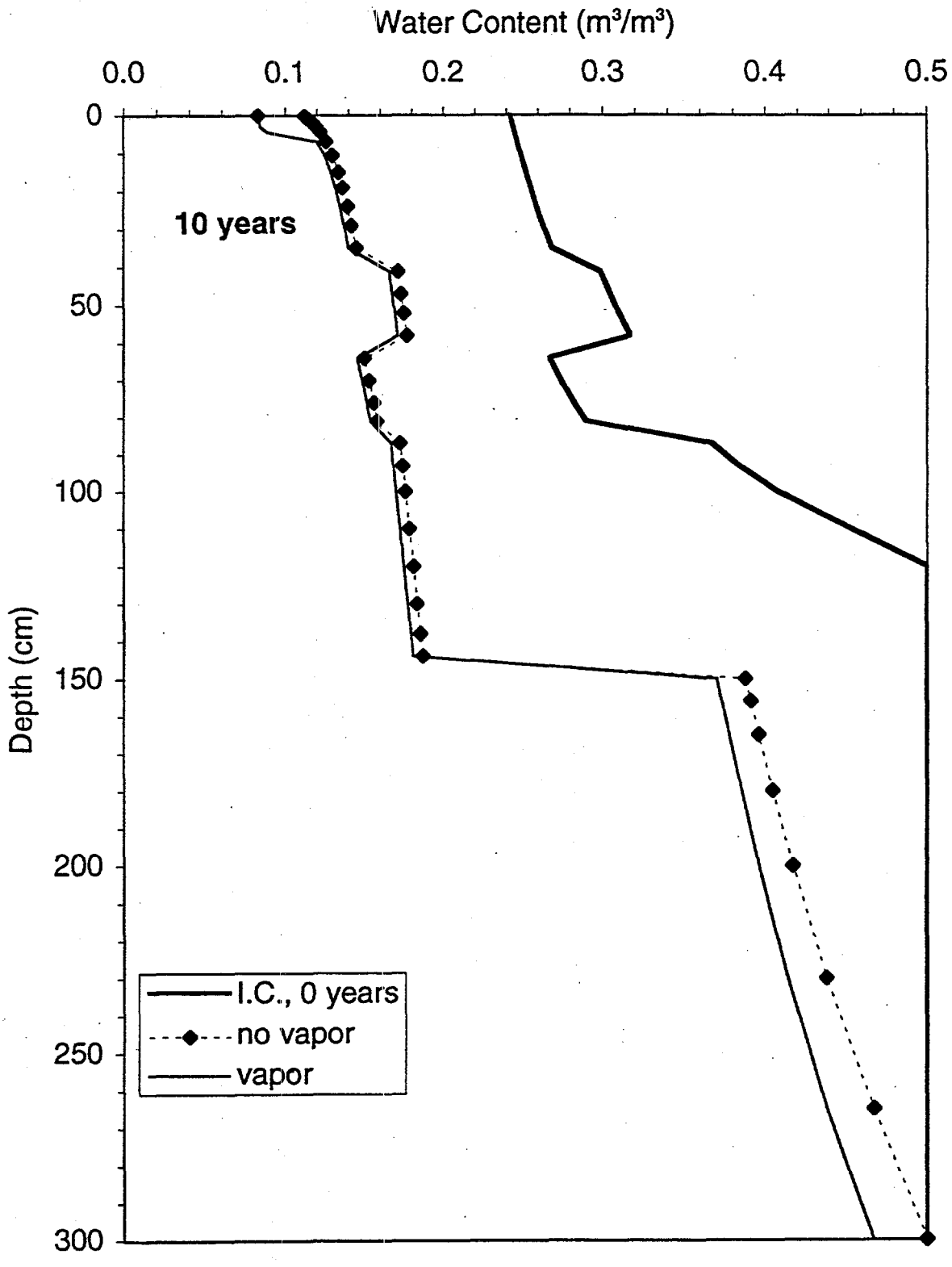

Figure B.3. Predicted Water Content Profile After 10 Years

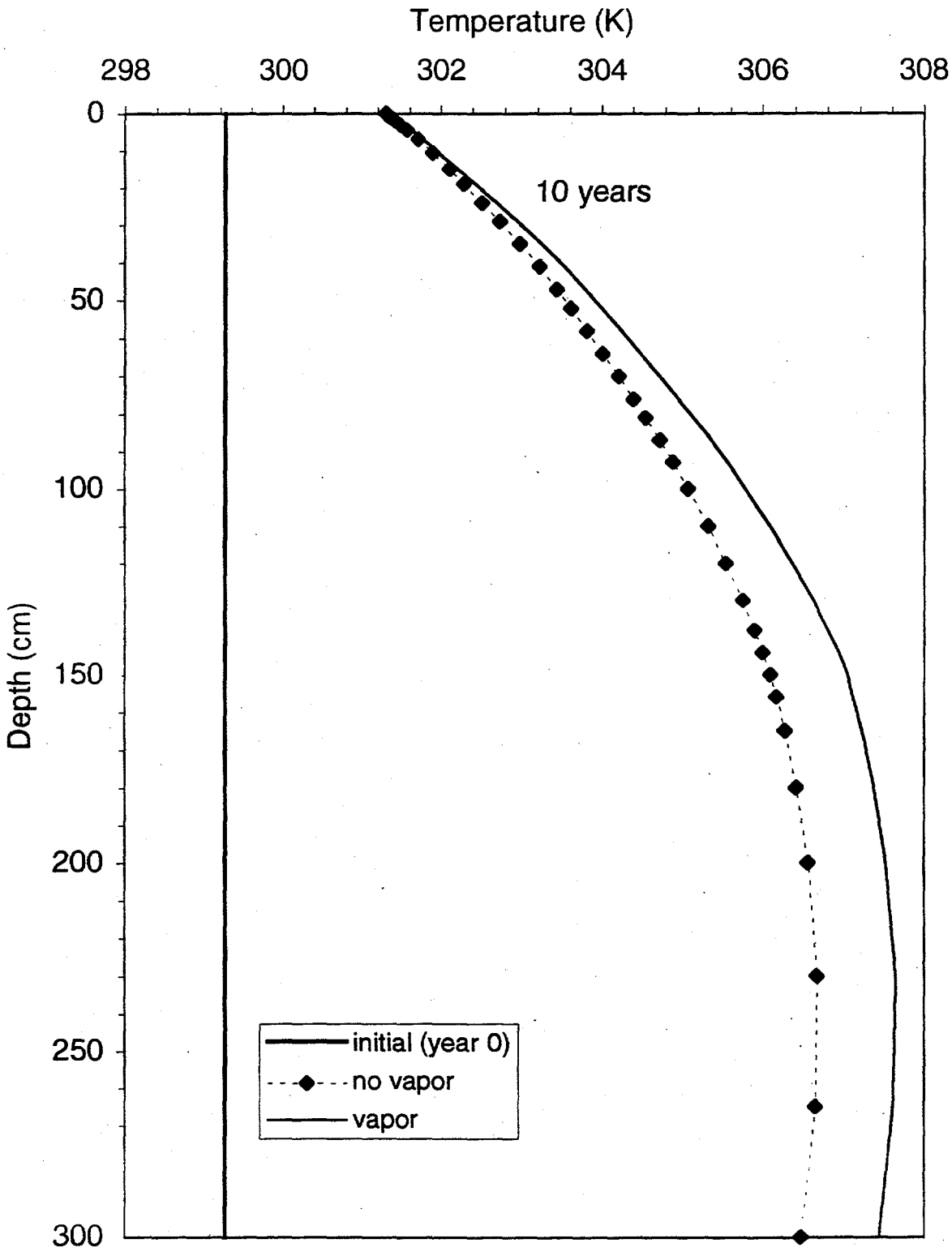

Figure B.4. Predicted Temperature Profile After 10 Years

B.4 Conclusions

The results showed clearly that the rate of water evaporation depended on the net longwave exchange between the waste and tank cover and on the aerodynamic resistance of the atmosphere within the tanks. The estimates provided by modeling can be verified by in-tank measurements (e.g., net radiometers).

The results showed the impact of osmotic potential in reducing (but not eliminating) evaporation rates. The results also showed the influence of the choice of water retention function. Laboratory measurements of retention and unsaturated conductivity can be used verify which function is most appropriate for representing the hydraulic behavior of tank wastes.

Finally, this study demonstrated that vapor flow within the waste becomes a significant water removal process only when the wastes have begun to dry out. As the wastes dry, the air space increases and allows vapor to flow. Eventually, the unsaturated liquid conductivity decreases till the liquid flux is less than the vapor flux. Beyond this stage, the evaporation rate is determined predominantly by the vapor flux. Thus, simulations that include vapor flow are more likely to simulate evaporation more accurately in situations where the waste surface is dry.

The preceding analyses were predicated on the assumption that any water that evaporated from the waste surface was immediately removed by some mechanism (e.g., venting), thus preventing a buildup of humidity and a concomitant decrease in the evaporation rate. If the rate of vapor removal from a tank air space is less than the evaporation rate such that the humidity increases, then the actual evaporation rates will be less than the estimates provided in this report.

B.5 References

Campbell GC. 1985. "Soil Physics with BASIC." *Developments in Soil Science 14*. Elsevier Science Publishing Co. Inc., New York.

Cass A, GS Campbell, and TL Jones. 1984. "Enhancement of thermal water vapor diffusion in soil." *Soil Sci. Soc. Am. J.* 48:25-32.

Crowe RD, M Kummerer, and AK Postma. 1993. *Estimation of Heat Load in Waste Tanks Using Average Vapor Space Temperatures*. WHC-EP-0709, Westinghouse Hanford Company, Richland, Washington.

Epstein M, HK Fauske, DR Dickinson, MD Crippen, JD McCormack, RJ Cash, JE Meacham, and CS Simmons. 1994. *Ferrocyanide Safety Program: An Assessment of the Possibility of Ferrocyanide Sludge Dryout*. WHC-EP-0816, Westinghouse Hanford Company, Richland, Washington.

Fayer MJ and TL Jones. 1990. *UNSAT-H Version 2.0: Unsaturated Soil Water and Heat Flow Model*. PNL-6779, Pacific Northwest Laboratory, Richland, Washington.

Simmons CS. 1996. *Modeling Water Retention of Tank Waste*. PNL-10831, Pacific Northwest National Laboratory, Richland, Washington.

Appendix C

EVAPLOSS: Head Space Evaporation Model

C. S. Simmons

Program EVAPLOSS: Version 3. Date Jan. 1997. This program calculates evaporation loss of moisture from a waste tank system under assumed steady-state heat transfer conditions. Developed by C.S. Simmons, PNNL from a previous program devised by Marty Plys (1994, FAI/94-95).

In this estimation, it is not assumed that the radiant energy emissivities for the dome cover, head space gas, or the waste surface are equal. Therefore, emissivities for each thermal region must be given. The head space gas is treated as a "gray" gas, which transmits most radiant energy through it, but some energy is absorbed to be reemitted. Relative humidity for at least one thermal region (dome cover, head space, or waste surface) must be known and given, as well as the relative humidity in the waste depending on the particular dissolved salts concentration. The outside temperature at the top of the dome overburden and the waste temperature at depth must be known also. The heat load for the tank may or may not be required; it can be estimated from the temperature information. Thermal conductivities for the waste and the soil overburden must be known. A steady breathing rate must be known to calculate the moisture loss rate. A porosity value for the water vapor in the liquid-drained surface region of waste is necessary to determine the vapor diffusion coefficient for evaporation of moisture.

Seven equations for the coupled steady flow of water vapor and heat are solved simultaneously. This is three equations for the transfer of water vapor and four for transfer of heat to the soil overburden surface. The equations are simple transfer type depending on large-scale transfer coefficients. Transfer of mass and energy is proportional to differences in the relative concentrations of water vapor and temperature, respectively. The set of assumed transfer coefficients are discussed by Plys (1994) in FAI/94-95, "Evaporative Losses from Hanford Single Shell Tanks".

For a tank with high active ventilation, an eddy diffusion transfer coefficient from Heard's report (1993, WHC-SD-WM-ER-202) can be used as an alternative description of vapor transfer from the waste surface to the head space. The equation must be turned on while turning off the Plys' equation.

$A := 410 \cdot m^2$ waste surface area

$Fo := 2 \cdot 10^3 \cdot \frac{m^3}{yr}$ breathing rate

$Q := \frac{0.66 \cdot 2550 \cdot watt}{A}$ heat output to waste surface - less sides/bottom

$f_{surf} := .8$ $Q = 4.10488 \cdot \frac{watt}{m^2}$

$Ta := 12$ outside atmosphere temp

$To := 13.5$ outside soil surface temp 13.5

$Tc := 26.5$ tank cover ceiling temp

$Tg := 26.6$ tank headspace gas temp 26.6

$Ts := 27.2$ waste surface temp 27.2

$Td := 52.5$ waste temp at ILL depth

52.5 43.5

$\theta s := 0.5$ porosity

$\theta := 0.05$ liquid content

$L := 13 \cdot ft$ waste surface height

$ILL := 7.44 \cdot ft$ liquid level BY-104

$\Delta Z := L - ILL$ vapor diffusion length

$\Delta Z = 1.69469 \cdot m$

$Lsoil := 13 \cdot ft$ soil cover depth

$Lsoil = 3.9624 \cdot m$

$r := 37.5 \cdot ft$ tank radius

$Vs := 0.2 \cdot \frac{ft}{sec}$ air velocity over waste surface or crust

$Ksoil := 1.0 \cdot \frac{watt}{m \cdot K}$ soil thermal conduct

$Kwaste := 0.25 \cdot \frac{watt}{m \cdot K}$ waste thermal conductivity

$RHd := 0.60$ RH in waste at depth

$\varepsilon := .9$ emissivity (overall)

$\sigma := 5.67 \cdot 10^{-8} \cdot \frac{watt}{m^2 \cdot K^4}$ Stefan-Boltzman constant

$Re := \rho_{air} \cdot Vs \cdot \frac{r}{\mu}$ Reynolds number

$Sc := \frac{\mu}{\rho_{air} \cdot Da}$ Schmidt number

$Tk := 273.16$ degrees Kelvin at 0 C

$Patm := 1.01 \cdot 10^5 \cdot Pa$ atmospheric pressure

$R := 8.314 \cdot \frac{joule}{K}$ per mole

$Mw := 0.018 \cdot kg$ per mole of water vapor

$Ma := 0.029 \cdot kg$ per mole of air

$Lheat := 2400 \cdot 10^3 \cdot \frac{joule}{kg}$ latent heat of water vapor

$T := (Tk + 20) \cdot K$ standard conditions

$p_{wv} := \frac{17.535}{760} \cdot Patm$ $\rho_a(T) := Patm \cdot \frac{Ma}{R \cdot T}$

$\rho_{wv} := p_{wv} \cdot \frac{Mw}{R \cdot T}$ $\rho_{air} := \rho_a(T)$

$\rho_{wv} = 0.01721 \cdot kg \cdot m^{-3}$ $\rho_{air} = 1.20172 \cdot kg \cdot m^{-3}$

Water vapor density at saturation:

$$\rho_v(T) := \left(1.323 \cdot \frac{kg \cdot K}{m^3}\right) \cdot \frac{\exp\left[17.27 \cdot \frac{(T - 273.16 \cdot K)}{(T - 35.86 \cdot K)}\right]}{T}$$

$\rho_v(T) = 0.01728 \cdot kg \cdot m^{-3}$

$Da := \left(229 \cdot \frac{m^2}{sec}\right) \cdot 10^{-7} \cdot \left(\frac{T}{273.16 \cdot K}\right)^{1.75}$ diffusion coeff in air

$Da = 2.59143 \cdot 10^{-5} \cdot m^2 \cdot sec^{-1}$

$D := 0.66 \cdot (\theta s - \theta) \cdot Da$ water vapor diffusion coefficient in waste

$\nu := 1.57 \cdot 10^{-5} \cdot \frac{m^2}{sec}$ kinetic viscosity of air

$Ka := 0.0262 \cdot \frac{watt}{m \cdot K}$ thermal conductivity of air

$Sa := 1010 \cdot \frac{joule}{kg \cdot K}$ air specific heat

$\mu := \rho_{air} \cdot \nu$ air dynamic viscosity

$\mu = 1.88671 \cdot 10^{-4} \cdot poise$

$\alpha := \frac{Ka}{\rho_{air} \cdot Sa}$ thermal diffusivity

$\alpha = 2.15862 \cdot 10^{-5} \cdot m^2 \cdot sec^{-1}$

$Re = 4.43804 \cdot 10^{4}$ $h_D := 0.039 \cdot Vs \cdot Re^{-0.206} \cdot Sc^{-1.5}$

$Sc = 0.60584$ $h_D = 5.5622 \cdot 10^{-4} \cdot m \cdot sec^{-1}$

Eddy diffusion mass transfer coefficient from Heard (1993, WHC-SD-ER-202.)

Transfer coefficients for energy and mass:

$$C1 := 0.156 \cdot Ka \cdot \left(\alpha \cdot \frac{\nu}{g}\right)^{-\frac{1}{3}}$$

$$C2 := C1 \cdot Da \cdot \frac{\rho_{air}}{Ka}$$

Defines the mass fraction variable Y as a function of temperature and vapor density:

$$p_V(T) := \frac{\rho_V(T)}{Mw} \cdot R \cdot T$$

$$y(T) := \frac{p_V(T)}{Patm} \cdot \frac{Mw}{Ma}$$ maximum

$C1 = 12.548 \cdot \frac{watt}{m^2 \cdot K}$ $C2 = 0.01491 \cdot kg \cdot m^{-2} \cdot sec^{-1}$

$Ta := (Tk + Ta) \cdot K$ $Tc := (Tk + Tc) \cdot K$ $Tg := (Tk + Tg) \cdot K$ $Ts := (Tk + Ts) \cdot K$ $Td := (Tk + Td) \cdot K$

$Ta = 285.16 \cdot K$ $Tc = 299.66 \cdot K$ $Tg = 299.76 \cdot K$ $Ts = 300.36 \cdot K$ $Td = 325.66 \cdot K$

$To := (Tk + To) \cdot K$ $Tcc := Tc$ $Tgg := Tg$ $Tss := Ts$ saves temps to constrain

Cover temp set assuming entire heat conducted out top

$$Tc := To + f_{surf} Q \cdot \frac{Lsoil}{Ksoil}$$ $hsoil := \frac{Ksoil}{Lsoil}$ soil cover transfer coeff

$\frac{Tc}{1 \cdot K} - Tk = 26.51214$ <-new estimate of ceiling temp--> $Tc = 299.67214 \cdot K$

$Hd := RHd$ $Hs := .55$ $Hg := .55$ $Hc := .55$ <--Relative humidity fractions

$Hd = 0.6$ $Hs := Hd_0$ $Hg := Hd_0$ $Hc := Hd_0$ $Ha := 0.54$ <--air outside

Water vapor concentrations

$Cd := Hd \cdot \rho_V(Td)$ $Cs := Hs \cdot \rho_V(Ts)$ $Cg := Hg \cdot \rho_V(Tg)$ $Cc := Hc \cdot \rho_V(Tc)$

$Ys := Hs \cdot y(Ts)$ $Yg := Hg \cdot y(Tg)$ $Yc := Hc \cdot y(Tc)$

$(Cd > Cs) = 1$ $(Ys > Yg) = 1$ $(Yg > Yc) = 1$ <check mass flow direction: No = 0

Define u as $u := \frac{Ma - Mw}{Mw}$ Transfer coefficients defined below:

$$Gc := \left|\frac{Tg - Tc}{Tg}\right| + u \cdot |Yg - Yc|$$ $$Gs := \left|\frac{Ts - Tg}{Tg}\right| + u \cdot |Ys - Yg|$$

$hcc := C1 \cdot Gc^{\frac{1}{3}}$ convection $hcs := C1 \cdot Gs^{\frac{1}{3}}$

$$hrc := \frac{\varepsilon}{2 - \varepsilon} \cdot \sigma \cdot \left(\frac{Ts^4 - Tc^4}{Tg - Tc}\right)$$ radiation $$hrs := \frac{\varepsilon}{2 - \varepsilon} \cdot \sigma \cdot \left(\frac{Ts^4 - Tc^4}{Ts - Tg}\right)$$ equal ε case

$hc := hcc + hrc$ heat $hs := hcs + hrs$

$hmc := C2 \cdot Gc^{\frac{1}{3}}$ mass $hms := C2 \cdot Gs^{\frac{1}{3}}$

CHECKS TRANSFER RATES BELOW

$\eta := 0.834$ <--enhancement factor for vapor diffusion 0.834

$hmd := \frac{\eta \cdot D}{\Delta Z}$ vapor diffusion transfer coeff through waste

$hd := \frac{Kwaste}{\Delta Z}$ heat transfer coeff through waste

$hd = 0.14752 \cdot kg \cdot sec^{-3} \cdot K^{-1}$

$Ca := Ha \cdot \rho_V(Ta)$ water vapor concentration in outside air

$fo := \frac{Fo}{A}$ air flow per unit surface area

Mass and heat transfer rate equations:

$Wd := hmd \cdot (Cd - Cs)$

$Qd := hd \cdot (Td - Ts) + Lheat \cdot Wd$ from waste depth to surface

$Ws := hms \cdot (Ys - Yg)$ $Ws := h_D \cdot (Cs - Cg)_n$ <-alternate surface transfer

$Qs := hs \cdot (Ts - Tg) + Lheat \cdot Ws$ from surface to gas

$Wc := hmc \cdot (Yg - Yc)$

$Qc := hc \cdot (Tg - Tc) + Lheat \cdot Wc$ from gas to tank cover

$Qg := Qs - Qc - ha \cdot (Tg - Ta)$ $ha := \rho_a(Ta) \cdot Sa \cdot fo$ <- air heat transfer coeff via heat capacity

$Wo := (Cg - Ca) \cdot fo$

$Qo := ha \cdot (Tg - Ta) + Lheat \cdot Wo$ from gas to outside

$Lheat \cdot Wd = 0.37608 \cdot \frac{watt}{m^2}$ $Lheat \cdot Ws = 1.98334 \cdot \frac{watt}{m^2}$ $Lheat \cdot Wo = 0.003 \cdot \frac{watt}{m^2}$

$Lheat \cdot (Wc + Wo) = 0.15331 \cdot \frac{watt}{m^2}$

$Qd = 4.10833 \cdot \frac{watt}{m^2}$ $Qs = 6.41821 \cdot \frac{watt}{m^2}$

$Qc + Qo = 3.67925 \cdot \frac{watt}{m^2}$ to equal $f_{surf} Q = 3.2839 \cdot \frac{watt}{m^2}$

$Qc = 3.67343 \cdot \frac{watt}{m^2}$ $Qo = 0.00582 \cdot \frac{watt}{m^2}$ $Qg = 2.74196 \cdot \frac{watt}{m^2}$

Calculating atmospheres of vapor partial pressure: $T_G := (Tk + 20) \cdot K$

$p_{sv} := \frac{R \cdot Tg}{Mw} \cdot \rho_V(T_G)$ $T_G = 293.16 \cdot K$ $Hg = 0.55$

$RHg := 1$

$p_{sv} = 2.39202 \cdot 10^3 \cdot Pa$

$\frac{p_{sv}}{Patm} \cdot RHg = 0.02368$ $\frac{p_{sv}}{Patm} \cdot RHg \cdot 760 = 17.99933$ mm Hg or torr

$$Fs(Ts,Tg,Cs,Cg) := \left[\frac{Ts-Tg}{Tg} + u\cdot\left(\frac{Cs}{\rho_a(Ts)} - \frac{Cg}{\rho_a(Tg)}\right)\right]^{\frac{1}{3}}$$

transfer functions in terms of water vapor concentration

$$Fc(Tg,Tc,Cg,Cc) := \left[\frac{Tg-Tc}{Tg} + u\cdot\left(\frac{Cg}{\rho_a(Tg)} - \frac{Cc}{\rho_a(Tc)}\right)\right]^{\frac{1}{3}}$$

$$Fs(Ts,Tg,Ys,Yg) := \left(\left|\frac{Ts-Tg}{Tg}\right| + u\cdot|Ys-Yg|\right)^{\frac{1}{3}}$$

In terms of mass fraction Y

$$Fc(Tg,Tc,Yg,Yc) := \left(\left|\frac{Tg-Tc}{Tg}\right| + u\cdot|Yg-Yc|\right)^{\frac{1}{3}}$$

Emissivities: $\varepsilon = 0.9$

surface	gas	cover	
$\varepsilon_s := .8$	$\varepsilon_g := 0.2$	$\varepsilon_c := .8$	<-set emissivities here

$$f_s := \frac{1-\varepsilon_s}{\varepsilon_s} \qquad f_c := \frac{1-\varepsilon_c}{\varepsilon_c}$$

$$Res := f_s + f_c + \frac{1}{1-\frac{\varepsilon_g}{2}}$$

$$b_s := \frac{1}{2}\cdot\left(1 + \frac{f_c - f_s}{Res}\right) \qquad b_c := \frac{1}{2}\cdot\left(-1 + \frac{f_c - f_s}{Res}\right)$$

$b_s = 0.5$ $\quad Res = 1.61111$ $\quad b_c = -0.5$

radiation heat transfer

$$Fr(Ts,Tc) := \frac{\sigma}{Res}\cdot\left(Ts^4 - Tc^4\right)$$

additional radiation from excess heat in head space gas is included in other balance equations

transfer coefficients

$hfs(Ts,Tg,Ys,Yg) := C1\cdot Fs(Ts,Tg,Ys,Yg)$

$hfc(Tg,Tc,Yg,Yc) := C1\cdot Fc(Tg,Tc,Yg,Yc)$

Heat

$hfms(Ts,Tg,Ys,Yg) := C2\cdot Fs(Ts,Tg,Ys,Yg)$

$hfmc(Tg,Tc,Yg,Yc) := C2\cdot Fc(Tg,Tc,Yg,Yc)$

Mass

Solving mass transfer equations $TOL := 10^{-10}$

$w := Wd$ Assumes known temperatures to find RH

Given

$hmd \cdot (Cd - \rho_a(Ts) \cdot Ys) - w = 0$

$hfms(Ts, Tg, Ys, Yg) \cdot (Ys - Yg) - w = 0$ $Ys > Yg$

$h_D \cdot (\rho_a(Ts) \cdot Ys - \rho_a(Tg) \cdot Yg) - w = 0$ <-eddy diffusion alternative when ventilation active

$hfmc(Tg, Tc, Yg, Yc) \cdot (Yg - Yc) + (\rho_a(Tg) \cdot Yg - Ca) \cdot fo - w = 0$

$y(Tc) \cdot Hc - Yc = 0$

$$\begin{bmatrix} w \\ YYs \\ YYg \\ YYc \end{bmatrix} := Find(w, Ys, Yg, Yc)$$

$YYs = 0.01184$

$YYg = 0.01176$

$YYc = 0.01161$

$w = 1.5829 \cdot 10^{-7} \cdot kg \cdot m^{-2} \cdot sec^{-1}$

replaces old Y with new:

$RHd = 0.6$

$Ys := YYs$

$Yg := YYg$

$Yc := YYc$

RH's: $\frac{YYs}{y(Ts)} = 0.53386$ $\frac{YYg}{y(Tg)} = 0.5491$ $\frac{YYc}{y(Tc)} = 0.54513$

<-Turn replacement off if RH are held as given

$Qg := 0 \cdot Qg$ $X := 0$

Solving heat transfer equations

Finds temperatures given RHs

Given

$hd \cdot (Td - Ts) + Lheat \cdot w - Q = 0$

$Qg - (1 - f_{surf}) \cdot Q = 0$ heat exits via gas - or $Qg = 0$ no heat from gas

$hfs(Ts, Tg, Ys, Yg) \cdot (Ts - Tg) + Lheat \cdot w + Fr(Ts, Tc) + b_s \cdot Qg - Q = 0$

$hfc(Tg, Tc, Yg, Yc) \cdot (Tg - Tc) + Lheat \cdot w + Fr(Ts, Tc) + b_c \cdot Qg + ha \cdot (Tg - Ta) - Q \cdot f_{surf} = 0$

$hsoil \cdot (Tc - To) + Lheat \cdot (\rho_a(Tg) \cdot Yg - Ca) \cdot fo + ha \cdot (Tg - Ta) - Q \cdot f_{surf} = 0$

$Hc \cdot y(Tc) - Yc = 0$

$X = 0$

$$\begin{bmatrix} Ts' \\ Tg' \\ Tc' \\ Qg \\ Q' \\ X \end{bmatrix} := \text{Find}(Ts, Tg, Tc, Qg, Q, X)$$

	previous	new
	$Ts = 300.36 \cdot K$	$Ts' = 300.38822 \cdot K$
	$Tg = 299.76 \cdot K$	$Tg' = 299.78879 \cdot K$
	$Tc = 299.67214 \cdot K$	$Tc' = 299.65895 \cdot K$
Assumes RH is known or found from above with given temperatures	$Q = 4.10488 \cdot \frac{watt}{m^2}$	$Q' = 4.10798 \cdot \frac{watt}{m^2}$

New RH's $\frac{Ys}{y(Ts')} = 0.53298$ $\frac{Yg}{y(Tg')} = 0.54817$ $\frac{Yc}{y(Tc')} = 0.54556$

Replace old temp $Qg = 0 \cdot \frac{watt}{m^2}$ $Fr(Ts', Tc') + b_s \cdot Qg = 2.7725 \cdot \frac{watt}{m^2}$

$Ts := Ts'$

$Tg := Tg'$

$Tc := Tc'$

Solving mass and heat transfer equations coupled $TOL = 1 \cdot 10^{-10}$

$QQ := Q$ saves initial Q $TOL := 10^{-12}$ * NOTE

Given

$hmd \cdot (Cd - \rho_a(Ts) \cdot Ys) - w = 0$ <<moisture mass flow balance eqs

$hfms(Ts, Tg, Ys, Yg) \cdot (Ys - Yg) - w = 0$

$h_D \cdot (\rho_a(Ts) \cdot Ys - \rho_a(Tg) \cdot Yg) - w = 0$ <-eddy diffusion alternative when ventilation active

$hfmc(Tg, Tc, Yg, Yc) \cdot (Yg - Yc) \cdot \Phi(Yg - Yc) + (\rho_a(Tg) \cdot Yg - Ca) \cdot fo - w = 0$

$hd \cdot (Td - Ts) + Lheat \cdot w - Q = 0$ <<heat flow balance eqs

$Qg - (1 - f_{surf}) \cdot Q = 0$ heat exits via gas - or $Qg = 0$ no heat from gas

$hfs(Ts, Tg, Ys, Yg) \cdot (Ts - Tg) + Lheat \cdot w + Fr(Ts, Tc) + b_s \cdot Qg - Q = 0$

$hfc(Tg, Tc, Yg, Yc) \cdot (Tg - Tc) + Lheat \cdot w + Fr(Ts, Tc) + b_c \cdot Qg + ha \cdot (Tg - Ta) - Q \cdot f_{surf} = 0$

$hsoil \cdot (Tc - To) + Lheat \cdot (\rho_a(Tg) \cdot Yg - Ca) \cdot fo + ha \cdot (Tg - Ta) - Q \cdot f_{surf} = 0$ <- adjusts Tc for heat loss

$Ys > 0$ $Yg > 0$ $Yc > 0$

$Tss - Ts = 0$ $Tgg - Tg = 0$ $Tcc - Tc = 0$ constrains temps

$y(Tc) \cdot Hc - Yc = 0$ $y(Tg) \cdot Hg - Yg = 0$ constrains RH for cover or gas

$Q - QQ = 0$ constrains heat load as if known

$$\begin{bmatrix} w \\ Q \\ Ys \\ Yg \\ Yc \\ Ts \\ Tg \\ Tc \\ Qg \end{bmatrix} := \text{Find}(w, Q, Ys, Yg, Yc, Ts, Tg, Tc, Qg)$$

$w \cdot A \cdot (1 \cdot yr) = 2.02331 \cdot 10^3 \cdot kg$

$Ys = 0.01227$

$Yg = 0.01219$

$Yc = 0.01206$

$Td = 325.66 \cdot K$

$Ts = 300.37821 \cdot K$

$Tg = 299.77896 \cdot K$

$Tc = 299.64836 \cdot K$

$Lheat \cdot w = 0.37531 \cdot \frac{watt}{m^2}$ evaporation transfer

$Q = 4.10488 \cdot \frac{watt}{m^2}$ total heat transfer

$Lheat \cdot \frac{w}{Q} \cdot 100 = 9.14313$ percent latent heat transfer

$Td - Tk \cdot K = 52.5 \cdot K$ $Ts - Tk \cdot K = 27.21821 \cdot K$ $Tg - Tk \cdot K = 26.61896 \cdot K$ $Tc - Tk \cdot K = 26.48836 \cdot K$

Relative Humidity $RHs := \frac{Ys}{y(Ts)}$ $RHg := \frac{Yg}{y(Tg)}$ $RHc := \frac{Yc}{y(Tc)}$

$RHd = 0.6$ $RHs = 0.55268$ $RHg = 0.56861$ $RHc = 0.5669$

Emissivities $\varepsilon_s = 0.8$ $\varepsilon_g = 0.2$ $\varepsilon_c = 0.8$

Diffusion enhancement $\eta = 0.834$

Check solution:

$hd \cdot (Td - Ts) + Lheat \cdot w = 4.10488 \cdot \frac{watt}{m^2}$ final value $Q = 4.10488 \cdot \frac{watt}{m^2}$

$Fo = 2 \cdot 10^3 \cdot \frac{m^3}{yr}$ flow rate initial value $QQ = 4.10488 \cdot \frac{watt}{m^2}$

$Wo := (\rho_a(Tg) \cdot Yg - Ca) \cdot fo$ moisture outflow

$Lheat \cdot Wo + ha \cdot (Tg - Ta) = 0.006 \cdot \frac{watt}{m^2}$ vented amount of heat

$ha \cdot (Tg - Ta) = 0.00282 \cdot \frac{watt}{m^2}$ transfer by heat capacity

$Wo \cdot A \cdot (1 \cdot yr) = 17.14161 \cdot kg$ external loss in one year

$w \cdot A \cdot (1 \cdot yr) = 2.02331 \cdot 10^{3} \cdot kg$ internal cycle per year

$hfmc(Tg, Tc, Yg, Yc) \cdot (Yg - Yc) \cdot \Phi(Yg - Yc) + Wo = 1.56381 \cdot 10^{-7} \cdot kg \cdot m^{-2} \cdot sec^{-1}$

above should equal moisture flow -> $w = 1.56381 \cdot 10^{-7} \cdot kg \cdot m^{-2} \cdot sec^{-1}$

$Qs := hfs(Ts, Tg, Ys, Yg) \cdot (Ts - Tg) + Lheat \cdot w$

$Qc := hfc(Tg, Tc, Yg, Yc) \cdot (Tg - Tc) + Lheat \cdot (w - Wo)$

$Qs = 1.33045 \cdot \frac{watt}{m^2}$ $Qg = 0 \cdot \frac{watt}{m^2}$ $Qc = 0.50348 \cdot \frac{watt}{m^2}$

$Q - Qs = 2.77443 \cdot \frac{watt}{m^2}$ $Fr(Ts, Tc) + b_s \cdot Qg = 2.77443 \cdot \frac{watt}{m^2}$ radiation heat

$\frac{Q - Qs}{Q} \cdot 100 = 67.58853$ percent radiation heat transfer

$\frac{Qs - Lheat \cdot w}{Q} \cdot 100 = 23.26834$ percent convection transfer

$Lheat \cdot \frac{w}{Q} \cdot 100 = 9.14313$ percent latent heat transfer

Vapor Pressure Conditions:

Depth		Surface	
$(Td - Tk \cdot K) \cdot (1 \cdot K)^{-1} = 52.5$		$Ts - Tk \cdot K = 27.21821 \cdot K$	
$p_{vd} := \frac{R \cdot Td}{Mw} \cdot \rho_v(Td)$	$RHd = 0.6$	$p_{vs} := \frac{R \cdot Ts}{Mw} \cdot \rho_v(Ts)$	$RHs = 0.55268$
$\frac{p_{vd}}{Patm} \cdot RHd \cdot 760 = 63.0209$	mm Hg or torr	$\frac{p_{vs}}{Patm} \cdot RHs \cdot 760 = 15.02513$	mm Hg or torr
$\frac{p_{vd}}{Patm} \cdot RHd = 0.08292$	atmospheres	$\frac{p_{vs}}{Patm} \cdot RHs = 0.01977$	atmospheres

Appendix D

Test Cases for Nonisothermal Moisture Distribution in a Saltcake Waste Tank

N. Aimo

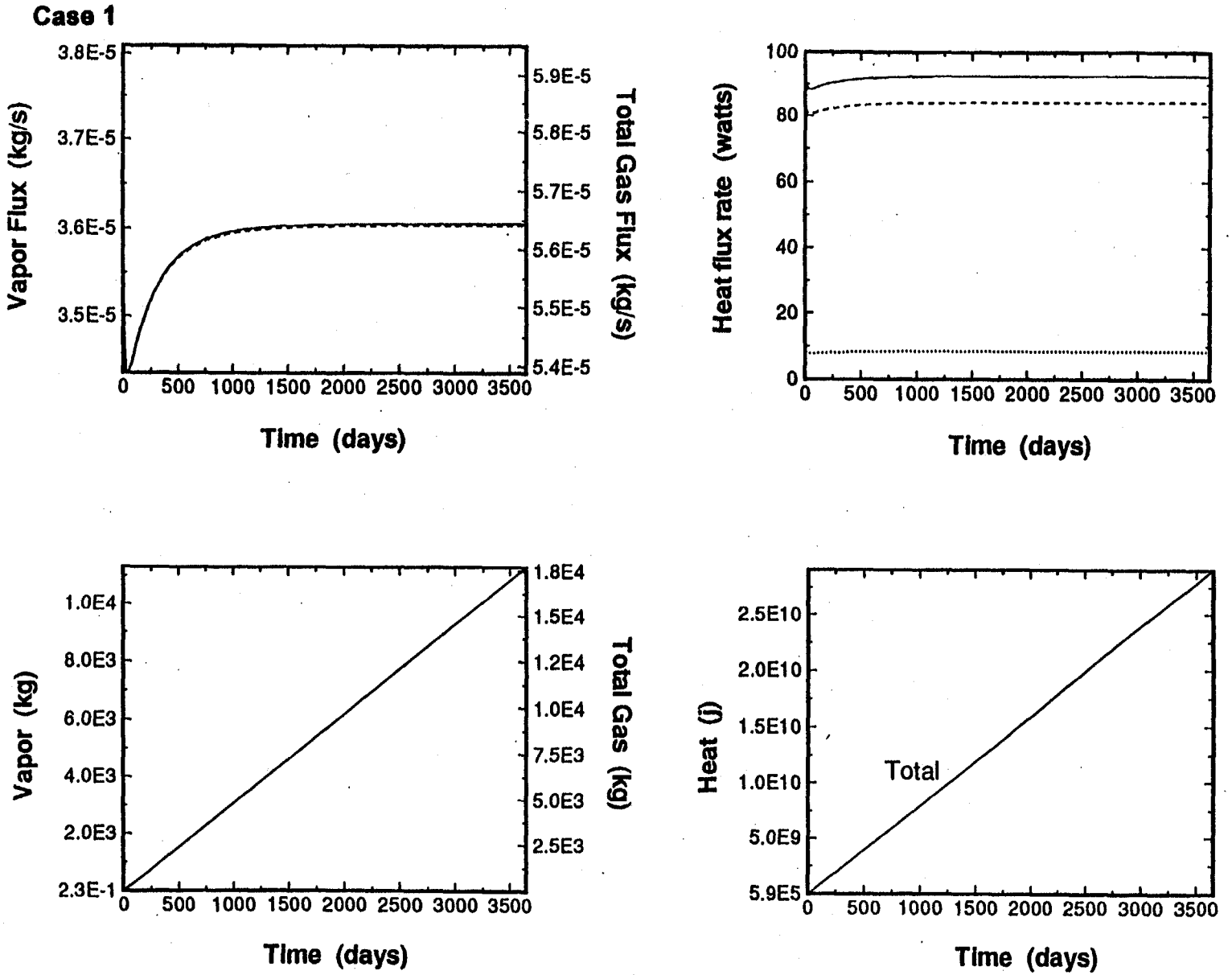

Figure D.1. Vapor and Heat Flux over Time for Test Cases 1 Through 12. For heat flux rate, dashed line is the heat transfer by advection of gas, and dotted line is that by diffusion only of water vapor.

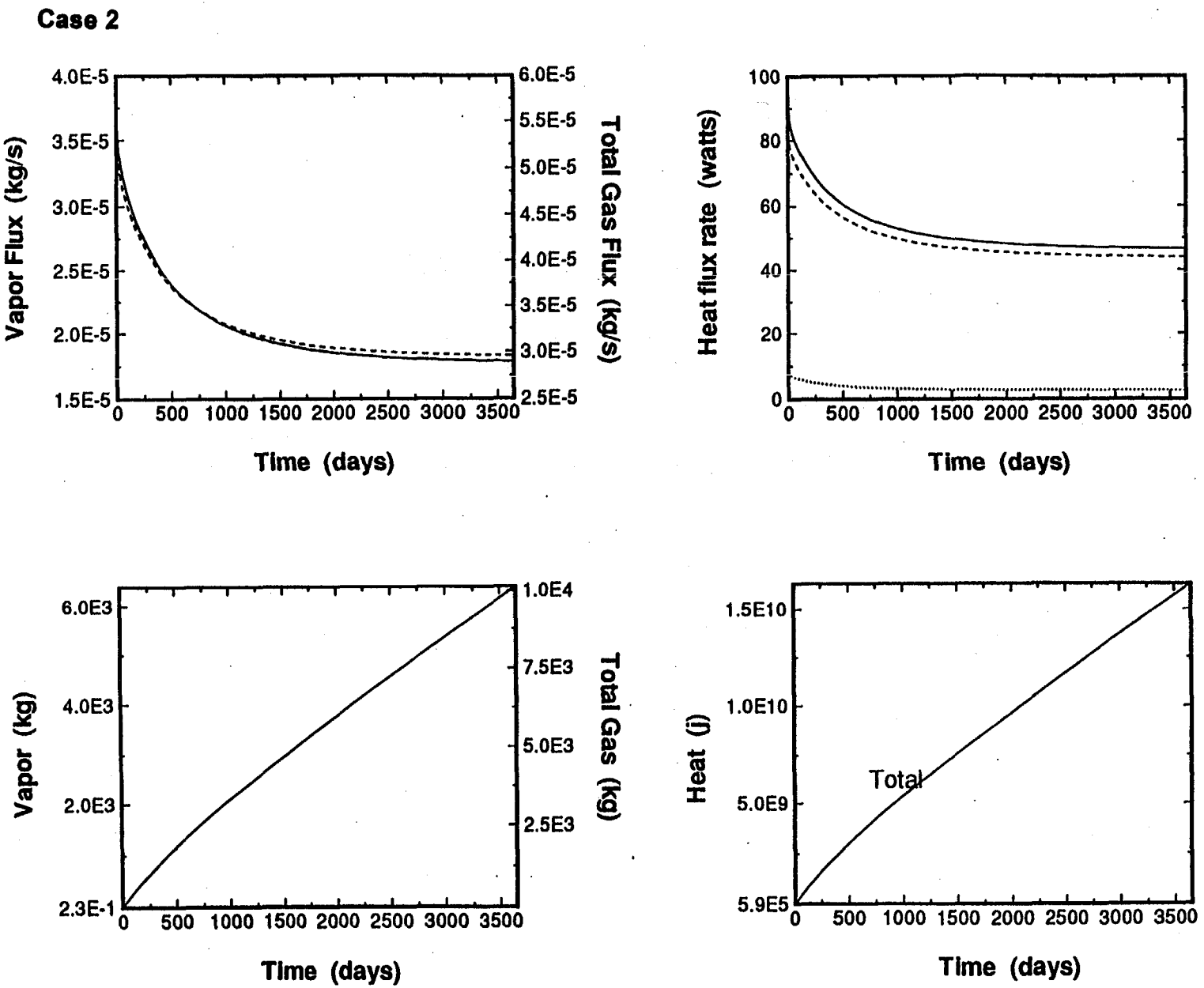

Figure D.1. Vapor and Heat Flux over Time for Test Cases 1 Through 12. For heat flux rate, dashed line is the heat transfer by advection of gas, and dotted line is that by diffusion only of water vapor.

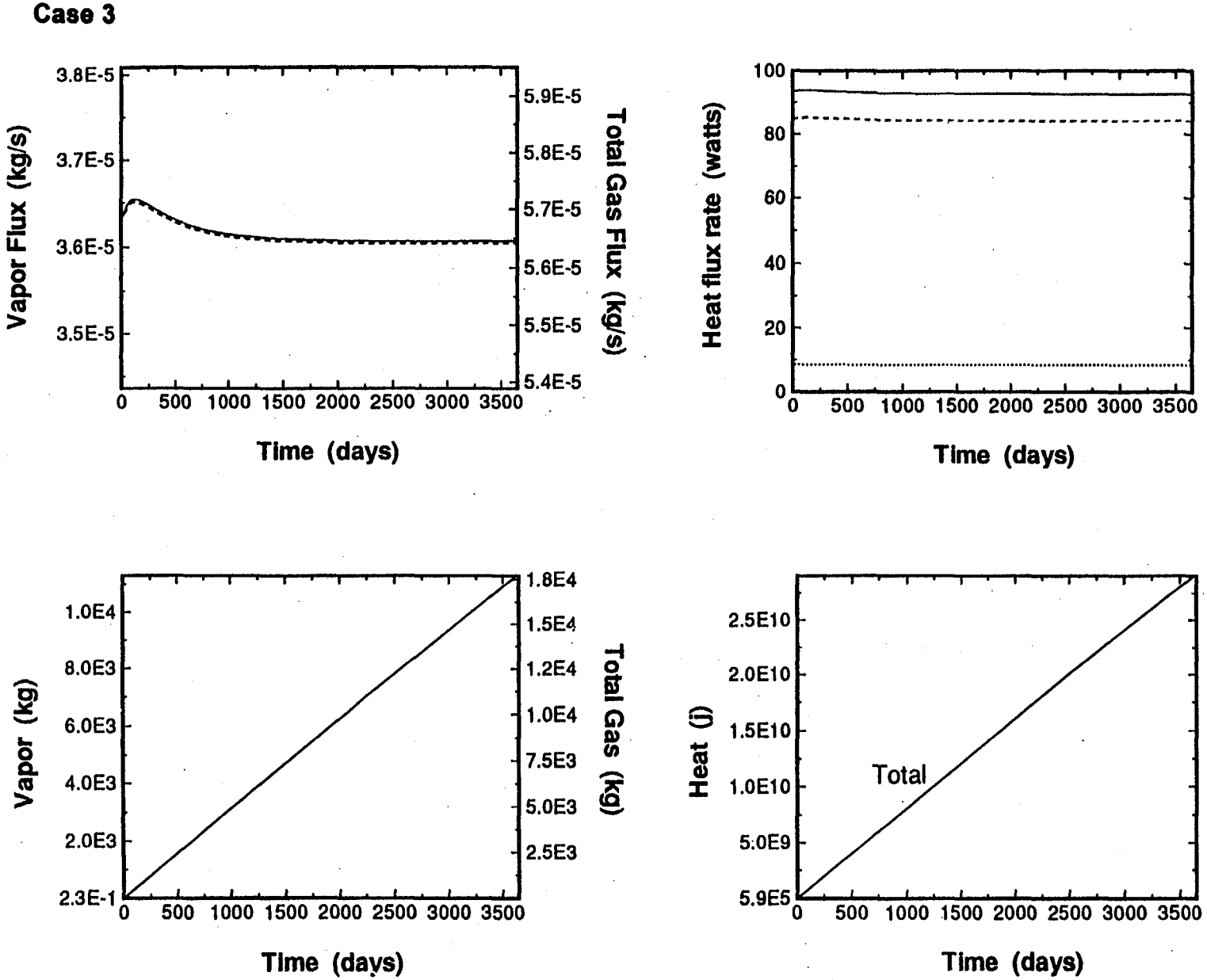

Figure D.1. Vapor and Heat Flux over Time for Test Cases 1 Through 12. For heat flux rate, dashed line is the heat transfer by advection of gas, and dotted line is that by diffusion only of water vapor.

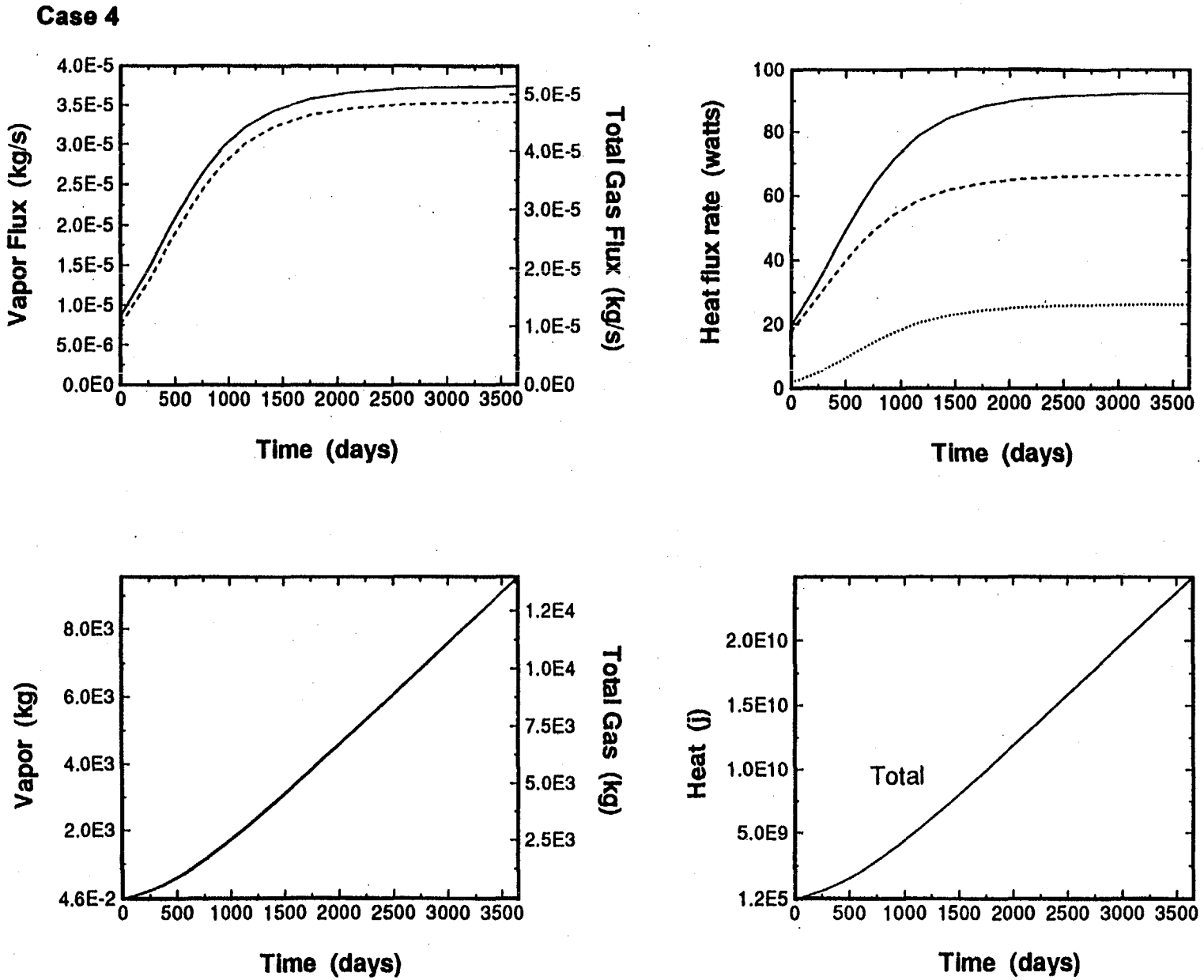

Figure D.1. Vapor and Heat Flux over Time for Test Cases 1 Through 12. For heat flux rate, dashed line is the heat transfer by advection of gas, and dotted line is that by diffusion only of water vapor.

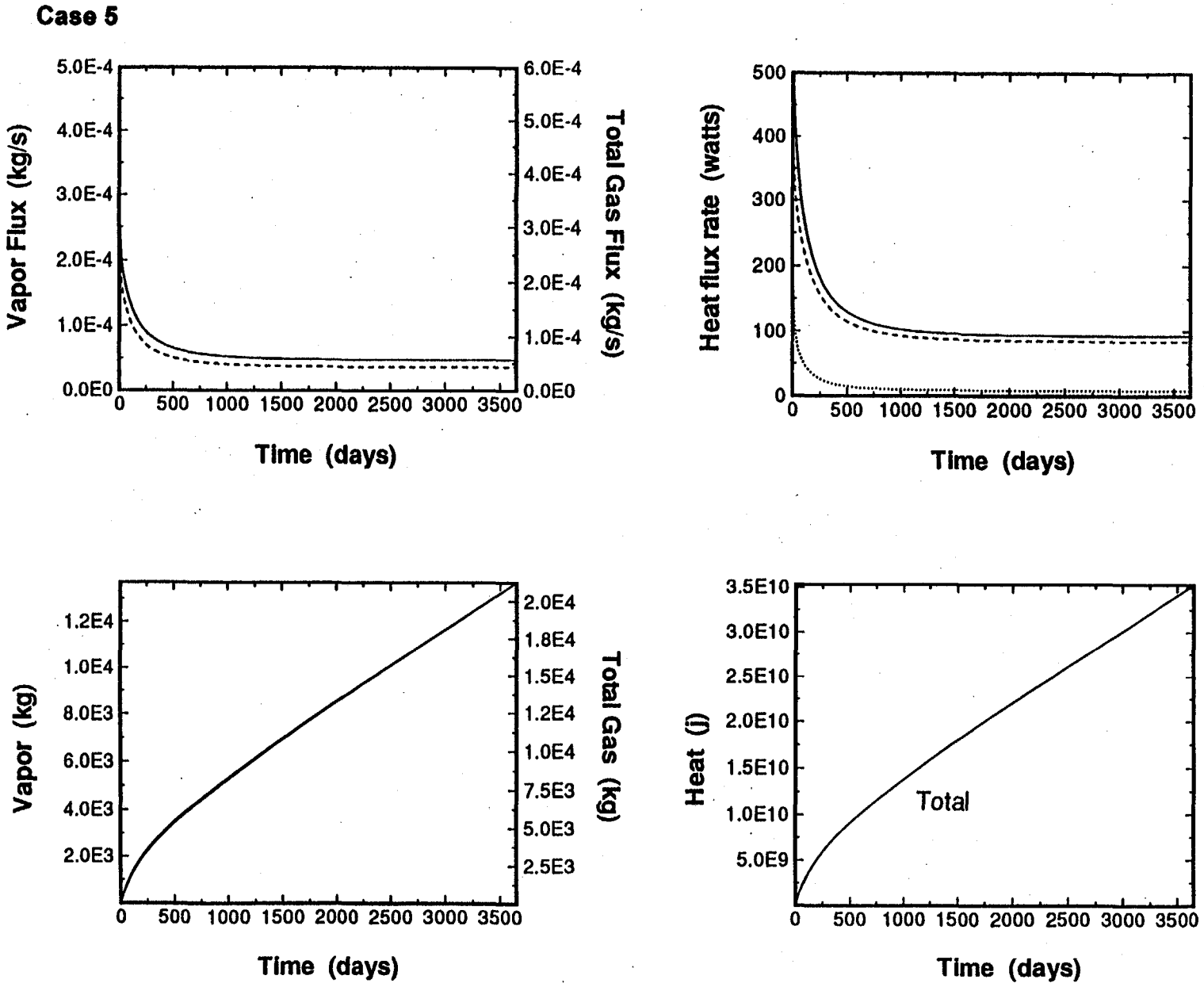

Figure D.1. Vapor and Heat Flux over Time for Test Cases 1 Through 12. For heat flux rate, dashed line is the heat transfer by advection of gas, and dotted line is that by diffusion only of water vapor.

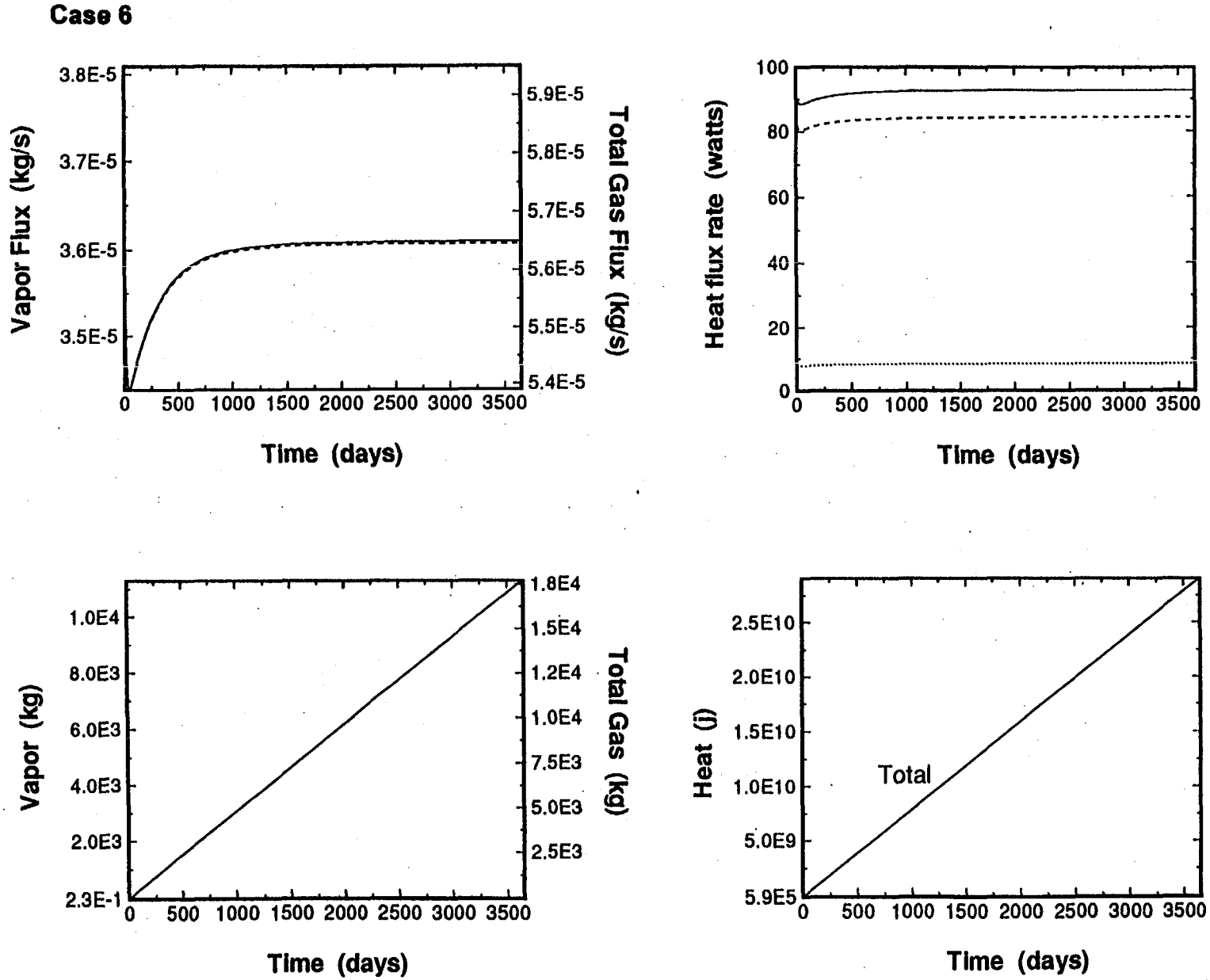

Figure D.1. Vapor and Heat Flux over Time for Test Cases 1 Through 12. For heat flux rate, dashed line is the heat transfer by advection of gas, and dotted line is that by diffusion only of water vapor.

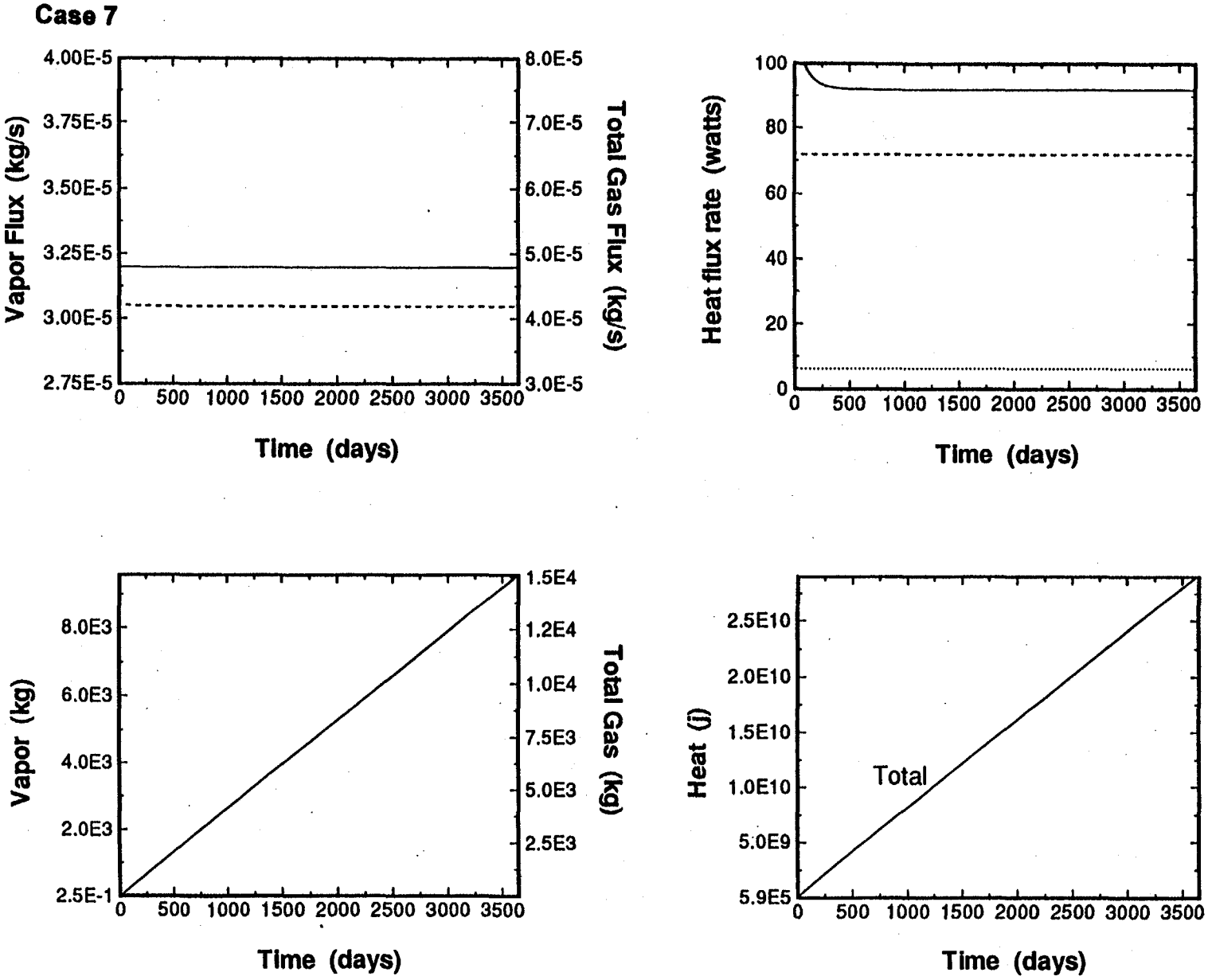

Figure D.1. Vapor and Heat Flux over Time for Test Cases 1 Through 12. For heat flux rate, dashed line is the heat transfer by advection of gas, and dotted line is that by diffusion only of water vapor.

Case 8

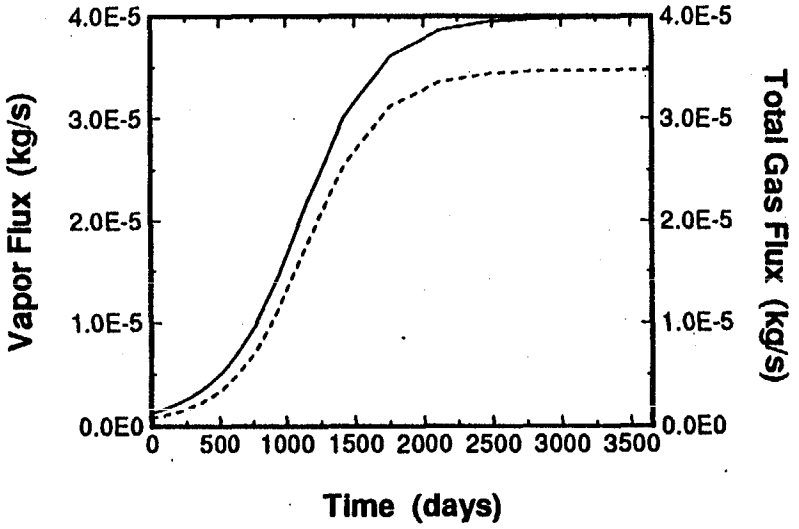

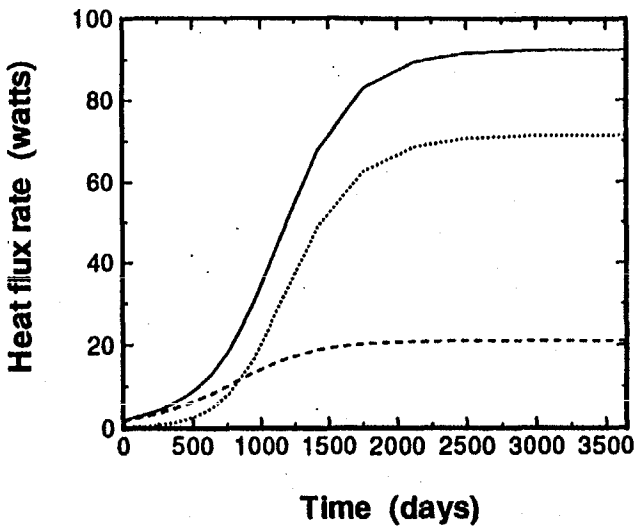

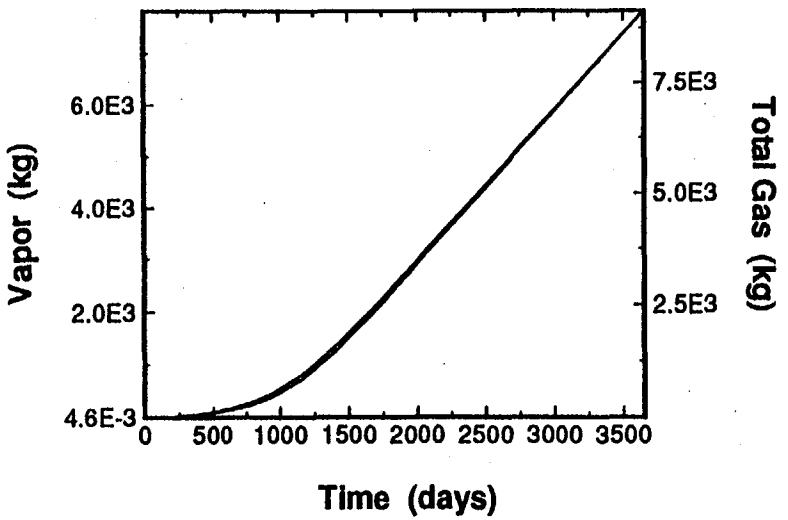

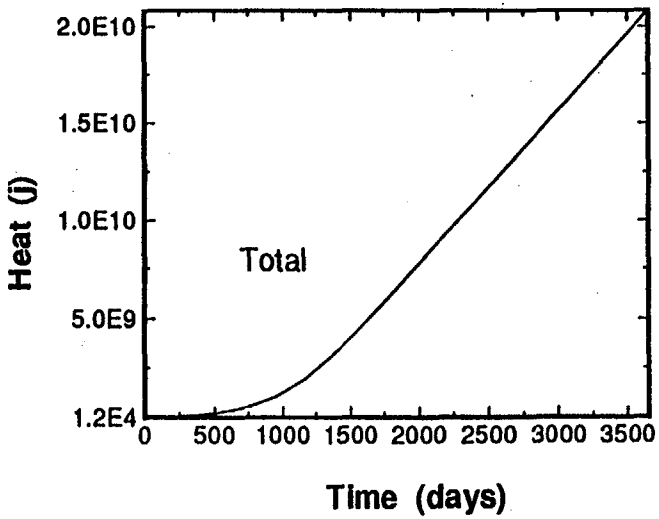

Figure D.1. Vapor and Heat Flux over Time for Test Cases 1 Through 12. For heat flux rate, dashed line is the heat transfer by advection of gas, and dotted line is that by diffusion only of water vapor.

Case 9

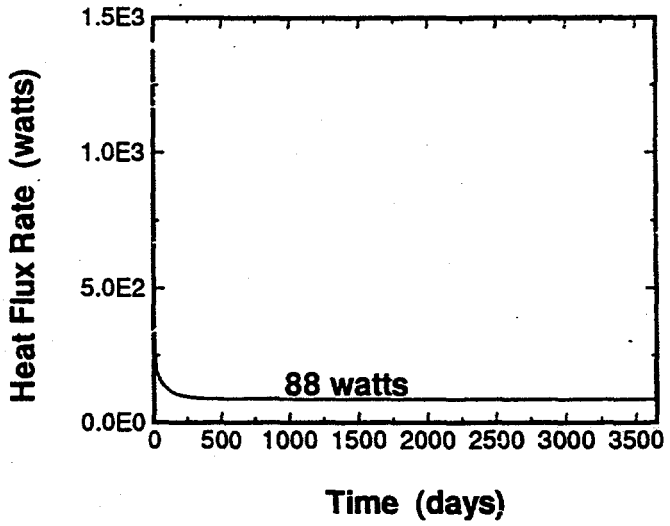

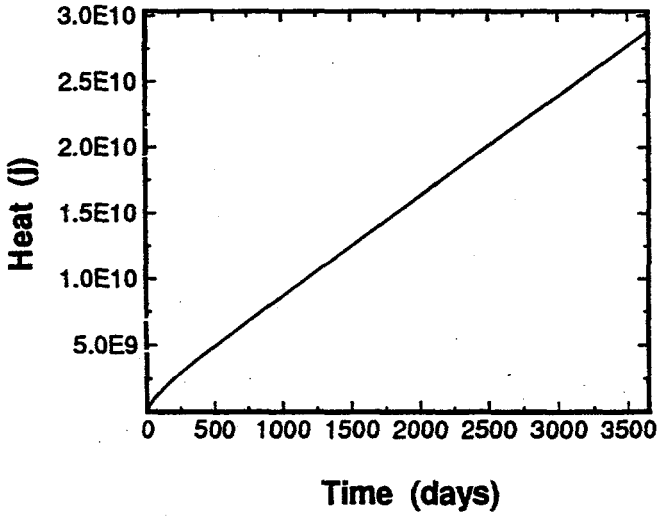

Figure D.1. Vapor and Heat Flux over Time for Test Cases 1 through 12. For heat flux rate, dash line is the heat transfer by advection of gas, and dotted line is that by diffusion only of water vapor.

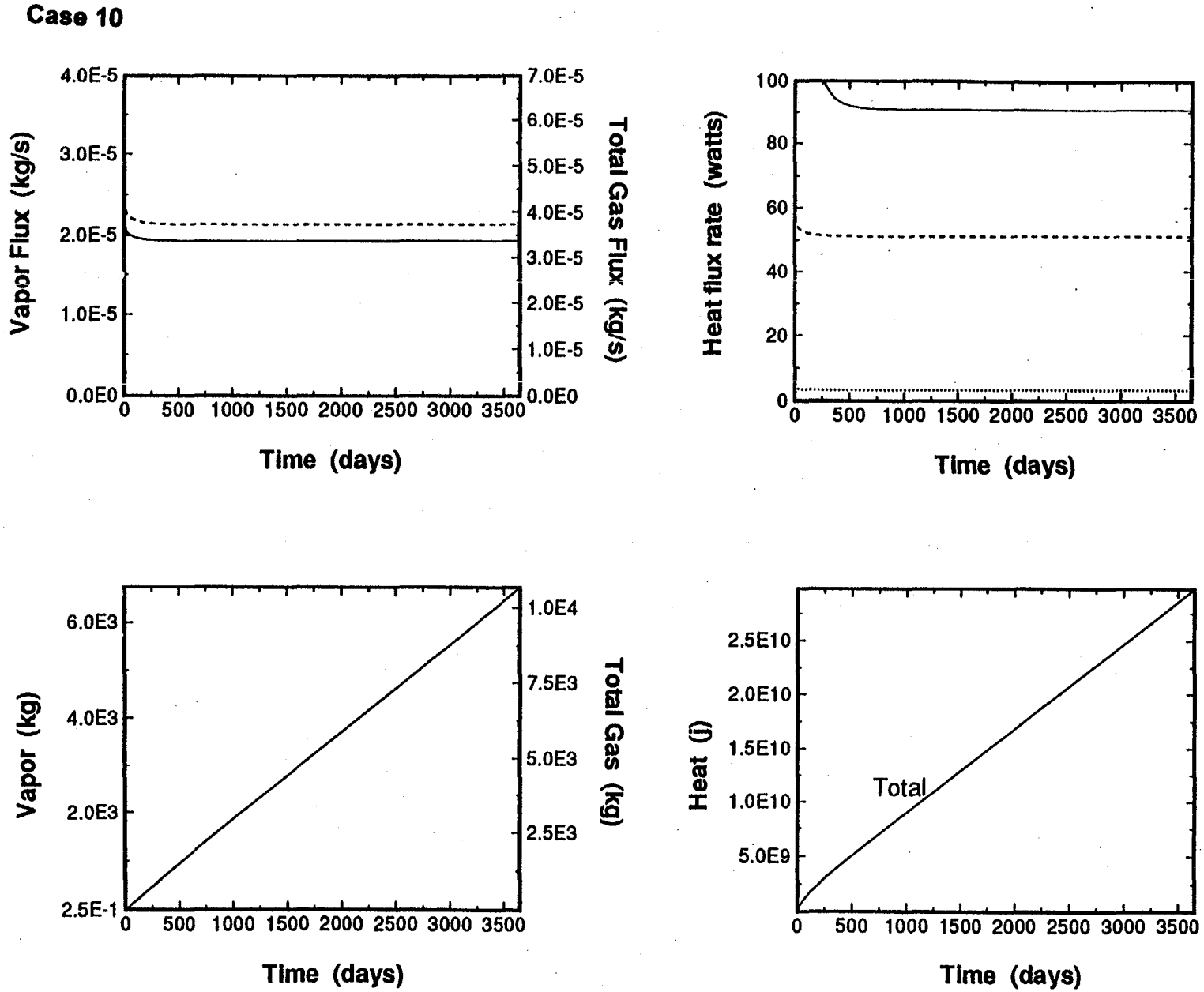

Figure D.1. Vapor and Heat Flux over Time for Test Cases 1 Through 12. For heat flux rate, dashed line is the heat transfer by advection of gas, and dotted line is that by diffusion only of water vapor.

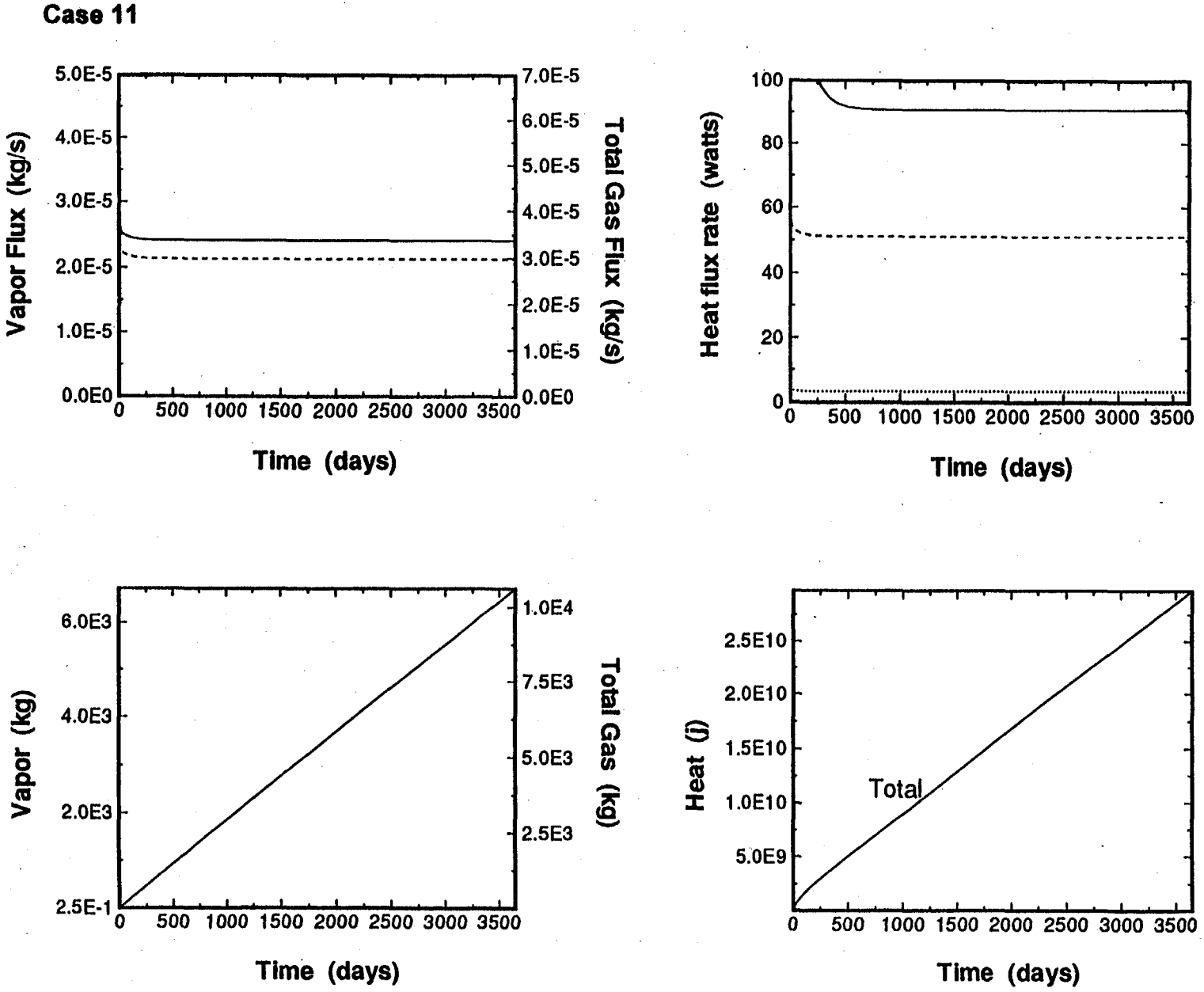

Figure D.1. Vapor and Heat Flux over Time for Test Cases 1 Through 12. For heat flux rate, dashed line is the heat transfer by advection of gas, and dotted line is that by diffusion only of water vapor.

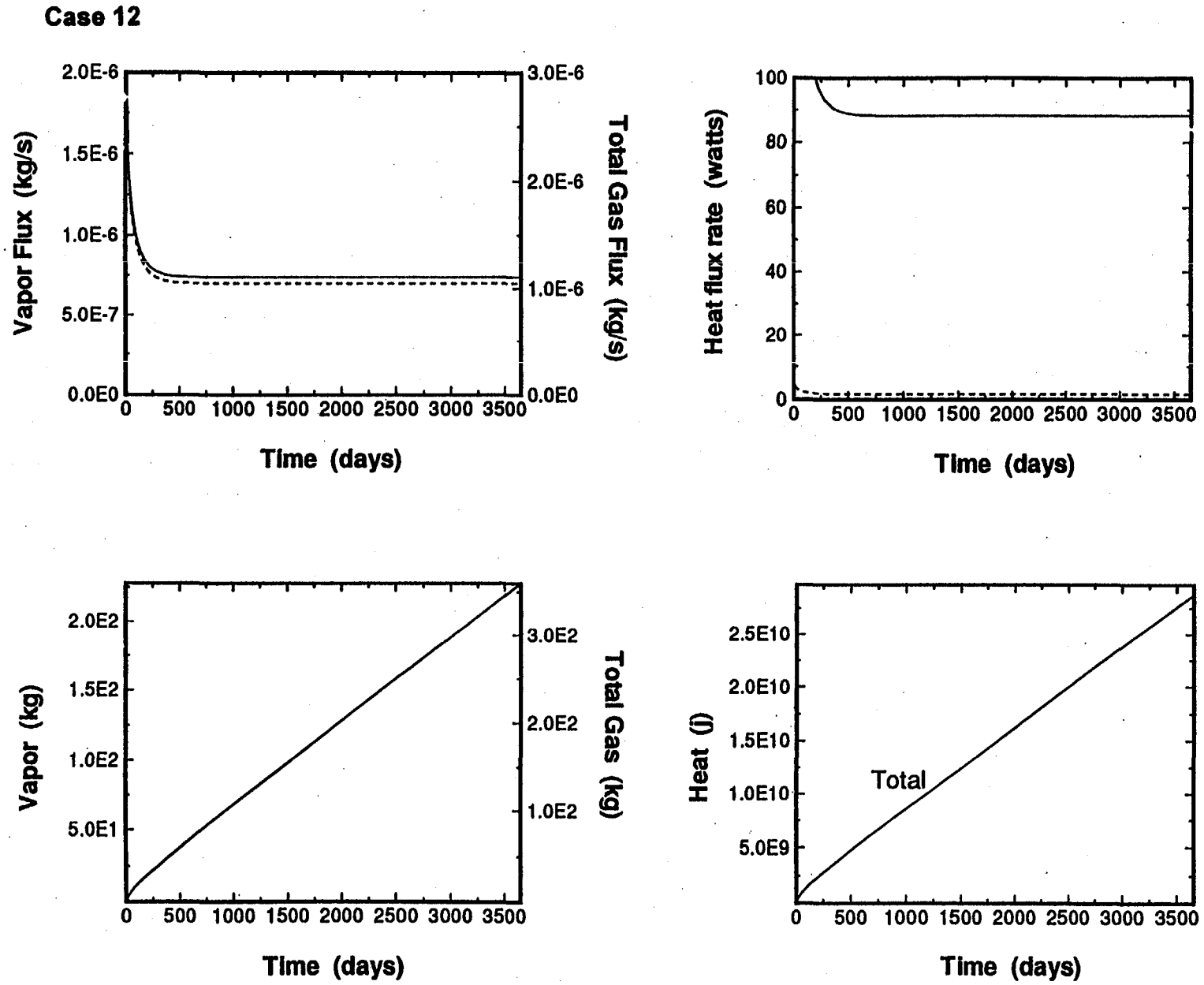

Figure D.1. Vapor and Heat Flux over Time for Test Cases 1 Through 12. For heat flux rate, dashed line is the heat transfer by advection of gas, and dotted line is that by diffusion only of water vapor.

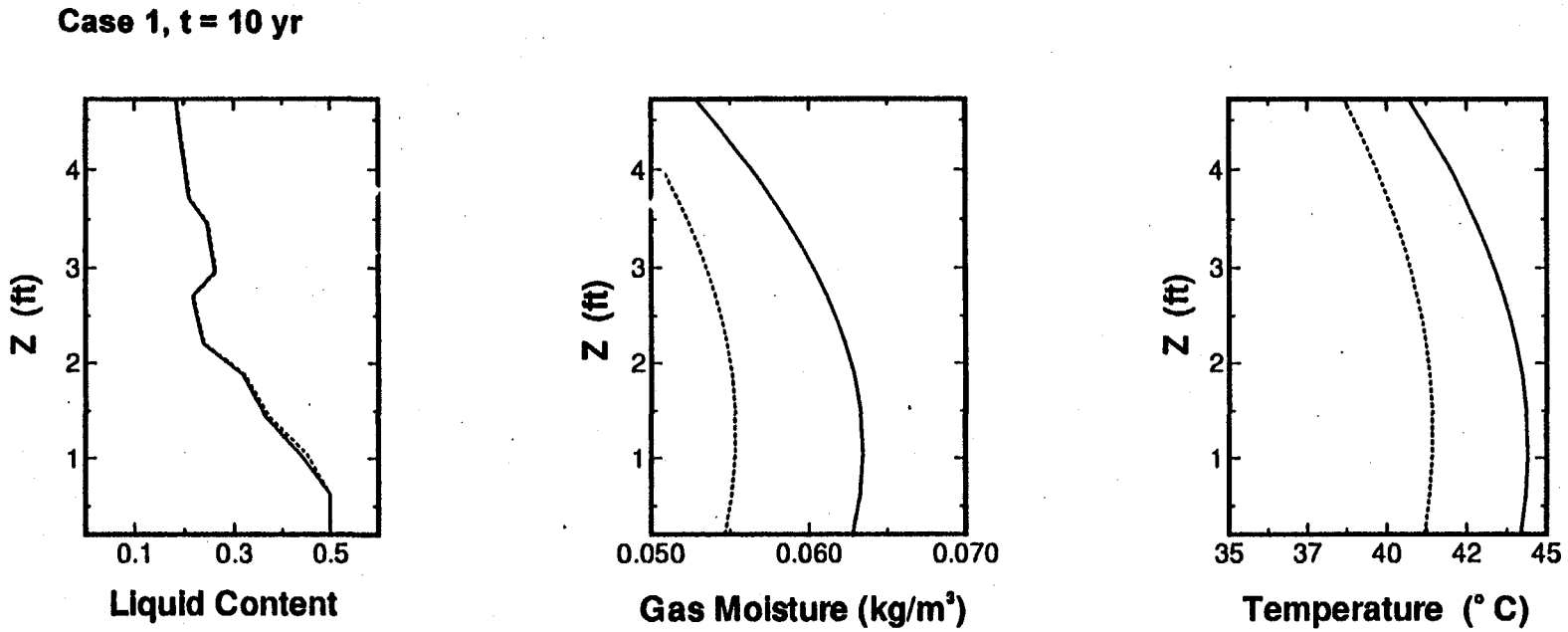

Figure D.2. Liquid Content, Gas Moisture Content, and Temperature Profiles for Test Cases 1 through 12. Solid curve is for radius 4.7 ft, and dotted curve is for radius 30 ft.

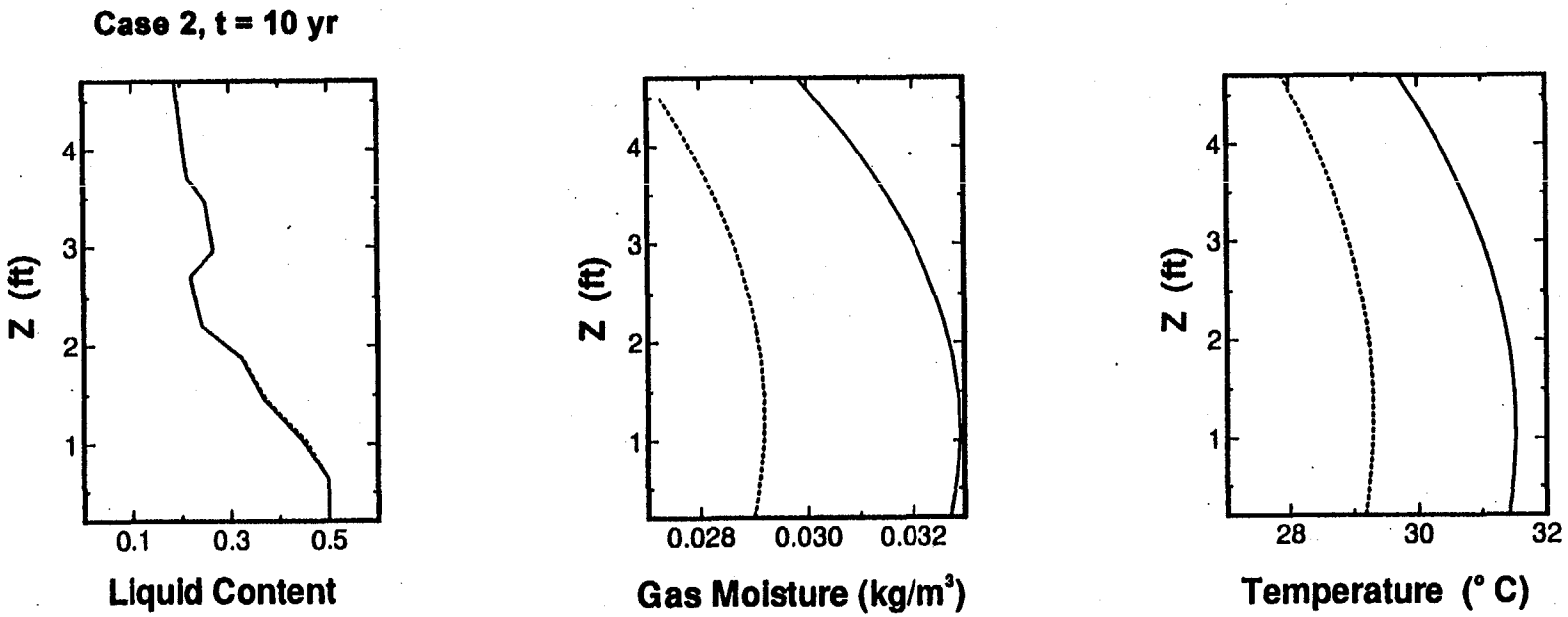

Figure D.2. Liquid Content, Gas Moisture Content, and Temperature Profiles for Test Cases 1 through 12. Solid curve is for radius 4.7 ft, and dotted curve is for radius 30 ft.

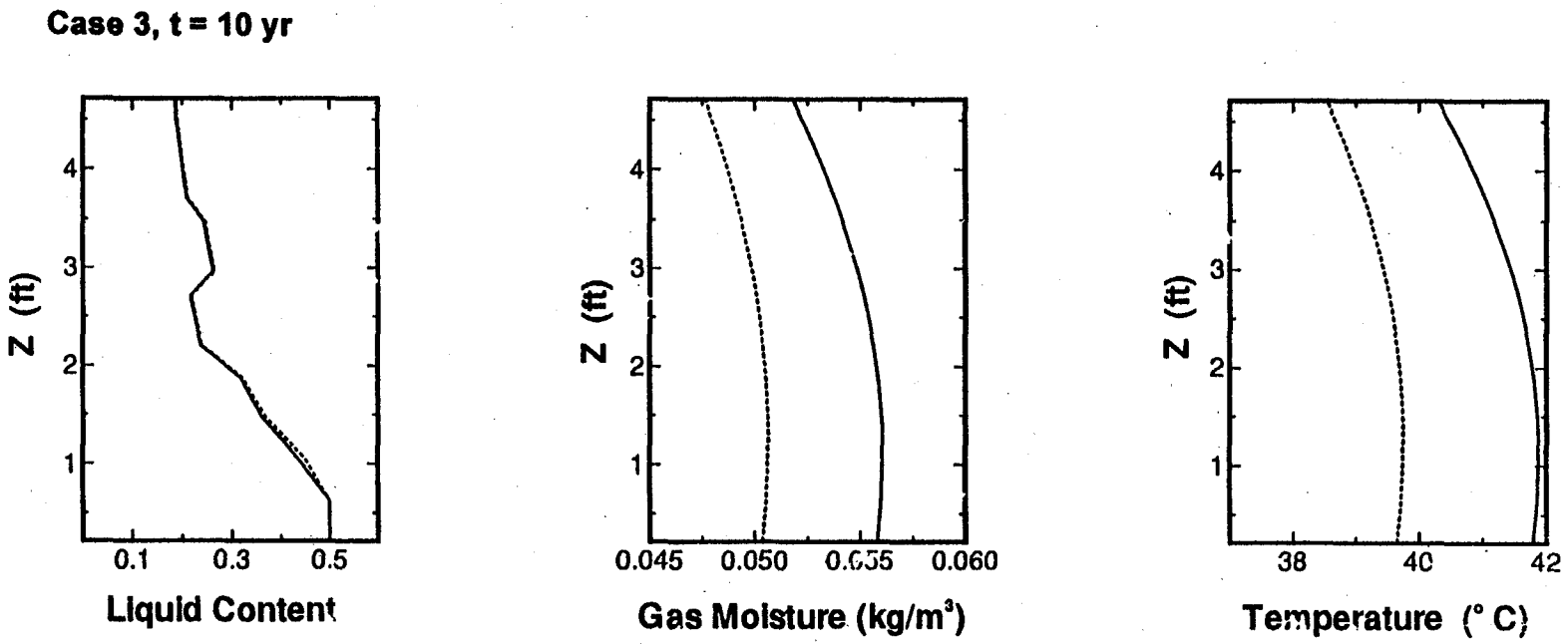

Figure D.2. Liquid Content, Gas Moisture Content, and Temperature Profiles for Test Cases 1 through 12. Solid curve is for radius 4.7 ft, and dotted curve is for radius 30 ft.

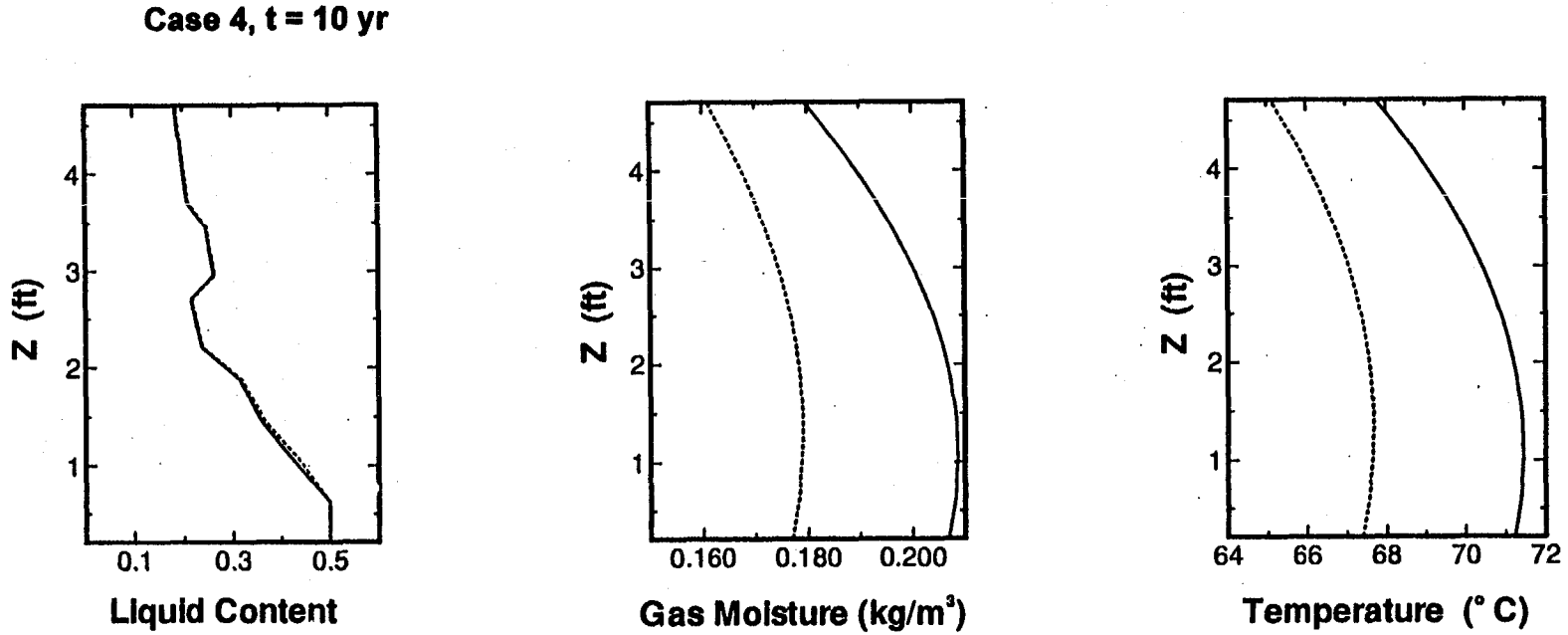

Figure D.2. Liquid Content, Gas Moisture Content, and Temperature Profiles for Test Cases 1 through 12. Solid curve is for radius 4.7 ft, and dotted curve is for radius 30 ft.

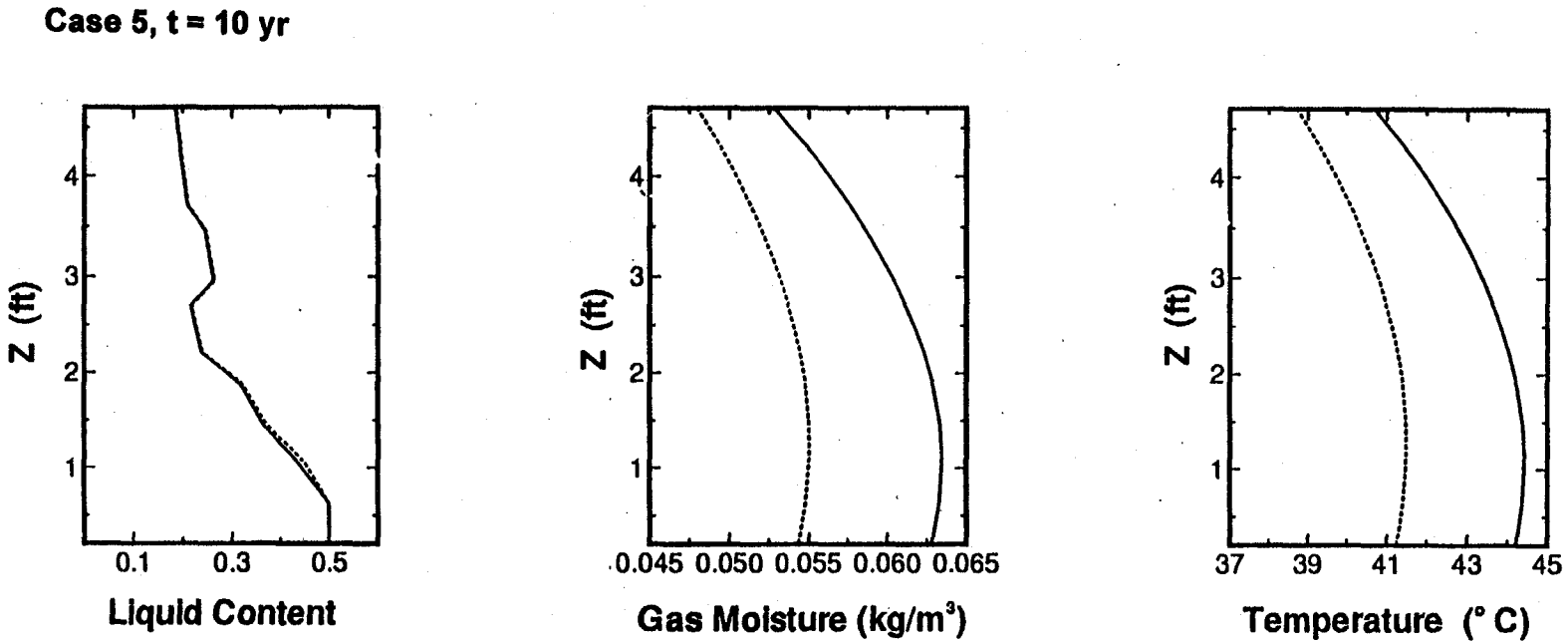

Figure D.2. Liquid Content, Gas Moisture Content, and Temperature Profiles for Test Cases 1 through 12. Solid curve is for radius 4.7 ft, and dotted curve is for radius 30 ft.

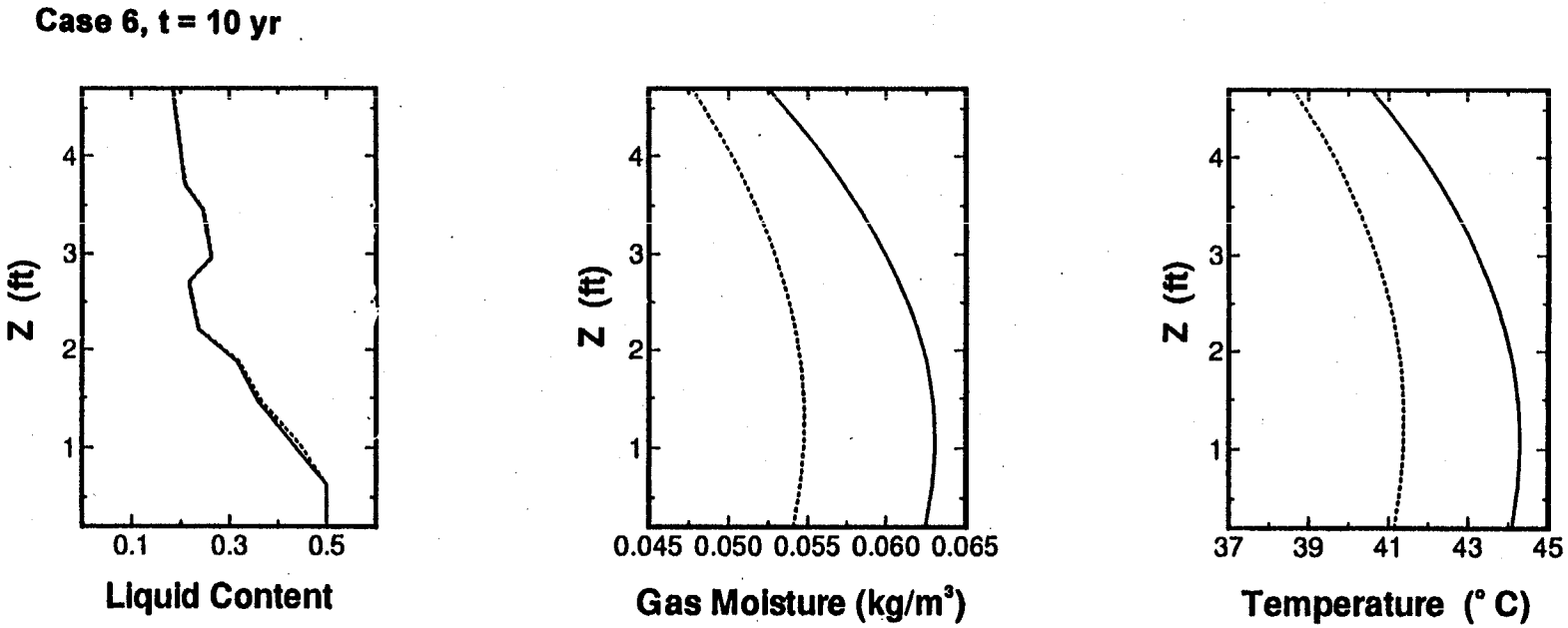

Figure D.2. Liquid Content, Gas Moisture Content, and Temperature Profiles for Test Cases 1 through 12. Solid curve is for radius 4.7 ft, and dotted curve is for radius 30 ft.

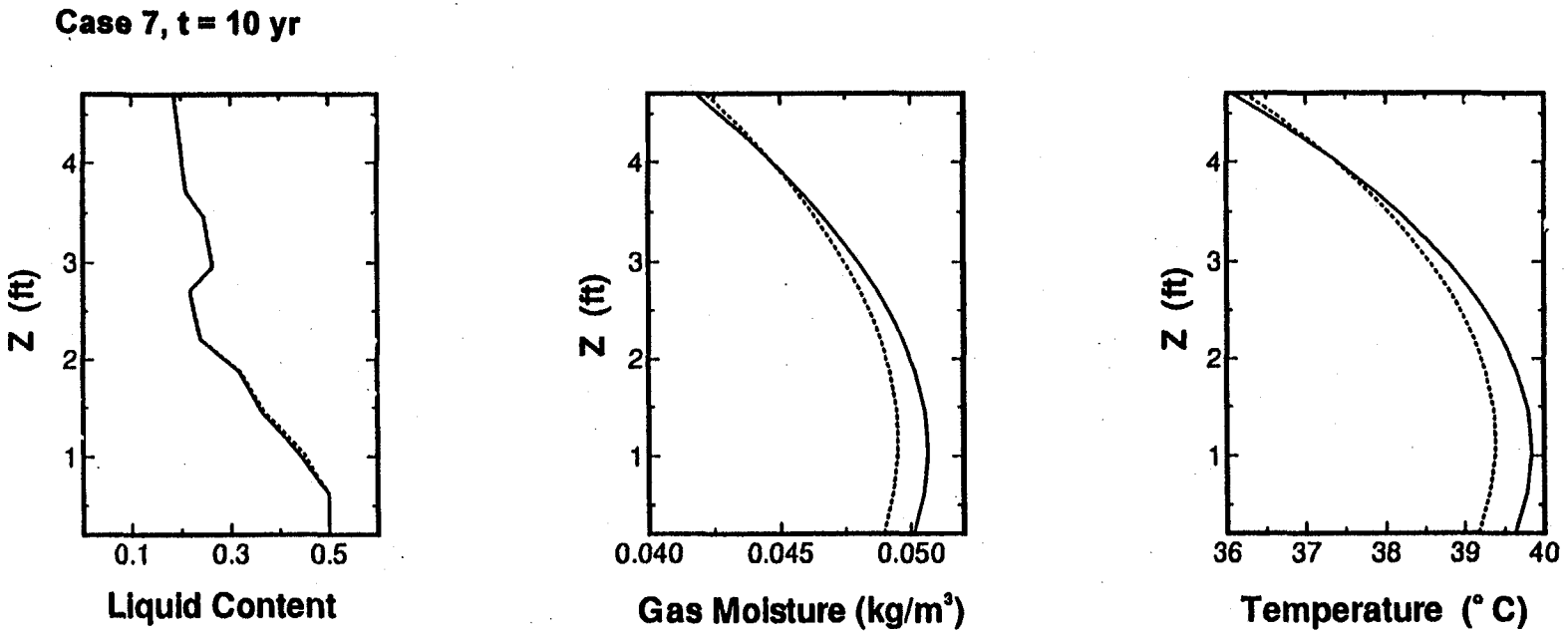

Figure D.2. Liquid Content, Gas Moisture Content, and Temperature Profiles for Test Cases 1 through 12. Solid curve is for radius 4.7 ft, and dotted curve is for radius 30 ft.

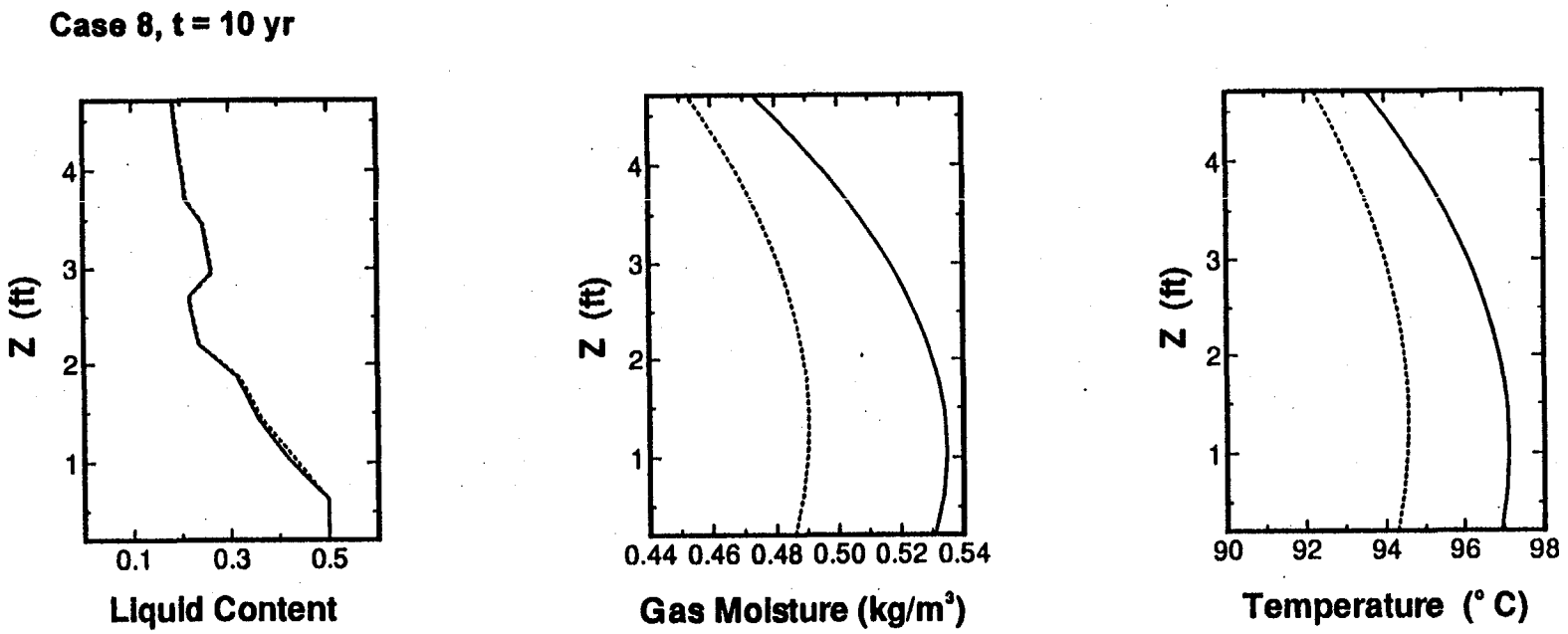

Figure D.2. Liquid Content, Gas Moisture Content, and Temperature Profiles for Test Cases 1 through 12. Solid curve is for radius 4.7 ft, and dotted curve is for radius 30 ft.

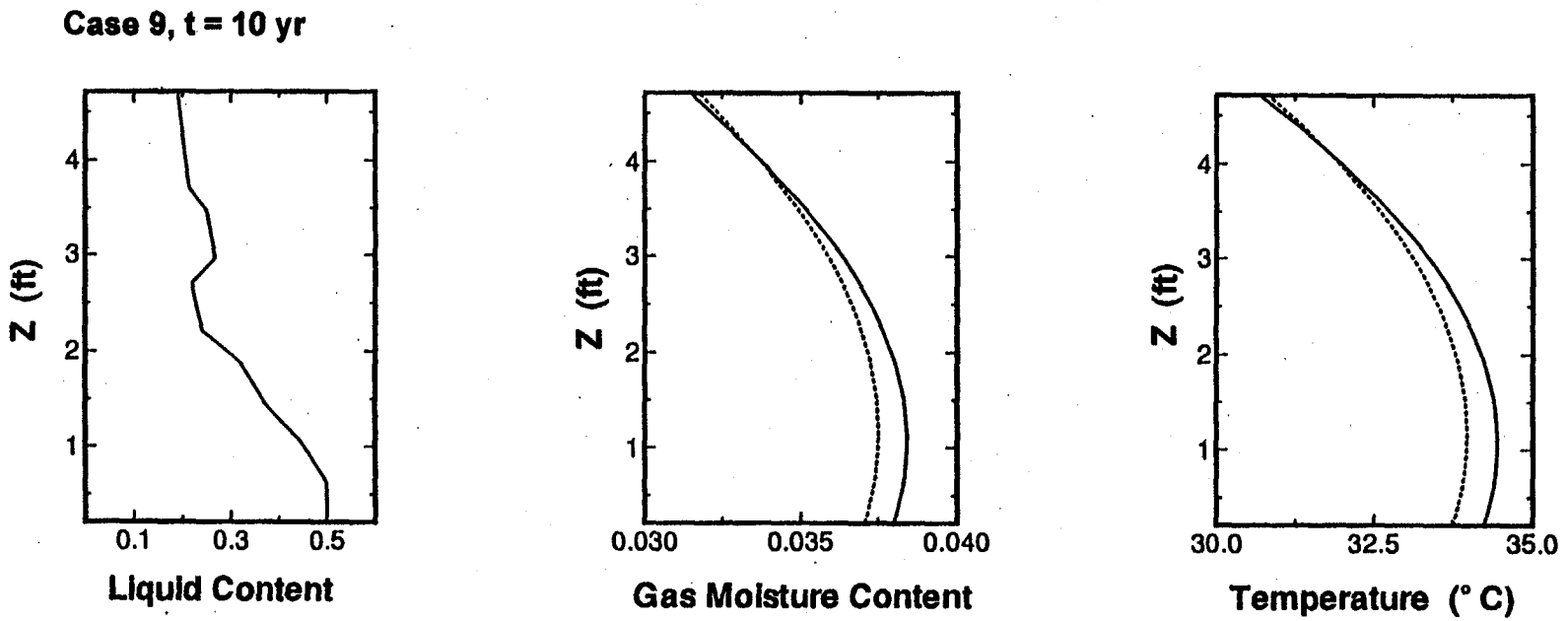

Figure D.2. Liquid Content, Gas Moisture Content, and Temperature Profiles for Test Cases 1 through 12. Solid curve is for radius 4.7 ft, and dotted curve is for radius 30 ft.

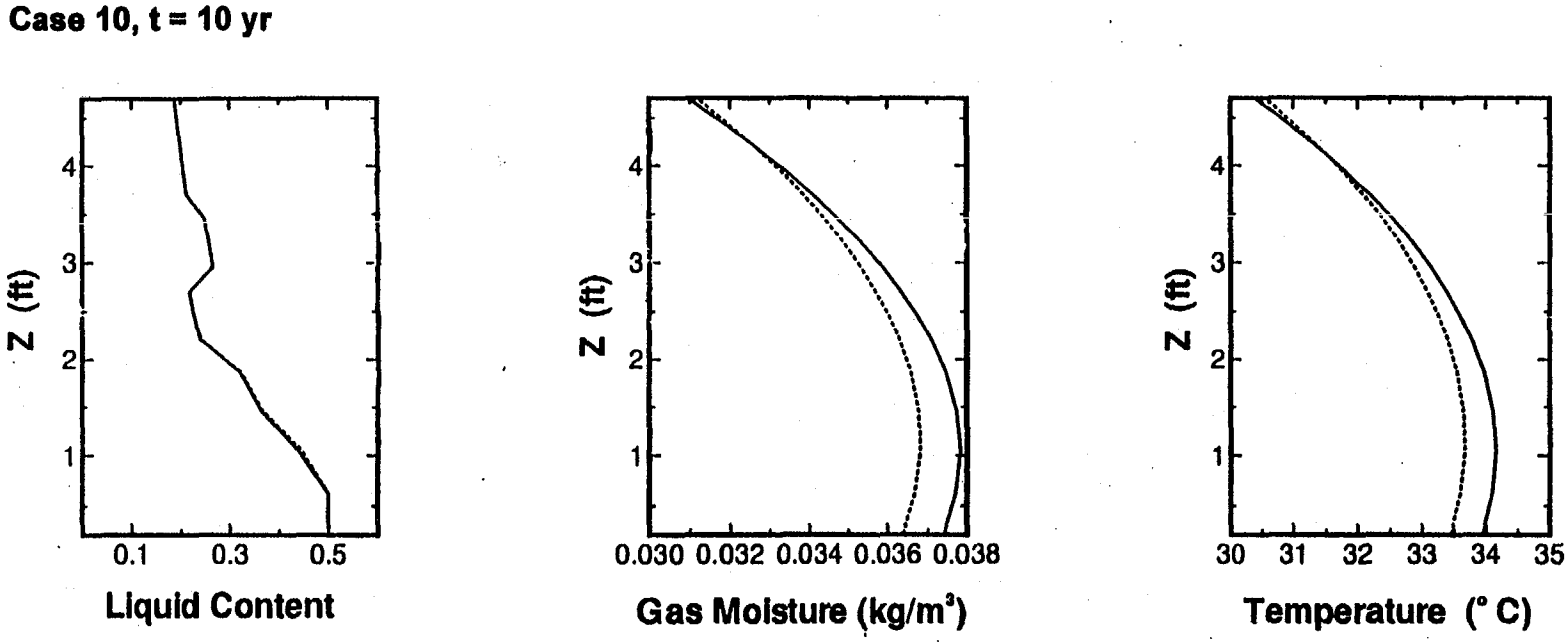

Figure D.2. Liquid Content, Gas Moisture Content, and Temperature Profiles for Test Cases 1 through 12. Solid curve is for radius 4.7 ft, and dotted curve is for radius 30 ft.

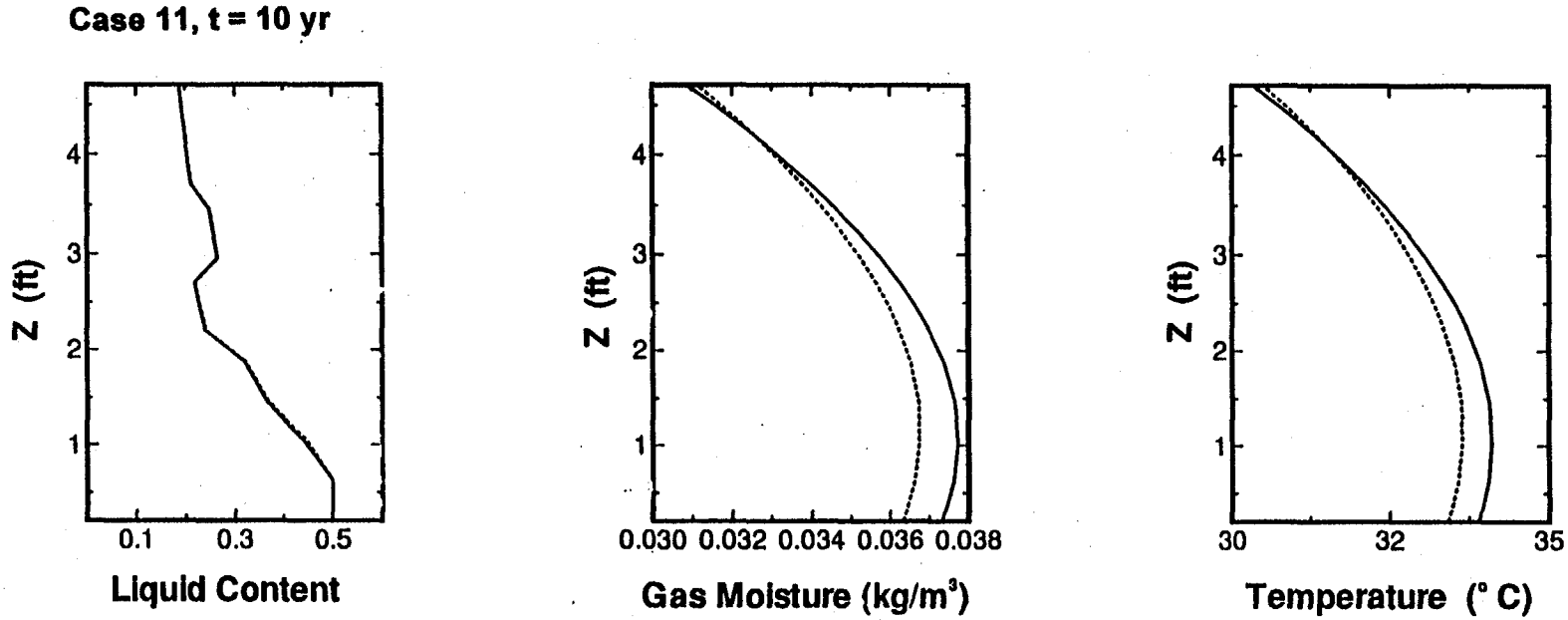

Figure D.2. Liquid Content, Gas Moisture Content, and Temperature Profiles for Test Cases 1 through 12. Solid curve is for radius 4.7 ft, and dotted curve is for radius 30 ft.

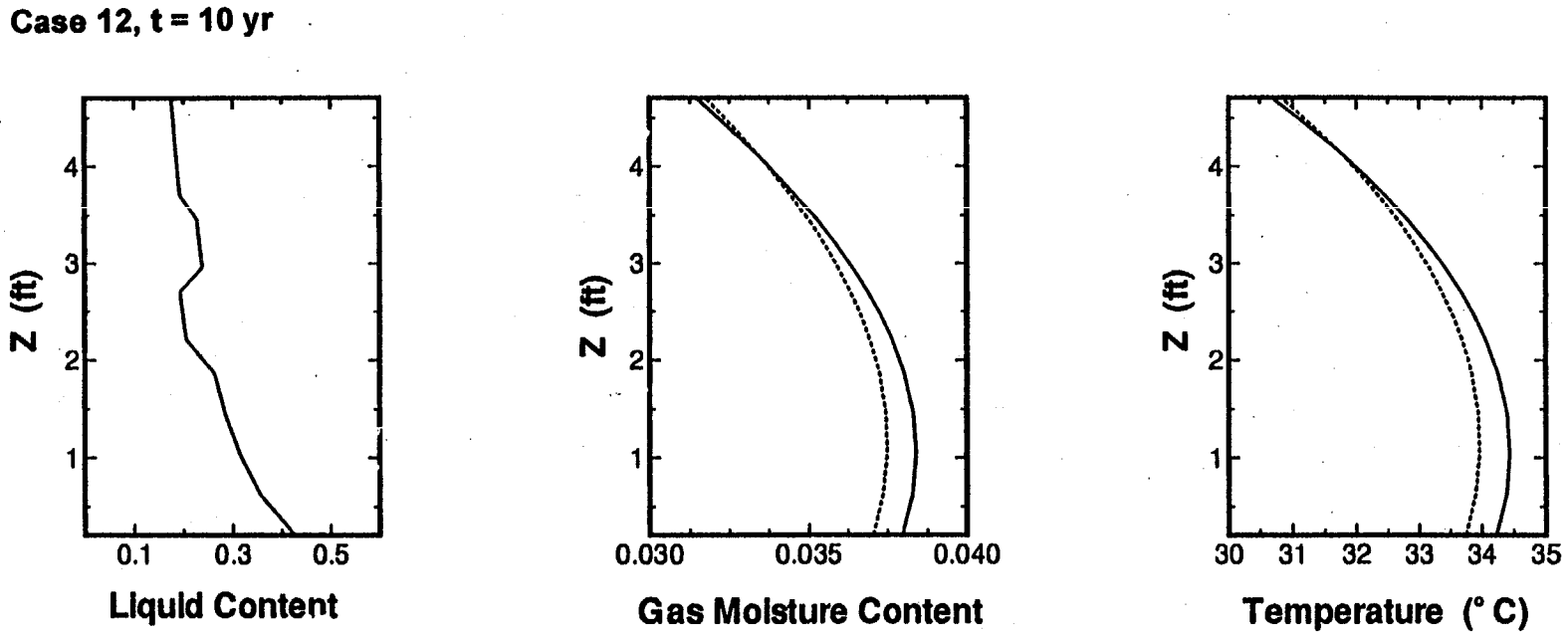

Figure D.2. Liquid Content, Gas Moisture Content, and Temperature Profiles for Test Cases 1 through 12. Solid curve is for radius 4.7 ft, and dotted curve is for radius 30 ft.

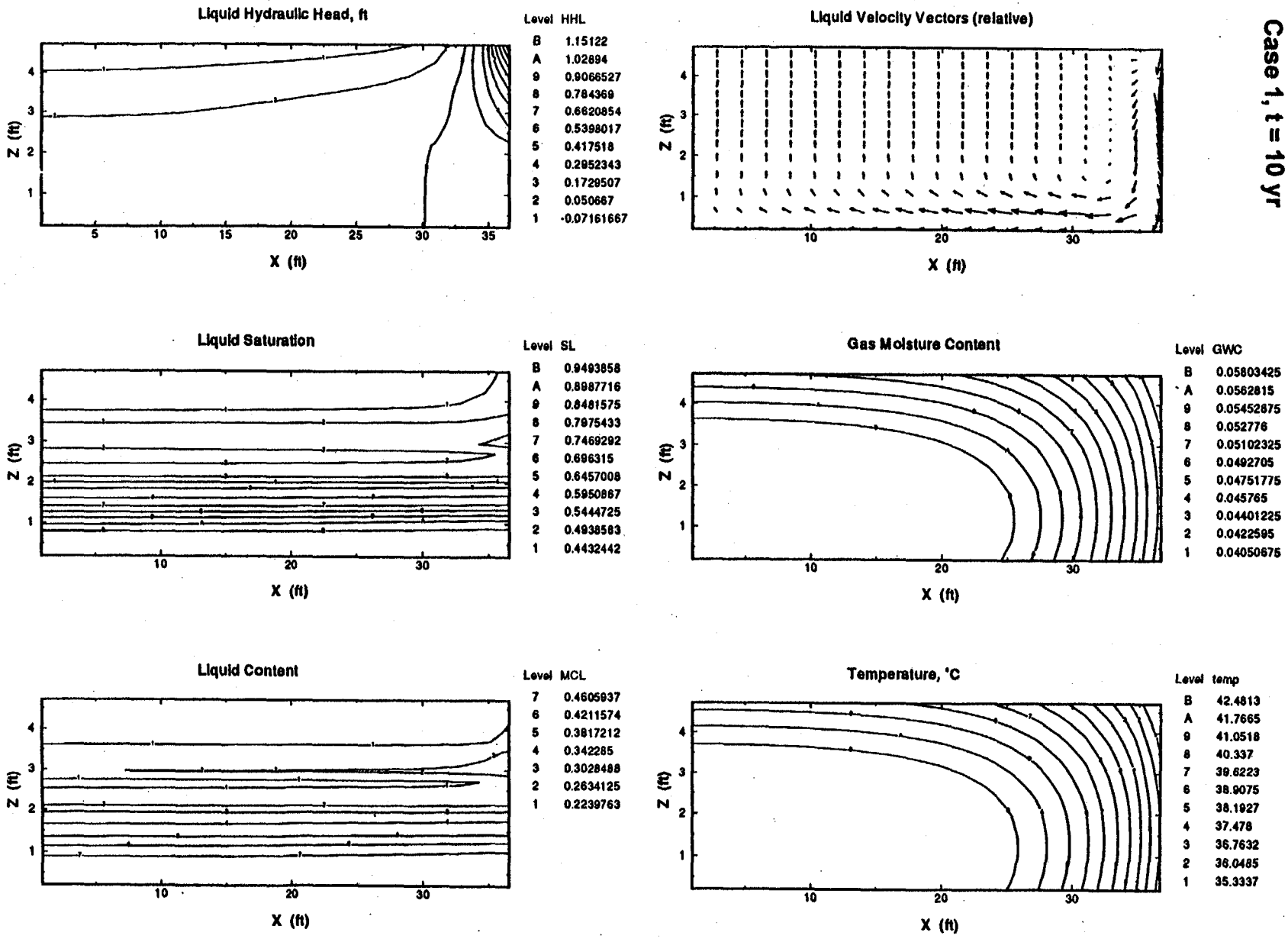

Figure D.3. Contour plots of Hydraulic Head, Liquid Saturation, Liquid Content, Liquid Velocity Vectors, Gas Moisture Content, and Temperature in a Radial Cross Section of a Waste Tank. Test Cases 1 through 12 are shown.

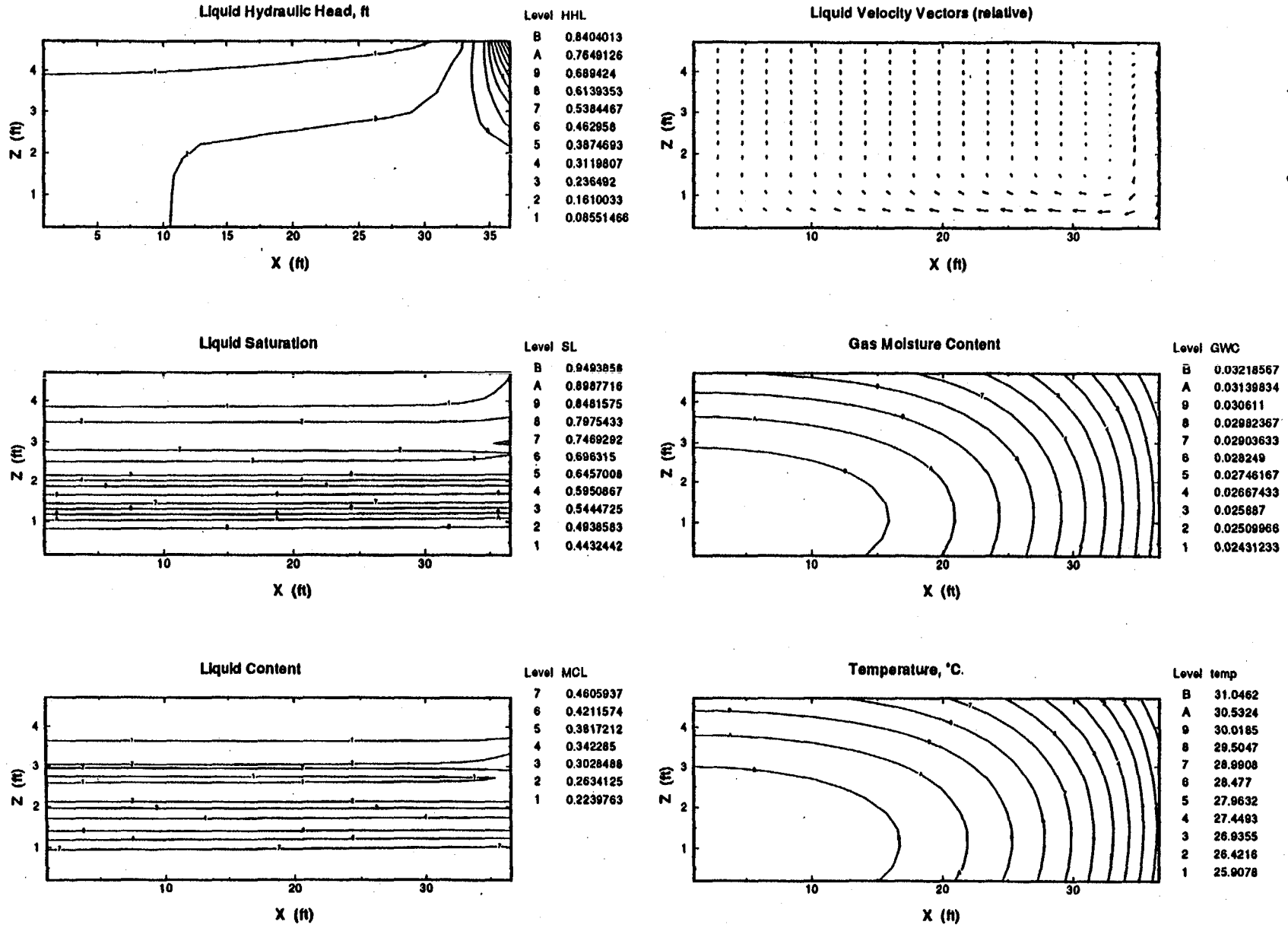

Figure D.3. Contour plots of Hydraulic Head, Liquid Saturation, Liquid Content, Liquid Velocity Vectors, Gas Moisture Content, and Temperature in a Radial Cross Section of a Waste Tank. Test Cases 1 through 12 are shown.

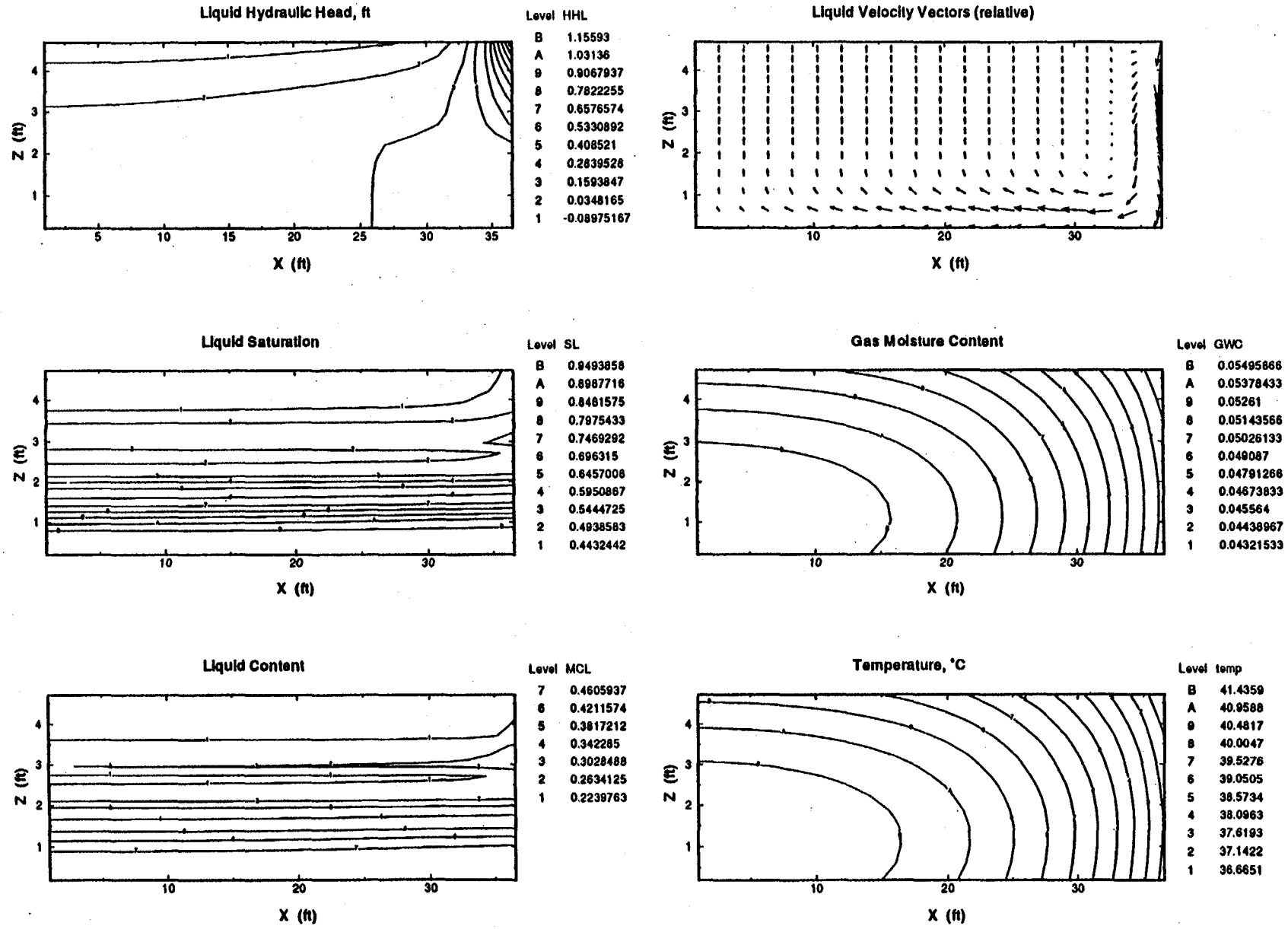

Figure D.3. Contour plots of Hydraulic Head, Liquid Saturation, Liquid Content, Liquid Velocity Vectors, Gas Moisture Content, and Temperature in a Radial Cross Section of a Waste Tank. Test Cases 1 through 12 are shown.

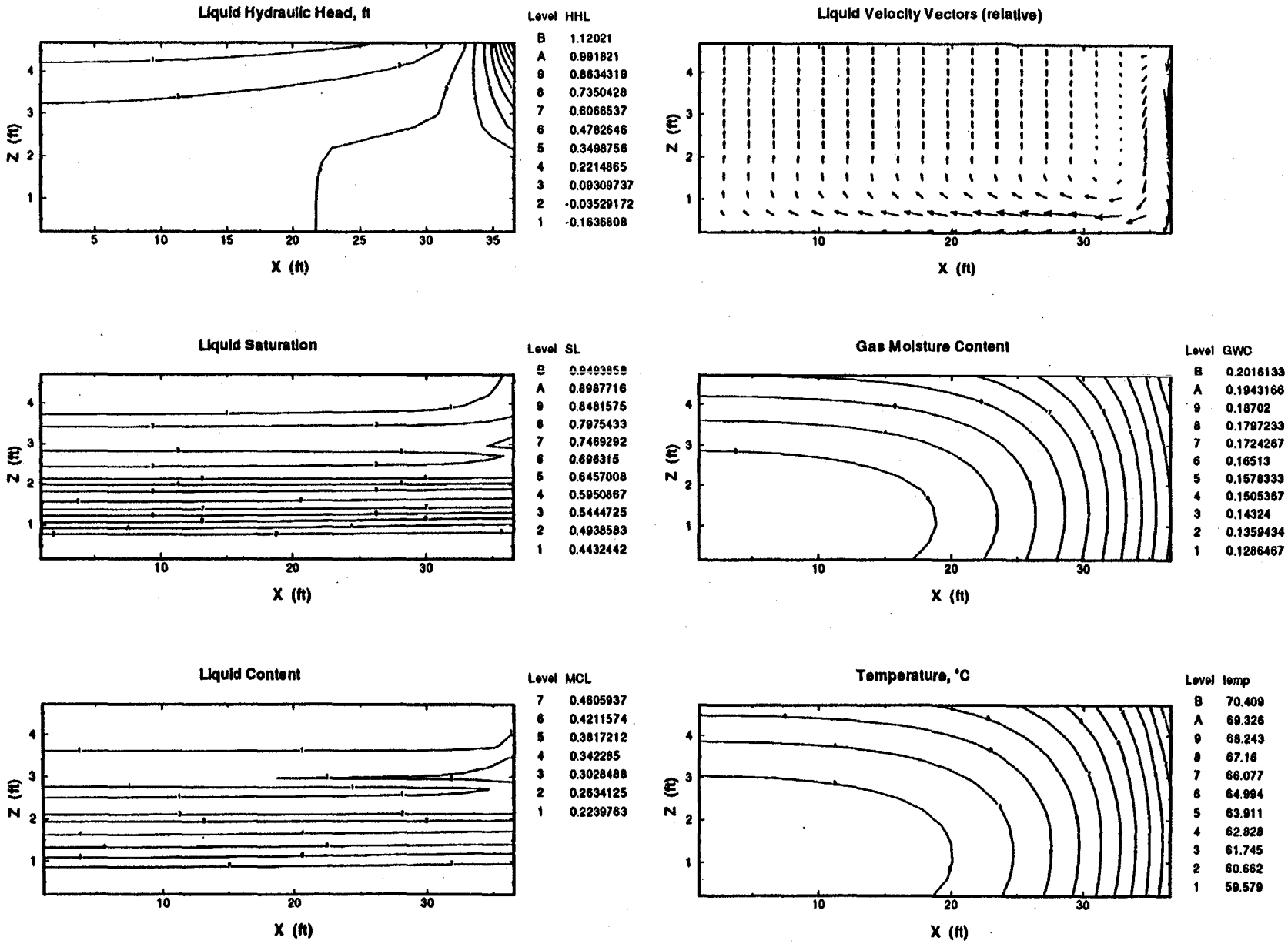

Figure D.3. Contour plots of Hydraulic Head, Liquid Saturation, Liquid Content, Liquid Velocity Vectors, Gas Moisture Content, and Temperature in a Radial Cross Section of a Waste Tank. Test Cases 1 through 12 are shown.

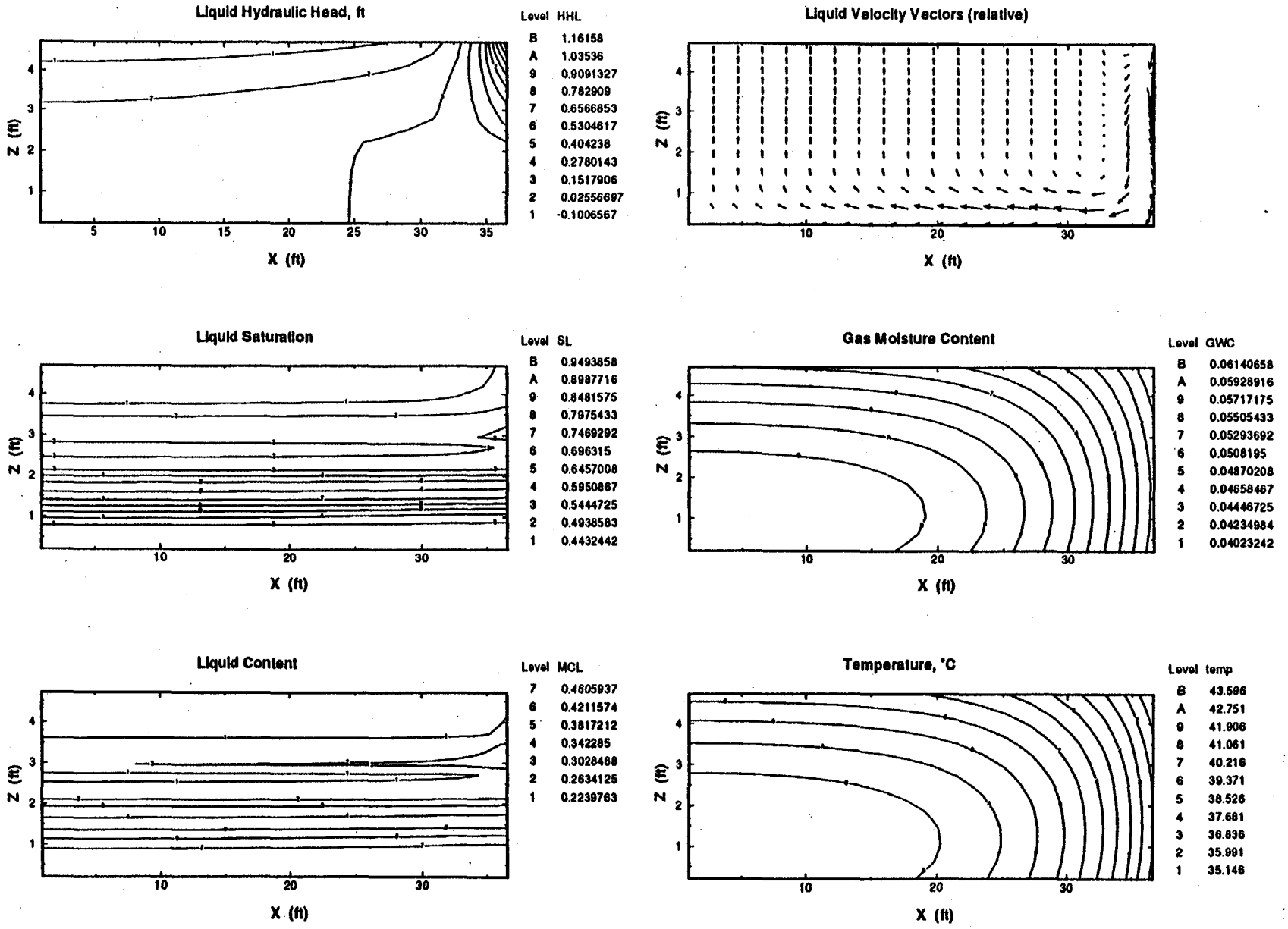

Figure D.3. Contour plots of Hydraulic Head, Liquid Saturation, Liquid Content, Liquid Velocity Vectors, Gas Moisture Content, and Temperature in a Radial Cross Section of a Waste Tank. Test Cases 1 through 12 are shown.

Case 5, t = 10 yr

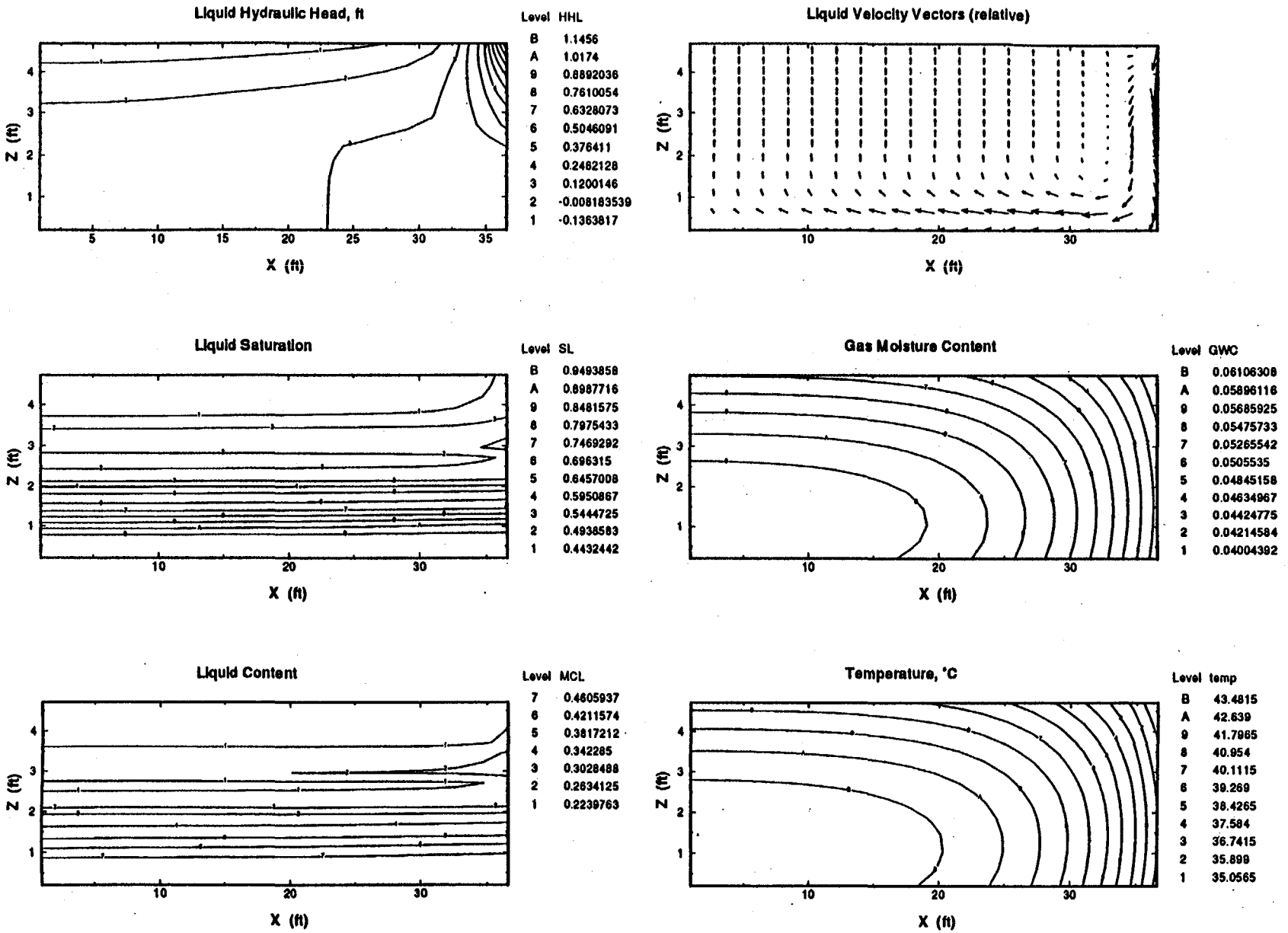

Figure D.3. Contour plots of Hydraulic Head, Liquid Saturation, Liquid Content, Liquid Velocity Vectors, Gas Moisture Content, and Temperature in a Radial Cross Section of a Waste Tank. Test Cases 1 through 12 are shown.

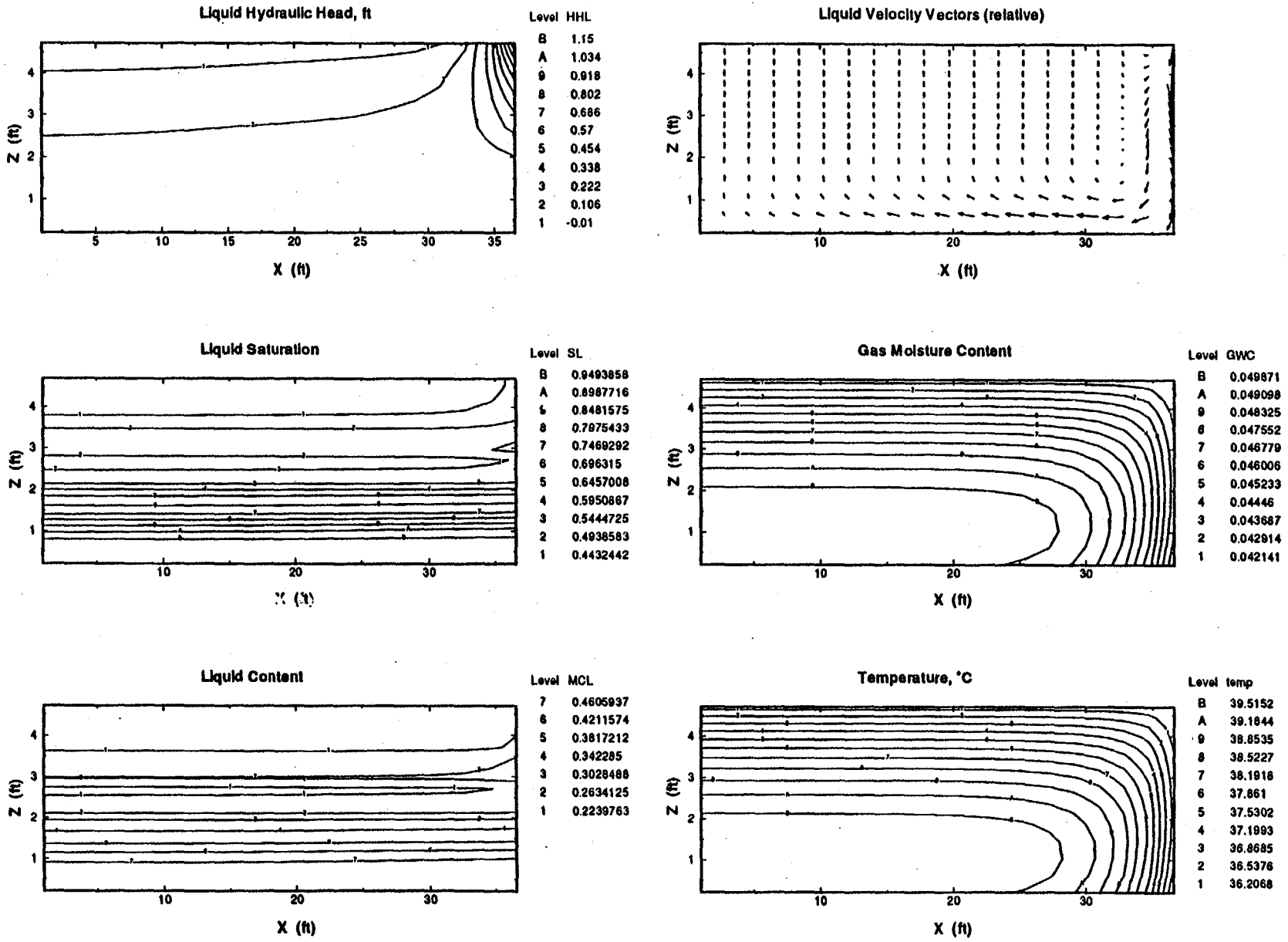

Figure D.3. Contour plots of Hydraulic Head, Liquid Saturation, Liquid Content, Liquid Velocity Vectors, Gas Moisture Content, and Temperature in a Radial Cross Section of a Waste Tank. Test Cases 1 through 12 are shown.

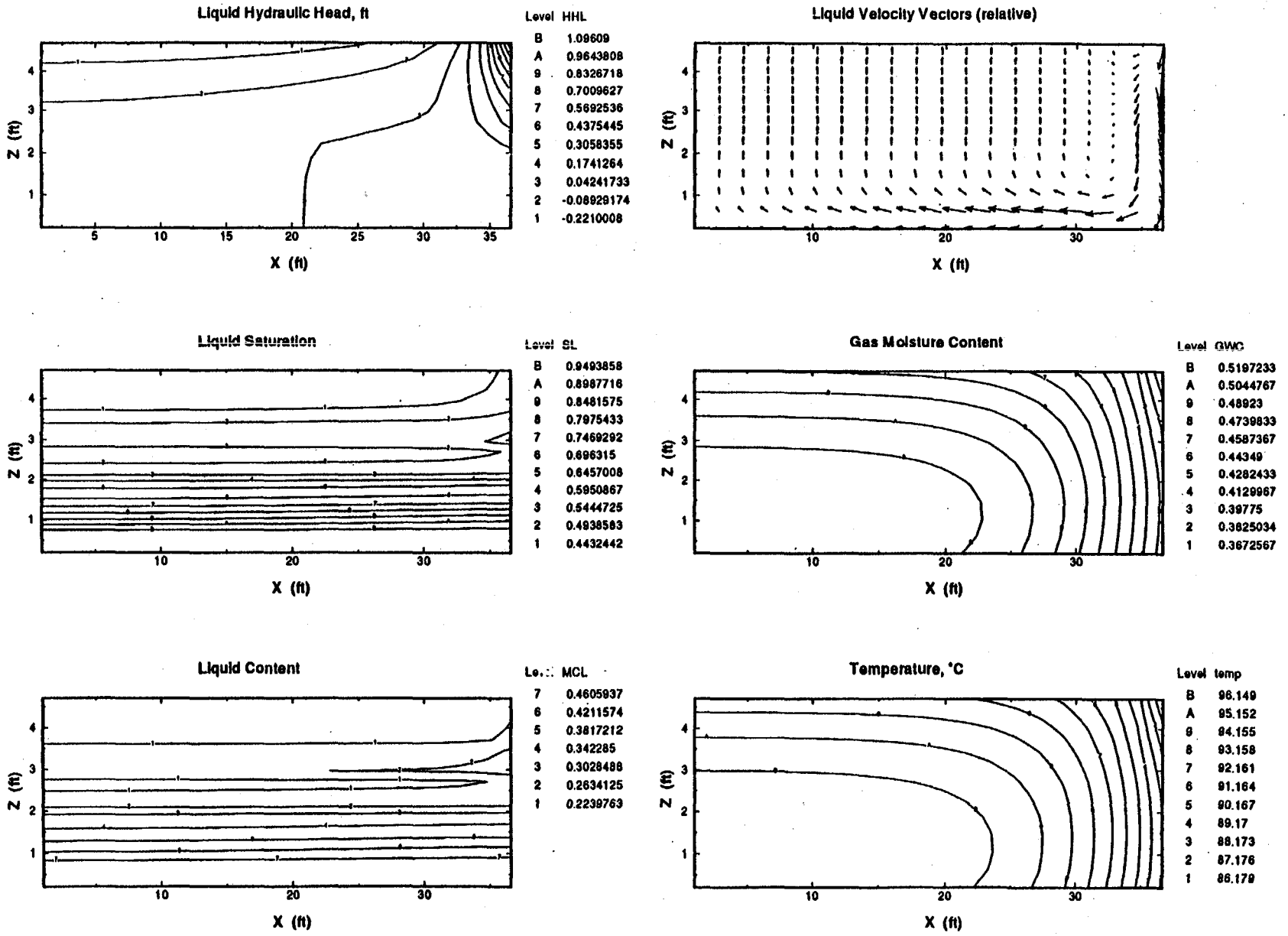

Figure D.3. Contour plots of Hydraulic Head, Liquid Saturation, Liquid Content, Liquid Velocity Vectors, Gas Moisture Content, and Temperature in a Radial Cross Section of a Waste Tank. Test Cases 1 through 12 are shown.

Case 9, t = 10 yr

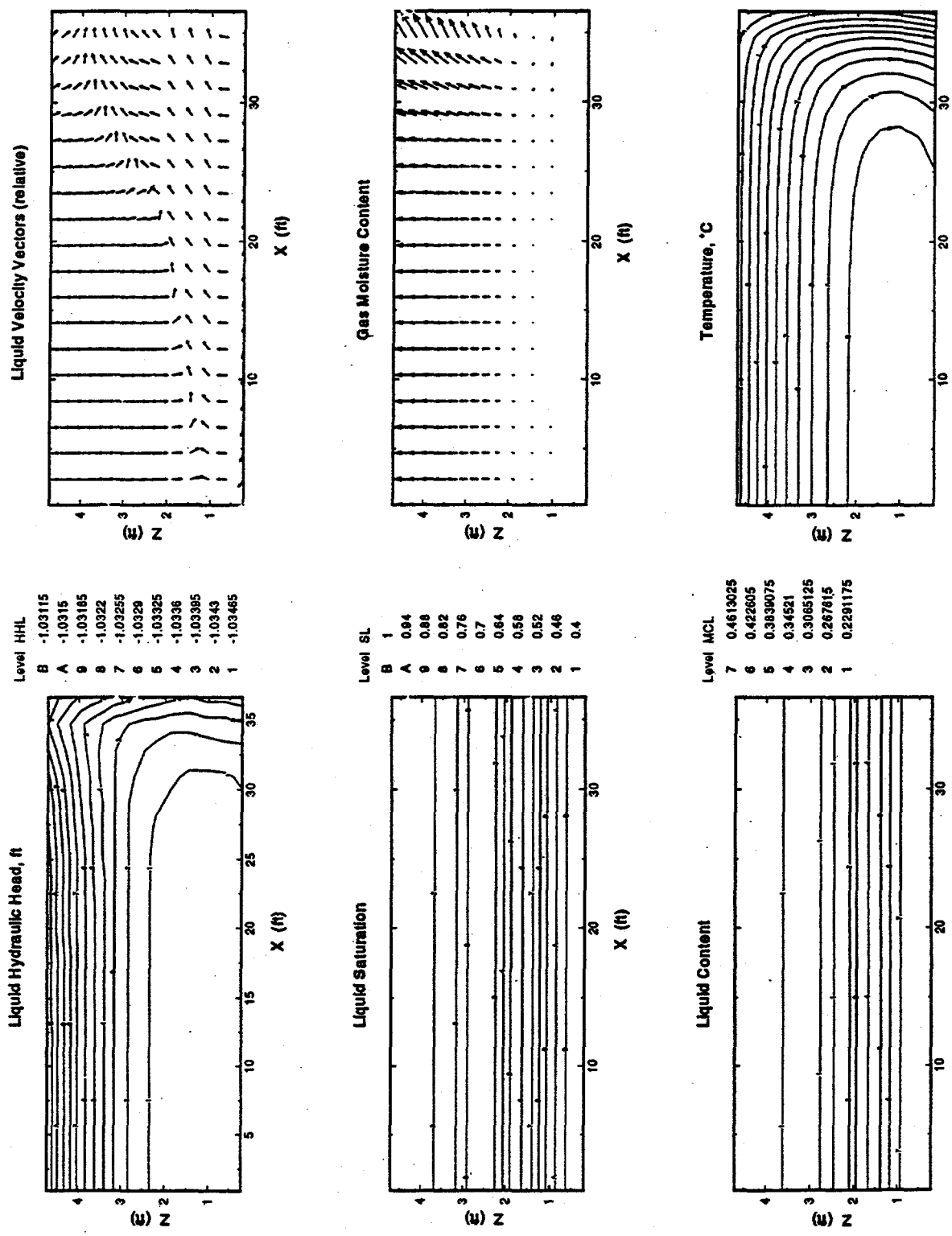

Figure D.3. Contour plots of Hydraulic Head, Liquid Saturation, Liquid Content, Liquid Velocity Vectors, Gas Moisture Content, and Temperature in a Radial Cross Section of a Waste Tank. Test Cases 1 through 12 are shown.

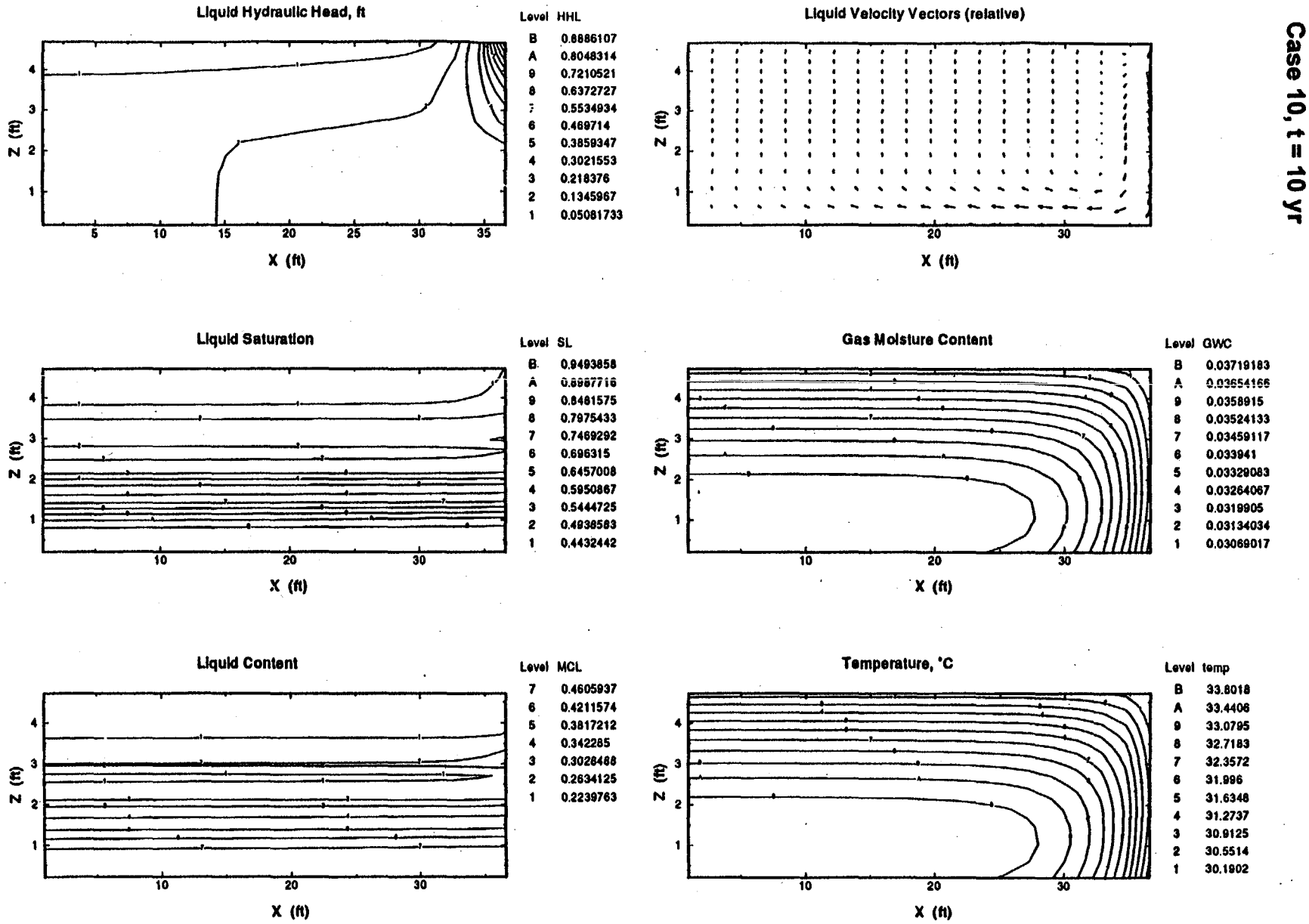

Case 10, t = 10 yr

Figure D.3. Contour plots of Hydraulic Head, Liquid Saturation, Liquid Content, Liquid Velocity Vectors, Gas Moisture Content, and Temperature in a Radial Cross Section of a Waste Tank. Test Cases 1 through 12 are shown.

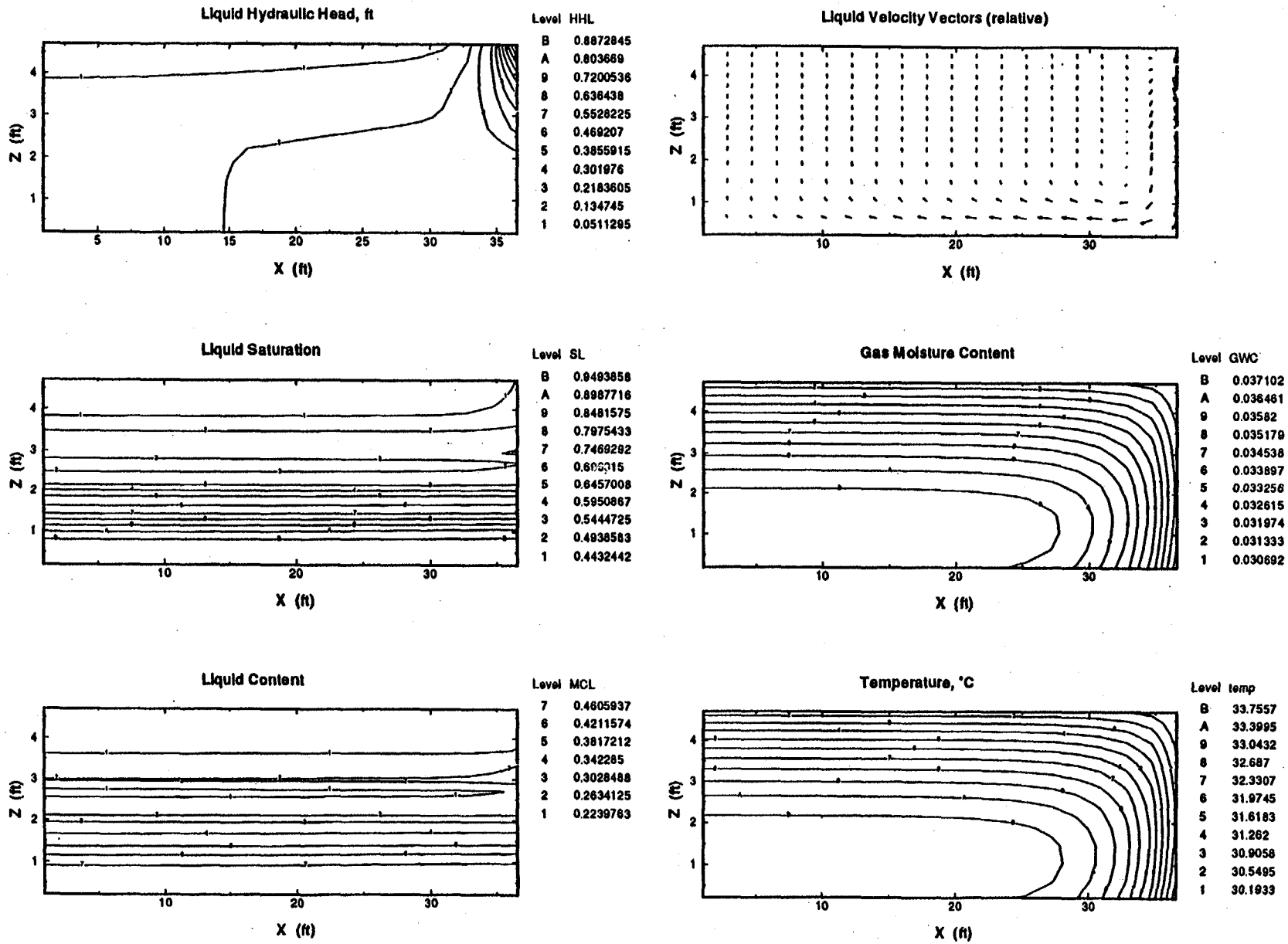

Figure D.3. Contour plots of Hydraulic Head, Liquid Saturation, Liquid Content, Liquid Velocity Vectors, Gas Moisture Content, and Temperature in a Radial Cross Section of a Waste Tank. Test Cases 1 through 12 are shown.

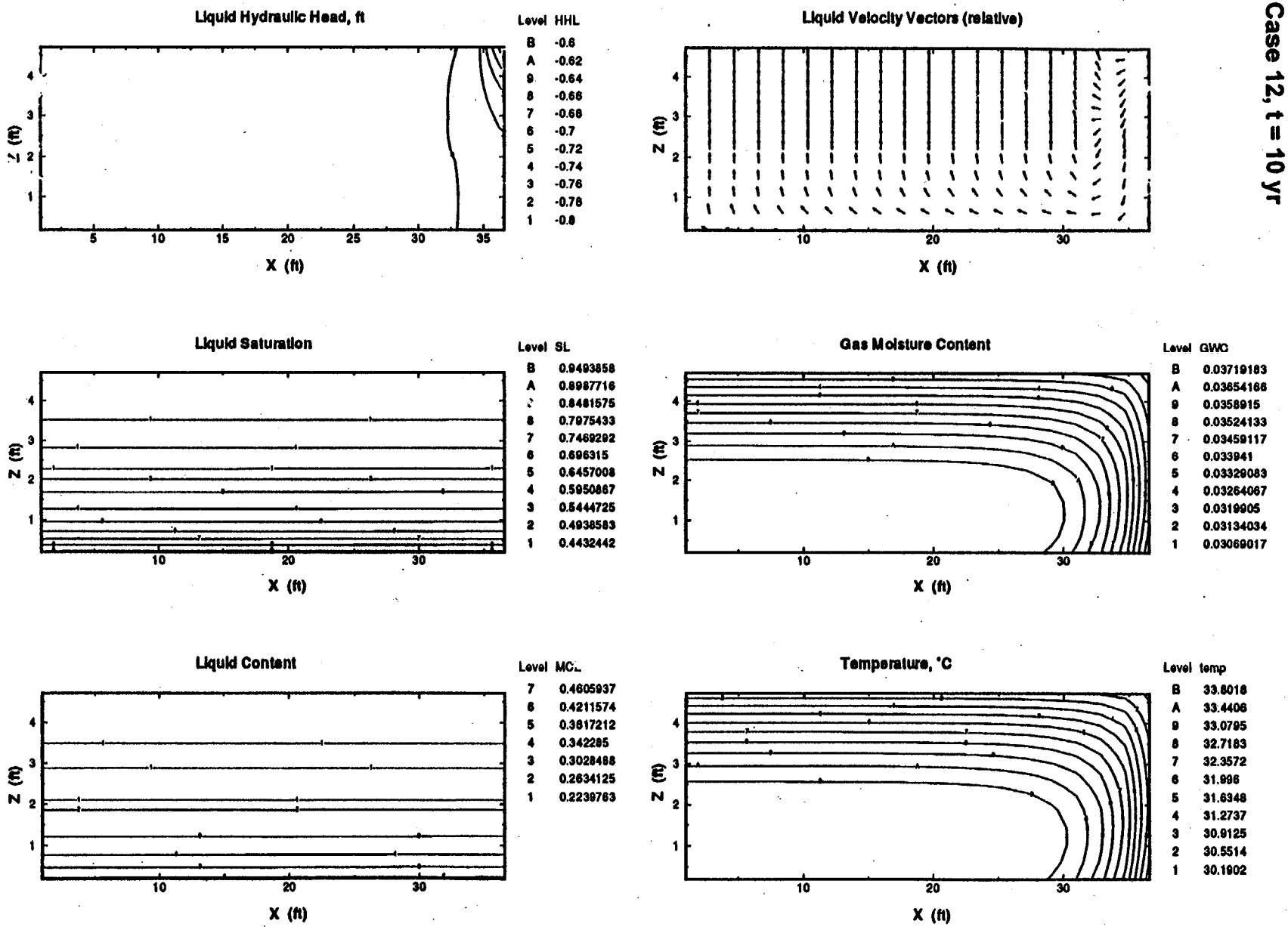

Figure D.3. Contour plots of Hydraulic Head, Liquid Saturation, Liquid Content, Liquid Velocity Vectors, Gas Moisture Content, and Temperature in a Radial Cross Section of a Waste Tank. Test Cases 1 through 12 are shown.

Appendix E

Drainable Porosity for Stabilized Saltcake Tanks

C. S. Simmons

Appendix E

Drainable Porosity for Stabilized Saltcake Tanks

When a saltcake tank is pumped, the volume fraction of interstitial liquid that is removed from the stabilized waste volume is called the drainable porosity. The drainable porosity is equal to

$$\text{PIL}/(\text{DILL} \times 2.75 \text{ kgal/in.})$$

where PIL is the pumped interstitial liquid (kgal), and DILL is the drop in the ILL (interstitial liquid level) from its stabilized starting liquid level. This stabilized starting liquid level should be the final surface level of the waste after supernatant liquid is removed and the surface of the solid waste has collapsed to its final level. Generally, when the waste profile is initially fully saturated with liquid up to the surface before pumping, the PIL is the liquid amount removed from below the final waste surface level and excludes the amount of pumped supernatant liquid. This means that the amount of liquid produced by collapse of the waste profile must be subtracted from the total amount pumped. Then

$$\text{PIL} = \text{Pumped Amount} - (\text{LS} - \text{L}) \times 2.75 \text{ kgal/in.}$$

and

$$\text{DILL} = \text{L} - \text{ILL}$$

where LS is the starting surface level, and L is the final collapsed surface level of the waste profile. That is, LS is the pre-stabilized waste level, and L is the post-stabilized waste level. L is also the starting level from which the interstitial liquid begins its decline during pumping.

To be stabilized, the ILL must be decreased as much as possible below the solid surface level. The smallest that the ILL can be decreased to is the capillary holdup height above the interface between the saltcake and sludge layer. Often the stabilization is not entirely completed (it is not practical to continue pumping long enough), and the final ILL stands above the sludge-saltcake interface, or above the tank bottom, by a height greater than the holdup height. Therefore, DILL is the drained waste depth affected by stabilization, and PIL is the amount actually removed from that affected drained waste volume. The amount given by (LS - L) x 2.75kgal/in., which is subtracted from the total pumpage, includes the supernatant liquid pumped and also the amount derived from collapse of the profile. If the amount of supernatant liquid standing above the starting solids level, LS, is known beforehand, it is also subtracted from the total pumpage.

The importance of the drainable porosity is that its value is used to estimate how much more liquid must be pumped out to lower the ILL by a depth of DILL. When fully stabilized, the remaining liquid is held up in a saltcake waste profile by capillary retention and cannot be further drained or leaked from the tank.

Letting P be the porosity, assumed as initially filled with interstitial liquid, and DP the drainable porosity, calculated as explained above, then P - DP is the retained volume fraction of liquid in the stabilized volume. The total amount of liquid retained by capillary retention is equal to (P - DP) x DILL x (2.75 kgal/in.). Also, there is the amount held below the ILL and above the sludge layer (when present): P x (ILL - Lsludge) x (2.75 kgal/in.), where Lsludge is the height of the sludge in inches. The smallest (ILL - Lsludge) can be is H, which is the holdup height. Generally, H is accepted to be about 12 in. in saltcake, although it varies among tanks. When a tank is not fully stabilized, DP x (ILL - Lsludge - H) x (2.75 kgal/in.) is the amount that could potentially still be drained or leaked. A sludge layer, if present, could also potentially drain additional liquid by consolidation of its volume, but the drainable porosity that applies is much smaller than for saltcake, generally accepted as about 12 vol% for sludge compared with 45 vol% for saltcake. Moreover, the effective capillary holdup height in sludge is much greater, and most sludge layers cannot be drained much. But the dryness of stabilized saltcake, not the drainable porosity of sludge, is considered here.

Figure E.1 gives the drainable porosity in volume percent for stabilized saltcake tanks. Drainable porosity is seen to be essentially independent of DILL in Figure E.1. The trend of PIL with DILL is shown in Figure E.2. The slope of the lines (curves) marked by "+" and "x" when divided by 2.75 kgal/in. constitute average drainable porosity for each of the two tank groups.

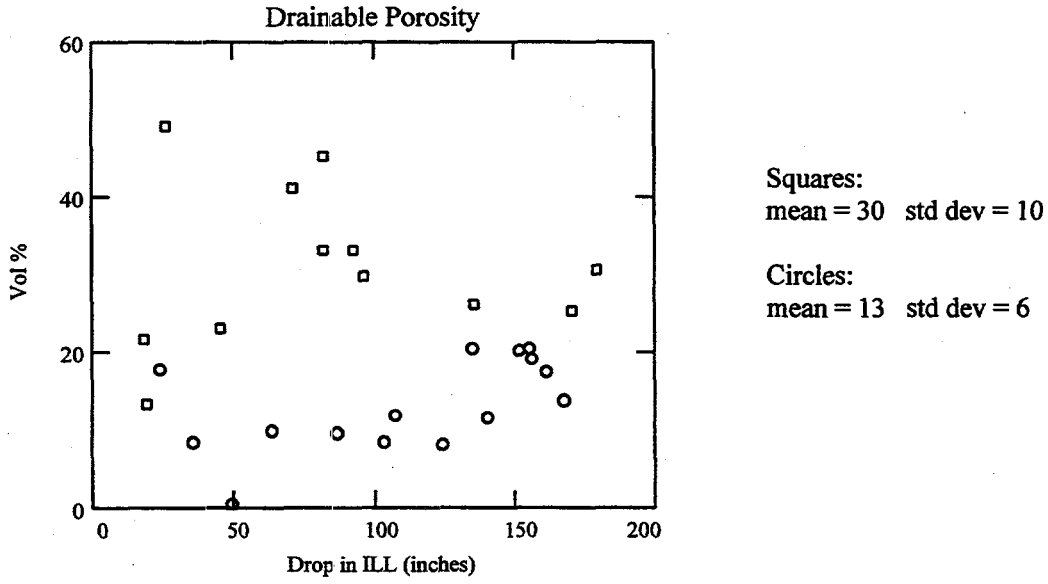

Figure E.1. Drainable Porosity for Two Groups of Stabilized Saltcake Tanks. Squares include most BY tanks and circles represent most TX tanks. The specific tank names in each group are provided in Figure E.2.

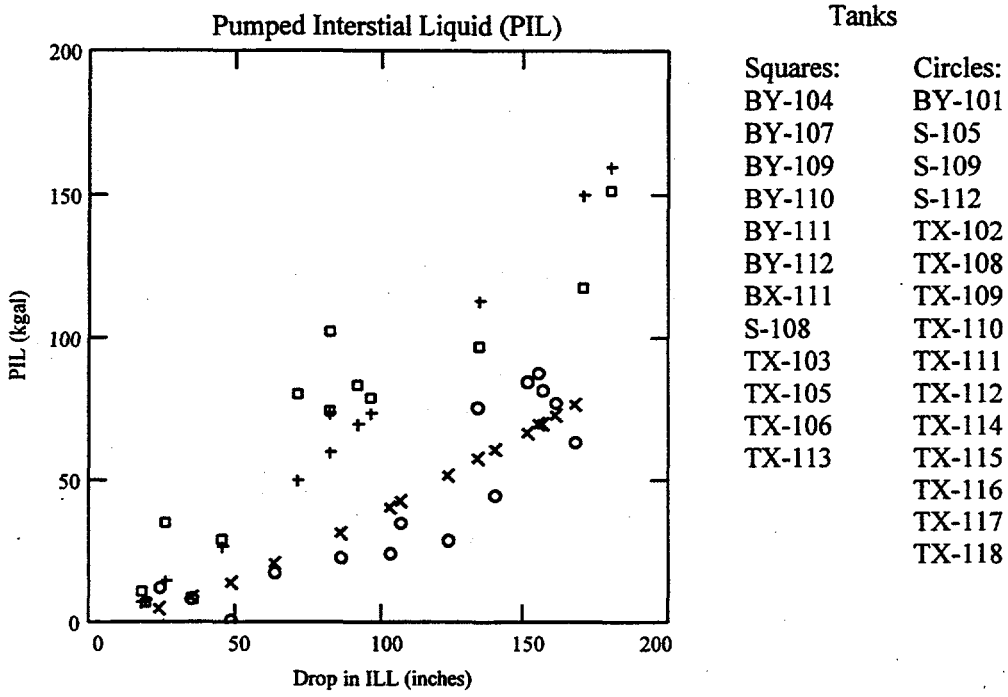

Figure E.2. PIL Depending on DILL for the Two Groups of Stabilized Tanks. The + and x show the trend predicted by using a single pore-size index, b, within each tank group.

The squares (first group including BY tanks) represent about an average of 30 vol%, whereas the circles (mostly TX tanks) represent average drainable porosity of about 13 vol%. (These values are direct averages given in Figure E.1 and not the slopes in Figure E.2.)

The trends shown by "+" and "x" in Figure E.2 are based on a capillary retention model called the Brooks-Corey model, which has the parameters P, H, and b, where "b" is the pore-size index that indicates how strongly liquid is held up above the holdup height H by capillarity in an unsaturated porous medium. That is,

$$\log(1 + h / H) = b \times \log(P / VLC)$$

where VLC is the volumetric liquid content that depends on the height, h, measured above the holdup height H. Note that (h + H)/H equals the ratio P/VLC raised to the power b. Notice where h is zero, right at the top of the holdup, VLC = P. For h becoming greater, VLC becomes smaller than P. Here h is the height measured above the ILL, so its maximum value is DILL at the waste's top. (Note the reference location is always a depth H below the ILL, and ILL is always the level of the saturated zone above a tank's bottom including the holdup height, H. For h measured above the ILL, the total height h + ILL above the bottom, the waste is unsaturated with VLC depending on h according to the Brooks-Corey equation.)

When a tank is drained by pumping down the ILL, the porosity P less the average VLC retained in the unsaturated volume equals the drainable porosity, DP. Therefore, when H and P (the liquid saturated value of VLC) are known, then "b" can be related to DP for each pumped tank profile. Thus DP is an average of the drained porosity and will depend on how much waste depth is stabilized. Contrary to common usage in the stabilization record (Swaney 1994), DP is not a constant value that applies to whatever waste depth is stabilized. Moreover, when DP is determined by partial stabilization from the drop in the ILL and the pumpage amount, PIL, this does not necessarily predict how much of the remaining liquid can be drained. The practice has been to use DP to estimate further possible drainage from the ILL that still stands a height greater than H above the saltcake-sludge layer interface or the tank bottom. Actually, DP depends on how deep the waste profile is stabilized, and DP is greater for greater DILL, assuming that a single b applies on the average to an entire waste profile.

In Figure E.2, the first tank group (squares) is represented by b = 1.4 and the second (circles) by b = 2.8. It was assumed that H = 12 in. and P is about 45 vol% for the first group (except that BY-112 and BX-111 had P of about 55 vol%) and 35 vol% for the second group. These two mean values of b are based on a regression fit of the Brooks-Corey retention model for each group. In general, a set of "b" values can be estimated corresponding to each tank so that predicted PIL or DP exactly equals the measured values of DP.

Figure E.3 gives the pore-size index evaluated for each tank of the two groups. Larger values of "b" are associated with the TX tanks having relatively smaller drainable porosity (circles in Figure E.1). The pore-size index has no apparent correlation with DILL, indicating that b is associated more with a waste's liquid retention than with the profile depth. Figure E.4 shows the correlation of pore-size index with drainable porosity over all stabilized tanks. This plot shows that "b" has a predictable dependence on DP.

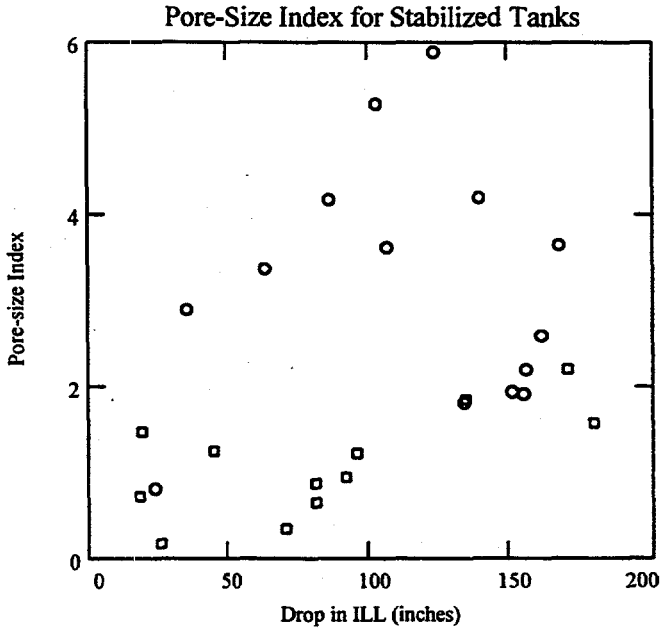

Figure E.3. Pore-size Index for the Two Groups of Stabilized Tanks

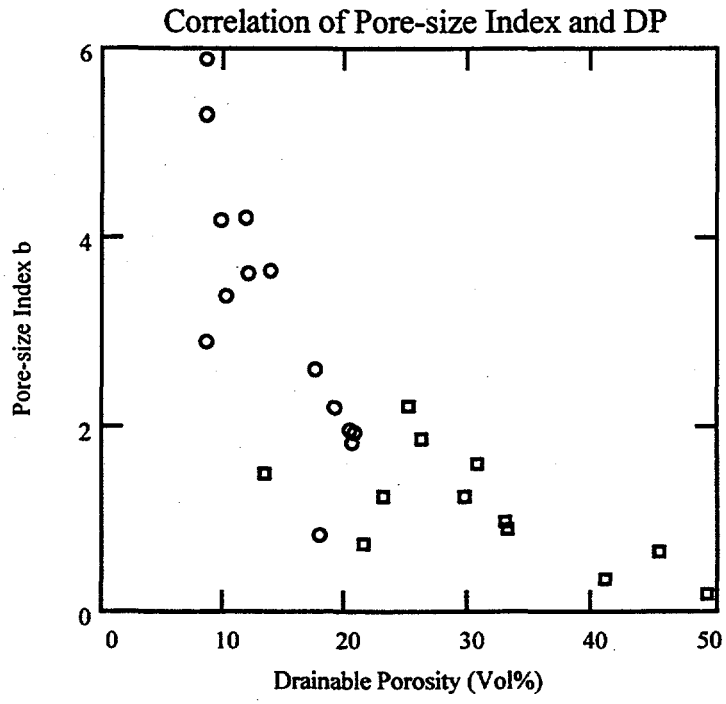

Figure E.4. Correlation of Pore-size Index and Drainable Porosity for All Stabilized Tanks in the Two Groups

The importance of estimating b values is that the Brooks-Corey retention model can then be used to estimate the average trend in the VLC with height above the ILL. By itself, the drainable porosity does not indicate how dry the surface may be relative to waste deeper in the profile. However, having a b value makes it possible to determine how much drier the surface might be relative to the deeper waste.

Values for the drainable porosity and pore-size index are different than those previously reported (Simmons 1995) because a different approach for estimating DP from tank pumping response data was used. The previous estimates made use of DeWeese's (1988) revised evaluation of drainable porosity based on including additional P-10 pumpage that was not originally included with the jet-pumped amount. These estimates did not always accurately account for the distinction between the amount of liquid pumped as supernatant liquid and the amount from below the final surface level as actual PIL.

E.1 Estimation Method

The evaluation of PIL was based on pumping records found in Hanlon (1995) and Swaney (1994). The P-10 pumping amount given by DeWeese (1988) was included with the jet pumped amount to define the total pumpage. Level information for the waste profile, before and after pumping, was taken from the plots published by Whitney (1995), who gives the necessary information on both liquid level determined from liquid observation well (LOW) records and surface level determined with manual tape or Food Instrument Corporation (FIC) gauge.

However, Whitney mainly describes conditions since about 1981. Dip tube measurement records of liquid level just after pumping were usually found in Swaney's records. Brevick (1994) was used for waste level before pumping. In some cases, it appears that DeWeese's estimates did not use the final waste solids level following pumping. In the method used here, the supernatant liquid pumped during collapse of the waste level was calculated rather than using amounts reported by Swaney. Often the amount derived from P-10 pumping was removed as supernatant liquid before the waste surface had collapsed to its final height. DeWeese sometimes attributed the entire amount to the initial profile height, LS, instead of L, as required to find actual PIL.

Generally, the drainable porosities evaluated here are substantially smaller than those revised by DeWeese. This is the case for TX tanks. Porosity values estimated here tend to be similar to the original values in Swaney's stabilization record. DeWeese's revisions are sometimes inappropriate because the P-10 pumpage was often attributed to the interstitial volume of the final waste profile when in fact it should have been derived as supernatant liquid from collapse of the starting waste profile. It appears that some TX tanks were pumped in two stages. The first stage included the P-10 pumping and placed the final ILL below the physical surface based on the waste volume. In the second stage, the ILL was further dropped to the final dip tube reading, and the stabilization record given by Swaney was used to estimate drainable porosity. Such drainable porosity estimates are usually much less than those recalculated by DeWeese that associated the entire pumpage with the starting waste level. The method proposed here, however, attributes all pumpage between the starting level and final waste level to supernatant liquid, and only the remaining amount is viewed as interstitial liquid, drawn from below the final waste solid level. Thus the same systematic procedure is applied to every stabilized tank, regardless of whether the tank was pumped in repeated stages.

Some examples are of value for considering the distinction in methods for finding drainable porosity. A good validation case is Tank BY-104 because the waste surface level was recorded during jet pumping using a manual tape. The waste starting level was 240 in. and the final level was 156 in. The ILL dropped to 48 in. (by dip tube) after pumping, and 330 kgal were pumped. Recorded supernatant liquid volume is determined as 231 kgal, and PIL is 99 kgal. Thus DILL = 156 in - 48 in., and drainable porosity is 99 kgal/108 in./(2.75 kgal/in.) or is equal to 0.33. The final ILL is actually 48 in. plus the unknown holdup height, which was taken as 12 in. for all tanks. The 33 vol% porosity is consistent with DeWeese's revised estimate.

Tanks TX-113 and TX-114 were P-10 pumped, and DeWeese revised the original drainable porosity recorded in Swaney. For TX-113, the drainable porosity estimates are 17, 35, and 26 vol%, respectively, for the Swaney original, DeWeese revised, and new proposed value. For TX-114, the three values are 22, 33, and 19 vol%, in the same order. Typically, it was found that more pumpage is attributed to collapse of the waste level in this estimation method proposed here. Also, starting waste levels recorded by Brevick for TX tanks are often greater than those based on Hanlon's waste volume record. The consequence is that the proposed method attributes a smaller amount of PIL to the final waste level, and hence drainable porosity is less.

The varying amounts of liquid pumped as supernatant liquid from different tanks are described by a collapse factor, Fc, which equals (2.75 kgal/in.) x (LS - L)/Vwaste, where Vwaste is the total initial waste volume. This factor is the volume fraction of supernatant liquid derived

from the collapse of the starting level, LS, when dropped to the final level, L. The collapse factor, Fc, determines the reduction in the starting average volumetric liquid content, VLCS, to the final waste porosity, P. That is,

$$P = (VLCS - Fc) / (1 - Fc)$$

Brevick provides estimates of the waste's beginning void fraction, which can be equated to VLCS. Then, given an estimate of Fc, the P can be estimated for the collapsed waste profile. The collapse factor accounts for pumpage that is not now included in the drainable porosity. DeWeese's revision did not always distinguish between pumpage as supernatant liquid and as PIL. The distinction is essential to calculate the capillary pore-size index of pumped and drained waste. Previous estimates of "b" (Simmons 1995) were subject to error because they were based directly on DeWeese's revised estimates of drainable porosity.

Figure E.5 gives values of Fc for the stabilized tanks. These values appear random over the starting waste level. A few of the BY tanks appear to exhibit greater collapse, possibly related to the sludge portion of the waste profile that is not present in the TX tanks. One hypothesis suggests that the collapse attributable to sludge consolidation contributes additional pumpage that appears to come from the saltcake as PIL. This sludge consolidation would cause tanks with saltcake-sludge layered waste to yield larger apparent drainable porosity because additional liquid is expelled upward into the saltcake from the sludge due to the increased effective weight (overburden) of the saltcake. When saturated with liquid, the saltcake layer is

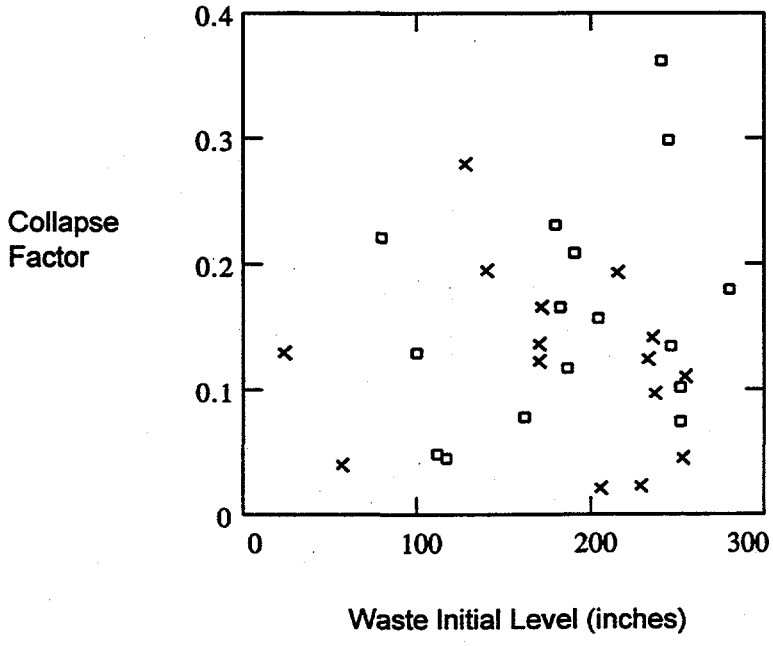

Figure E.5. Collapse Factors for BY and S Tanks (squares) and TX Tanks (X). Points indicate 31 jet-pumped tanks.

partly supported by buoyancy. When unsaturated by pumping, the saltcake overburden is increased; and the sludge layer beneath is subject to greater internal effective stress, which drives consolidation and expels liquid.

An equation can be derived for correcting DP that takes into account the liquid expelled into the saltcake layer from a consolidated sludge layer beneath. Letting DPO be the apparent drainable porosity based on the entire estimated PIL, the actual DP excluding liquid acquired from the sludge is given by

$$DP = (DPO - a \times Lsludge)/(1 - a \times Lsludge)$$

where "Lsludge" is the sludge layer thickness, and "a" is a volume compressibility coefficient, with units of 1/in. Here "a" is the actual sludge volume compressibility multiplied by the interstitial liquid's specific gravity. Laboratory measurements of "a" for sludge simulants yield values about 0.001/in. A comparison of observed DP for BY tanks having sludge layers and for TX tanks suggests an "a" value around 0.005/in. for actual in-tank sludge. The equation above was used to modify the estimates of DP for tanks BY-104, BY-107, BY-109, BY-110, BY-111, BX-111, and TX-103. For tank BY-104, the DP was changed from 0.38 to 0.3, for instance. Tank TX-103, which actually has a substantial sludge layer, showed the greatest revision, from about 0.4 to 0.13. These revised DP values tended to give a pore-size index greater than 1, whereas prior to correction, the b value was less than one. A list of the revised drainable porosity for these particular tanks is given below. Estimates of pore-size index are based on these revised values rather than on the uncorrected original value of DP (given in Tables E.1 and E.2).

Revised Drainable Porosity accounting for Liquid from Sludge Layer Consolidation

Tank	Drainable Porosity
BY-104	0.3
BY-107	0.23
BY-109	0.22
BY-110	0.33
BY-111	0.26
BX-111	0.49
TX-103	0.13

Tables E.1, E.2, and E.3 summarize the quantities discussed. The three estimates of DP are compared, and two sets of pore-size indexes are listed along with the associated saturated liquid contents. The first list of pore-size indexes is based on a guess of what the porosity might be in the saltcake for present tank conditions. The second set represents the tanks just after stabilization, and the porosities are based on collapsing Brevick's estimates of the initial waste void fraction. Together, the two sets suggest what the range in "b" is likely to be in stabilized tanks. The drop in the ILL (DILL) for past conditions (post-pumped) is used along with PIL estimates to calculate the proposed DP values. Using the DILL for past conditions and the given DP, the PIL can be back-calculated. Total pumpage is provided for comparison. But recall that PIL will generally be much less than the total pumpage, as reflected by the collapse factor, which indicates how much supernatant liquid was pumped before the PIL. Depth of saltcake is the

Table E.1. Drainable Porosity Estimates and Related Tank Waste Data[aa,b,c,d,e]

Tank Farm	Tank Number	Pumpage kgal total	Pore Size Index (1)	Porosity *(1)	Pore Size Index (2)	Porosity *(2)
BY	101	68	3.617	0.35	7.18	0.621
BY	104	330	1.225	0.45	1.58	0.515
BY	107	56.4	1.24	0.45	1.99	0.622
BY	109	128	0.7339	0.45	0.973	0.544
BY	110	213	0.886	0.45	1.61	0.608
BY	111	313	1.852	0.45	2.41	0.529
BY	112	116	0.646	0.55	1.02	0.654
BX	111	117	0.1855	0.55	0.272	0.589
S	105	114	5.903	0.35	6.78	0.395
S	108	152	0.9567	0.45	0.861	0.432
S	109	111	4.166	0.35	5.05	0.411
S	112	125	1.824	0.35	2.7	0.449
TX	102	94.4	52.2	0.35	69.6	0.466
TX	103	68.3	1.484	0.45	1.71	0.505
TX	105	165	1.573	0.45	2.66	0.608
TX	106	135	0.3528	0.45	0.859	0.569
TX	108	13.7	2.898	0.35	5.4	0.605
TX	109	72.3	0.8228	0.35	1.66	0.576
TX	110	155	4.2	0.35	7.11	0.542
TX	111	98.5	5.302	0.35	9.2	0.569
TX	112	94	3.644	0.35	7.15	0.602
TX	113	192	2.195	0.45	3.21	0.578
TX	114	159	2.2	0.35	4.35	0.566
TX	115	99	1.926	0.35	4.36	0.614
TX	116	145	1.952	0.35	3.99	0.57
TX	117	165	2.588	0.35	4.81	0.552
TX	118	89	3.363	0.35	5.83	0.559

Notes:

(a) The original list of jet pumped tanks includes BY-102, 103, 105, 106, & 108. It was not possible to find drainable porosity for these tanks for various reasons.

(b) Tanks BY-102 & 103 had no dip tube liquid level record available, and the present liquid level is near or above the solids surface. Thus no apparent PIL was removed.

(c) Tank BY-105 had cement added to the surface, and now waste surface and liquid levels are equal.

(d) Information on recently pumped BY-106 is still incomplete.

(e) This proposed method showed no PIL removed from Tank BY-108; waste collapse accounted for all pumpage. DP, therefore, is 0, although DeWeese assigned a DP of 23 vol% while the Swaney estimate is 12 vol%. No LOW is available to confirm ILL.

Table E.2. Estimates of Pore-Size Index and Corresponding Porosity[a,b,c,d,e]

Tank Farm	Tank Number	DP Original	DP DeWeese	Drainable Porosity	Collapse Factor	Pumped Effectiveness	Drop in ILL - past	Drop in ILL - now	Depth Saltcake
BY	101	10	19	11.9	0.078	100	107	68	103
BY	104	45	34	37.5	0.361	78.7	96	37	134
BY	107	45	32	34.4	0.048	68.5	45	42	77.7
BY	109		***	36.4	0.232	19.9	18	6	102
BY	110	13	43	48.1	0.208	86.2	82	24	107
BY	111	45	52	31.7	0.299	91.9	135	79	159
BY	112	42	42	45.4	0.045	81.2	82	69	113
BX	111		***	55.9	0.221	100	26	26	37.6
S	105		***	8.45	0.158	77	124	82	173
S	108		***	32.9	0.102	42.8	92	38	227
S	109		***	9.73	0.134	45.3	86	32	202
S	112		***	20.5	0.074	60.4	134	75	234
TX	102	36	36	0.68	0.28	58.4	48.5	21	95
TX	103	25	25	41.3	0.228	100	19	9	0.455
TX	105	38	30	30.6	0.023	85.2	180	171	223
TX	106	47	41	41	0.123	51.4	71	38	150
TX	108	2	13	8.52	0.04	81.4	35	35	55
TX	109	45	45	17.9	0.135	17.6	24	5	148
TX	110	26	32	11.7	0.193	85.9	140	99	175
TX	111	18	18	8.58	0.165	78	103	81	144
TX	112	17	17	13.9	0.045	72.8	168	115	242
TX	113	17	35	25.2	0.11	79.1	170	147	227
TX	114	22	33	19.1	0.124	80.8	156	125	205
TX	115	25	25	20.6	0.02	81.6	155	122	202
TX	116	21	27	20.3	0.096	74.4	151	148	215
TX	117	16	27	17.4	0.141	84.3	161	122	203
TX	118	35	35	10.1	0.195	61.2	63	13	115

Notes:

(a) The original list of jet pumped tanks includes BY-102, 103, 105, 106, & 108. It was not possible to find drainable porosity for these tanks for various reasons.

(b) Tanks BY-102 & 103 had no dip tube liquid level record available, and the present liquid level is near or above the solids surface. Thus, no apparent PIL was removed.

(c) Tank BY-105 had cement added to the surface, and now waste surface and liquid levels are equal.

(d) Information on recently pumped BY-106 is still incomplete.

(e) This proposed method showed no PIL removed from tank BY-108; waste collapse accounted for all pumpage. DP, therefore, is 0, although DeWeese assigned DP of 23 vol%, while the Swaney estimate is 12 vol%. No LOW is available to confirm ILL.

Table E.3. Drainable Porosity Spreadsheet

Drainable Porosity

$kgal := 1000 \cdot gal$

Tank TX-113
Jet pumped: 19.2 kgal
P-10 pumped: 173 kgal
Starting Liquid Level: 88 in.
Final Liquid Level (Dip tube): 47 in.
Starting Waste Level: 254 in. (Brevick record)
Final Waste Level: 228 in.

$$\frac{19.2 \cdot kgal}{(88 \cdot in - 47 \cdot in) \cdot \left(2.75 \cdot \frac{kgal}{in}\right)} = 0.17$$ Swaney original

$$\frac{192 \cdot kgal - (235 \cdot in - 228 \cdot in) \cdot 2.75 \cdot \frac{kgal}{in}}{(228 \cdot in - 47 \cdot in) \cdot 2.75 \cdot \frac{kgal}{in}} = 0.347$$ DeWeese revised

$$\frac{192 \cdot kgal - (254 \cdot in - 228 \cdot in) \cdot 2.75 \cdot \frac{kgal}{in}}{(228 \cdot in - 47 \cdot in - 12 \cdot in) \cdot 2.75 \cdot \frac{kgal}{in}} = 0.259$$ New proposed

Tank TX-114
Jet pumped: 104 kgal
P-10 pumped: 55 kgal
Starting Liquid Level: 213 in.
Final Liquid Level (Dip tube): 37 in.
Starting Waste Level: 213 in + 55 in/(2.75 kgal/in) = 233 in
Final Waste Level: 205 in.

$$\frac{104 \cdot kgal}{(213 \cdot in - 37 \cdot in) \cdot 2.75 \cdot \frac{kgal}{in}} = 0.215$$ Swaney original

$$\frac{159 \cdot kgal}{(213 \cdot in - 37 \cdot in) \cdot 2.75 \cdot \frac{kgal}{in}} = 0.329$$ DeWeese revised

$$\frac{159 \cdot kgal - (233 \cdot in - 205 \cdot in) \cdot 2.75 \cdot \frac{kgal}{in}}{(205 \cdot in - 37 \cdot in - 12 \cdot in) \cdot 2.75 \cdot \frac{kgal}{in}} = 0.191$$ New proposed

difference between the post-stabilized waste level and the sludge level, i.e., L - Lsludge. The drop in the ILL-past (the quantity DILL) is usually much less than the saltcake depth, because the pumping is not completely effective—not all of the available interstitial liquid was pumped. Pumped effectiveness, therefore, is the ratio of DILL/(L - Lsludge - H) in percent. For example, Tanks S-108 and S-109 were apparently only about 43 to 45% effectively pumped, whereas BY-101 is completely stabilized. Most tanks that are stabilized have about 80% pumped effectiveness. A plot of pumped effectiveness versus collapse factor reveals no obvious correlation or trend, so the effectiveness of stabilization does not have any apparent connection to how much the waste profile collapses or how much pumpage is supernatant liquid. This is expected because the amount of supernatant liquid pumped from any particular tank seems random and does not relate in any apparent way to the original amount of waste, as shown in Figure E.5.

The post-stabilized tank waste profile is not static after being pumped. Apparently, from surface level graphs and neutron logs in LOWs reported by Whitney (1995), the DILL has decreased substantially over time in most cases. In Tank BY-104 the ILL has increased considerably with time, and the surface level has dropped. But most of the change in DILL is attributed to the increased ILL relative to the solid waste surface. A possible cause is that porosity below the ILL is becoming less as crystal growth continues by dissolution and re-crystallization of saltcake. This would displace liquid upward. Also, salt is likely crystallizing and filling in liquid within the dissolution gap around each LOW pipe produced when the LOW was first drilled into the waste. It is unlikely that condensation of moisture from the outside atmosphere or leakage into so many tanks could account for the observed rise of the ILL or the apparent decrease of DILL with time. Regardless of the time since being stabilized, the DILL exhibits a consistent trend as shown in Figure E.6.

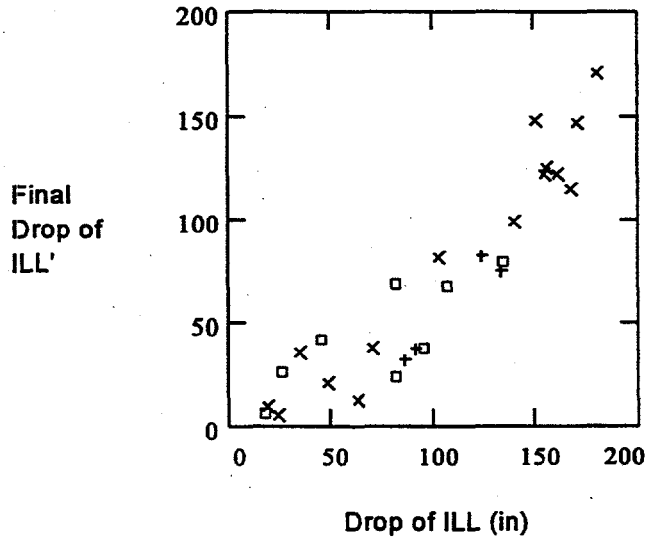

Figure E.6. Trend of the Present DILL with the Past Value Just After Stabilization. BY tanks (squares), TX tanks (X) and S tanks (+) are indicated. The final drop of ILL (the present DILL) is the same as "DILL-now." "DILL-past" was used to find drainable porosity. The mean ratio of DILL-now/DILL-past is 0.64 with std. dev. of 0.24 and a correlation of 0.92.

E.2 Summary

The drainable porosity of stabilized tanks was evaluated with a newly proposed procedure intended to distinguish better between supernatant liquid and interstitial liquid pumped from saltcake waste. The drainable porosity can then be used to estimate the pore-size index of the Brooks-Corey capillary retention curve, which gives the volumetric liquid content at a particular height above the saltcake-sludge layer interface or above the actual ILL. However, the pore-size index depends on the unknown porosity of the saltcake in its present physical condition, which is very uncertain for the tanks at this time. It is difficult to pin down the drainable porosity because the distance between the waste surface and the ILL, called DILL, has been changing over time, as determined from LOWs. Moreover, an accurate PIL is not easy to find from past waste level and stabilization records. The pore-size index and porosity as physical variables that replace the drainable porosity are essential to know if it is required to estimate the liquid content at the drained waste surface.

A recommendation from this study is that a greater effort is essential to measure the porosity of typical saltcake in a drained condition. The porosity is also essential to convert the volumetric liquid content into an estimate of weight percent water of saltcake. To more accurately estimate total weight percent water, measurement of the moisture content associated with the saltcake crystal structure (bound water) is needed also, because the capillary retention model describes only the so-called free liquid held in the interstitial volume. Furthermore, there is still a need to describe the crystal structure or grain size distribution of actual in-tank saltcake to determine the correct capillary retention model that is applicable.

Distribution

No. of Copies

OFFSITE

2 DOE/Office of Scientific and Technical Information

H. Babad
2540 Cordoba Court
Richland, WA 99352

D. O. Campbell
102 Windham Road
Oak Ridge, TN 37830

2 Fauske and Associates, Inc.
16W070 W. 83rd St.
Burr Ridge, IL 60521
Attn: M. G. Plys
H. K. Fauske

C. W. Forsberg
Oak Ridge National Laboratory
P.O. Box 2008
MS-6495
Oak Ridge, TN 37831-6495

A. K. Postma
G & P Consulting, Inc.
3640 Ballard Road
Dallas, OR 97338

B. C. Hudson
202 Northridge Court
PO Box 271
Lindsborg, KA 67456

No. of Copies

J. L. Kovach
Nuclear Consulting Services, Inc.
P.O. Box 29151
Columbus, OH 43229-0151

T. S. Kress
102-B Newridge Road
Oak Ridge, TN 37839

T. E. Larson
2711 Walnut St.
Los Alamos, NM 87544

3 Los Alamos National Laboratory
P.O. Box 1663
Los Alamos, NM 87545
Attn: W. L. Kubic K557
K. Pasamehmetoglu K557
C. Unal K557

2 Sandia National Laboratories
P.O. Box 5800
Albuquerque, NM 87185
Attn: D. A. Powers MS-0744
S. E. Slezak MS-0741

A. Stone
Washington State Department of Ecology
1315 W. 4th Avenue
Kennewick, WA 99336

3 U.S. Department of Energy
EM-38, Trevion II
12800 Middlebrook Road
Germantown, MD 20874
Attn: H. Calley
K. Lang
D. Pepson

No. of Copies

ONSITE

5 **DOE Richland Operations Office**

S. O. Branch	S7-54
C. A. Groendyke	S7-54
W. F. Hendrickson	S7-54
D. H. Irby	S7-54
G. W. Rosenwald	S7-54

19 **Hanford Contractors**

G. S. Barney	T5-12
W. B. Barton	R2-12
D. B. Bechtold	T6-07
W. S. Callaway	S3-90
R. J. Cash (2)	S7-14
J. M. Grigsby	R1-49
G. D. Johnson	S7-14
N. W. Kirch	R2-11
J. E. Meacham (5)	S7-14
D. A. Reynolds	R2-11
E. F. Riedel	S3-90
E. R. Siciliano	H0-31
L. M. Stock	S7-14
A. B. Webb	R1-44

No. of Copies

38 **Pacific Northwest National Laboratory**

Z. I. Antoniak	K7-15
J. M. Bates	K7-15
S. Q. Bennett	K7-90
J. W. Brothers	K9-20
S. A. Bryan	P7-25
S. M. Caley	P7-41
D. M. Camaioni	K2-44
C. D. Carlson	P7-25
P. A. Gauglitz	P7-41
R. T. Hallen	P8-38
P. G. Heasler	K5-12
J. L. Huckaby	K6-80
L. A. Mahoney	K7-15
B. J. Palmer	K7-15
L. R. Pederson	K2-44
L. M. Peurrung	P7-41
S. D. Rassat	P7-41
D. R. Rector	K7-15
H. C. Reid	K7-15
R. D. Scheele	P7-25
A. Shekarriz	K7-15
C. S. Simmons (10)	K9-33
C. W. Stewart	K7-15
J. J. Toth	K7-94
Information Release (5)	K1-06